The tetrapeptide Ac-SDKP and angiotensin converting enzyme in tuberculous pericarditis and fibrosis

by

VINASHA RAMASAMY

RMSVIN001

SUBMITTED TO THE UNIVERSITY OF CAPE TOWN

In fulfilment of the requirements for the degree

DOCTOR OF PHILOSOPHY IN CHEMICAL AND SYSTEMS BIOLOGY

Faculty of Health Sciences

UNIVERSITY OF CAPE TOWN

May 2020

Supervisor: Professor Edward Sturrock, Co-supervisor: Professor Mpiko Ntsekhe

Integrative Biomedical Sciences, University of Cape Town

DECLARATION

I, …Vinasha RAMASAMY…, hereby declare that the work on which this dissertation/thesis is based is my original work (except where acknowledgements indicate otherwise) and that neither the whole work nor any part of it has been, is being, or is to be submitted for another degree in this or any other university.

I empower the university to reproduce for the purpose of research either the whole or any portion of the contents in any manner whatsoever.

Signature: Signed by candidate

Date: …5.10.2020.……

Abstract

Tuberculous pericarditis is an extra pulmonary form of tuberculosis (TB) which leads to a life-threatening form of pericardial fibrosis in up to 25% of patients despite anti tuberculous therapy. The mechanisms leading to the fibrotic phenotype following infection are poorly understood. A proof of concept study revealed decreased levels of the antifibrotic N-acetyl-seryl-aspartyl-lysyl-proline or Ac-SDKP in tuberculous pericardial fluid as compared to control (non infectious) pericardial fluid. Ac-SDKP is a physiological peptide that is synthesised from its precursor protein thymosin β4 by the sequential action of meprin-α and prolyl oligopeptidase (POP) and is cleaved by angiotensin-1 converting enzyme (ACE). Importantly, a role of ACE and Ac-SDKP in the regulation of inflammation and fibrosis in multiple tissues and organs has been increasingly described in the literature. This has prompted interest in both the mechanisms of and potential for protective benefits of ACE inhibitors and Ac-SDKP analogue administration in fibrotic disease. The aim of this project was to investigate a) the molecular mechanisms of the antifibrotic effects of Ac-SDKP in the development of fibrosis, particularly in TB pericarditis, and b) the potential of ACEi and Ac-SDKP analogues *in vitro* in fibrosis prevention.

Pericardial fluid and blood samples from patients with TB pericarditis or undergoing coronary artery bypass surgery (non-infectious controls) was used to investigate the metabolism of Ac-SDKP in the tuberculous pericardium. Ac-SDKP levels as measured by ELISA, were significantly decreased (2.3 fold) in TB pericardial fluid as compared to controls. This reduction in Ac-SDKP levels was accompanied by a local 28% increase in the enzymatic activity of ACE, but no change in POP enzyme activity levels, both of which were measured using fluorogenic assays. This suggests that an increase in ACE activity in the pericardium following infection by the mycobacterium leads to a reduction of the levels of the antifibrotic peptide which is likely to contribute to the pathophysiology of fibrosing pericarditis.

A mass spectrometric (MS) approach was employed in order to identify proteins whose expression is modulated by the effect of Ac-SDKP in the proteome and secretome of a human lung fibroblast cell line (WI-38). Label free quantitative MS was employed to identify 114 and 44 differentially expressed proteins in Ac-SDKP fibroblast proteome and secretome respectively. Various extracellular matrix components and their related factors such as collagens, cytoskeletal proteins and inflammatory proteins, were identified among the

differentially regulated proteins. Reactome pathway analysis confirmed the significant enrichment of Ac-SDKP-related extracellular matrix proteoglycans and extracellular matrix in the differentially expressed proteins of the secretome.

Using the same cell line, the antifibrotic effects of Ac-SDKP analogues and ACE inhibitors were investigated through quantitative western blotting for transforming growth factor β (TGF-β) and Smad 3 levels, and using a hydroxyproline assay. Ac-SDKP prevented TGF-β and collagen expression through inhibition of Smad 3 phosphorylation. The Ac-SDψKP analogue (whereby the peptide bond between the aspartate and lysine is reduced) alone prevented TGF-β mediated collagen secretion. The combination of Ac-SDKP and the N domain-selective inhibitor RXP407, but not the non-selective lisinopril had an additive effect on the inhibition of collagen in fibroblasts. However, the antifibrotic effect of Ac-SDψKP was comparable to the combination of Ac-SDKP and RXP407 and was not improved with added ACE inhibition. Finally, the ACE signalling response to Ac-SDKP and the ACE inhibitors RXP407 and lisinopril was investigated using mass spectrometry and quantitative western blotting for phospho JNK and JNK. The ACE inhibitors as well as Ac-SDKP triggered the ACE signalling cascade to induce JNK phosphorylation. This highlights a potential new mechanism for the anti-inflammatory and antifibrotic effects of Ac-SDKP and the inhibitors.

This thesis has demonstrated an altered metabolism of Ac-SDKP is associated with increased ACE activity in the tuberculous pericardium. It has also provided a deeper understanding of the antifibrotic action of the tetrapeptide, and *in vitro* evidence for the use of the analogue Ac-SDψKP and inhibtion of N domain catalytic activity for decreasing fibrosis. These findings form a solid basis for future *in vivo* pharmacological studies on the effects of Ac-SDKP analogues and ACE inhibitors in the prevention and management of fibrotic conditions. Importantly, these therapeutic options present an exciting avenue to follow in the prevention of fibrosing pericarditis in TB pericarditis.

ACKNOWLEDGEMENTS

I would like to express my heartfelt gratitude to my supervisors Prof Edward Sturrock and Prof Mpiko Ntsekhe: Ed for your steadfast support and guidance, for your positive attitude and for all the opportunities you have provided me throughout the years. Mpiko for your unwavering dedication, your insight and for your guidance in navigating the clinical world.

I thank the National Research Foundation of South Africa for funding this degree.

I extend sincere thanks to the following people who have contributed to the work in this thesis:

Dr Arthur Mutyaba, Dr Alfred Mureko and Dr Paresh Keshaw for much appreciated collaboration in the collection of patient samples.

All the staff of the C25 Cath Lab at the Groote Schuur Hospital who have been involved in patient sample collection throughout the years.

Prof Ntobeko Ntusi and Stephen Jermy for their analysis of patient cardiac magnetic resonance data.

To various members of the Blackburn Lab: Dr Nelson Soares, Dr Bridget Calder, Dr Andrew Nel and Brandon for their invaluable help with mass spectrometry techniques and experiments. Special thanks to Bridget for critical reading of the thesis.

I am also thankful to past and present members of the ACE lab: Ross, Dale, Karabelo, Albert, Nailah, Afolake, Bertus, Lauren, Siya and especially Palesa, Kate and Lizelle for making this journey fun and memorable. To Sylva, thank you for being always ready to help, to support and to listen, for reading my thesis and for our recipe sharing moments.

To my parents Saloni and Viiay, I am immensely grateful for all the sacrifices you have made to allow me to pursue my dreams. I also thank the rest of my family for their constant encouragement: Nityam, Maa, Youvin, Auntie Veena and Ton Ramesh.

Last, but certainly not least, I thank my husband Kurvin for the love and support. Without you, I would not be on this journey in the first place. You are my cheerleader, my confidante and my goofiest friend all in one.

Abbreviations and Acronyms

ACE: Angiotensin converting enzyme.

ACEi: ACE inhibitor.

AChE: acetyl-cholinesterase.

ACN: Acetonitrile.

Ac-SDKP: N-acetyl-seryl-aspartyl-lysyl-proline.

ADA: adenosine deaminase.

AMC: amino methyl coumarin.

Ang 1-7: Angiotensin 1-7.

AngI: angiotensin I.

AngII: angiotensin II.

AP-1: apoprotein-1.

ARBs: angiotensin receptor blockers.

AT_1: angiotensin receptor type I. ,

Bcl2: B-cell lymphoma 2.

bFGF: basic fibroblast growth factor.

BiNGO: Biological Networks Gene Ontology tool.

BK: bradykinin.

BMP-2: bone morphogenetic protein 2.

BSA: Bovine serum albumin.

CHO: Chinese Hamster Ovary.

CK-2: casein kinase-2.

CMR: cardiac magnetic resonance. ,

Co-Smads: common-partner Smads.

COX-2: cyclooxygenase-2.

CRD: carbohydrate recognition domain.

CTGF: connective tissue growth factor.

DMSO: dimethyl sulfoxide.

ECG: electrocardiogram.

ECM: extracellular matrix accumulation.

ECP: Effusive Constrictive Pericarditis.

ELISA: Enzyme Linked Immunosorbent Assay.

EMT: epithelial-mesenchymal transition.

EndMT: endothelial-to-mesenchymal transition. ,

ESI: electrospray ionisation.

ET-1: endothelin-1.

FA: formic acid.

FASP: Filter aided sample preparation.

FCS: foetal calf serum.

FDR: false discovery rate.

FGF: fibroblast growth factor.

FT-MS: Fourier transform ion cyclotron.

Gal-3: galectin-3.

GnRH: Gonadotropin Releasing Hormone.

GO: Gene Ontology.

HIV: Human Immunodeficiency Virus.

HL: Histidyl-Leucine.

IFN-γ: interferon-gamma.

IL: Interleukin.

ILK: integrin-linked kinase.

IMPI: Investigation of the Management of Pericarditis.

I-Smads: inhibitory Smads.

iTRAQ: Isobaric Tags for Relative and Absolute Quantitation.

JNK: c-Jun N-terminal kinases.

KKS: Kallikrein-Kinin System.

KLB: β-klotho protein.

LAP: Latency Associated Protein.

LC-MS/MS: liquid chromatography tandem MS.

LFQ: label free quantification.

LTBP: Latent TGF-β Binding Proteins.

M.Tb: Mycobacterium tuberculosis.

m/z: mass-to-charge ratio.

MALDI: matrix assisted laser desorption ionisation.

MAP4K4: mitogen-activated protein kinase kinase kinase kinase 4.

MAPKs: mitogen-activated protein kinases.

MI: myocardial infarction.

mins: minutes.

MKK7: Map kinase kinase 7.

MMP: matrix metalloprotease. ,

MMPs: matrix metalloproteases.

MS: mass spectrometry.

MWCO: molecular weight cut off.

NADPH: nicotinamide adenine dinucleotide phosphate.

PAGE: polyacrylamide gel electrophoresis.

PDGF: platelet derived growth factor.

PEP: posterior error probability.

PICs: Pericardial interstitial cells.

QE: Q-Exactive.

RAAS: Renin-Angiotensin-Aldosterone System.

R-Smads: receptor-regulated Smads.

SDS: sodium dodecyl sulphate.

SEM: standard of the mean.

SHP-2: Src homology 2-containing protein tyrosine phosphatase-2.

SILAC: Stable Isotope Labelling by/with Amino acids in Cell culture.

Smad: small mother against decapentaplegic.

Smurfs: Smad ubiquitination regulatory factors.

SPARC: secreted protein acidic and rich in cysteine. ,

STRING: search tool for the retrieval of interacting genes/proteins.

TB: Tuberculosis.

TB-: TB negative.

TB+: TB positive.

TGF-β: transforming growth factor-β.

Th-1: T helper-1.

TIC: total ion counts.

TNF-α: tumour necrosis factor-α.

TOF: time-of-flight.

Tβ4: thymosin β4.

uIFNγ: unstimulated IFN-γ.

VEGF: vascular endothelial growth factor.

WHO: World Health Organisation.

ZFHL: Z-Phenylalanine-L-histidyl-L-leucine.

Table of Contents

List of Figures

List of Tables

I. Introduction

Constrictive pericarditis is a common, and potentially life-threatening, complication of tuberculous pericarditis (Mayosi et al., 2005). Tuberculosis (TB), caused by the pathogen Mycobacterium tuberculosis (*M.tb*) is still widely prevalent in the developing world, where socio-economic conditions are poor and access to healthcare is scarce. Compounded by the Human Immunodeficiency Virus (HIV) pandemic, the incidence of TB and its manifestation in the heart such as TB pericarditis is high and contributes to the burden of cardiovascular disease in South Africa (Ntsekhe and Mayosi, 2012). The pathophysiological mechanisms leading to constriction following infection by the bacterium are poorly understood. A proof of concept study by Ntsekhe *et al.* revealed the presence of the antifibrotic N-acetyl-seryl-aspartyl-lysyl-proline (Ac-SDKP), a physiological peptide cleaved by angiotensin-1 converting enzyme (ACE), in normal and tuberculous pericardial fluid. The levels of Ac-SDKP were significantly lower in TB pericardial fluid suggesting a potential disruption of the ACE/Ac-SDKP balance in TB pericarditis which could potentially contribute to the onset and/or progression of fibrosis (Ntsekhe et al., 2012).

ACE is predominantly known for its role in the Renin-Angiotensin-Aldosterone System (RAAS) and the Kallikrein-Kinin System (KKS), where it is involved in blood pressure and fluid homeostasis. The centrality of ACE in the RAAS has led to the development of ACE inhibitors (ACEi), which are widely used in the treatment of hypertension and cardiovascular disease. However, it has become increasingly apparent that the physiological functions of ACE extend well beyond blood pressure regulation, reflecting the diversity of substrates of the enzyme. Among many peptides, ACE cleaves the amyloid-β protein, (the deposition and accumulation of which in the brain, is associated with Alzheimer's disease), Gonadotropin Releasing Hormone (GnRH) and the aforementioned Ac-SDKP (Skidgel and Erdös, 1985)(Hemming and Selkoe, 2005). The role of ACE and Ac-SDKP in the prevention and reversal of tissue and organ fibrosis, both *in vitro* and *in vivo,* has prompted interest in the protective benefits of ACEi in fibrotic disease (Brilla et al., 2000) (Gross et al., 2004) (Kumar and Yin, 2018).

This chapter provides insights into the molecular mediators of the fibrotic progression to constrictive pericarditis from various studies. It also details the ACE/Ac-SDKP axis of fibrosis and the signalling mechanisms involved in the antifibrotic action of Ac-SDKP as well as the rationale for and the research questions of the current study.

1.1. The pericardium and its response to pericardial insult/injury

1.1.1. The normal pericardium

The pericardium is a double layered flask-like sac which encloses the heart through its attachments to the great vessels, namely the vena cava, aorta, and pulmonary artery and vein. Whilst the pericardium is not essential for normal cardiac function, it has multiple functions. These include, but are not restricted to, lubricating the heart surface for reduced friction upon motion, anchoring the heart in its correct anatomic position, shielding the heart from surrounding structures to prevent adhesion formation and the spread of inflammation or neoplasia, and restricting any excessive dilatation of the cardiac chamber. The pericardium has an independent blood supply from the internal mammary arteries and is innervated by the phrenic nerve (Holt, 1970)(Spodick, 1992)(Shabetai et al., 1979).

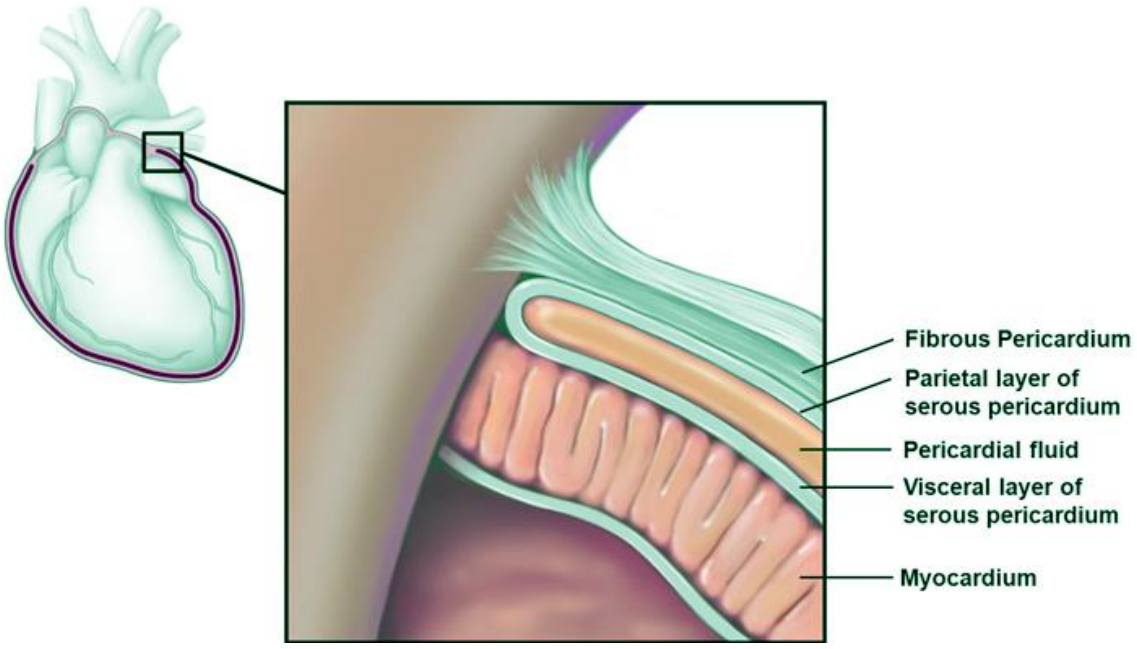

Figure 1-1: An illustration of the different layers of the pericardium.
Adapted from: http://www.clevelandclinicmeded.com/medicalpubs/diseasemanagement/cardiology/pericardial-disease/

The pericardium is lined by an outer fibrous layer of connective tissue rich in elastic fibres and collagenous fibres (Figure 1-1). This fibrosa is supplied by a network of blood and lymphatic vessels and it contains macrophages and fibroblasts. The inner serous pericardium is composed of a single layer of flat, irregular, ciliated mesothelial cells resting on a thin basement membrane and separated from the fibrous layer by a thin sub-mesothelial space. The serosa

comprises a visceral layer and a parietal layer coating the heart and the fibrous pericardium respectively (Ishihara et al., 1980)(Mutsaers, 2002). These two layers of the pericardium are 1 to 2 mm thick and give rise to a cavity which contains on average 10 to 35 ml of pericardial fluid, under normal physiological conditions (Little and Freeman, 2006). Pericardial fluid is formed from ultrafiltration of plasma and comprises largely globular proteins, phospholipids and surfactant-like prostaglandins (Spodick, 1992).

1.1.2. Pericarditis

The pathophysiological response of the pericardium to injury results in the clinical syndrome of pericarditis. Pericarditis refers to the inflammation of the pericardium and it is a common disorder (Imazio et al., 2015). Clinically, pericarditis often presents with prolonged pleuritic chest pain, which radiates to the neck, back and left arm. A pericardial friction rub is a pathognomonic sign of acute pericarditis and is detected in 60% to 85% of cases. Abnormal electrocardiogram (ECG) findings are common with a classical initial profile of ST-segment elevations, sometimes accompanied by PQ or PR segment depression. The progression of ECG changes has been described to happen in stages; from ST elevations in stage 1 and their return to the isoelectric position in stage 2, negative T waves in stage 3 and a restoration to the baseline ECG in stage 4 (Sagristà Sauleda et al., 2005)(Spodick, 2003).

The accumulation of pericardial fluid rich in inflammatory cells and fibrin in the pericardium following pericarditis can compromise cardiac function by compressing the underlying myocardium and causing cardiac tamponade. Chronic inflammation of the pericardium can result in thickening, adhesion, fibrosis calcification of the pericardium, obliteration of the pericardial space and constrictive pericarditis (Singhal et al., 2016). Both cardiac tamponade with and without hemodynamic instability in the short term, and constrictive pericarditis with and without effusion in the long term are major complications of pericarditis (Little and Freeman, 2006).

1.1.3. Aetiology of pericarditis

Pericarditis may arise from a range of aetiologies, both infectious and non-infectious (summarised in Table 1-1)(Maisch et al., 2004). Pericarditis can present clinically as acute dry pericarditis (non-effusive), effusive pericarditis, effusive constrictive pericarditis (ECP) and non-effusive constrictive pericarditis (Imazio et al., 2015). A pericardial effusion is said to be present when the amount of fluid exceeds the normal 10 to 35ml in the pericardial space (Spodick, 2003).

Table 1-1: A summary of the common aetiologies of pericarditis

Infectious	**- Viral:** Enteroviruses (Coxsackie viruses, echoviruses); herpes viruses (Epstein-Barr virus, cytomegalovirus, human herpes virus 6) and adenoviruses **- Bacterial:** *M.tb*, Coxiella burnetii and Borrelia burgdorferi **- Fungal:** Histoplasma, Aspergillus, Blastomyces, and Candida species **- Parasitic:** Echinococcus and Toxoplasma species
Autoimmune and auto-inflammatory	**- Systemic autoimmune diseases:** systemic lupus erythematosus, rheumatoid arthritis and systemic sclerosis - **Type 2 auto-immune processes following infection/surgery:** rheumatic fever, post-cardiotomy syndrome, post-myocardial infarction syndrome, epistenocardica and auto-reactive (chronic) pericarditis
Malignant	- **Secondary metastatic tumours:** lung and breast cancer, leukaemia, lymphoma, melanoma and cancers of contiguous anatomical structures such as the oesophagus
Metabolic	**- Renal insufficiency**: uraemia **- Myxoedema**
Traumatic pericarditis	- **Direct injury:** penetrating thoracic injury and oesophageal perforation - **Indirect injury:** radiation injury - **Drug-related:** procainamide, hydralazine, isoniazid, phenytoin, penicillins, and doxorubicin

Adapted from (Maisch et al., 2004) and (Imazio and Gaita, 2015).

1.1.4. Constrictive pericarditis

Constrictive pericarditis is a clinical syndrome, characterised by a thickened, stiff and non-compliant pericardium, which restricts cardiac filling (Goldstein, 2004). Constrictive pericarditis arises as a result of severe acute inflammation or recurrent inflammatory events over a highly variable time course from the period of injury (Syed et al., 2014)(D'Elia et al., 2019). However, the risk factors for the progression to constriction are poorly understood. Table 1-2 summarises some of the potential pathophysiological mechanisms of constriction in pericardial diseases which commonly progress to constriction.

The incidence of constrictive pericarditis following the inflammatory process depends on the aetiology of the pericarditis. Whilst idiopathic and viral pericarditis have a low incidence of constrictive complications, tuberculous and purulent pericarditis result in a large proportion of pericardial constriction (Imazio et al., 2015).

The most apparent pathological features of constrictive pericarditis are the thickening and fibrosis of the thin and elastic parietal and visceral pericardial linings. The pericardium commonly bears areas of inflammation of the serosa, scarring, and fibro-calcification (Goldstein, 2004). This leads to a classical haemodynamic profile arising from altered pericardial compliance and impaired ventricular diastolic function and ventricular interdependence. Atrial filling pressures increase whilst cardiac output decreases, eventually leading to diastolic heart failure (Myers and Spodick, 1999)(Shabetai et al., 1970). This haemodynamic pattern is reflected in elevated waveforms in the jugular venous pulse and right atrial pressures, accompanied by prominent A waves. A distinctive RV waveform shape, referred to as a "dip and plateau" or "square root" pattern, indicates the resistance to ventricular filling (Goldstein, 2004).

Table 1-2: Pathophysiological manifestations in common causes of constrictive pericarditis.
(Excluding TB pericarditis, discussed separately)

Manifestations and potential underlying causes of constrictive pericarditis		References
Uraemic pericarditis	Serous/haemorrhagic effusions typically evolve into a fibrinous state with irregular, scattered adhesions in a "*bread and butter*" pattern but can also progress to densely adherent pericarditis and gross pericardial thickening. Pericarditis is more frequent in cases of severe uraemia, but there is no correlation between blood urea and creatinine levels and the degree of constriction.	(Kumar and Lesch, 1980) (Reyman, 1969) (de Gouveia et al., 2016) (Lindsay et al., 1970) (Bailey et al., 1968)
Radiation pericarditis	Radiation toxicity can cause micro-vascular damage and episodic pericardial ischemia, leading to permeable neovascularization and fibrous deposition. There is also evidence of vascular and lymphatic fibrosis. The degree of inflammation and thickening corresponds to the x-ray exposure, suggesting a cellular injury and necrosis induced inflammatory response.	(Botti et al., 1968) (Morton et al., 1973) (Taunk et al., 2015)
Systemic sclerosis	Pericardial manifestations include effusions, fibrous pericarditis, pericardial adhesions or constrictive pericarditis. However, the pathogenesis is believed to differ from the traditional inflammatory pathways as evidenced by a 'non-inflammatory' profile of the pericardial fluid but may instead be due to the release of fibroblast growth factor (FGF) and histamine by mast cells.	(Lambova, 2014) (Byers et al., 1997)
Episteno-cardica	Vascular injury and myocardial necrosis have been associated with increased incidence of pericarditis, suggesting an inflammatory response to injury. Fibrous deposits and adhesions often develop in the visceral and parietal pericardium covering the area of infarction but may also involve wider and more diffuse pericardial surfaces (Roberts, 2005.	(Roberts, 2005) (Dorfman and Aqel, 2009) (Sugiura et al., 1990)
Post cardiac surgery pericarditis	Adhesions and fibrous patches in the pericardium post-surgery can lead to constrictive pericarditis. The presence of blood in the pericardial cavity may play a role, with failure to drain bloody effusions being a risk factor for the development of fibrosis. Blood in the pericardium may result in irritation of the serosal layer and inflammation, but fibrosis can occur in its absence.	(Cohen and Greenberg, 1979) (Matsuyama et al., 2001) (Gaudino et al., 2013)
Malignant pericarditis	Effusions are common in neoplastic pericarditis and can be bloody. Malignant invasion of the heart and the deposition of fibrous tissue often lead to constriction. Sub-acute inflammation with lymphocytic accumulation and mesothelial hyperplasia has been described in primary pericardial mesothelioma.	(Thurber et al., 1962) (Smets et al., 2013) (Wilkes et al., 1995)

1.2. Tuberculous pericarditis

1.2.1. Tuberculosis in South Africa

Tuberculosis contributes an enormous global burden of disease concentrated in Asia, Africa and Latin America. An estimated 10.0 million cases of TB have been recorded in 2018 alone ("WHO | Global tuberculosis report 2019," n.d.). HIV infection not only represents a potent risk factor for TB but also results in the aggressive latent reactivation of TB and rapid progression of newly acquired or reinfection with *M.tb* (Daley et al., 1992)(Corbett et al., 2003). It is hence not surprising that in South Africa, where the incidence and prevalence of HIV is high (Figure 1-2), there is an accompanying high TB incidence (227 999 new and relapse notified cases in 2018 alone), with a disproportionately higher rate of mortality when both co-morbidities are present ("WHO | Global tuberculosis report 2019," n.d.).

1.2.2. Tuberculous pericarditis

TB pericarditis is a form of extra-pulmonary tuberculosis which affects the pericardium. Tuberculosis is a major cause of pericardial diseases in both HIV-uninfected and HIV-infected populations in Sub Saharan Africa (Noubiap et al., 2019)(Syed and Mayosi, 2007). This is in contrast to the developed world where TB pericarditis accounts for only a small proportion of cases of acute pericarditis and constrictive pericarditis (Fowler NO, 1991). Whilst TB pericardial disease accounted for 4% of admission in a Spanish case series, pericardial effusions in South Africa are predominantly caused by TB infection, ranging from 64.9 to 70% (Isiguzo et al., 2020). This is in part due to the HIV pandemic with HIV co-infection not only increasing the number of TB pericarditis cases but has also changing its clinical manifestations and therapeutic considerations (Ntsekhe and Mayosi, 2012).

Patients with TB pericarditis present predominantly with effusive pericarditis, with a smaller percentage having ECP and myopericarditis (Noubiap et al., 2019). TB pericarditis has a poor outcome bearing a mortality rate of up to 40% in those patients coinfected with HIV as compared to 17% in patients without HIV at 6 months (Mayosi et al., 2008). Given that many patients are not on ARV therapy, it is likely that the difference is attributable to the impaired response to the presence of the mycobacterium, with fewer granulomas observed in the tuberculous pericardium. Mortality results primarily from heart failure arising from constrictive disease and cardiac tamponade (Mayosi et al., 2005)(Noubiap et al., 2019).

Estimated TB incidence rates, 2018

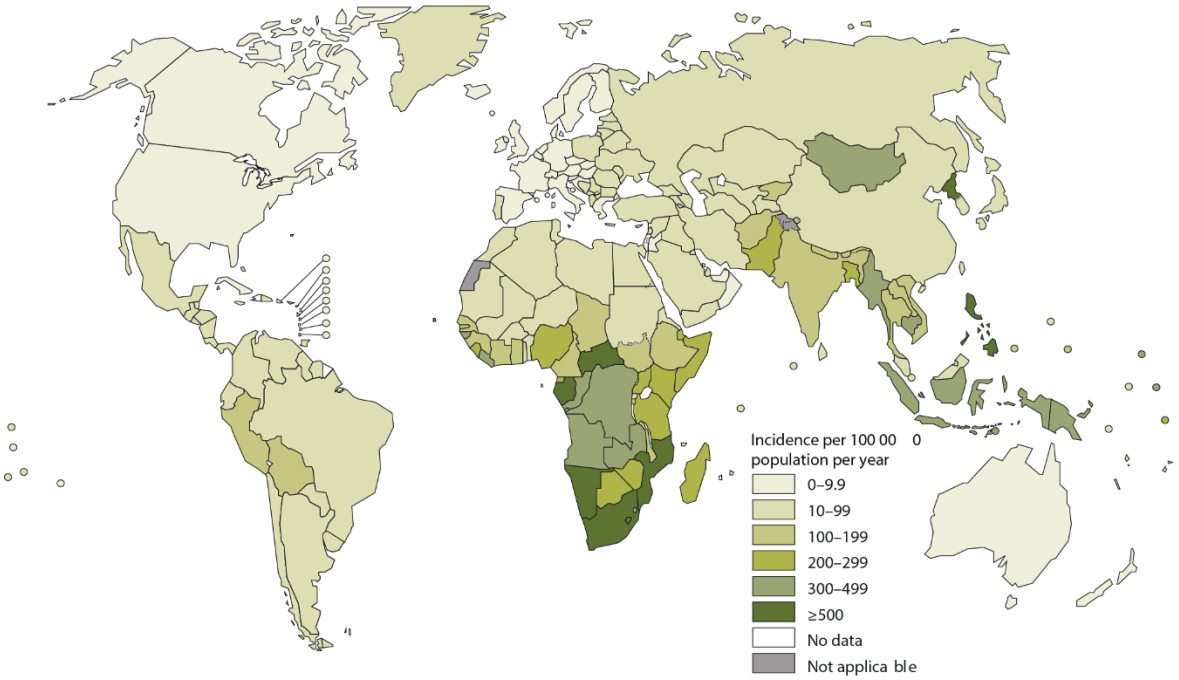

Estimates of the case fatality ratio (CFR), including HIV-negative and HIV-positive people, 2018

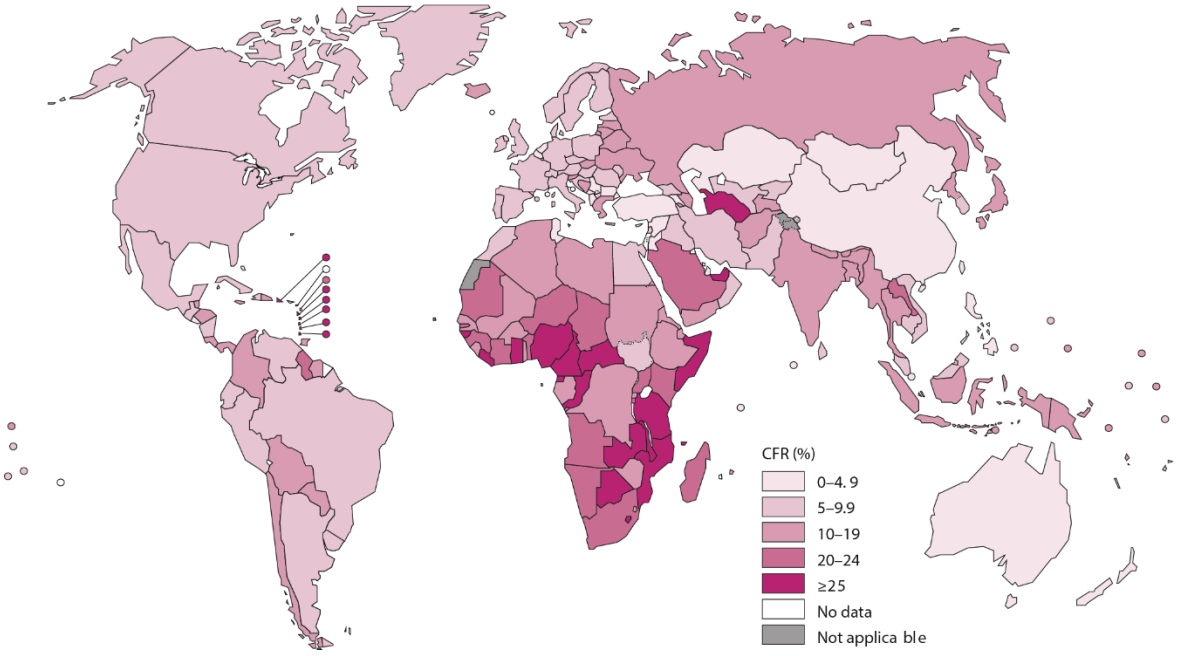

Figure 1-2: Worldwide TB incidence and fatalities adapted from the WHO Global Tuberculosis Report 2018. As depicted in the map, South Africa has one of the highest incidence rates and case fatality ratios for Tuberculosis worldwide.
Available at: https://www.who.int/tb/publications/global_report/en/

1.2.3. Pathophysiology of TB pericarditis

The spread of *M.tb* to the pericardium occurs either through retrograde lymphatic spread or through haematogenous spread from primary sites of infection (Mayosi et al., 2005) (Myers and Spodick, 1999). Among both HIV-infected and HIV-uninfected patients, high *M.tb* bacillary loads have been identified suggesting that the condition is not paucibacillary, as previously believed (Isiguzo et al., 2020).

Infection of the pericardium with the bacilli elicits an immune response, stimulating lymphocytes to release cytokines which activate macrophages and influence granuloma formation. Marked elevations of Interleukin-10 (IL-10) and interferon-gamma (IFN-γ) accompanied by low levels of bioactive transforming growth factor-β (TGF-β) levels in tuberculous pericardial fluid suggest a T helper-1 (Th-1) mediated delayed type hypersensitivity response to the pathogen (Ntsekhe et al., 2013). Similarly, Reuter *et al*, measured significantly increased IFN-γ levels in the pericardial fluid and observed large numbers of mesothelial cells in tuberculous pericardial aspirates (Reuter et al., 2006). A role for complement fixing antimyolemmal antibodies has also been suggested in the development of exudative tuberculous pericarditis through cardiocyte cytolysis (Maisch et al., 1982). The inflammatory process in TB pericarditis follows a sequence of pathological events. An early fibrinous exudate is formed with leucocytosis, accompanied by early granuloma formation, followed by a sero-sanguineous effusion with a predominantly lymphocytic exudate. The effusion gradually recedes whilst the granulomatous architecture is organised to restrict mycobacterial spread. Fibrin, collagen and extracellular matrix deposition lead to pericardial thickening and fibrosis (Mayosi et al., 2005).

1.2.4. Diagnosis and treatment of TB pericarditis

A definitive diagnosis of tuberculous pericarditis is made by isolating the acid-fast tubercle bacilli from pericardial fluid or by demonstrating its presence through pericardial histology or culture. However, isolating the organism is often challenging. A diagnosis can also be made with evidence of other forms of TB in a patient, accompanied by otherwise unexplained lymphocytic predominant exudative pericarditis and where other infectious agents have been excluded (Reuter et al., 2006) (Mayosi et al., 2005). Elevated pericardial adenosine deaminase (ADA) activity, lysozyme levels and un-stimulated IFN-γ (uIFN-γ) have also been associated with

TB pericarditis, and considered of significant value in the diagnosis of TB pericarditis (Reuter et al., 2006) (Pandie et al., 2014) (Kim et al., 2018)(Seo et al., 2020).

The poor definition of end points makes TB pericarditis a therapeutic challenge (Sharma and Mohan, 2019). The immediate goal of treatment involves symptomatic relief for the patient whereas the long term management plan centres on the prevention of constrictive pericarditis (Mayosi et al., 2005). The standard of care for TB pericarditis is similar to the management of TB and involves a minimum of six months of therapy with two months of intensive drug phase using four anti-tuberculous drugs namely rifampicin, isoniazid, ethambutol, and pyrazinamide followed by at least four months of dual drug therapy (Isiguzo et al., 2020).

1.2.5. Tuberculous constrictive pericarditis

Constrictive pericarditis represents the end stage of TB pericarditis pathology. It is characterised by thickening, fibrotic scarring and/or calcification of the visceral and parietal pericardial pleura, which restricts diastolic cardiac filling, hence leading to cardiac failure (Mayosi et al., 2005). Up to 26% of patients with TB pericarditis develop constrictive pericarditis if untreated; effective antituberculous medication including rifampicin-based therapy merely reduces this progression rate to around 17% (Trautner and Darouiche, 2001)(Mayosi et al., 2008)(Noubiap et al., 2019)(D'Elia et al., 2019). The evolution of TB pericarditis to constriction with or without an effusion is the fastest of all the different forms of pericarditis, which explains the poor short term prognosis of the disease (Mayosi et al., 2008). This may be due to the poor penetration and rapid clearance of rifampicin into the pericardial space. A decreased penetration of the drug has been measured in the pericardium over time, supporting previous observations of the rapid progression to thickening and fibrosis of the pericardium in TB pericarditis (Shenje et al., 2015).

Recently, the debate surrounding the use of corticosteroids in the management of the condition was addressed by the Investigation of the Management of Pericarditis (IMPI) trial which revealed a significantly reduced rate of constrictive pericarditis in both HIV negative and positive patients on prednisone (Mayosi et al., 2014). Corticosteroids also reduce the need for repeat pericardiocentesis and deaths from pericarditis in HIV negative patients. However in the same trial, corticosteroids increased the risk of opportunistic malignancies and a subsequent Cochrane review found that their efficacy in the HIV positive population not

conclusive (Wiysonge et al., 2017). The value of routine surgical drainage in the effusive stage of pericarditis as a preventative measure remain unclear (Schwefer et al., 2009)

The treatment of choice for those with established constrictive pericarditis is a pericardiectomy with complete decortication of the pericardium (Depboylu et al., 2017). To date, there are no effective predictors for constrictive pericarditis, and a lack of prophylactic therapy. Cardiac tamponade in the early clinical stage of TB pericarditis is the best predictive factor of subsequent constrictive pericarditis (Schwefer et al., 2009). High ADA levels are also prognostic for the development of constrictive pericarditis (Burgess et al., 2002). Importantly, the degree of fibrosis of the pericardium at the onset of treatment may constitute the most important determinant of whether or not constriction develops (Suwan and Potjalongsilp, 1995). Further, the rates of constrictive pericarditis are considerably lower in patients with effective pericardiocentesis, suggesting that the removal of pro-inflammatory and profibrotic cytokines from the pericardium may thereby reduce the fibrotic process (Naicker and Ntsekhe, 2020).

1.3. Fibrosis in constrictive TB pericarditis

Fibrosis refers to the hyper-proliferation, hardening and tissue scarring which arises as a result of collagen and extracellular matrix accumulation (ECM). Fibrosis and fibrotic disorders arise in a number of organ systems as a result of interstitial fibroblast proliferation from marrow stromal cell progenitors or epithelial-mesenchymal transition (EMT) (Iwano et al., 2002). In contrast to the controlled fibroblast to myofibroblast transformation which promotes wound contraction and healing in acute inflammation, fibrosis is usually a consequence of chronic inflammation. An increased turnover of the net collagen and ECM levels arises in chronic inflammation leads to the gradual formation of fibrotic scar tissue and subsequent loss of organ function, typical of organ fibrosis (Wynn, 2007) (Wynn, 2008).

1.3.1. Aetiology of fibrosis

Fibrosis represents the pathological end stage of various inflammatory diseases; Table 1-3 summarises the most common organs/tissues affected by fibrosis and lists some of the associated diseases.

Table 1-3: Major organ systems affected by fibrogenesis.

Liver	Viral hepatitis, alcohol-abuse, related pathologies, schistosomiasis, hepatocellular cancer
Lung	Idiopathic lung disease, pulmonary hypertension, right sided heart failure, sarcoidosis, silicosis, infections, rheumatoid arthritis, systemic sclerosis
Kidney	Diabetes, hypertension, anaemia
Heart/ vascular	Myocardial infarction, hypertension, atherosclerosis, restenosis, infections, arrhythmias
Eye	Macular degeneration, retinal and vitreal retinopathy, strabismus
Skin	Systemic sclerosis, scleroderma, burns, keloids and hypertrophic scars
Pancreas	Diabetes, malabsorption, cancer

Adapted from (Wynn, 2008) and (Rockey et al., 2015).

1.3.2. Molecular mechanisms of fibrosis

Molecular mechanisms of fibrogenesis involve unique contributing factors for different pathologies; however, certain key processes and pathways are common to most fibrotic events. The fibrotic cascade of events is triggered upon insult to epithelial or endothelial cells which release inflammatory mediators resulting in the activation of the coagulation cascade. The formation of blood clots gives rise to a provisional ECM to which platelets are exposed (Diegelmann, 2004). They respond by aggregating and propagating the blood clot before releasing a plethora of effector proteins through degranulation and lysis which induce vasodilation and enhance blood vessel permeability. Simultaneously, the epithelial or endothelial cells, aided by stimulated myofibroblasts, produce matrix metalloproteases (MMPs) which degrade the basement membrane. The combination of these processes results in the recruitment of inflammatory cells to the site of injury (Kalluri and Neilson, 2003). The initial inflammatory response is characterised by the release of various pro-inflammatory cytokines, including tumour necrosis factor-α (TNF-α)(Wynn, 2007)(Wynn, 2008). TNF-α is a pleiotropic cytokine with a central role in the activation and recruitment of immune cells and the regulation of pro-inflammatory cytokine production (Parameswaran and Patial, 2010). Activated leukocytes then proceed to release pro-fibrotic cytokines such as IL-13 and TGF-β which drive EMT and ECM component production. These include hyaluronic acid, fibronectin, proteoglycans, and interstitial collagens which accumulate to form the fibrotic scar (Frantz et al., 2010).

1.3.3. TGF-β: a master regulator of fibrosis

TGF-β belongs to the TGF-β super-family of secreted polypeptide factors comprising BMPs, activins, inhibins, and other growth and differentiation related factors. The TGF-β family regulates a range of cellular responses in various cell types, including growth, differentiation, migration and apoptosis (Miyazono, 2000).

TGF-β responses are not only diverse, but highly complex. The cytokine mediates different effects in different physiological contexts; it also has antithetic effects in cells of different developmental lineages (Lai et al., 2005)(Moustakas et al., 2002). For example, TGF-β stimulates ECM deposition, cardiomyocyte hypertrophy and fibroblast proliferation in the heart, leading to overall cardiac hypertrophy and dysfunction (Rosenkranz, 2004). In the blood vessel however, TGF-β inhibits leukocyte recruitment and activation, migration of vascular smooth muscle cells and prevents formation of unstable lesions; these processes exert a protective role in atherosclerosis (Grainger, 2004). The physiological role of TGF-β and its centrality in various signalling pathways is highlighted in various TGF-β knock-out mice models where mice present with life-threatening systemic inflammation, rapid wasting and premature death (Kulkarni et al., 1993)(Shull et al., 1992). Whilst some TGF-β antagonists effectively reduced rates of metastasis in mice without significant side effects, the mouse immune response to a simultaneous infection or environmental stressor remains to be investigated (Yang et al., 2002)(Akhurst, 2002).

1.3.3.1. Synthesis of the TGF- β complex

TGF-β occurs as three isoforms (β1, β2, and β3) transcribed from three separate genes and encoded as large precursor proteins, linked to a unique Latency Associated Protein (LAP), of 390–412 amino acids in size (Massague et al., 1994). The precursor proteins are processed in various stages in the Golgi apparatus and the endoplasmic reticulum prior to being secreted (Figure 1-3). Briefly, two TGF-β precursor proteins dimerise via disulphide bridge formation. Furin then cleaves the TGF-β dimer between amino acids 278 and 279 to yield the N-terminal LAP protein, and the 25KDa C-terminal mature TGF-β dimer. These two portions however remain connected by non-covalent bonds, termed the small latent TGF-β complex (Tran, 2012) (Hayashi and Sakai, 2012). The LAP is necessary for proper TGF-β homo-dimer folding and its secretion from cells. Various Latent TGF-β Binding Proteins (LTBP) such as LTBP-1, LTBP−3 and

LTBP−4, can thereafter bind to LAP to yield a large latent TGF-β complex which further facilitates the secretion of TGF-β and its incorporation into the ECM (Massagué et al., 2000).

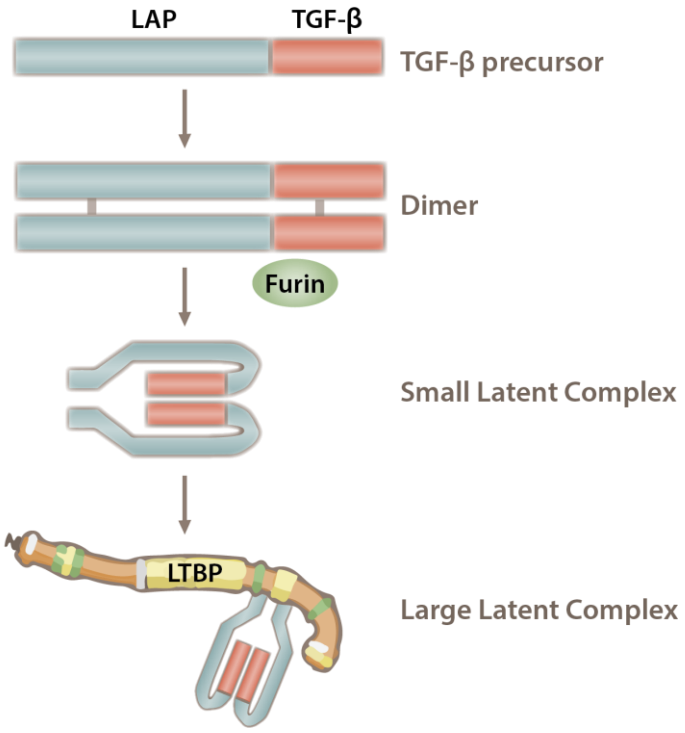

Figure 1-3: TGF-β synthesis in the cell.
Following dimerisation of the precursor, furin cleaves the Latency Associated Protein- LAP from the TGF-β homo-dimer. LAP and mature TGF-β remain associated in a non-covalent fashion in the small latent complex which can bind Latent TGF- β binding protein- LTBP to form the large latent complex.
Adapted from (Hayashi and Sakai, 2012)

1.3.3.2. TGF- β signalling

TGF-β is a key mediator of the fibrotic response and it acts via canonical (small mother against decapentaplegic (smad)-dependent) and non-canonical (non-Smad-based) signalling pathways to coordinate an ECM accumulation through increased synthesis as well as a reduced degradation of ECM components (Branton and Kopp, 1999)(Moustakas et al., 2001)(Zhang, 2009).

In the canonical TGF-β/Smad pathway, TGF-β family members activate type I and type II serine/threonine kinase receptors on the cell surface membrane (Figure 1-4)(Dijke and Hill, 2004). Ligand binding to the type II receptor results in type I receptor kinase activation through the phosphorylation of a glycine-serine rich region of the juxta-membrane domain of the type I receptor. The type I receptor propagates an intracellular signalling cascade by phosphorylating (Smad) proteins (Miyazono *et al.*, 2000). Smad proteins are grouped into

three subclasses namely the receptor-regulated Smads (R-Smads), common-partner Smads (Co-Smads) and inhibitory Smads (I-Smads). R-Smads (Smad 1, Smad 2, Smad 3, Smad 5 and Smad 8) anchored to the cell surface membrane are activated via phosphorylation by the type I receptor and recruit Smad 4 (the Co-Smad) to form heteromeric complexes. These complexes translocate to the nucleus where they recruit histone acetyl-transferases to induce transcription of their target genes. The I-Smads, Smad 6 and Smad 7, are antagonists of the R-Smads and inhibit their signalling by various mechanisms. They inhibit R-Smad binding to the type I receptor by acting as competitive inhibitors and recruit Smad ubiquitination regulatory factors (Smurfs) to activate type I receptors, promoting their ubiquitination and degradation (Miyazono, 2000)(Dijke and Hill, 2004)(Lai et al., 2005).

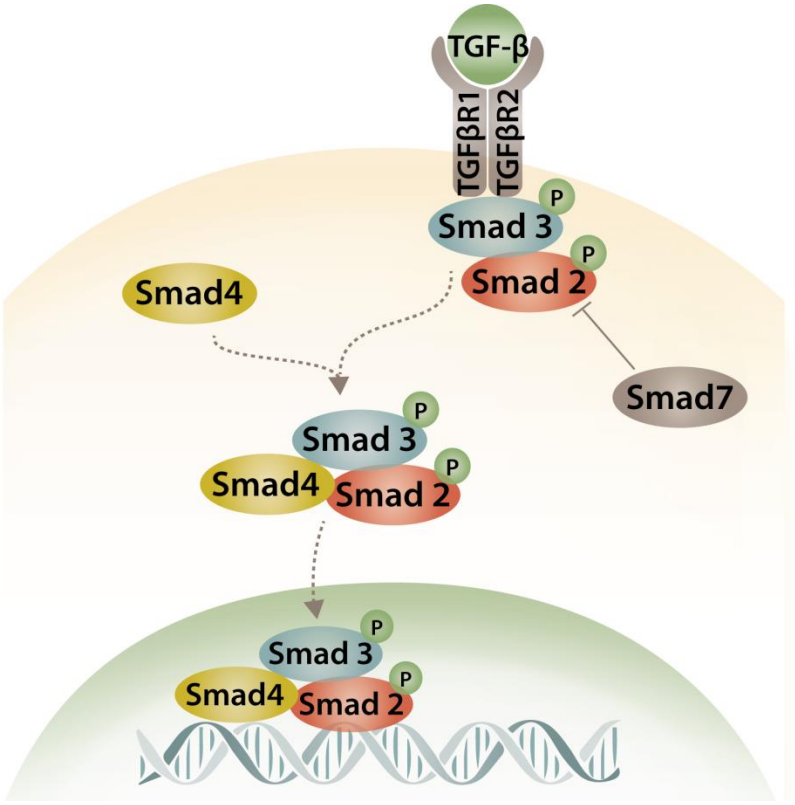

Figure 1-4: Illustration of TGF-β/Smad signalling in fibrosis.

TGF- β binding to its receptor induces dimerisation of the Type I and Type II receptors which get activated to induce on the cytosolic side, R-Smad (Smad2/3) phosphorylation and activation. The R-Smads associate with Smad-4 to form a heteromeric complex which translocates to the nucleus to induce the transcription of ECM components.

1.3.4. Molecular mechanisms of constrictive pericarditis

Molecular mechanisms of pericardial constriction remain to be fully elucidated but are likely to follow a classical pattern of pericardial inflammation mediated by various cytokines (Table 1-4), including TNF-α, followed by abnormal healing with an exaggerated TGF-β mediated pro-fibrotic response leading to pericardial fibrosis. Both experimental mice models of acute pericarditis and pericardial fluid from patients with tuberculous ECP (associated with a high incidence of pericarditis), demonstrate a mixed picture of both pro-inflammatory IFN-γ, and anti-inflammatory cytokines IL-8, and IL-10 (Fairweather et al., 2004), but their exact roles are as yet unclear.

Patterns of inflammation and fibrosis in the pericardium suggest that both myocardial and pericardial cells play a role in the pathogenesis of pericarditis and constriction. A change in mesothelial cell morphology has been consistently described in various forms of pericarditis. Further, a loss of the mesothelial cell architecture, as well as mesothelial desquamation often accompanies constrictive pericarditis. The transition from a 'flat' to a 'cuboidal' shape has been associated with an 'activation' of mesothelial cells and a distinct enzymatic profile of the cells with functions being geared towards oxidative stress and inflammatory responses (Vogiatzidis et al., 2015)(Whitaker et al., 1982). Activated mesothelial cells secrete chemokines and adhesion molecules to aid in the recruitment and migration of leukocytes across the mesothelium. They are also known to mediate the inflammatory process and produce ECM components (Mutsaers et al., 2015). Further, mesothelial cells can undergo phenotypic changes similar to EMT transition to adopt fibroblast-like morphology and function in the healing serosa (Yáñez-Mó et al., 2003)(Mutsaers, 2002). The active regulation of both pro- and anti-inflammatory mediators by mesothelial cells suggests a key role for the cells in maintaining pericardial homeostasis and in the pathogenesis of pericardial fibrosis. Pericardial interstitial cells (PICs) have also been implicated in the production of ECM and calcification in the pericardium (Liu et al., 2012). PICs have a comparable immune phenotype to mesenchymal stem cells. PICs cultured from fibro-calcific human samples could be differentiated into myofibroblasts and osteoblasts which are central to the development of fibrosis and the production of extra-osseous calcification. TGF-β and bone morphogenetic protein 2 (BMP-2) are associated with the trans-differentiation process.

Table 1-4: Summary of inflammatory and fibrotic cytokines and growth factors (detected in pericardial fluid) likely to modulate the pathophysiological processes leading to chronic fibrosis in the pericardium.

Inflammatory/ Fibrotic Mediator	Major roles in Inflammation and Fibrosis	References
TGF- β	Anti-inflammatory mediator ECM deposition and remodelling	(Yarnold and Vozenin Brotons, 2010) (Ristić et al., 2013) (Ntsekhe et al., 2013) (Afanasyeva et al., 2004)
CTGF	Myofibroblast activation ECM deposition and remodelling	(Yarnold and Vozenin Brotons, 2010)
TNF-α	Inducer and regulator of inflammation Macrophage and Natural Killer cell recruitment	(Ristić et al., 2013) (Pankuweit et al., 2000)
IL-6	Late role in inflammatory cascade Adaptive Immune system activation	(Ristić et al., 2013) (Pankuweit et al., 2000)
IL-8	Later role in inflammatory cascade Neutrophil cell recruitment	(Ristić et al., 2013) (Pankuweit et al., 2000)
IL-10	Inflammatory mediator	(Ntsekhe et al., 2013)
IFN-γ	Immune response modulation Macrophage and NK cell activation Antifibrotic	(Ristić et al., 2013) (Pankuweit et al., 2000) (Karatolios et al., 2012) (Ntsekhe et al., 2013) (Kulkarni et al., 1995)
VEGF	Angiogenesis and fibrosis promotion Fibrosis resolution	(Karatolios et al., 2012)
bFGF	ECM deposition	(Karatolios et al., 2012) (Byers et al., 1997)
Ac-SDKP	Major role in the inhibition of fibrosis	(Ntsekhe et al., 2012)
Gal-3	Myofibroblast activation ECM deposition	(Ntsekhe et al., 2012)

Increased pericardial fluid and serum levels of TGF-β have been described in various forms of pericarditis and have been associated with increased collagen synthesis. Thus, TGF-β might play a key role in the development of fibrosis in the pericardium. Interestingly, Ristic *et al.* did not detect any increase in TGF-β levels in viral pericardial fluid and this could account for the low proportion of constrictive pericarditis arising in this group (Ristić et al., 2013).

An increase in connective tissue growth factor (CTGF) was associated with ECM deposition and pericardial remodelling (Yarnold and Vozenin Brotons, 2010). This is not surprising as CTGF expression is known to be induced by TGF-β in cardiac fibroblasts and cardiac myocytes, whereby it contributes to the expression of fibronectin, collagen type I and plasminogen

activator inhibitor-1 (Chen et al., 2000). Interestingly, a decrease in vascular endothelial growth factor (VEGF) was observed in viral pericarditis which rarely results in a constrictive pericarditis. Whilst VEGF mediated angiogenesis is known to be important for the promotion of fibrosis, it also plays a role in fibrosis resolution (Yang et al., 2014). Indeed, an angio-fibrotic switch of VEGF and CTGF has been described in proliferative diabetic retinopathy, whereby the VEGF to CTGF ratio closely dictates the progression to fibrosis (Geest et al., 2012) (Kuiper et al., 2008). CTGF has also been shown to bind to VEGF and to inhibit its angiogenic functions (Inoki et al., 2002). It is possible that such CTGF-VEGF interplay is also involved in the progression to fibrosis in the pericardium. This would further explain the high VEGF levels coinciding with low levels of basic fibroblast growth factor (bFGF) in viral pericardial fluid.

Galectin-3 (Gal-3) levels were found to be mildly but non-significantly up-regulated in TB pericardial fluid (Ntsekhe et al., 2012). Gal-3, also referred to as MAC-2 antigen belongs to a large family of β-galactoside-binding adhesion and growth-regulation lectins. Gal-3 expressed by inflammatory cells is a major player in cardiac inflammation and fibrosis. Elevated Gal-3 levels induce the release of various fibrotic mediators, including, IL-1 and IL-2 to promote cardiac fibroblast proliferation, collagen deposition (De Boer et al., 2010) (Henderson et al., 2006).

Finally, Ac-SDKP, which is known to decrease TGF-β signalling (Castoldi et al., 2009) (Kanasaki et al., 2003) (Pokharel et al., 2004) (Lin et al., 2008), may play a role in the progression of pericardial fibrosis. As previously mentioned, patients with TB pericarditis, have been found to have diminished Ac-SDKP levels compared to participants without pericarditis (Ntsekhe et al., 2012). Lowered Ac-SDKP levels could arise from an increase in ACE activity, which is known to degrade Ac-SDKP (Azizi et al., 2001) (Inoue et al., 2011).

On a gene expression level, a range of changes in various forms non-coding RNAs, including microRNAs (miRNAs), long non-coding RNAs (lncRNAs) and circular RNAs (circRNAs) are likely to influence signalling pathways involved in the fibrotic process. A recent study on differential gene expression in patients with constrictive pericarditis has identified a plethora of differentially expressed mRNAs likely to contribute to the pathological processes involved in constriction (Chen et al., 2020). These RNA functions were mapped predominantly to inflammation processes, including apoptotic process, regulation of immune system process, cell activation and adhesion, chemokine signalling and leukocyte activation. Importantly,

deregulation of the known inflammatory STAT1 and RUNX3 transcriptional factors were also observed (Chen et al., 2020).

1.4.The Ac-SDKP/ACE axis in fibrosis

1.4.1. ACE in the RAAS and KKS

ACE is a key enzyme of the RAAS which has two components: a circulating RAAS is involved in the homeostasis of systemic perfusion and a tissue RAAS operates at the local tissue level. Whilst the functions of the circulating and tissue RAAS and their effects differ, the pathways are common for both (Xiao et al., 2004). ACE hydrolyses the metabolically inactive decapeptide angiotensin I (AngI) generating the octapeptide angiotensin II (AngII) and a histidyl-leucine (HL) dipeptide (Skeggs Jr et al., 1954)(Skeggs Jr et al., 1956). AngII is a potent vasopressor which mediates its effects via the angiotensin receptor type I (AT_1). These effects include sodium reabsorption, growth and differentiation, and aldosterone secretion (Kaschina and Unger, 2003). AngII binding to the AT_1 receptor also influences cell growth, inflammation and fibrosis besides mediating circulatory integrity (Suzuki et al., 2003).

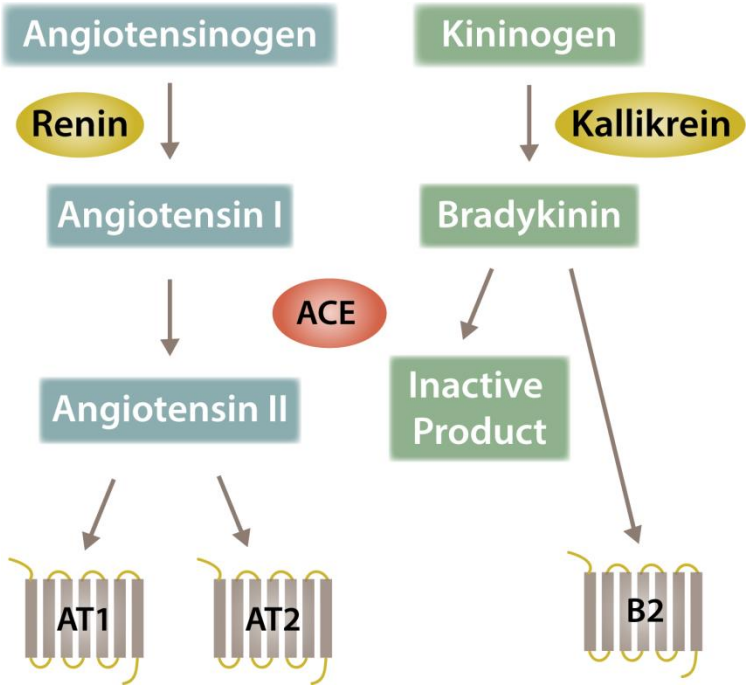

Figure 1-5: Schematic representation of the RAAS and KKS.

ACE cleaves Ang I, resulting in the formation of angiotensin II, which predominantly mediates vasoconstriction, aldosterone secretion, renal sodium reabsorption and cell growth and migration by binding the commonly expressed AT1 receptor. ACE also degrades BK preventing the vasodilation and nitric oxide release which occurs upon its binding to the B2 receptor.

Ang II can also bind the angiotensin receptor type II (AT_2) to mediate a plethora of counter-regulatory effects including immune modulation, the prevention of inflammation and fibrosis, neuroprotection and neuroregeneration, as well as antihypertensive and antiapoptotic actions (Namsolleck et al., 2014) (Steckelings et al., 2017).

ACE also hydrolyses the vasodilator bradykinin (BK) in the KKS, thus preventing its binding to the bradykinin B_2 receptor (Yang et al., 1971). Operating as a central node in the RAAS and KKS (Figure 1-5), ACE is thus critical for the physiological regulation of blood pressure, by mediating both a downstream increase in vasoconstriction (AT_1) and decrease in vasodilation (B_2).

1.4.2. Properties of ACE

ACE (EC 3.4.15.1) is a zinc dipeptidyl carboxypeptidase of the M2 gluzincin family, involved in the hydrolysis of dipeptides from the carboxyl terminus of a range of oligopeptides (Sturrock et al., 2004) (Hooper, 1994).

There are two distinct isoforms of ACE in human tissue: a somatic form (sACE) and a smaller germinal form found in the testes (tACE) (Soubrier et al., 1988) (Ehlers et al., 1989). Both sACE and tACE are transcribed through two alternate promoters from a single 21kb gene on chromosome 17, which comprises 26 exons, to give rise to the 170kDa and 110kDa protein respectively (Hubert et al., 1991) (Ehlers et al., 1989).

Approximately 90% of the sACE exists as a membrane bound form on the plasma membranes of vascular endothelial cells, microvillar brush border epithelial cells, and neuro-epithelial cells (Caldwell et al., 1976) (Ryan et al., 1976). The ACE protein is composed of a larger ectodomain which is found in the extracellular space and a shorter C-terminal intracellular cytoplasmic region (Figure 1-6). A small trans-membrane region anchors the enzyme on the cell surface (Soubrier et al., 1988). Both sACE and tACE are solubilised from their membrane form, through the proteolytic cleavage of a protease (‘sheddase’) at identical sites in the juxtamembrane or stalk region (Ehlers et al., 1996).

Figure 1-6: Schematic representation of sACE
TM: transmembrane region, CT: cytoplasmic tail region

1.4.3. ACE protein domains

Somatic ACE comprises two individual domains termed the N and C domains which share an overall 60% sequence identity and 90% identity in their catalytic active sites (Soubrier et al., 1988). The two domains are joined via a small linker region and likely occured as a result of a gene duplication event in their evolutionary history (Hubert et al., 1991). Each domain contains within its active site, a His-Glu-X-X-His motif which tetrahedrally coordinates a zinc atom (Wei et al., 1991). Both the N and C domains exhibit independent catalytic activity, but they are not catalytically equal (Wei et al., 1991). The enzymatic activity of the C domain is heavily reliant on chloride ion concentration as compared to the N domain (Wei et al., 1991). Importantly, the rates of substrate hydrolysis and the sensitivity to inhibitors differ across the two domains (Wei et al., 1992) (Jaspard et al., 1993).

1.4.4. ACE substrates

ACE cleaves a myriad of peptides or varying sizes besides Ang I and BK. As mentioned, the two domains of ACE display substrate selectivity making them preferential sites of hydrolysis for certain substrates. For instance, the cleavage of AngI is carried out predominantly by the C domain (Fuchs et al., 2008) (Wei et al., 1991) whereas the N domain is predominantly responsible for the metabolism of other biologically active peptides including amyloid beta-peptide (Aβ), Ac-SDKP and GnRH (Zou et al., 2007)(Rieger et al., 1993)(Skidgel and Erdös, 1985). Given the wide range of physiological peptides cleaved by ACE, it is no surprise that the known roles of ACE have vastly expanded beyond those of blood pressure regulation and fluid homeostasis in the RAAS to important functionalities in inflammation, haematopoiesis and immune modulation in more recent years (Bernstein et al., 2018).

1.4.5. Ac-SDKP

Ac-SDKP, previously known as goralatide or seraspenide, was first extracted from fetal calf bone marrow as an inhibitor of haematopoietic cell proliferation, specifically of the spleen colony forming unit (Frindel and Guigon, 1977). It was subsequently purified and its tetrapeptide amino acid sequence identified in 1989 (Lenfant et al., 1989). Ac-SDKP is ubiquitously found in mammalian tissues, with a higher level of expression in the spleen (Pradelles et al., 1990)(Pradelles et al., 1991).

1.4.5.1. **Biological synthesis of Ac-SDKP**

Ac-SDKP is formed from the enzymatic cleavage of its precursor thymosin β4 (Tβ4): an exogenous addition of Tβ4 to kidney homogenates *in vitro* results in an increase in the production of Ac-SDKP (Lenfant et al., 1991) (Cavasin et al., 2004). Tβ4 is a small intracellular peptide of the thymosin family, composed of 43 amino acid residues. It was first isolated from bovine thymus tissue as one of the biologically active peptides in thymosin fractions, which are involved in the regulation and differentiation of lymphocytes of thymic origin (Low et al., 1981) (Low and Goldstein, 1982). Various functions have been attributed to Tβ4 including the sequestering of intracellular actin through binding and stabilising of monomeric G-actin, cardioprotection, wound healing and angiogenesis (Mannherz and Hannappel, 2009).

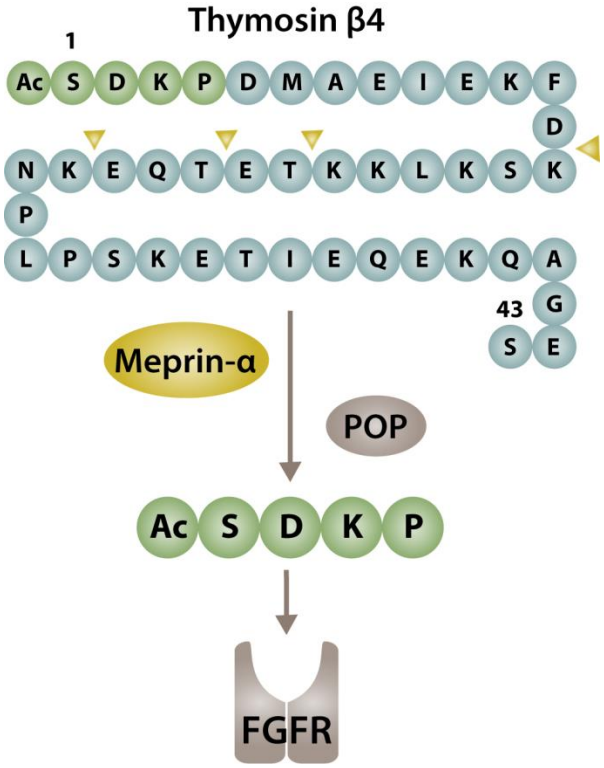

Figure 1-7: Biological synthesis of Ac-SDKP
Ac-SDKP is formed from the sequential cleavage of thymosin β4 by the enzymes meprin-α (at putative cleavage sites indicated by the yellow arrows) and POP. The tetrapeptide mediates its effects through the fibroblast growth factor receptor-1, FGFR1.

Ac-SDKP represents the N terminal sequence of Tβ4 and is generated by a two-step hydrolysis process (Figure 1-7). The first step, mediated by meprin-α, produces an NH_2-terminal intermediate peptide and the second step involves the cleavage of a Pro-Asp bond by the enzyme prolyl oligopeptidase (POP)(Kumar et al., 2016) (Crockford et al., 2010) (Cavasin et al., 2004) (Grillon et al., 1990). Long term POP inhibitor administration has been shown to significantly reduce circulating plasma levels of Ac-SDKP *in vivo* without affecting blood pressure levels (Cavasin et al., 2004)(Cavasin et al., 2007).

The precise mechanism of Ac-SDKP binding and interaction with the FGFR1 receptor has not been elucidated. However, colocalisation of Ac-SDKP with the receptor to induces its phosphorylation has been observed (Li et al., 2017). FGFR1 is a known inhibitor of fibrosis by inhibiting the TGF-β/Smad pathway. These observations have led to speculation that the FGFR-1 receptor might be the endogenous receptor or one of the endogenous receptors for Ac-SDKP (Li et al., 2017). Phosphorylation of FGFR1 on the cytoplasmic side upon binding/ interaction in the extracellular environment results in the mitogen-activated protein kinase kinase kinase kinase 4 (MAP4K4) being recruited and phosphorylated both *in vitro* and *in vivo.* Phosphorylated MAP4K4 suppresses integrin-β1, which is a potent activator of TGF-β.

An alternate mechanism of activation has been proposed by Gao et al., which involves the β-klotho protein (KLB) of the newly defined klotho protein group (R. Gao et al., 2019). There are type I single-pass trans-membrane proteins, which have a high degree of homology to family 1 β-glycosidases, involved in fibrosis regulation (Doi et al., 2011)(Satoh et al., 2012). Ac-SDKP was shown to increase KLB expression through interaction with FGFR1. KLB expression inhibits EndMT through inhibition of MEK1/2 and ERK1/2 phosphorylation (R. Gao et al., 2019).

1.4.5.2. **Cleavage of Ac-SDKP by ACE**

ACE is the predominant enzyme responsible for Ac-SDKP hydrolysis *in vivo*; an acute inhibition of ACE by the slightly N domain-selective inhibitor captopril resulted in almost total abolition of [3H]-Ac-SDKP (radiolabelled tetrapeptide) hydrolysis. Importantly, single dose administration of captopril caused an approximately 5.5-fold increase in plasma levels of Ac-SDKP in healthy human subjects (Azizi et al., 1996) (Inoue et al., 2011). Similarly, chronic ACE inhibition by ACEi, regardless of their chemical characteristics, resulted in approximately a five-fold increase in Ac-SDKP levels in both hypertensive and normotensive subjects (Azizi et al., 1997). A massive accumulation of Ac-SDKP during chronic ACEi therapy has not been observed,

however. This is due to an intermittent reactivation of ACE in between doses of ACEi as well as an increase in the glomerular filtration of Ac-SDKP by the kidney. A 2- to 5-fold increase in urinary Ac-SDKP concentration is observed in chronic ACE inhibition (Azizi et al., 1999) (Comte et al., 1997).

Ac-SDKP displays similar affinities for the N and C domains of ACE. However, in studies whereby one of the ACE domains was catalytically inactivated by a mutation of the zinc coordinating residue, the N domain was found to be 40 times more effective at cleaving Ac-SDKP as compared to the C domain. Further, a monoclonal antibody to the N domain resulted in a similar level of inhibition in both the wild type recombinant somatic ACE as compared to the ACE N active mutant of ACE (C domain inactive), suggesting that the N domain is the primary site of Ac-SDKP hydrolysis (Rousseau-Plasse et al., 1996). Abz-SDK(Dnp)P-OH, a fluorescent analogue of Ac-SDKP-OH, in which Abz and Dnp (2,4-dinitrophenyl) are the fluorescent donor-acceptor pair was hydrolysed with high specificity by the N domain of ACE at the D-K(Dnp) bond with hardly any cleavage by the C domain (Araujo et al., 2000). Hence, ACE cleaves Ac-SDKP by a dipeptidase activity, generating the C-terminal dipeptide Lys-Pro from Ac-SDKP. Hydrolysis by ACE is believed to be the first limiting step of Ac-SDKP degradation in human plasma (Rieger et al., 1993).

1.4.6. Ac-SDKP as an inhibitor of cell proliferation

Ac-SDKP was discovered with regards to its ability to inhibit haematopoietic stem cell proliferation. The protective effect of Ac-SDKP is conferred by its ability to reversibly inhibit the high proliferative activity of most primitive haematopoietic cells as well as their progenitors at nanomolar concentrations (Cashman et al., 1994) (Bonnet et al., 1993). Ac-SDKP demonstrated the ability to prevent G_0/G_1 progression into S phase in continuous cell lines *in vivo* as well as *in vitro* (Volkov et al., 1996). Ac-SDKP at physiological levels was shown to inhibit the entry of cardiac and renal cells into the S phase of the cell cycle (Iwamoto et al., 2000)(Peng et al., 2001). Importantly, Ac-SDKP improved the recovery of haematopoietic progenitor cells *in vivo* against 5-fluoroacil with a significant increase in the number of colony forming units after exposure to the chemotherapeutic agent (Aidoudi et al., 1996). Administration of Ac-SDKP also allows for protection from Ara-C, as shown by higher levels of circulating blood cells in recovery periods (Bogden et al., 1998).

Initial interest into the therapeutic potential of exogenous Ac-SDKP administration was centred on haematopoietic cell protection during cancer chemotherapy (Carde et al., 1992). However, further studies have not been reported.

1.4.7. Ac-SDKP as an inhibitor of fibrosis

A physiological role for Ac-SDKP in preventing fibrosis has been shown by Cavasin *et al.* By inhibiting POP which releases Ac-SDKP from Tβ4, there was increased collagen deposition in various organ tissues leading to cardiac and renal perivascular fibrosis and nephro-sclerosis, thereby implicating Ac-SDKP in the prevention of organ fibrosis (Cavasin et al., 2007).

1.4.7.1. Ac-SDKP in cardiac fibrosis

Cardiac remodelling in hypertensive and ischaemic pathologies is a major cause of chronic heart failure and is characterised by cardiac hypertrophy and fibrosis. Both in cardiac failure and post MI, inflammatory responses play a key role in the pathogenesis of interstitial and perivascular cardiac fibrosis. ACEi have been shown to exert protective effects in ischaemic pathology with a regression of myocardial fibrosis and an improvement in left ventricular function on lisinopril therapy (Brilla et al., 2000).

Various studies, outlined below, suggest a role for Ac-SDKP in the protective effects of ACE inhibition in cardiovascular pathology. An increase in the endogenous expression of cardiac ACE was correlated with a decrease in Ac-SDKP levels in the heart giving rise to cardiac fibrosis (Pokharel et al., 2004). Ac-SDKP has been shown to inhibit cardiac fibroblast proliferation as measured by serum-stimulated ^{3}H-thymidine incorporation (Rhaleb et al., 2001b).

In a 2-kidney, 1-clip (2K-1C) rat model of hypertension, small levels of Ac-SDKP were able to reduce cell proliferation, macrophage infiltration as well as collagen synthesis in the left ventricular (LV) interstitial spaces and to prevent right ventricular fibrosis (Rhaleb et al., 2001a). Ac-SDKP specifically decreased the cardiac infiltration of pro-inflammatory M1 macrophages but not M2 macrophages and neutrophils in a mice model of heart failure (Nakagawa et al., 2018). However, the peptide failed to reduce the dry weight of the ventricles, implicating a different mechanism for the prevention of LV hypertrophy during ACE inhibition (Peng et al., 2001). Yang *et al.*, observed that treatment with Ac-SDKP not only prevented cardiac fibrosis but also reversed the fibrotic process in non-infarcted regions of the myocardium. The

tetrapeptide has been shown to inhibit the inflammatory process associated with infarction (Yang et al., 2004) (Song et al., 2014).

Ac-SDKP was also found to be an inhibitor of aortic fibrosis (Lin et al., 2008). Moreover, Ac-SDKP protects against diabetic cardiomyopathy with marked reduction in interstitial and perivascular collagen deposition in diabetic rats even under conditions whereby their blood glucose levels and blood pressure were high. Ac-SDKP administration partially abolished the diastolic dysfunction associated with diabetes (Castoldi et al., 2010).

1.4.7.2. **Ac-SDKP in renal fibrosis**

Ac-SDKP has demonstrated beneficial effects on renal inflammation and fibrosis in various models of renal pathology (Chan et al., 2015) (Rhaleb et al., 2001b). Mesangial cell proliferation and mesangial cell hypertrophy occurs in a range of glomerular pathologies. Ac-SDKP was observed to inhibit mesangial cell DNA synthesis and hence proliferation without affecting their viability (Kanasaki et al., 2006).

In aldosterone-salt hypertension rats which develop renal fibrosis, Ac-SDKP markedly reduced interstitial collagen deposition and fibroblast proliferation (Peng et al., 2001). Furthermore, Ac-SDKP reduced urinary albuminuria and reduced macrophage infiltration in salt-sensitive hypertension model of kidney disease (M. Wang et al., 2010).

Ac-SDKP administration in diabetic rats was also effective at decreasing glomerular, and perivascular fibrosis, conferring better protection than the ACE inhibitor ramipril. Co-treatment with both Ac-SDKP and ramipril further reduced fibrosis, demonstrating an additive effect of Ac-SDKP with respect to ACE inhibition only (Castoldi et al., 2013). In unilateral ureter obstruction models, a reduction in renal interstitial inflammation and fibrosis caused by the ACEi captopril was found to be mediated by the increase in Ac-SDKP levels (Chan et al., 2018).

1.4.7.3. **Ac-SDKP in other forms of fibrosis**

Ac-SDKP also exerted protective effects in bile duct ligation-induced liver fibrosis and ameliorated carbon tetrachloride-induced liver fibrosis (Zhang et al., 2012). In cases of lung silicosis, Ac-SDKP reduced the extent of collagen deposition and myofibroblast differentiation (Xu et al., 2012)(Deng et al., 2016)(Y. Sun et al., 2010)(Xiaojun et al., 2016)(X. Gao et al., 2019). Ac-SDKP treatment reversed AngII mediated collagen deposition through a restoration of the

protective arm of the RAAS axis, namely the ACE2/Angiotensin 1-7 (Ang 1-7)/Mas in silicotic rats and in fibroblasts (X. Gao et al., 2019).

1.5. Molecular mechanisms of the antifibrotic action of Ac-SDKP

Antifibrotic effects of Ac-SDKP appear to be mediated by numerous cell signalling pathways, likely to involve an Ac-SDKP receptor. Using the radioactive analogue ^{125}I-Hpp-Aca-SDKP, Zhuo *et al.*, demonstrated the presence of a single class of high-affinity and highly specific receptor binding sites for Ac-SDKP in cardiac fibroblasts (Zhuo et al., 2007).

A wide range of cytokines which promote cell growth and proliferation as well as ECM accumulation contribute to the development of organ fibrosis. Some of the major drivers of fibrosis include TGF-β, PDGF, CTGF, endothelin-1 (ET-1) and AngII (Leask, 2010). Hence, various studies have investigated the role of Ac-SDKP in modulating the signalling pathways initiated by these cytokines.

1.5.1. Ac-SDKP modulation of the TGF-β pathway

Ac-SDKP decreases levels of TGF-β in a dose-dependent manner by decreasing TGF-β transcription (Castoldi et al., 2010). Administration of the tetrapeptide in rat cardiac fibroblasts significantly reduced the luciferase signal in a Smad-sensitive luciferase construct in cardiac fibroblasts. The phosphorylation of Smad2 and Smad3 and their translocation to the nucleus is inhibited by Ac-SDKP in the cells *in vitro* and *in vivo* (Pokharel et al., 2002) (Kanasaki et al., 2003) (Pokharel et al., 2004)(Lin et al., 2008)(Castoldi et al., 2010). Furthermore, Ac-SDKP increases the cytoplasmic distribution of I-Smad (Smad 7).

Interestingly, AngII is known to modulate TGF-β expression through the AT_1 receptor in cardiac myocytes and fibroblasts. This results in activation of nicotinamide adenine dinucleotide phosphate (NADPH) oxidase which stimulates TGF-β production (Bataller et al., 2003) (Rosenkranz, 2004). Ac-SDKP also prevents AngII-mediated TGF-β expression and significantly inhibited the 5-fold increase in Smad-2 phosphorylation induced by AngII (Lin et al., 2008). Further, an increase in the levels of CTGF was attenuated by Ac-SDKP in the heart, probably

due to inhibition of TGF-β/Smad signalling (Peng et al., 2003). While the relationship between Ac-SDKP and TGF- β has been demonstrated in both *in vivo* and *in vitro* rat and cell culture models, whether the same pathways and mechanisms are involved within the pericardium is not known.

1.5.2. Ac-SDKP and Map kinase signalling

The cytosolic serine/threonine kinases, MAPKs are involved in cellular growth and proliferation pathways and they respond to various growth stimuli (Blenis, 1993). MAPKs play a vital role in fibroblast cell proliferation and have been implicated in AngII-mediated DNA synthesis and cardiac fibroblast proliferation via the AT_1 receptor (Pagès et al., 1993)(Schorb et al., 1995).

ET-1 is a potent vaso-constrictive peptide found at high circulating levels in various pathologies (Masaki, 2004). It has been found to increase the synthesis of collagen and the proliferation of cardiac fibroblasts (Guarda et al., 1993) (Gray et al., 1998). Ac-SDKP inhibits ET-1–induced collagen synthesis and reduces ET-1 dependent extracellular signal-regulated kinase (ERK1/2) phosphorylation by up-to 50% (Zhuo et al., 2007). Ac-SDKP also attenuates the ET-1-mediated increase in intracellular calcium from basal levels (Zhuo et al., 2007). Calcium signalling pathways play an important role in cell growth and proliferation by inducing the transcription of genes that allow cells in the resting (G0) stage to enter the mitotic cell cycle (Berridge, 1995)(Berridge et al., 2000).

In rat mesangial cells, ET-1 was shown to rapidly induce MAPK activation via the activation of protein kinase C and protein tyrosine kinases (Wang et al., 1992). Ac-SDKP has indeed been shown to inhibit MAPK p44/42 activation in a biphasic and concentration-dependent fashion (Rhaleb et al., 2001a). Peng *et al.*, found that Ac-SDKP failed to inhibit ET-1 induced p44/42 MAPK phosphorylation in cells where the Src homology 2-containing protein tyrosine phosphatase-2 (SHP-2) was knocked down. SHP-2 is an unusual protein tyrosine phosphatase (PTP) which mediates Ras-MAPK activation by receptors for various cytokines as opposed to the negative regulatory functions of other PTPs (Matozaki et al., 2009). It is thus highly likely that Ac-SDKP prevents p44/42 MAPK activation via SHP-2 activation (Peng et al., 2012).

PDGF is a potent stimulant of cellular growth and proliferation of connective tissue including smooth muscle cells and fibroblasts (Bornfeldt et al., 1995). Stimulation of cardiac fibroblasts with PDGF was shown to increase cellular proliferation. An observed upregulation in ERK1/2 and c-Jun N-terminal kinases (JNK) phosphorylation is a likely downstream effect of PDGF

receptor binding as simultaneous treatment of PDGF with ERK1/2 and JNK inhibitors significantly reduced fibroblast proliferation.

Ac-SDKP inhibited PDGF-induced ERK1/2 and JNK phosphorylation with a concomitant reduction of fibroblast proliferation and collagen expression suggesting that Ac-SDKP may inhibit fibrosis by inhibiting ERK1/2 and JNK pathway activation (Zhang et al., 2011). JNK is an effector of the MAPK signalling pathway. The JNK pathway is triggered in response to a wide variety of stimuli including cytokines and environmental stressors. Downstream effects of the JNK pathway include a range of cellular responses such as differentiation, proliferation, inflammation and apoptosis (Robinson and Cobb, 1997).

The inhibition of PDGF induced JNK signalling by Ac-SDKP is achieved by upregulating the cell cycle modulators p53 and $p27^{kip1}$ protein and Ac-SDKP was also shown to inhibit PDGF induced expression of cyclin D1 (Kanasaki et al., 2006).

Finally, endothelial-to-mesenchymal transition (EndMT) is known to significantly contribute to fibrotic pathologies in various organs. TGF-β/Smad signalling is a major driver of EndMT and Ac-SDKP has been shown to inhibit TGF-β mediated EndMT through interaction with FGFR1 to phosphorylate MAP4K4. To date the role of Ac-SDKP in Map kinase signalling has not been investigated in pericardial fluid so whether the findings above are relevant in patients with TB pericarditis is not known and would need to be verified.

1.5.3. Ac-SDKP and ACE signalling

Observations of ACEi potentiation of bradykinin responses lead to the discovery of an ACE signal transduction pathway, illustrated in Figure 1-8 (Kohlstedt et al., 2004). Briefly ACEi binding to ACE on the cell surface membrane triggers ACE dimerisation, the initial step in the cascade (Kohlstedt et al., 2006). Upon dimerisation, a serine residue on the cytoplasmic tail at position 1270 of the ACE sequence (ser1270) undergoes casein kinase-2 (CK-2) mediated phosphorylation. This leads to the activation of the c-Jun NH2-terminal kinase (JNK) with the likely involvement of Map kinase kinase 7 (MKK7) which is co-immunoprecipitated with the ACE-CK2 complex (Tournier et al., 1997)(Kohlstedt et al., 2004). Increased JNK activity causes c-jun to phosphorylate and translocate to the nucleus whereby it dimerises into the apoprotein-1 (AP-1) transcription factor. AP-1 induces the expression of ACE (ACE99 gene) and of cyclooxygenase-2 (COX-2) (Kohlstedt et al., 2004)(Kohlstedt et al., 2005). COX-2 is a pro-inflammatory agent which has been implicated in pathological processes via its ability to induce

the local production of prostaglandins and is targeted by COX-2 inhibitors in the treatment of inflammatory processes (Crofford, 1997).

In porcine aortic endothelial cells, the presence of a functional C-terminal active site, as seen in the C domain knock out mutant (two zinc coordinating histidines converted to lysines thus inactivating only the C domain) was crucial for sACE dimerisation (Kohlstedt et al., 2006). However, a C domain knock out murine sACE construct was able to activate JNK in a Chinese Hamster Ovary cell line (CHO) (X. Sun et al., 2010) (Kohlstedt et al., 2004). In studies in murine sACE whereby either the N or C domains or both were inactivated, Ac-SDKP was shown to induce JNK phosphorylation in the N or C domain mutant only, which was abolished by a CK-2 inhibitor (Y. Sun et al., 2010). Thus Ac-SDKP requires binding to either the N or C domain to induce ACE signalling via Ser1270 phosphorylation. However, the pathway appears to be species specific with no signalling response registered to AngI in porcine cells expressing human sACE but a definite increase in JNK levels on AngI binding to murine sACE in CHO cells (Kohlstedt et al., 2005). Whether such an ACE signal transduction pathway is active in normal pericardial fluid and in the pericardial fluid of participants with TB pericarditis is not known and may have implications for the potential to prevent pericardial fibrosis.

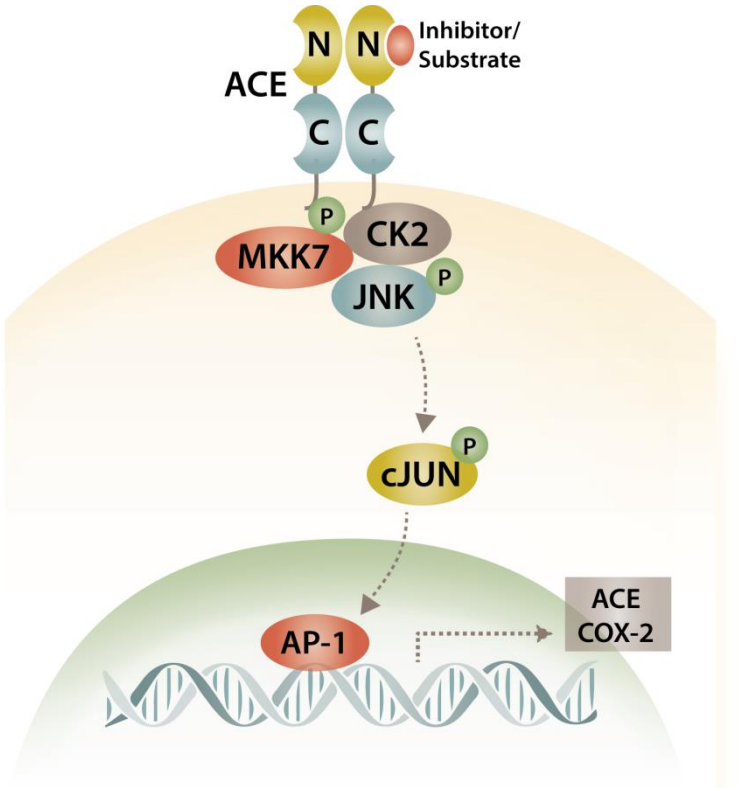

Figure 1-8: Schematic of the ACE signalling cascade

ACEi or substrate binding on the N terminus of the protein induces phosphorylation of the C-terminal cytoplasmic tail serine residue and subsequent JNK and AP-1 mediated signalling.

1.5.4. ACE inhibitors in fibrosis

1.5.4.1. ACE inhibitors in clinical practice

An understanding of the RAAS physiology allows for the prediction of the beneficial effects of ACE antagonism: an inhibition of AngII formation, a decrease in the systolic and diastolic pressure with no effect on the cardiac output and a decrease in bradykinin breakdown. This lead to the search for and development of the first ACEi captopril, for the treatment of hypertension (raised mean arterial blood pressure: systolic pressure >140mmHg and diastolic pressure >90mmHg, WHO guidelines) (Whitworth, 2003) (Cushman and Ondetti, 1991). Various ACEi have since been developed (enalapril, lisinopril, benazepril, fosinopril, quinapril, moexipril, perindopril and ramipril among others) and are widely used in the management hypertension, a range of conditions primarily involving the cardiac system including chronic heart failure, acute myocardial infarction (MI), arrhythmia, atherosclerotic vascular diseases, stroke, and coronary artery disease, and finally in renal failure. Interestingly, the beneficial effects of ACEi in cardio- and nephro-protection cannot be simply explained by their blood pressure-lowering effects (Wong et al., 2004). Nevertheless, despite these beneficial effects, ACEi are associated with side effects which have been attributed to BK accumulation. The two principal adverse effects include life-threatening angioedema and a persistent dry cough arising in 10-44% of patients which reduces adherence to the long term administration required for the preventative management of cardiovascular events (Kulkarni et al., 2006) (Fox et al., 1996) (Agostoni et al., 1999). An alternative way of inhibiting the RAAS, through the means of AT_1 receptor blockers (ARBs) such as candesartan and losartan, is often utilised in

patients who cannot tolerate ACEi. However, each class of drugs offers unique protective effects and combination therapy of ACEi and ARBs is often the most effective in therapy (McMurray et al., 2003) (Laverman et al., 2002). The development of next generation, domain-selective ACEi, targeting the cleavage of specific ACE substrates has hence been proposed as a means to avoid the adverse effects (Acharya et al., 2003).

1.5.4.2. **ACE inhibitors in fibrotic conditions**

The role of the RAAS in cardiac inflammation and fibrosis is well established; its activation results in up-regulated AngII levels, and the subsequent expression of pro-inflammatory and pro-fibrotic cytokines (Brilla et al., 1993). It is hence no surprise that antifibrotic effects of ACEi are increasingly being reported. However, prospective trials of ACEi with clinical end points comparing markers of fibrosis in chronic inflammatory conditions are scarce. A clinical trial assessing the 6-month outcome of ACEi therapy in hypertensive patients revealed a significant regression in myocardial fibrosis evidenced by a reduction of left ventricular collagen volume fraction and myocardial hydroxyproline levels (Brilla et al., 2000).

Protective effects of ACEi have however been reported in mouse and rat models of diverse diseases ranging from radiation-induced pulmonary injury, tubule-interstitial fibrosis and progressive renal fibrosis, bleomycin-induced lung fibrosis, liver fibrosis, peritoneal fibrosis to Duchenne muscular dystrophy (Morrissey et al., 1996)(Gross et al., 2004)(A. Molteni, 2000) (Yoshiji et al., 2006)(Wang et al., 2000)(Yoshiji et al., 2005)(Morales et al., 2013)(Sawada et al., 2002)(Takeda et al., 2010). The antifibrotic mechanisms of action of the ACEi were similar in most studies involving: a reduction in fibroblast activation or cellular transition to adopt fibroblast-like function; a decrease in TGF-β expression both at the protein and mRNA levels; down-regulation of MMP activity, and an overall reduction in collagen levels (Jonsson et al., 2001)(Kuno et al., 2003). In some of these studies the effects of ACEi was compared to ARBs, but there was no overall consensus: whilst similar efficacy was observed in certain disease models, ACEi showed different mechanisms of action or improved/reduced protection against fibrosis in other studies (Yu et al., 2001) (A. Molteni, 2000). For instance, ramipril as compared to candesartan showed enhanced reduction in glomerular and tubulo-interstitial fibrosis and an overall decrease in the number of fibroblasts through a greater down-regulation of TGF-β, CTGF and MMP levels (Gross et al., 2004). Further, in a ventricular fibrosis model, ACEi and ARBs differentially regulated collagen gene expression and MMP activity but the overall

suppression of fibrosis was similar (Yamamoto et al., 2005). These observations further support a role for ACEi extending beyond the mere inhibition of the formation of the pro-fibrotic AngII. Indeed, the accumulation of Ac-SDKP as well as the anti-inflammatory RAAS peptide Ang 1-7 has been increasingly recognised as a mechanism of action of ACEi (Carretero, 2005). These findings and observations may have important implications for the potential role of ACE inhibitors in the prevention post tuberculous pericardial fibrosis.

1.6.Galectin-3 in fibrosis

1.6.1. Galectin-3

Gal-3 belongs to the galectin protein family characterised by evolutionarily conserved amino acid sequences in their carbohydrate-binding site and an affinity for β-galactoside (Leffler et al., 2002). Fifteen galectins have been identified, belonging to three main groups; a prototype group bearing a single carbohydrate recognition domain (CRD)(galectins 1, 2, 5, 7, 10, 11, 13, and 14), a tandem repeat group containing two CRDs (galectins 4, 6, 8, 9, and 12) and a chimera group (galectin-3) containing a proline- and glycine- rich domain (Liu et al., 2002).

Gal-3, previously referred to as Mac-2 antigen, IgE-binding protein, L-29 and CBP30, is a circulating 35kDa lectin with a C-terminal CRD connected to a long N-terminal domain, coded for by the singular *LGALS3* gene located on chromosome 14 (locus q21-22)(Dumic et al., 2006). Gal-3 is expressed in inflammatory cells as well as different types of activated microglial cells. Gal-3 can be found in most subcellular compartments, but the localisation of Gal-3 is dependent on the cell type and proliferation stage of the cell. It is ubiquitously distributed in tissues including haematopoietic tissue, lymph nodes, respiratory, digestive and urinary tracts and skin (H. Kim et al., 2007)(Li et al., 2020).

1.6.2. Galectin-3 structure

Gal-3 bears one C-terminal CRD and a flexible N-terminal domain (Dumic et al., 2006) (Birdsall et al., 2001). The N domain comprises 7–14 repeats of specific nine amino acid long sequence of Pro-Gly-Ala-Tyr-Pro-Gly-X-X-X. It is important for the oligomerisation of

Gal-3 as well as its secretion and nuclear translocation (Massa et al., 1993)(Gong et al., 1999).

The CRD of Gal-3 is around 130 amino acids long and forms a globular structure with five- and six-stranded β-sheets arranged in a β-sandwich (Seetharaman et al., 1998). The CRD bears a NWGR (Asp-Trp-Gly-Arg) motif which allows binding to β-galactosides. This motif also present in members of the B-cell lymphoma 2 (Bcl2) apoptotic protein family also contributes to the anti-apoptotic action of Gal-3 (Akahani et al., 1997).

Gal-3 occurs primarily as a monomer in solution (Morris et al., 2004). However, it can form homodimers through the CRD and polymerise in the presence of carbohydrate binding counterparts through its N domain (Massa et al., 1993)(Yang et al., 1998)(Ahmad et al., 2004). Extracellular gal-3 commonly multimerises and cross-links with cell surface ligands to form complexes which initiate cell surface molecule-associated cellular signalling (Ochieng et al., 2002).

1.6.3. Physiological roles of Galectin-3

The physiological functions of Gal-3 are wide ranging: it has been implicated in processes ranging from cellular proliferation, cell adhesion, inflammation to immune regulation (Newlaczyl and Yu, 2011). Gal-3 localises predominantly to the cytoplasm but it can also shuttle into the nucleus (Yang et al., 1996). Further, it is secreted into the extracellular environment and biological fluids. The varying locations of the molecule contribute to its plethora of biological functions. In the cellular environment, cytoplasmic Galectin-3 plays a vital role to cell survival through its interactions with anti-apoptotic Bcl-2 proteins and activated guanosine-5'-triphosphate-bound K-Ras (Akahani et al., 1997)(Yang et al., 1996)(Shalom-Feuerstein et al., 2005). Nuclear galectin-3 induced pre-mRNA splicing and functions to regulate gene transcription (Dumic et al., 2006) (Elad-Sfadia et al., 2004). Finally, extracellular galectin-3 is involved in cell-cell interaction modulation, including extracellular matrix regulation (Ochieng et al., 2002).

1.6.3.1. Galectin-3 in fibrosis

In fibroblasts and macrophages, gal-3 secretion can be triggered as a result of various stress stimuli including heat shock and irradiation (Sato and Hughes, 1994). Secreted gal-3 plays a role

in EMT, scar tissue formation as well as pathological remodelling of tissue architecture (Li et al., 2014). Gal-3 has been implicated in fibrotic pathway modulation in various tissues including the liver, heart, vascular tissue, kidney, and lungs (Calvier et al., 2013)(Li et al., 2014).

1.6.3.2. **Galectin-3 in cardiac fibrosis**

Gal-3 plays a role in the modulation of pro-inflammatory and pro-fibrotic pathways in cardiac regulation (Sharma et al., 2004)(Yu et al., 2013). Gal-3 is known to regulate the integrity of the cardiac matrix and myocardial Gal-3 levels in rodents correlate with the degree of hypertrophy in hearts which are prole to failure (Schroen Blanche et al., 2004). Further, exogeneous administration of gal-3 into rodent heart promotes cardiac hypertrophy, pathological fibrotic remodelling and eventually leads to heart failure (Sharma et al., 2004). This is supported by observations of suppressed inflammation, and collagen type I deposition in response to aldosterone in gal-3 knock out mice (Calvier et al., 2013). Further both pharmacological and genetic inhibiton of gal-3 lead to a reduction in collagen I and III formation, processing, cleavage, cross-linking, and deposition leading to an inhibition in left ventricular dysfunction and fibrosis (Yu et al., 2013). Moreover, Gal-3 has emerged as a prognostic marker in cardiac fibrosis for the risk for heart failure (D. J. A. Lok et al., 2010)(Ho et al., 2012)

1.7. Study rationale and research questions

Tuberculous pericarditis is prevalent in South Africa, where 10 million cases of TB were recorded in 2018 alone. TB pericarditis is associated with the development of constrictive pericarditis, a complication which arises in up to 26% of patients. The treatment of choice for severe constrictive pericarditis involves the surgical resection of the pericardium. This procedure has a poor post-operative prognosis and is not available in most of sub Saharan Africa. Thus, the identification of preventative strategies for the development of fibrosis in TB pericarditis is strongly warranted. Importantly, the mechanisms underlying the molecular processes leading to the pathophysiological manifestations of fibrotic disease have not been well established. Therefore, a better understanding of the key molecular pathways and mediators of fibrosis in TB pericarditis will pave the way to the identification of potential targets to prevent the onset of fibrosis in these patients.

A significant down regulation of Ac-SDKP levels as well as a mild increase in Gal-3 levels has been demonstrated in TB pericardial fluid in a small study. Ac-SDKP is a physiological tetrapeptide degraded by ACE, Gal-3 is a lectin which plays an important role in cardiac inflammatory and fibrotic pathways. However, the role played by these molecules in the development of constrictive pericarditis is poorly understood. An implication of altered Ac-SDKP regulation in TB pericarditis could pave the way for the implementation of already available ACEi in the management of the condition.

ACEi and Ac-SDKP analogues are promising approaches not only for the treatment of constrictive pericarditis but various other fibrotic conditions. Despite the vast array of manifestations of fibrosis which translates into a major cause of morbidity and mortality in many chronic inflammatory diseases, there are currently very few treatment strategies which specifically target the pathophysiological processes occurring in fibrosis. Thus, further studies on the antifibrotic potential of ACEi and Ac-SDKP as well as their precise mechanisms of action are warranted.

1.7.1. Aims and Objectives

The aim of this project is to increase our current understanding of the molecular mechanisms and mediators involved in the development of fibrosis, particularly in TB pericarditis by: a] investigating the role played by Ac-SDKP, ACE, POP and Gal-3 in the pathophysiology of constrictive TB pericarditis; b] investigating the *in vitro* potential of ACEi and Ac-SDKP analogues as therapeutic targets in the progression to fibrosis; and c] investigating the molecular mechanisms of action of Ac-SDKP.

The objectives are as follows:

1) To investigate the deregulated Ac-SDKP metabolism in TB pericardial fluid.
2) To determine the molecular specificity of the antifibrotic action of Ac-SDKP.
3) To investigate the *in vitro* antifibrotic potential of Ac-SDKP analogues and ACE inhibitors.
4) To characterise the signalling mechanism of the Ac-SDKP mediated effect on fibrosis.

2. Dysregulation of Ac-SDKP metabolism in TB pericardial fluid

2.1. Background

Tuberculous pericarditis remains an important challenge in sub-Saharan Africa owing to the endemicity of TB and the HIV/AIDs pandemic. Most of the scientific studies conducted in sub-Saharan Africa in the field of tuberculous heart diseases have occurred over the past couple of decades (Zumla et al., 2015). While progress has been made in the understanding of the immune responses within the pericardium, diagnostic approaches and overall survival, important gaps remain.

A major complication of TB pericarditis is constrictive pericarditis which is characterised by fusion of the visceral and parietal pericardium with progressive fibrosis (Mutyaba and Ntsekhe, 2017). This manifests as a loss of compliance of the pericardium, eventually leading to heart failure. Constrictive pericarditis arises in up to 26% of patients and has a poor prognosis (Noubiap et al., 2019). This highlights the need for better predictors of constrictive pericarditis and development of targeted fibrosis prevention strategies in those treated for TB pericarditis.

Infection of the pericardium by *M.tb* is likely to elicit an initial inflammatory reaction which when poorly resolved progresses on to the fibrotic phenotype of TB constrictive pericarditis (Mayosi et al., 2008). Various studies have established a distinct profile of TB pericardial fluid as compared to normal pericardial fluid (Matthews et al., 2015)(Ntsekhe et al., 2013).

Importantly, when paired TB pericardial fluid and blood samples were tested for a panel of inflammatory and fibrotic mediators, a strong profibrotic gene expression response was observed, with an accompanying pro-inflammatory response in the pericardial fluid at the protein level (Matthews et al., 2015).

In 2012, it was shown for the first time that Ac-SDKP and Gal-3 could be detected in pericardial fluid (Ntsekhe et al., 2012). Ac-SDKP is a physiological antifibrotic tetrapeptide generated from the protein Tβ4 by the enzymatic action of POP and primarily hydrolysed by ACE (Azizi et al., 1997). ACE, as previously described is known to play a role in inflammation and fibrosis by cleaving AngI into the pro-inflammatory AngII, a potent inducer of cardiac fibrosis (Schnee and

Hsueh, 2000)(Lijnen et al., 2004). Gal-3, on the other hand, has been associated with various fibrotic conditions; its expression leading to fibroblast activation and collagen synthesis both *in vitro* and *in vivo* (De Boer et al., 2010)(Henderson et al., 2006). An upregulation in Gal-3 has been implicated in the pathophysiology of cardiac failure and its potential as a biomarker and as pharmacological target in the treatment of cardiac failure has been assessed (D. J. Lok et al., 2010). Ntsekhe *et al.*, compared the levels of Gal-3 and Ac-SDKP in pericardial fluid from control patients and TB pericarditis patients in a small study. Whilst no significant difference was observed in Gal-3 levels, Ac-SDKP levels in TB pericardial effusions were significantly reduced. These findings suggest a possible physiological role for these molecules in maintaining pericardial homeostasis and possibly in the pathogenesis of pericardial fibrosis.

An understanding of mechanisms of pericardial fibrosis is key to the identification of novel strategies to curb the progression to constriction in TB pericarditis. Further study is hence warranted to determine the mechanism for the reduction in Ac-SDKP levels. This will provide useful information regarding the pathophysiology of pericardial fibrosis and potential pharmacological targets for TB constrictive pericarditis. An increase in ACE serum levels has been reported in granulomatous conditions including *M.tb* infection and sarcoidosis. Levels of sACE correlate well with the disease progression and are believed to arise from an overflow of ACE produced by the macrophages and phagocytes in the granulomatous lesions into the circulation (Weinstock, 1986)(Brice et al., 1995)(Ainslie and Benatar, 1985). However, increased activity of POP in experimentally produced granulomatous skin and liver inflammation has also been described (Nozaki et al., 1992).

2.2. Study objectives

The objective of this chapter was to investigate the metabolism of Ac-SDKP in TB pericardial fluid by:

- identifying any dysregulation of Ac-SDKP levels, of its synthesising enzyme POP and its degrading enzyme ACE
- identifying any dysregulation in Gal-3 levels
- analyzing whether Ac-SDKP metabolism was affected locally in the pericardium, or systemically by contrasting with serum levels

2.3. Materials and methods

2.3.1. Patient recruitment

This was a sub study of the ***I***nvestigation in the ***M***anagement of ***P***ericardit***I***s (IMPI registry) (UCTHREC 102/2003 sub studies 492/2007 and HREC 289/2007). Patients with effusive pericarditis suspected to be of tuberculous origin referred to Groote Schuur Hospital in Cape Town between July 2014 and December 2018 at Groote Schuur Hospital, Observatory, Cape Town were recruited to participate in the registry. Consenting adults (age >18) who were undergoing diagnostic and therapeutic pericardiocentesis, gave permission to have their pericardial fluid analysed and investigated for the molecular mechanisms and mediators of fibrosis. Participants were in the analysis if they had definite and probable TB pericarditis as defined in the Introduction (see section 1.2.4).

Participants in the control group were screened and recruited from adult patients (age >18) undergoing elective coronary artery bypass surgery at Groote Schuur Hospital during the same period (patients on ACEi were excluded from the study). All participants provided written, informed and voluntary consent and permission to conduct the sub-study was provided by the University of Cape Town Health Research Ethics Committee.

2.3.2. Biological sample processing

Pericardial fluid and blood samples were collected from patients at the time of enrolment and a blood sample was collected upon follow up. Pericardial fluid was collected in sodium heparin tubes (BD Vacutainer, UK) and blood was collected in SSTTM II Advance Plus blood collection tubes (BD Vacutainer, UK). Baseline pericardial fluid and blood samples, as well as follow up blood samples were processed in a biosafety level 3 facility. Briefly, Heparin tubes containing pericardial fluid and serum tubes containing whole blood were centrifuged at 3000 *g* for 15 minutes (mins) to collect the supernatant Pericardial Cell Free Fluid (PCFF) and serum respectively. These were filtered (0.2 μm syringe filters, LASEC, South Africa) and cryopreserved at -80^{o}C until ELISAs and enzymatic assays were performed.

2.3.3. Ac-SDKP and Gal-3 enzyme linked immunosorbent assay

2.3.3.1. Ac-SDKP ELISA

A competitive ELISA (SPI Bio, France) was used for the quantitative measurement of Ac-SDKP levels in PCFF, according to manufacturer's protocol (adapted from (Engvall and Perlmann, 1971). The principle of the assay is based on the competition for specific rabbit anti-Ac-SDKP antiserum sites between unlabelled Ac-SDKP (from standard or sample) and Ac-SDKP linked to acetyl-cholinesterase (AChE) (tracer). The AChE activity of the tracer was measured from the intensity of the yellow product formed from its reaction with Ellman's reagent (Ellman et al., 1961). The absorbance was measured using a spectrophotometer (iMARK^{TM}, Biorad) at 412 nm and was proportional to the amount of tracer and hence inversely proportional to the amount of Ac-SDKP from the standard or sample solution. A sigmoidal standard curve was used to quantify the amounts of Ac-SDKP in the biological samples (see Appendix).

2.3.3.2 Gal-3 ELISA

Gal-3 levels in pericardial CFF were measured using a specific Sandwich ELISA kit, according to manufacturer's protocol (eBioscience, USA). Briefly, an anti-human Gal-3 antibody adsorbed onto the wells of the plate captures Gal-3 from the samples/standard solutions. The wells were incubated with a biotin-conjugated anti-human Gal-3 antibody which binds the captured Gal-3. A streptavidin-horseradish peroxidase was then added which recognises the biotin-conjugated anti-human Gal-3 antibody prior to a chromogenic substrate solution (TMB) (Mesulam, 1978). Absorbance was measured with a spectrophotometer (iMARK^{TM}, Biorad) at 450 nm and the amount of human Gal-3 in each sample was quantified using a Gal-3 standard curve (see Appendix).

2.3.4 Enzyme assays

2.3.4.1 Prolyl oligopeptidase assay

POP hydrolyses peptide bonds on the carboxyl side of L-proline. POP activity was measured by a fluorometric assay using the substrate Z-Gly-Pro-Amino-Methyl Coumarin (Bachem, Switzerland) (adapted from (Browne and O'Cuinn, 1983)). The assay is based on the generation of the fluorescent product amino methyl coumarin (AMC) from cleavage of the substrate by POP. The substrate was dissolved in dimethyl sulfoxide (DMSO, 2% of final volume) and made up to a final concentration of 0.1 mM in 0.1 M of potassium phosphate buffer (pH 7.4) and 30 mM of DL-dithiothreitol (Sigma, USA). The assay was performed in a 96 well plate by incubating 10 µl of sample with 40 µl Z-Gly-Pro-AMC at 37 °C for 60 min. The reaction was stopped by adding 100 µl of 1.5 M acetic acid (pH 4.2) and fluorescence was read at $\gamma_{excitation}$ and $\gamma_{emission}$ of 370 and 440 nm, respectively (Varian Cary Eclipse, Agilent). Background fluorescence was measured in controls where the sample was not added. Relative fluorescence was thereupon converted to AMC concentration using an AMC (Bachem, Switzerland) standard curve (see appendix). Activities are expressed as pmol of AMC released per millilitre of sample.

2.3.4.2 ACE assay

ACE catalyses the hydrolysis of dipeptides from the carboxy-terminus of oligopeptides. A fluorometric assay for measuring ACE activity was performed using the substrate Z-Phenylalanine-L-histidyl-L-leucine (ZFHL) (Bachem, Switzerland) which yields the HL peptide upon cleavage by ACE. The fluorescent adduct of the HL, upon *o*-phthaldialdehyde (Sigma, USA) derivitization, was quantified fluorimetrically. HL formation from the substrate was quantified by using an adapted protocol from Schwager *et al.* (Schwager et al., 2006). Briefly 6µl of diluted sample was incubated in 30 µl of 1 mM *Z*-FHL and incubated at 37^{o}C for 20 mins. The reaction was stopped with 125 µl of 0.4 M NaOH. Endogenous fluorescence was measured by adding the sample to the mixture after the NaOH addition. Derivitisation was carried out by adding 10 µL of 24 mg/ml *o*-phthaldialdehyde, shaking at room temperature for 10 mins and the reaction stopped with 30 µL 3M hydrochloric acid. The plate was centrifuged at 2800 *g* for 15 mins at 18°C and the supernatants were transferred to a fresh 96 well plate. Fluorescence was measured at $\gamma_{excitation}$ of 360 nm and $\gamma_{emission}$ of 485 nm (Varian Cary Elipse, Agilent). A HL (Sigma, USA) standard curve was

generated to convert relative fluorescence into milliunits (mU) ACE activity: where 1 unit is defined as 1nmole of HL produced/minute/mL, by ACE, at 37^{o}C (see Appendix).

2.3.6 Statistical analysis

Data analysis was performed using the statistical software GraphPad PRISM 6.0 (GraphPad software Inc, USA). A Shapiro-Wilks test was used to determine whether distributions followed a Gaussian pattern. Significant differences between the TB pericarditis and control groups were investigated accordingly: two tailed un-paired student t-tests or Mann-Whitney tests were used with a cut off for statistical significance of $p<0.05$. Pearson's correlation was used for correlation analysis.

2.4. Results

2.4.1. Ac-SDKP and Gal-3 level comparison

2.4.1.1. Determination of Gal-3 levels in PCFF of TB+ and TB- patients

For the determination of Gal-3 levels in PCFF, a specific ELISA kit was used. Gal-3 levels in 35 TB PCFF (TB+) and 20 control (TB-) PCFF samples were determined. Median Gal-3 concentrations in the TB+ group were 7.38 ng/ml (IQR 4.38- 9.77) and 8.37 ng/ml (IQR 5.34- 14.11) in the TB- group (Figure 2-1). There was no significant difference in Gal-3 levels between the TB+ and the TB- group. This finding is in concordance with previous measurements of Gal-3 in PCFF by Ntsekhe *et al.* (Ntsekhe et al., 2012).

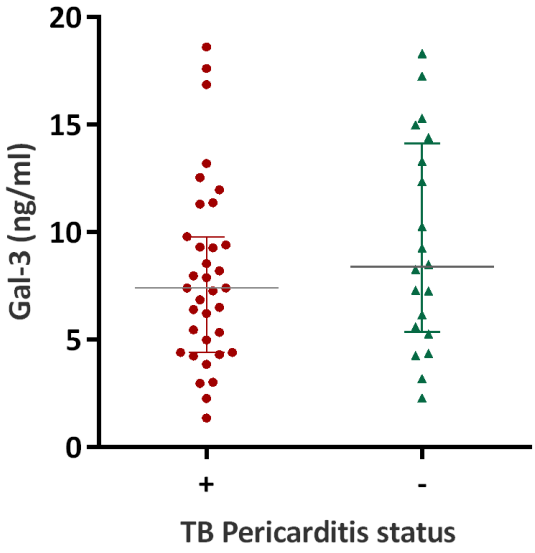

Figure 2-1: Scatterplot of Gal-3 levels grouped by TB pericarditis status. Gal-3 levels were measured in 35 TB+ and 20 TB- PCFF samples, revealing no significant difference between the two groups.

2.4.1.2. Determination of Ac-SDKP levels in PCFF of TB+ and TB- patients

A significant difference in Ac-SDKP levels was previously measured between TB pericarditis and controls in PCFF (Ntsekhe et al., 2012). We used a specific ELISA kit to validate these findings in our study population. Briefly, Ac-SDKP levels in 35 TB+ PCFF and 20 TB- PCFF samples were measured. The median Ac-SDKP level in TB+ group was 0.191 ng/ml (IQR 0.085-0.344) and in TB- group was 0.443ng/ml (IQR 0.169-0.613)(Figure 2-2). Ac-SDKP levels followed a Gaussian distribution for both the TB+ and TB- groups (Shapiro Wilk: 0.74 and 0.86 respectively); an unpaired t-test was used to compare between the two groups. A significant difference (p=0.048) in Ac-SDKP levels was revealed in our study group, in accord with Ntsekhe *et al.* (Ntsekhe et al., 2012).

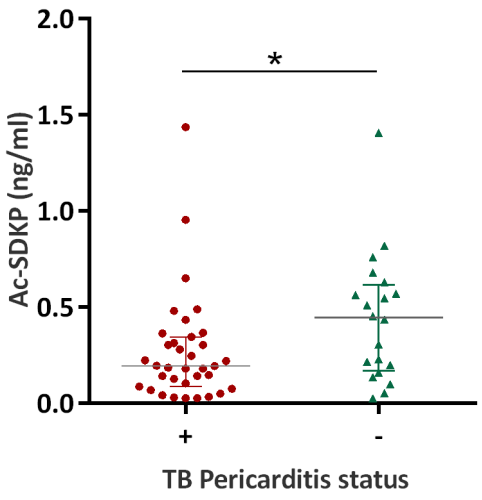

Figure 2-2: Scatterplot of Ac-SDKP levels grouped by TB pericarditis status.
Ac-SDKP levels were significantly different between 35 TB+ and 20 TB- PCFF samples. Significance is represented with a * ($p<0.05$).

2.4.1.3. **Gal-3/Ac-SDKP ratios in TB pericarditis vs controls**

The Gal-3/Ac-SDKP ratios were compared between the two groups (Figure 2-3). Whilst no significant difference was observed in the Gal-3/Ac-SDKP ratios, the TB+ group had some samples with markedly high Gal-3/Ac-SDKP ratios, driven predominantly by higher Gal-3 levels.

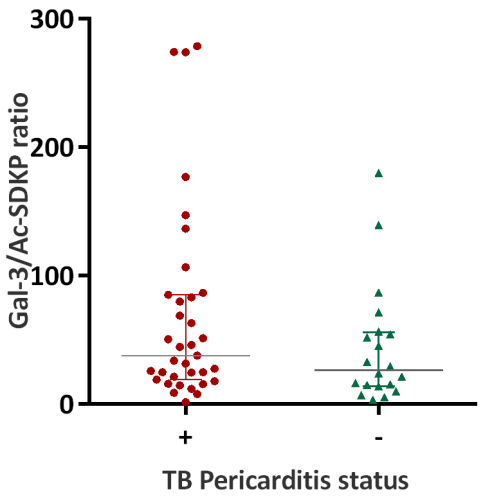

Figure 2-3: Scatterplot of Gal-3/Ac-SDKP ratios grouped by TB pericarditis status.
No significantly difference was observed. However, a mild increase in the ratios were found in the TB+ with 3 samples having a markedly increased Gal-3/Ac-SDKP proportion.

2.4.2. Enzymatic activity of ACE and POP in TB pericarditis vs controls

In order to investigate the mechanism for the decreased Ac-SDKP levels measured in our TB+ group, the enzymatic activities of POP and ACE in the PCFF were investigated. POP is the rate limiting enzyme for the synthesis of Ac-SDKP, whilst ACE is the only known physiological peptide to efficiently degrade Ac-SDKP (Grillon et al., 1990)(Azizi et al., 1996). Enzymatic activities were investigated in both PCFF and serum in order to establish whether any observed enzyme activity dysregulation was a systemic effect or a localised one.

2.4.2.1. **POP activities in PCFF and serum**

To determine whether the rate of synthesis of Ac-SDKP from Tβ4 differed between the two groups, POP activities were quantified using the substrate Z-Gly-Pro-AMC which it cleaves into AMC.

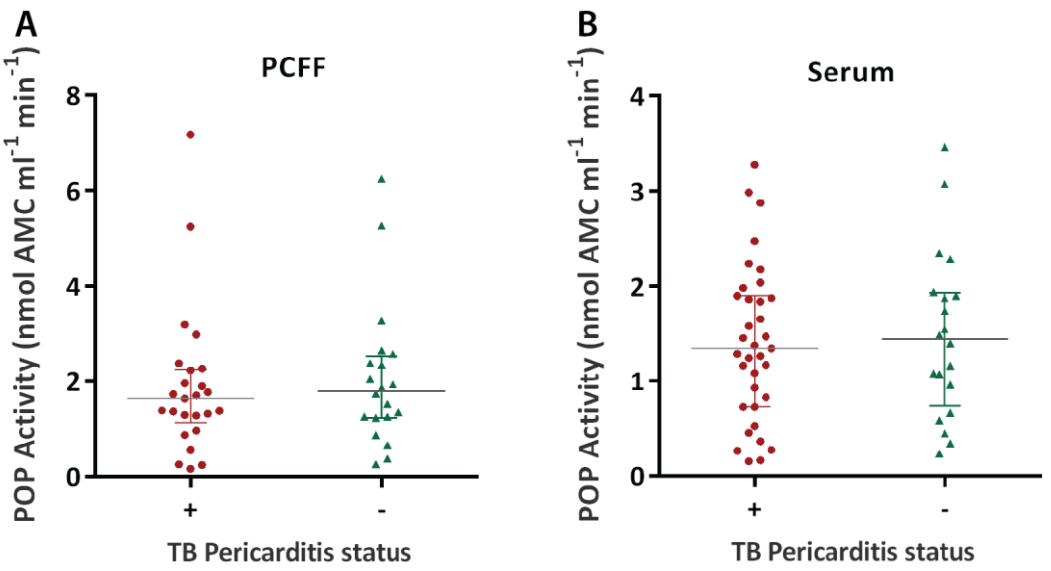

Figure 2-4: POP activities grouped by TB pericarditis status.
Scatterplot of POP activity levels measured in **A. PCFF.** POP activities in PCFF were comparable between the TB+ and TB- group **B. Serum.** Lower serum POP activities were measured than PCFF suggesting the local production of POP in the pericardium.

POP activities in PCFF ranged from 1.02-2.25 nmol AMC ml^{-1} min^{-1} in the TB+ group and from 1.24-2.53 nmol AMC ml^{-1} min^{-1} in the TB- group. In serum, POP activities ranged from 1.35-3.27 and from 1.44-3.46 nmol AMC ml^{-1} min^{-1} in the two groups respectively. No difference in POP activities were seen in the PCFF and in serum.

Serum POP levels observed were comparable to previous studies using the same substrate. However, POP activity in pericardial fluid has not been previously measured as far as can be seen in the literature. Higher pericardial POP levels were measured as compared to the serum suggesting a local production of POP in the pericardium.

2.4.2.2. **ACE activities in PCFF and serum**

To investigate the rate of degradation of Ac-SDKP between the two groups, ACE activities were quantified using the substrate ZFHL which is cleaved by ACE to release HL.

ACE activities in PCFF ranged from 1.02-2.25 nmol HL ml^{-1} min^{-1} in the TB+ group and from 1.24-2.53 nmol HL ml^{-1} min^{-1} in the TB- group (Figure 2-5). This represents a significant difference in ACE activities in the PCFF between active and control groups (p= 0.038). In serum, ACE activities ranged from 1.35-3.27 in the active and from 1.44-3.46 nmol HL ml^{-1} min^{-1} in the controls, suggesting no significant difference in the two groups.

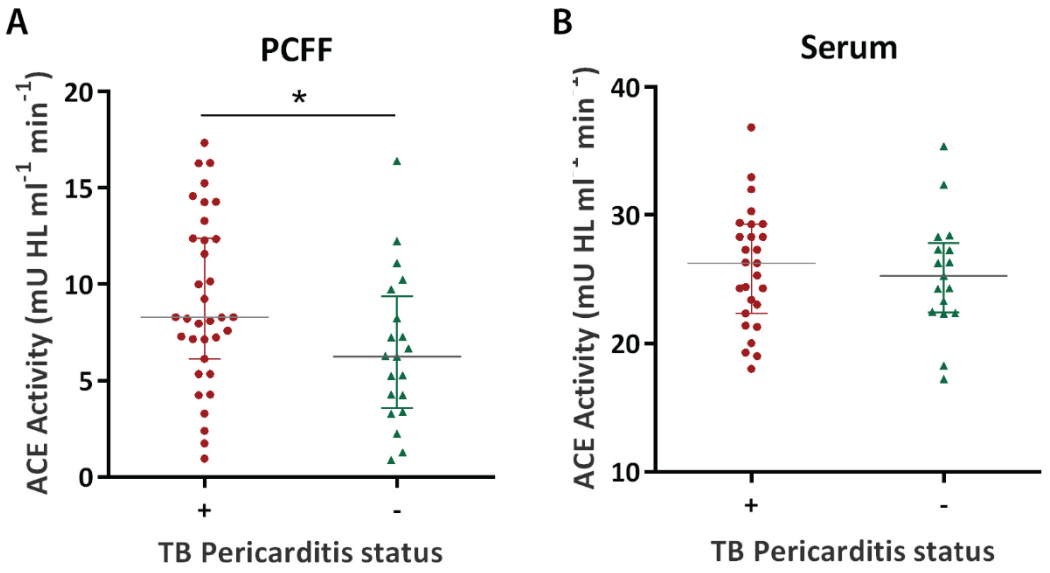

Figure 2-5: ACE activities grouped by TB pericarditis status.
Scatterplot of ACE activity levels measured in **A. PCFF. Significantly higher** ACE activities were measured in TB+ PCFF as compared to the TB- group **B. Serum.** Serum ACE activities were comparable between the two groups.

Further, ACE activities were lower in PCFF as compared to serum. ACE activity in pericardial fluid has not been previously described. This may be an indication that ACE from the pericardial fluid originates predominantly from the plasma ultrafiltrate. Importantly, serum ACE levels measured were comparable between the two groups. This indicates a localised dysregulation of ACE levels localised to the pericardial environment.

2.4.3. Correlation between Ac-SDKP levels and enzymatic activity

To determine whether Ac-SDKP levels correlated with either POP levels or ACE levels, a Pearson's correlation test was performed.

2.4.3.1. Ac-SDKP and POP correlation

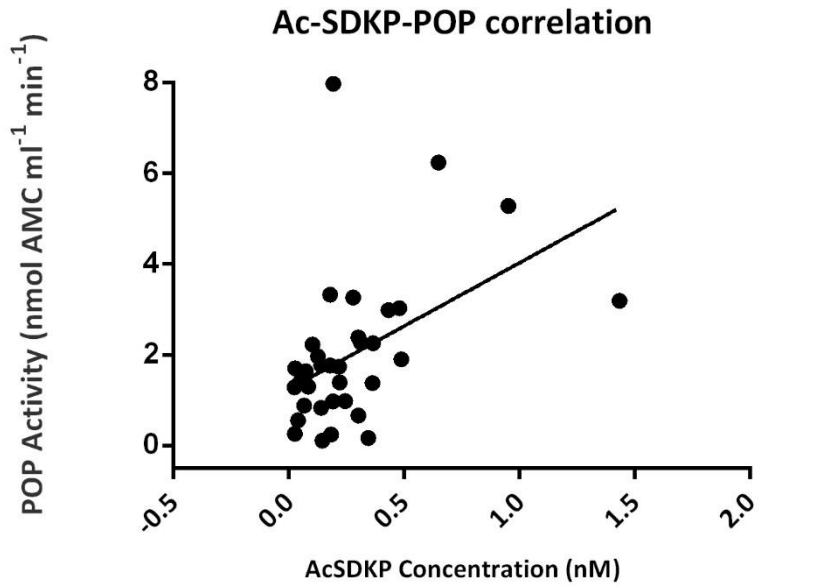

Pearson r			
r	0.4606	P value	
95% confidence interval	0.1503 to 0.6882	P (two-tailed)	0.0054
R square	0.2121		

Figure 2-6: Correlation between Ac-SDKP and POP levels
A significant (p=0.005) correlation between Ac-SDKP and POP levels were observed in the PCFF.

A plot of POP activity (Figure 2-6) against corresponding Ac-SDKP levels measured revealed a R coefficient of 0.46 with p=0.005.

2.4.3.2. **Ac-SDKP and ACE correlation**

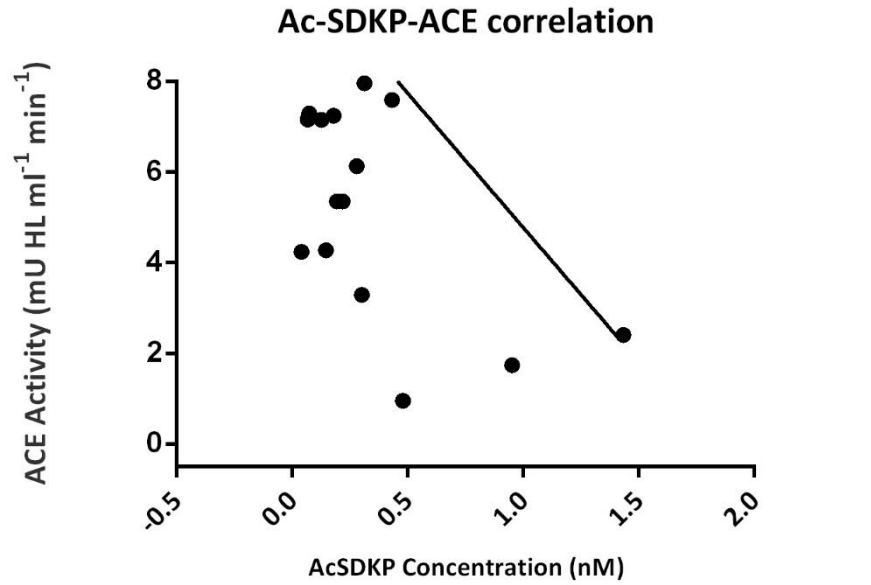

Pearson r			
r	-0.3802	P value	
95% confidence interval	-0.6333 to -0.05370	P (two-tailed)	0.0243
R square	0.1446		

Figure 2-7: Correlation between Ac-SDKP and ACE levels
A significant (p=0.02) correlation between Ac-SDKP and ACE levels were observed in the PCFF.

Ac-SDKP levels and corresponding ACE activities were plotted (Figure 2-7) and a Pearson's correlation was performed. Similar to the Ac-SDKP/POP correlation analysis, a significant (R: -0.38, p=0.02) correlation was observed between Ac-SDKP and ACE levels.

Thus, it would appear from our results that Ac-SDKP levels in PCFF are influenced by both its rate of synthesis by POP and degradation by ACE.

2.5. Discussion

There were four main findings from this study. The first two key findings were that Ac-SDKP was detectable in both TB and control pericardial fluid and the levels of Ac-SDKP were significantly decreased in TB pericardial fluid compared to normal fluid confirming similar observations made in a proof of concept study reported by Ntsekhe *et al*. The third finding is that there was a significant increase in ACE activity in the pericardial fluid of those with TB. This novel finding which was noted only in pericardial fluid and not in serum and implicates local intra-pericardial TB bacillus induced inflammation as a key regulator of ACE activity. The finding is also important because It suggests that an increase in cleavage of Ac-SDKP by ACE is a potential mechanism for the observed decrease in Ac-SDKP levels. The fourth and final key finding in this study which the first is to investigate the presence of POP and its enzymatic activity in pericardial fluid, was that there were no notable differences in POP enzymatic levels or activities measured between participants with and without disease.

The measurement of Ac-SDKP as well as the rate-limiting enzyme responsible for its formation, POP suggests a possible local production of Ac-SDKP in the pericardium. Whilst it is not known whether the POP is produced within the pericardial, this is entirely possible as POP has been shown to be expressed in most human cell types including fibroblasts, epithelial, endothelial and mesenchymal cells (Goossens et al., 1996) (Myöhänen et al., 2012). The detection of ACE activity was expected as ACE has previously been detected in pericardial fluid (Gomes et al., 2008). Further, a mass spectrometric based technique was utilised to quantify the levels of RAAS metabolites in pericardial fluid in our group revealing the presence of AngI as well as AngII in the pericardial environment (data unpublished). Ac-SDKP levels correlated mildly but significantly with both ACE (R: -0.38) and POP (R: 0.46) levels. This is unsurprising as Ac-SDKP has a short half-life of approximately 80 minutes, suggesting that it is constantly being synthesised and degraded in tissues (Rieger et al., 1993). The local synthesis of Ac-SDKP would support a role for Ac-SDKP in pericardial homeostasis, thus strengthening our hypothesis that Ac-SDKP may be involved in the prevention of pathological fibrotic remodelling of the pericardium.

Levels of Ac-SDKP measured in our study (0.19ng/ml) were ultimately comparable to those measured by Ntsekhe. *et al*, (1.56ng/ml) in the affected population (this is because our Ac-SDKP measurement protocol did not include an extraction step which results in a roughly 10-fold increase in Ac-SDKP levels but increases intra-sample variability). Similarly, to Ntsekhe. *et al*,

significantly reduced Ac-SDKP concentrations were measured in TB pericardial fluid as compared to the controls. This was accompanied by an increase in ACE activity levels as measured by the ZFHL assay. However, POP activity levels were comparable between the TB+ and control groups. We thus conclude that the reduced Ac-SDKP levels are likely a result of increased cleavage by ACE in the pericardial environment. Interestingly, the upregulated Ac-SDKP levels in the pericardium were not accompanied by an decrease in serum ACE levels. A few studies have revealed an increase in ACE levels in instances of granulomatous lesions (Thillai et al., 2012)(Mehta et al., 1990), but the precise mechanism for the ACE upregulation is unknown. Importantly, accumulation of ACE is known to arise in cardiac inflammation through an influx of macrophages at the site of inflammation (Diet Frank et al., 1996).

Levels of Galectin-3 measured in our current disease population (median 7.38 ng/ml in TB+ and 8.37 in TB-) are also comparable to those observed by Ntsekhe (median 11ng/ml, IQR 7.55-15.60). Once again, we observed a similar trend with no significant increase in Gal-3 levels in the TB+ group. This finding corroborates observations by Fernandes et al., of no difference in plasma Gal-3 levels in patients with chronic constrictive pericarditis as compared to healthy individuals (Fernandes et al., 2020).

The Ac-SDKP/Gal-3 ratios did not reveal any significant difference. However, certain TB+ patients had disproportionately higher Ac-SDKP/Gal-3 which may constitute a predisposing factor for the development of fibrosis.

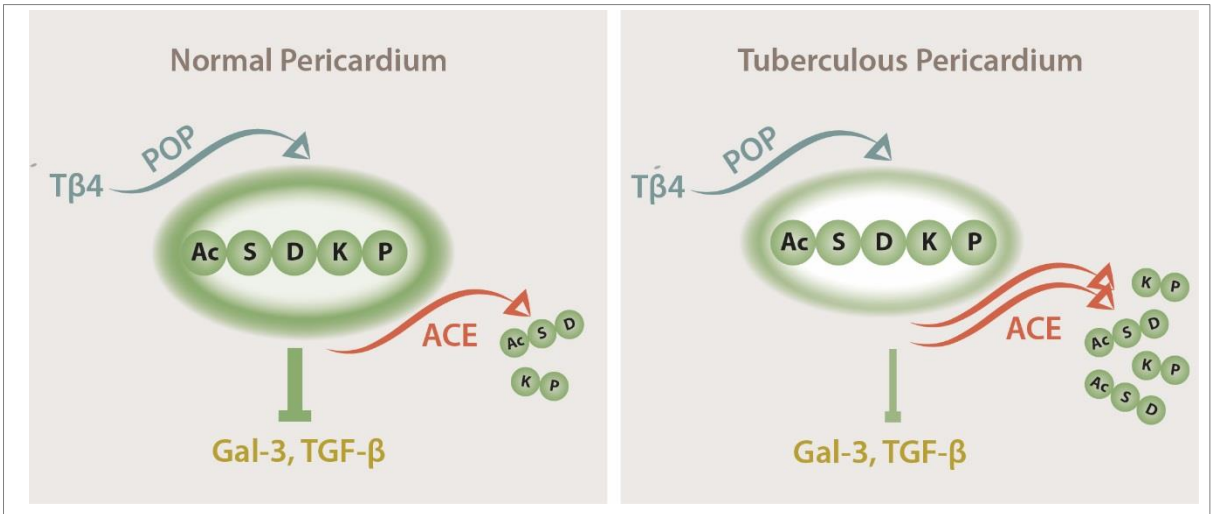

Figure 2-8: Dynamic Ac-SDKP metabolism in the normal versus tuberculous pericardium.
An increase in ACE in the TB pericardial fluid results in increased cleavage of Ac-SDKP and hence its lowered concentration. This is likely to result in a decrease in Gal-3 and TGF-β inhibition or an increase in fibrosis and fibrosis gene expression.

Pathophysiological processes in TB pericardial remodelling are likely to involve in part mesothelial cells of the pericardium which undergo EMT-like transition to demonstrate fibroblast-like morphology and function (Yáñez-Mó et al., 2003)(Mutsaers, 2002). Central to EMT transition and fibrotic gene expression are TGF-β signalling and in the cardiac context, Gal-3 (Zeisberg et al., 2007)(Ignotz and Massagué, 1986). Ac-SDKP is known to inhibit both Gal-3 and TGF- β, to prevent collagen deposition thus conferring a crucial protective role in fibrosis (Rhaleb et al., 2001a) (Peng et al., 2010).

The main complication of TB pericarditis is a reduction in visceral pericardial compliance which progresses to a constrictive pathophysiology. Chronic inflammatory and fibrotic processes are likely to be involved in this progression. A hypothesis driven study was performed by Ntsekhe *et al.*, to investigate the levels of the antifibrotic Ac-SDKP in TB pericarditis, revealing decreased levels in Ac-SDKP in TB pericardial fluid (Ntsekhe et al., 2012). We sought to confirm the finding of decreased Ac-SDKP levels in TB pericarditis and to further probe mechanisms of action for these diminished levels by investigating the enzymatic activities of POP and ACE which synthesise and degrade Ac-SDKP respectively. In general, our findings are consistent with previous observations by Ntsekhe *et al.* and confers reproducibility to the original findings. Further, we teased out a likely mechanism for the Ac-SDKP downregulation in TB pericardial fluid, implicating an overactive RAAS in the pericardial milieu (Figure 2-8). These findings thus form the basis for future investigations into the deregulated RAAS in TB pericarditis. This could provide exciting new avenues for the management of TB pericarditis with widely available RAAS therapeutics including ACEi.

3. The molecular specificity of the antifibrotic action of Ac-SDKP

3.1. Background

Angiotensin Converting Enzyme inhibitors (ACEi) reverses cardiac fibrosis in patients in various models of heart disease, an effect that was found to be independent of blood pressure regulation (Brilla et al., 2000)(Brilla et al., 1991)(Brown et al., 1999). This suggests an alternative mechanism for fibrosis protection and reversal that is not mediated by a reduction in the pro-inflammatory AngII levels. These findings, coupled with the findings of increased plasma Ac-SDKP levels in the presence of an ACEi, led to the suggestion that Ac-SDKP may be the alternative pathway through which fibrosis prevention occurs and spawned a number of studies to investigate the antifibrotic action of Ac-SDKP (Azizi et al., 1996)(Rhaleb et al., 2001a)(Peng et al., 2001).

This hypothesis-driven approach confirmed the antifibrotic effects of Ac-SDKP, and in 2007 Cavasin *et al.* robustly demonstrated the physiological importance of Ac-SDKP in preventing disseminated multi-organ fibrosis. Studies into the molecular mechanisms of action of Ac-SDKP have largely focused on well-established fibrotic pathways and mediators, particularly the TGF-β/Smad and MAPK pathways (Pokharel et al., 2002)(Zhuo et al., 2007).

While both our own group and other groups have established that Ac-SDKP inhibits TGF-β/Smad signalling to prevent collagen deposition, the precise physiological effects and mechanisms of actions of Ac-SDKP remain unclear and are likely to be more complex and to involve other signalling pathways (Kanasaki et al., 2003)(Pokharel et al., 2004)(Lin et al., 2008)(Castoldi et al., 2010). In particular, a better knowledge of the extracellular and intracellular proteins that are regulated by Ac-SDKP and elucidating the related complex regulatory networks would improve the current understanding of the Ac-SDKP mechanisms of action and identify potential targets for the physiological modulation of fibrosis.

An analysis encompassing the whole cell machinery and extracellular environment would facilitate the ability to obtain a complete snapshot of the proteins and processes regulated by Ac-SDKP. One approach that would enable such a comprehensive analysis is mass spectrometry (MS)-based discovery proteomics (Aebersold and Mann, 2003). The robustness of mass

spectrometry in the identification of proteins from small amounts of starting material has led to its widespread use in proteomic analysis (Aebersold and Mann, 2003).

The two main approaches to MS-based proteomics are top-down and bottom-up proteomics (Zhang et al., 2013). The former involves the study of proteins as intact entities, while bottom up proteomics refers to the identification of peptides generated by enzymatic digestion of intact proteins. Bottom-up proteomics is generally experimentally and computationally less complex than top-down and is therefore more commonly used. A schematic of a typical bottom-up proteomic approach is shown in Figure 3-1.

A mass spectrometer comprises an ion source and a mass analyser to measure the mass-to-charge ratio (m/z) of ionised analytes, which is registered by a detector. Large biomolecules such as peptides are ionised primarily by electrospray ionisation (ESI) when they are in a mobile or liquid phase, or by matrix assisted laser desorption ionisation (MALDI), where a sample is spotted onto an energy-absorbing matrix prior to desorption and laser-induced ionisation of the matrix (Ho et al., 2003)(Caprioli et al., 1997). Following ionisation, peptide ions are detected by the mass analyser. The four main types of mass analysers include the ion trap, time-of-flight (TOF), quadrupole, and Fourier transform ion cyclotron (FT-MS) analysers. These analysers each exploit diverse physical properties of ions to determine their m/z, and can either be used alone or in combination (Aebersold and Mann, 2003).

For the analysis of complex samples, integrated liquid chromatography (LC) ESI-MS systems are favoured as high-performance LC allows separation of peptides over time for higher rates of identification. In the current study, a Q-Exactive hybrid quadrupole-Orbitrap (Thermo) was used. Ion trap analysers in which ions are 'trapped' prior to MS analysis are known for their robustness and sensitivity, but have the inherent disadvantage of lower mass accuracy (Aebersold and Mann, 2003). Orbitraps operate by trapping ions in an orbital motion around a central spindle electrode (Hu et al., 2005) and then Fourier transforming the resultant rotational signal into mass spectra. Orbitraps have an excellent mass accuracy and are extremely fast, and therefore are well suited to the analysis of complex samples. Quadrupoles are parallel charged rods that allow analytes with a specific m/z to pass through the field in their centre. The Q-Exactive features a combination of a quadrupole mass filter with an Orbitrap analyser to produce a high resolution instrument that is widely used in proteomic analysis (Michalski et al., 2011). The benefits of this hybrid technology are excellent speed, resolution, and mass accuracy, all of which contribute to the popularity of this platform in modern proteomics workflows.

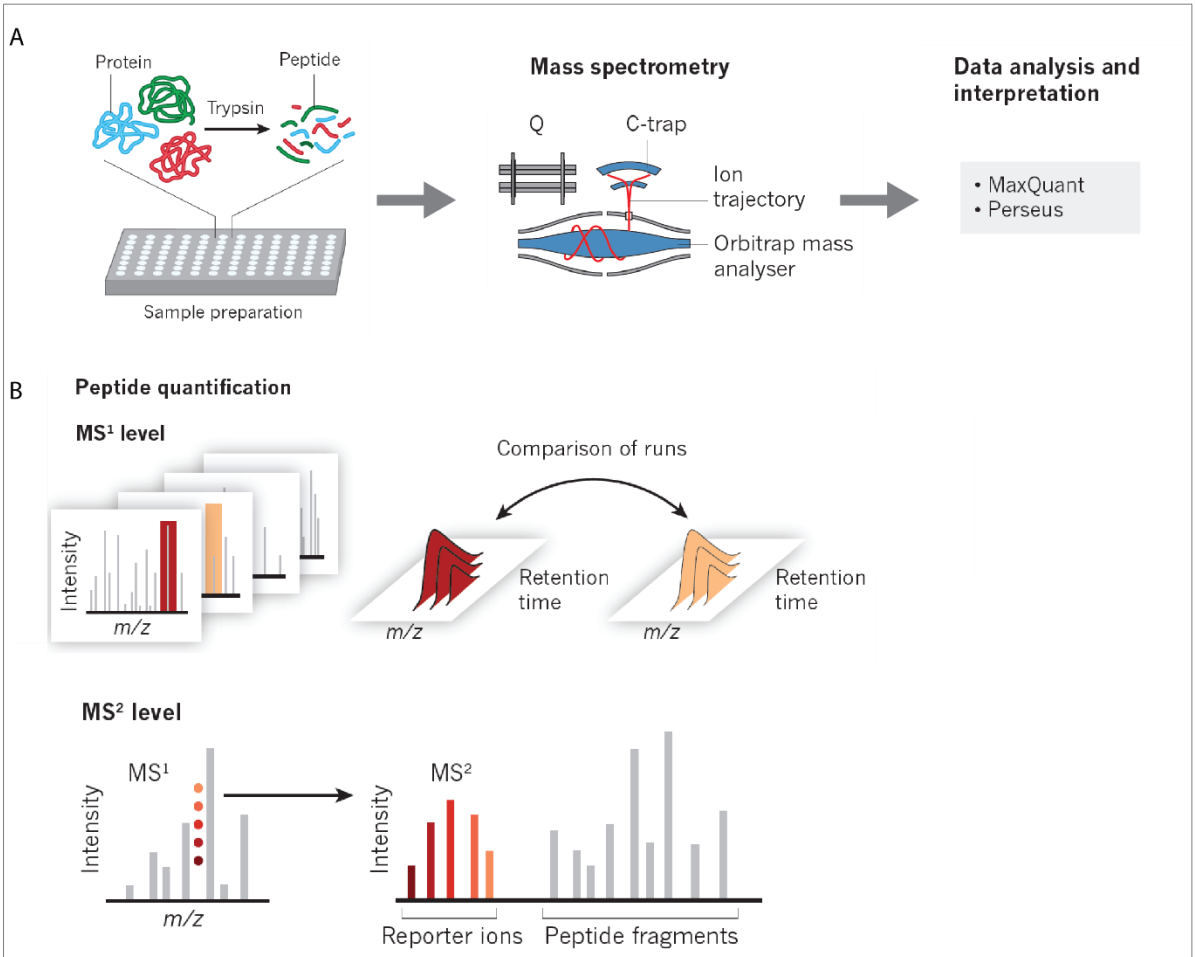

Figure 3-1: Bottom-up discovery proteomics workflow.

A. Sample preparation involves the extraction and digestion of proteins by a sequence-specific enzyme, trypsin being the most commonly used. Peptides are then separated by HPLC, ionized, and filtered by a quadrupole prior to detection in the Orbitrap mass analyser to obtain MS1 and MS2 scans. Raw MS data can be interpreted using software packages such as MaxQuant and the downstream Perseus environment.

B. Peptide quantification generally uses the intensity of the MS1 peak of the precursor ion as a proxy for peptide quantity. MS2 scans of the fragmented precursors then allow identification of the parent ion. Advanced alignment and normalisation algorithms can be used to compare different peptides across multiple runs, enabling label-free quantitative proteomics. Image adapted from **(Aebersold and Mann, 2016)**.

3.2. Study objectives

The objective of the present chapter is to investigate the molecular effects of Ac-SDKP by using MS-based discovery proteomics to survey the intracellular and extracellular proteins that are regulated by Ac-SDKP through the:

1. identification, through label free quantification, of differentially expressed proteins upon Ac-SDKP treatment of TGF-β stimulated fibroblasts.
2. characterisation of these differentially expressed proteins using gene ontology terms to clarify the mechanisms of Ac-SDKP protein modulation.

3.3. Materials and Methods

3.3.1. Cell culture

WI-38 (American Type Culture Collection- ATCC® CCL-75™) lung fibroblasts (a kind gift from the Leaner group, UCT) were used to assess the effects of Ac-SDKP on intracellular and secreted protein levels. The cells were reconstituted into 75 cm^2 flasks and grown in 10 ml of growth medium (100% HAMS-F12 (Sigma, USA), 20 mM HEPES buffer, pH 7.5, supplemented with 10% foetal calf serum (FCS) [heat-inactivated for 30 min at 56°C], and 1% Non-Essential Amino Acids (BioWhittaker®, USA). Cells were grown to 70% confluency, lifted using Trypsin-EDTA (Gibco®, USA) and seeded into 10 cm dishes. All flasks and plates were incubated at 37°C, 5% CO_2 and 80% humidity.

3.3.2. Treatment with Ac-SDKP

Cells were treated with 100 nM Ac-SDKP for 1 h prior to TGF-β stimulation to induce fibrosis. TGF-β (5 ng/ml) was added in the presence of ascorbic acid (50 µg/ml) for 6 to 48 h. To assess the effects of Ac-SDKP, cells in a 75 cm^2 flask were lysed in 300 µl of radioimmunoprecipitation assay buffer (RIPA) (100 mM Tris-HCl, pH 7.6, 1% SDS, 150 mM NaCl, 0.5% Sodium deoxycholate, with 1 mM PMSF-supplemented protease inhibitor cocktail (Set III, Calbiochem, USA)). The lysate was centrifuged at 10000 *g* at 4°C and the supernatant was removed for downstream analysis.

3.3.3. Sample preparation

3.3.3.1. Protein quantitation and concentration

Protein quantitation from the cell lysates and cell culture supernatants was performed in parallel according to the Biorad Protein Assay Kit (Bio-Rad, USA). Bovine serum albumin (BSA) was used as a standard and absorbance was read at 595 nm on a Biorad iMark™ microplate reader using the Microplate Manager software (version 6.1).

3.3.3.2. Cell supernatant concentration and purification

The concentration of protein available in the culture supernatant is extremely low due to the high volume of the culture medium. In addition, the culture supernatant contains potential contaminants that may affect downstream MS analysis. Prior to tryptic digest, the cell supernatant samples were therefore first concentrated centrifugally on a 10 kDA molecular weight cut off filter (MWCO) (Merck, USA), and then purified by methanol chloroform precipitation at room temperature. Aliquots of concentrated cell culture supernatant (400 µl) were mixed with 400 µl of methanol by vortexing. Subsequently, 400 µl of chloroform was added, and the mixture was vortexed again. The sample was then centrifuged at 13 000 rpm for 5 min and the aqueous methanol layer was carefully removed from the top of the sample, preserving the protein interphase. The proteins were then washed with 300 µl of methanol by vortexing and pelleted by centrifuging at 13 000 rpm for 15 minutes. The supernatant was gently decanted taking care not to dislodge the pellet. The protein pellet was air dried before being resuspended in 100 µl deionised water and quantified using as per *3.3.3.1*.

3.3.3.3. Filter aided sample preparation (FASP)

Filter aided sample preparation (FASP) was used to obtain tryptic digests of all samples for the discovery proteomics experiments (Wiśniewski, 2017). Briefly, 200 µg of cell lysate or precipitated proteins from cell culture supernatants (see 3.3.2 and 3.3.3.2) were denatured by incubating with 0.1 M DTT in 50 mM NH_4CO_3 buffer for 30 mins. The denatured proteins were loaded onto a 30 kDa molecular weight cut off filter (Millipore) and buffer exchange was performed with a urea buffer (8 M Urea, 0.1 M Tris; pH 8.5). The proteins were then alkylated with 0.05 M iodoacetamide (prepared in 50 mM NH_4CO_3) for 20 minutes in the dark at room temperature. The samples were washed with an 8 M urea solution twice prior to buffer exchange with 50 mM NH_4CO_3 three times. Tryptic digest was performed using a 1:100 trypsin to protein ratio. Trypsin (Promega, USA) was reconstituted in 50 mM NH_4CO_3 buffer containing 20 mM $CaCl_2$, and samples were incubated in a wet chamber at 37°C for 16 hours. Peptides were eluted by centrifuging the filter units at 15 000 rpm for 10 mins, followed by a second wash with 40 µl NH_4CO_3 which was centrifuged under the same conditions. The enzymatic reaction was stopped by the addition of formic acid (FA) to a final concentration of 0.1%.

3.3.3.4. **Sample desalting**

Prior to MS analysis, tryptic peptides were desalted on a C18 stage tip packed in-house with 2 x 5 µg binding capacity C18 resin discs (Millipore, USA) to remove any potentially contaminating salts. C18 stage tips were activated with 80% MS grade acetonitrile (ACN) acidified with 0.1% FA (Sigma, USA). Each stage tip was then equilibrated with 2% ACN with 0.1% FA prior to loading 10 µg of peptide from each sample. The samples were washed in 2% ACN acidified with 0.1% FA a total of three times. Peptides were then eluted into glass vials with 60% ACN acidified with 0.1 % FA. Desalted peptides were thereafter dried in a Savant^{TM} SpeedyVac (ThermoFischer Scientific, USA) and resuspended in 2% ACN and 0.1% FA for MS analysis.

3.3.4. Mass spectrometry

Desalted tryptic digests were analysed by liquid chromatography tandem MS (LC-MS/MS) on a Q-Exactive (QE) quadrupole-orbitrap MS coupled to a Dionex Ultimate 3500 RSLC nano LC system (Thermo Scientific, USA). The sample was loaded on a 30 cm C18 analytical column packed in-house with Aeris peptide 3.6 µM beads (Phenomenex, USA). Thereafter, elution was carried out using a curved gradient of 6-40% acetonitrile and 0.1% formic acid at a constant flow rate of 300 nl/min over 120 minutes. MS scan parameters are outlined in Table 3-1 below. Data acquisition was performed using Xcalibur software (Thermo scientific, v2.2).

Table 3-1: Mass spectrometry parameter settings

MS LEVEL	PARAMETER	SETTINGS
MS1	Run time	120 minutes
	Polarity	positive
	Default charge state	2
	Scan range	300-1750 m/z
	Resolution	70000
	Automatic gain control target	3e6
	Maximum injection time	250 ms
MS2	Resolution	17500
	Automatic gain control target	5e4
	Maximum injection time	80 ms
	TopN	10
	Isolation window	2 m/z
	Scan range	200-2000 m/z
	Intensity threshold	6.3e3
	Dynamic exclusion	30 s

3.3.5. Data processing and analysis

Raw data processing was performed using MaxQuant software (version) for peptide identification and label free quantification (LFQ) (Cox and Mann, 2008). Settings were set to default with the following modifications: a fixed modification of carbamidomethylation and variable modifications of oxidation and acetylation were selected. The false discovery rate (FDR) was set at 1% against a reverse decoy of the database and 2 missed cleavages were allowed. Unique peptides were used in the identification of protein groups. Andromeda, the inbuilt search engine in MaxQuant, was used for protein group identification against the 2018 UniProt Human proteome database. The LFQ algorithm was selected for quantification and only protein groups identified in all replicates from each treatment condition, and which satisfied a posterior error probability (PEP) score of lower than 0.01, were used for all downstream analysis.

Initial protein group analysis was performed with Perseus (version 1.6.1.3). All peptides identified as contaminants, reverse/decoy, or identified only by site were excluded. A Student's t-test was performed to compare the different treatment groups and a p-value < 0.05 was used as a cut-off for significance.

3.3.6. Functional enrichment and interaction analysis

For the analysis of protein-protein interaction, search tool for the retrieval of interacting genes/proteins (STRING) was used (https://string-db.org/)(Szklarczyk et al., 2017). Active interaction sources were set to only include 'experiments' and databases and network edges were set to indicate confidence with thicker lines being indicative of the strength of data support. The level of confidence was set at high confidence for the proteome but at medium confidence for the secretome, given the smaller data set.

Functional classification analysis and gene annotation were performed using the Biological Networks Gene Ontology tool (BiNGO) on biological networks visualized in Cytoscape version 3.7.2 (Maere et al., 2005) (Shannon et al., 2003). Significantly overrepresented Gene Ontology (GO) terms were determined using a hypergeometric test with a significance threshold of 0.05. Resulting p-values were corrected by applying the Benjamini-Hochberg false discovery rate. Proteins were compared against the full human annotation GO database for the proteome and against the ExoCarta database for the secretome. ExoCarta is a manually curated web-based compendium of exosomal proteins, RNAs and lipids (http://www.exocarta.org/)(Simpson et al., 2012). To summarise long lists of GO terms generated from BiNGO, the clustering algorithm REVIGO was used (http://revigo.irb.hr/)(Supek et al., 2011).

Pathway analysis was performed in Reactome to investigate biological pathways (https://reactome.org/)(Croft et al., 2011).

3.4. Results

3.4.1. Proteome and secretome MS data

3.4.1.1. Proteome and secretome raw data processing

Acquisition of MS1 and MS2 data from label-free peptides generated from lysates and cell culture supernatants of Ac-SDKP treated or untreated fibroblasts was performed on a QE MS instrument as described in 3.3.4. Representative chromatograms of the total ion counts (TIC) and MS2 data are presented in Figure 3-2.

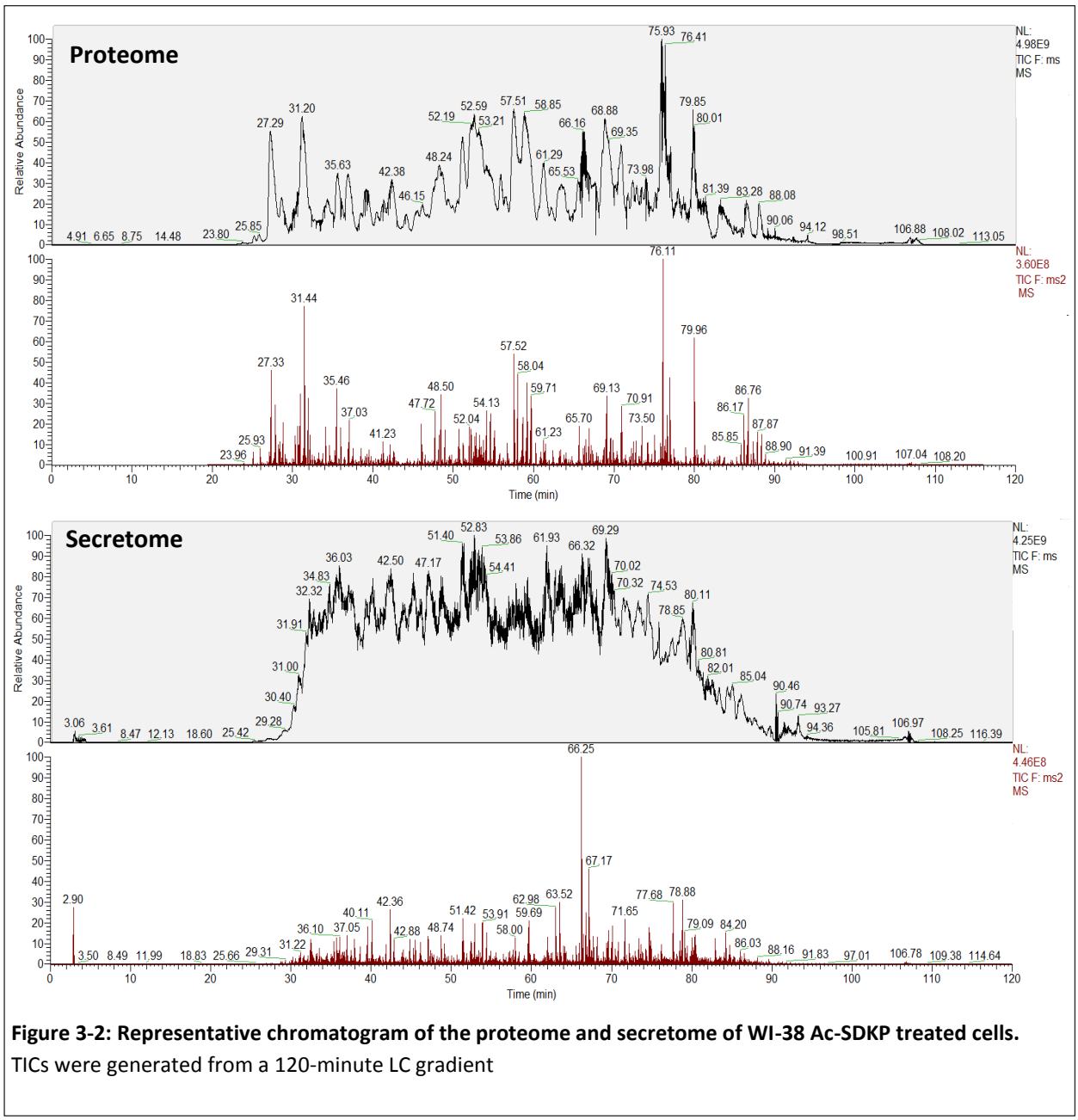

Figure 3-2: Representative chromatogram of the proteome and secretome of WI-38 Ac-SDKP treated cells. TICs were generated from a 120-minute LC gradient

Raw data files were analysed using the MaxQuant software package. A total of 102103 spectra from fibroblast lysates were submitted for analysis, of which 44.8% were identified and mapped to human peptides from the Uniprot database. These corresponded to 2870 protein groups, of which 1210 (FDR < 0.01) were present across all triplicates. The percentage of contaminants across all samples was 0.59% of total protein groups, and the percentage of decoy hits was 0.87%. The number of missed cleavages is depicted in Figure 3-3A.

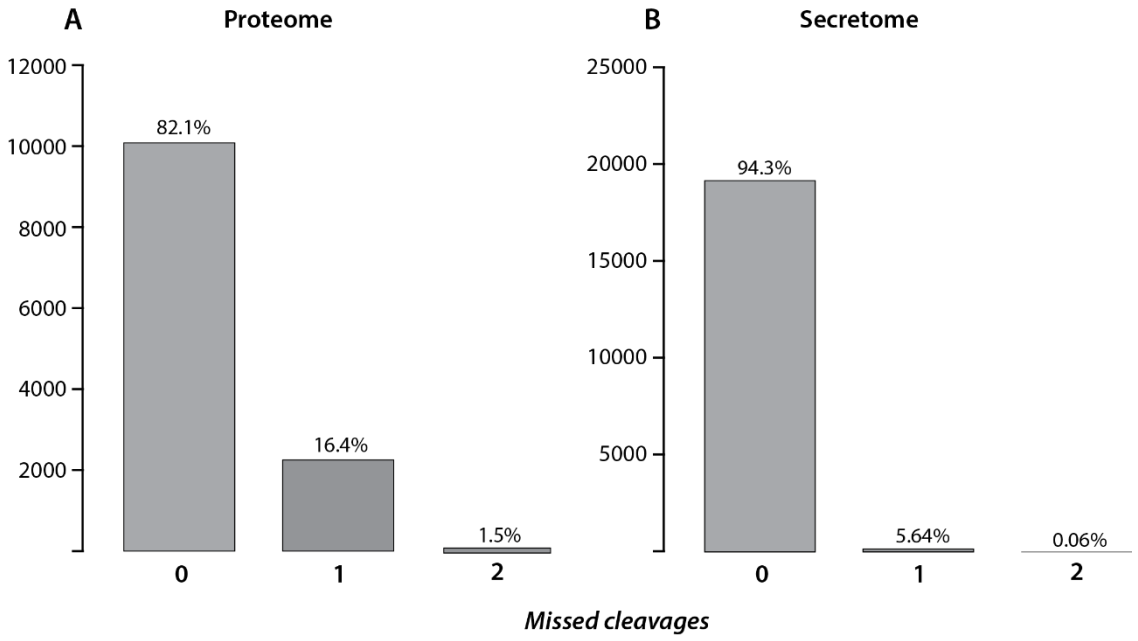

Figure 3-3: Assessment of tryptic digest efficiency.
Both the proteome and secretome display good tryptic digest efficiency with 82.1% and 94.3% of no missed cleavages respectively.

A total of 149110 spectra from the cell culture medium were submitted for analysis but only 14.1% of spectra were identified and mapped to the Uniprot database. This was likely due to the presence of a low concentration of foetal calf proteins in the cell culture supernatant, which were excluded in the peptide mapping. A challenge in the profiling of secreted proteins in a cell culture environment arises as a result of overlap between bovine and human peptide sequences. This is especially relevant for extracellular proteins including fibronectin, fibulin-1, and pigment epithelium derived factor, which share up to 90% sequence similarity to their human counterparts (Hathout, 2007). The quantification of proteins in the secretome was performed using only peptide sequences that are unique to human proteins. A total of 6470 peptides mapping to 315

human protein groups were detected in the cell culture supernatant, with 189 being detected across all replicates. The proportion of missed cleavages is presented in Figure 3-3B.

3.4.1.2. Proteome and secretome data quality and quantification

Label-free quantitative proteomic methods, including the MaxQuant LFQ algorithm, are inherently less sensitive than label-based methods such as stable isotope labelling by/with amino acids in cell culture (SILAC) and isobaric tags for relative and absolute quantitation (iTRAQ). It was thus important to establish that any observed differences in protein levels between the treated and control groups were not caused by technical variation. The correlation between biological replicates of both the proteome and secretome were assessed using Pearson's co-efficient, which was greater than 0.95 across all comparisons (Figure 3-4). This indicated that the technical variation between replicates was minimal.

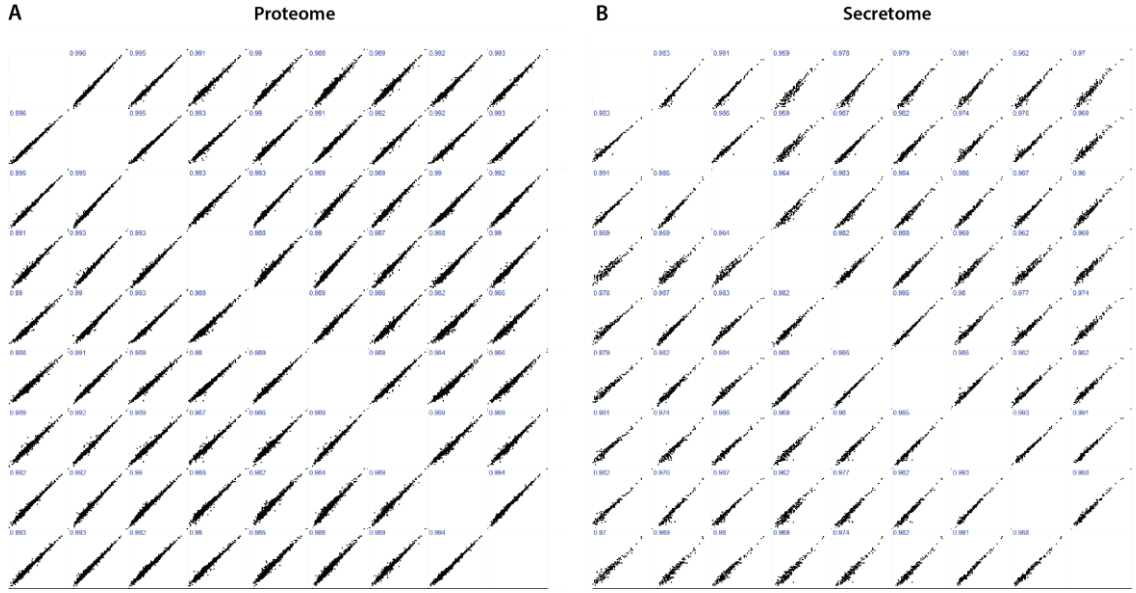

Figure 3-4: Scatterplot of the biological triplicates.
A. The proteome and B. secretome triplicates were compared using Pearson's correlation co-efficient (R^2) indicated in blue.

3.4.2. Effect of Ac-SDKP treatment on the secretome

A total of 58 proteins were found to have significantly different expression levels ($p<0.05$). Of these 23 proteins had higher expression levels and 35 proteins had decreased expression levels in the Ac-SDKP group. The fold change in protein expression levels ranged from 1.67- to 5.19- fold with an average of 3.25- fold change.

3.4.2.1. STRING interactions of differentially expressed proteins

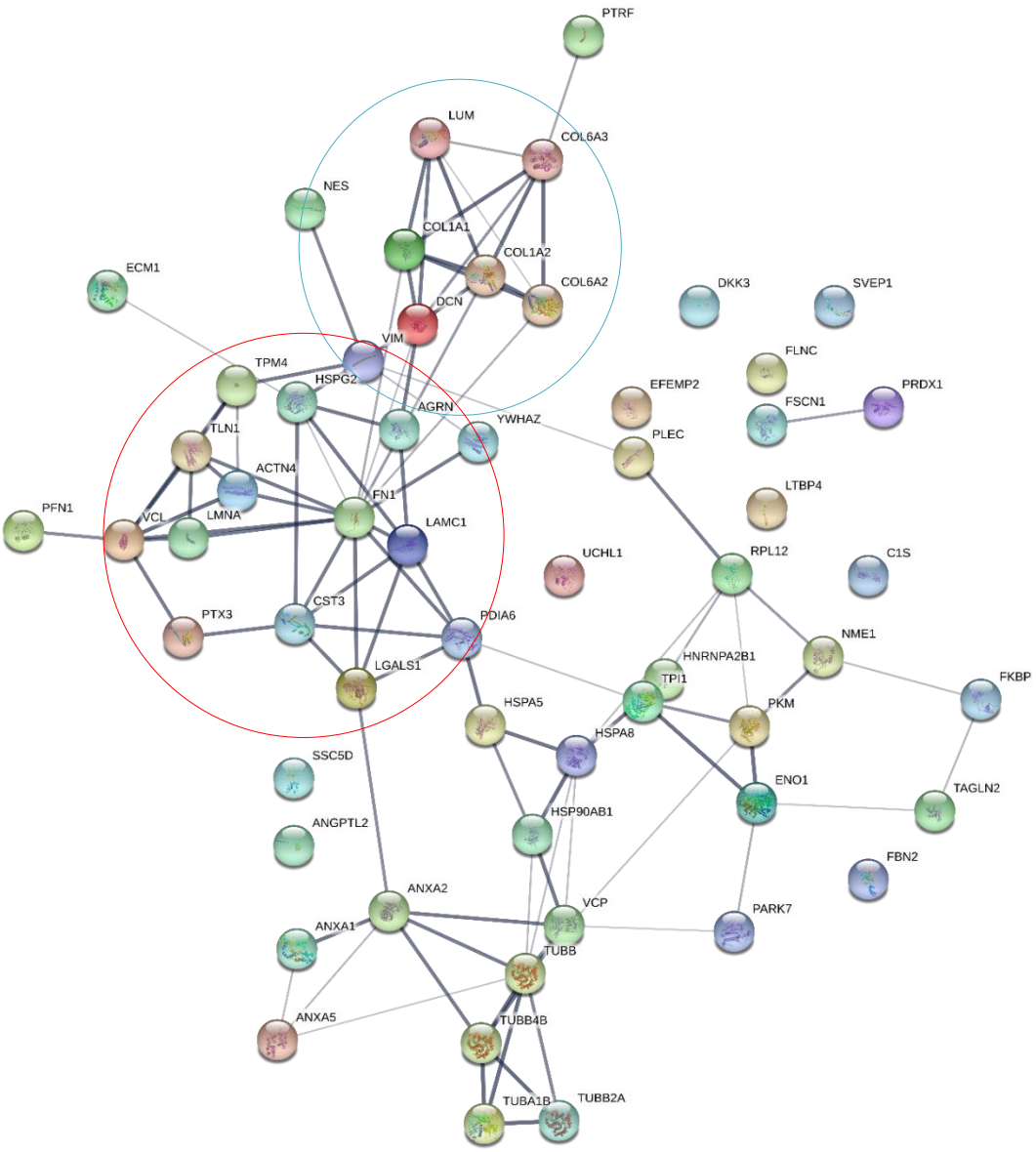

Figure 3-5: String interactions of differentially expressed protein groups in the secretome following Ac-SDKP treatment.

In order to visualise the interactions between the significant protein groups, String analysis was performed (Figure 3-5). The STRING database contains all published interactions between proteins (Szklarczyk et al., 2017). The protein interaction network contains 58 nodes with 99 protein-protein interactions. The interactions with the strongest evidence (thicker lines) revealed two clusters involved in extracellular matrix remodelling: a first cluster of collagen and ECM proteins circled in blue, and a second cluster of inflammatory and EMC modulating proteins circled in red.

3.4.2.2. **GO enrichment of differentially expressed secretome proteins**

To identify the relevant biological pathways that were significantly modulated by Ac-SDKP treatment, GO term enrichment was performed using BiNGO in Cytoscape. The string network analysis from *3.4.2.1* was used as the input network in Cytoscape.

A total of 40 biological pathway terms and 29 molecular function terms were significantly enriched ($p < 0.05$) in the Ac-SDKP treated secretome.

In the Molecular Function category, the two most significantly differentially expressed proteins mapped primarily to *extracellular matrix organization (GO:0030198)* and to *extracellular structure organization (GO:0043062)*(Table 3-2)(Figure 3-6).

Enriched biological functions in the secretome included *structural molecule activity (GO:0005198*), *extracellular matrix structural constituent (GO:0005201), phospholipase inhibitor activity (GO:0004859)* and *extracellular matrix binding (GO:0050840)* among others (Table 3-3)(Figure 3-6).

Table 3-2: Top 10 enriched molecular functions in the secretome

GO ID	GO Description	p-value
30198	extracellular matrix organization	2.54E-06
43062	extracellular structure organization	2.54E-06
32501	multicellular organismal process	2.54E-05
48731	system development	5.20E-05
16043	cellular component organization	7.28E-05
48856	anatomical structure development	1.93E-04
7275	multicellular organismal development	1.93E-04
48513	organ development	4.39E-04
32502	developmental process	1.05E-03
30199	collagen fibril organization	1.97E-03

Table 3-3: Top 10 enriched biological processes in the secretome

GO ID	GO Description	p-value
5198	structural molecule activity	2.52E-11
5201	extracellular matrix structural constituent	8.61E-9
4859	phospholipase inhibitor activity	3.50E-5
50840	extracellular matrix binding	5.01E-5
5509	calcium ion binding	8.94E-5
30674	protein binding, bridging	1.00E-4
55102	lipase inhibitor activity	1.01E-4
43236	laminin binding	1.34E-4
5544	calcium-dependent phospholipid binding	2.72E-4
4857	enzyme inhibitor activity	3.49E-4

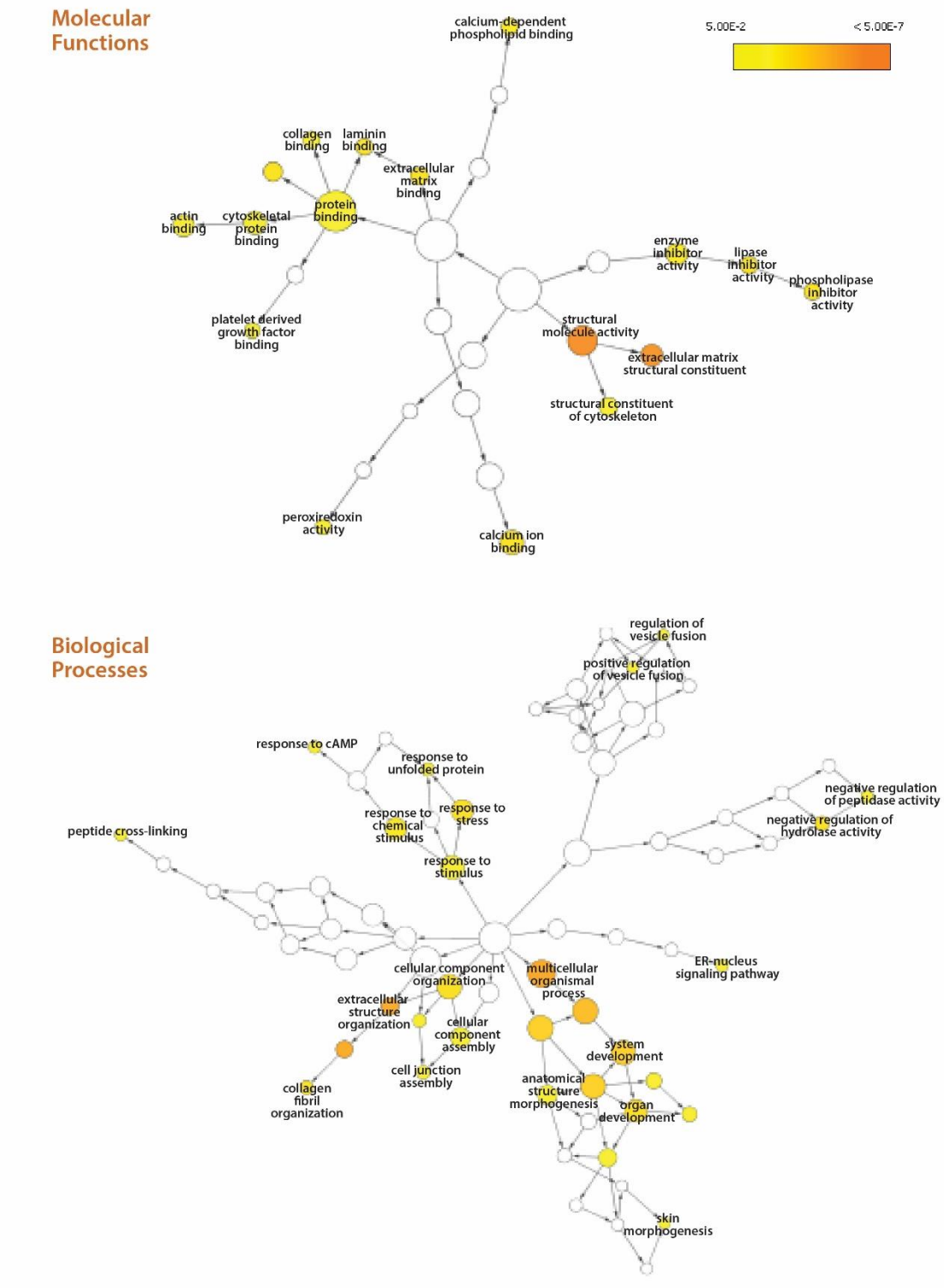

Figure 3-6: BiNGO generated biological processes and molecular function networks for differentially expressed proteins in the secretome of Ac-SDKP treated fibroblasts.

Colour of the nodes is indicative of the p-value for the statistical significance of the enrichment of a GO term while node size is indicative of the number of proteins associated with a GO term.

3.4.2.3. Enriched Reactome pathways in the secretome

To investigate which pathways are affected by Ac-SDKP in the secretome, the differentially expressed protein list was input into the online Reactome Pathway Database. The top 10 results are shown in Table 3-4 below).

Table 3-4: Ac-SDKP mediated Reactome pathway enrichment in the secretome

Pathway name	Entities				Reactions	
	found	ratio	pValue	FDR	found	ratio
ECM proteoglycans	10/79	0.006	3.18E-11	1.16E-08	14/23	0.00187
Extracellular matrix organization	15/329	0.024	4.55E-10	8.32E-08	120/318	0.02584
Interleukin-4 and Interleukin-13 signalling	12/211	0.015	2.64E-09	3.22E-07	3/46	0.00374
Integrin cell surface interactions	8/86	0.007	3.47E-08	3.16E-06	10/54	0.00439
Signalling by Interleukins	17/639	0.045	8.08E-08	4.89E-06	7/490	0.03981
Platelet degranulation	9/137	0.010	8.81E-08	4.89E-06	5/11	8.94E-04
Platelet activation, signalling and aggregation	12/293	0.021	9.41E-08	4.89E-06	37/114	0.00926
Response to elevated platelet cytosolic Ca2+	9/144	0.010	1.34E-07	6.01E-06	5/14	0.00114
HSP90 chaperone cycle for steroid hormone receptors (SHR)	7/70	0.005	1.60E-07	6.05E-06	12/12	9.75E-04
Degradation of the extracellular matrix	9/148	0.010	1.68E-07	6.05E-06	19/105	0.00853

The most enriched pathways include *ECM proteoglycans*, *Extracellular matrix organization*, *Interleukin-4 and Interleukin-13 signalling,* and *Signalling by Interleukins*. These findings support a role for Ac-SDKP in the modulation of the extracellular matrix.

3.4.2.4. Fibrotic proteins identified in the secretome

Some of the differentially regulated secretome proteins may be involved in conferring the antifibrotic effect of Ac-SDKP. The Reactome pathway analysis data was manually scanned to identify pathways and their respective entity proteins likely to be involved in the fibrotic processes (Table 3-5).

Table 3-5: Reactome pathways entities putatively involved in the fibrotic process in the secretome

Reactome Groups	Protein Entities
ECM proteoglycans	*LAMC1 FN1 COL6A3 LUM COL6A2 COL1A1 COL1A2 AGRN DCN HSPG2*
Extracellular matrix organisation ***Collagen chain trimerisation*** ***Collagen formation*** ***Collagen degradation***	*LAMC1 COL6A3 COL6A2 FBN2 EFEMP2 PLEC AGRN FN1 LTBP4 LUM COL1A1 COL1A2 DCN HSPG2*
Interleukin-4 and Interleukin-13 signalling	*FN1 FSCN1 VIM HSPA8 ANXA1 COL1A2*
Degradation of the extracellular matrix	*COL1A1 FBN2 COL1A2 COL6A2 FN1 COL6A3 LAMC1 HSPG2 DCN*
Signalling by TGF-beta family members ***TGF-beta receptor signalling in EMT (epithelial to mesenchymal transition)***	*FKBP1A COL1A2*

The proteins identified are listed by name in Table 3-5 and grouped according to whether they were over-expressed or under-expressed in the Ac-SDKP treated secretome (Table 3-6). Ac-SDKP is seen to lead to a decrease in the expression of various collagens and ECM proteins as well as TGF-β mediated proteins (*Latent-transforming growth factor beta-binding protein 4* and *Peptidyl-prolyl cis-trans isomerase).* However, Ac-SDKP treatment led to a decrease in the expression of some tubulins and other filament proteins.

Table 3-6: Ac-SDKP mediated differentially secreted proteins putatively involved in the fibrotic process

Up regulated proteins	Down regulated proteins
Heat shock protein HSP 90-beta	*Collagen alpha-3(VI) chain*
Plectin	*Collagen alpha-2(VI) chain*
	Collagen alpha-2(I) chain
	Collagen alpha-1(I) chain
	Lumican
	Decorin
	Agrin
	Fibronectin-1
	Fibrillin-2
	Laminin subunit gamma-1
	Filamin-C
	Tropomyosin alpha-4 chain
	Talin-1
	EGF-containing fibulin-like extracellular matrix protein 2
	Latent-transforming growth factor beta-binding protein 4
	Peptidyl-prolyl cis-trans isomerase

3.4.3. Effect of Ac-SDKP on the proteome

3.4.3.1. STRING interactions of differentially expressed proteins in the proteome

In the proteome, a total of 114 differentially expressed proteins were identified between the Ac-SDKP and TGF-β-only treated proteomes following Student's t-test comparisons ($p < 0.05$). Of these 52 proteins had higher expression levels and 62 proteins had decreased expression levels in the Ac-SDKP group. The fold change in protein expression levels ranged from 1.21- to 4.85- fold with an average of 3.15- fold change.

String analysis of differentially regulated proteins in the proteome revealed multiple clusters in the interaction network including i) proteins of the cellular transcription and translation machinery, and ii) fibrotic and inflammatory proteins (Figure 3-7).

Fibrotic and inflammatory proteins are circled in red and magnified in Figure 3-7.

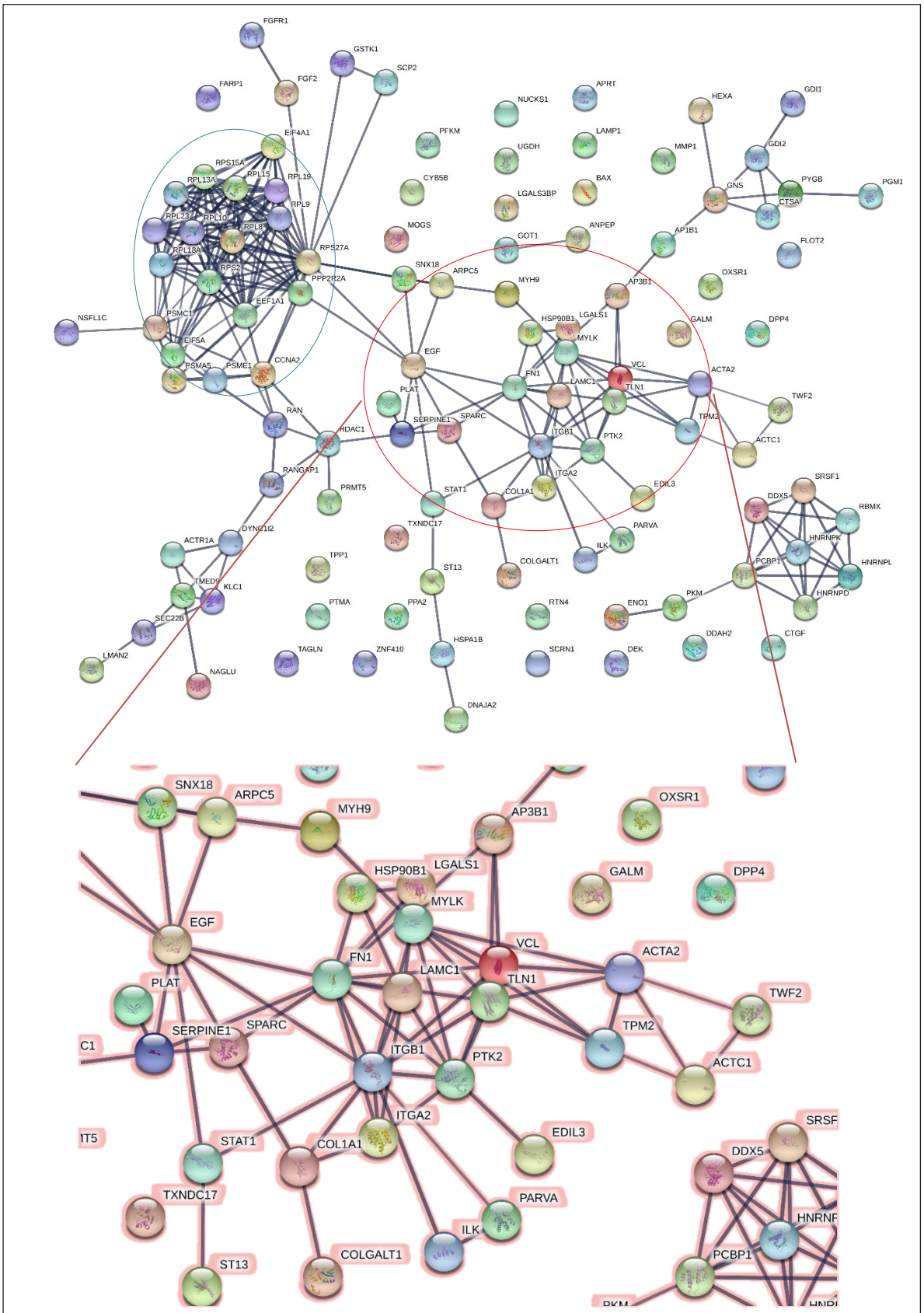

Figure 3-7: String interaction network of Ac-SDKP differentially expressed protein groups in the proteome.

The cluster with the most evidence contains proteins of the cellular transcription and translation machinery**.**

3.4.3.1. GO enrichment of differentially expressed proteome proteins

In the Ac-SDKP treated proteome, 34 molecular function terms and 201 biological pathway terms were significantly enriched ($p < 0.05$) in BiNGO (Figure 3-8). BiNGO terms for the biological pathways were further summarised using REVIGO.

The most highly enriched molecular functions (Table 3-7) in the proteome were *protein binding (GO:0005515)* and *structural constituent of ribosome (GO:0003735)*. *Extracellular matrix binding (GO:0005201)*, *integrin binding (GO:0005178)* and *collagen binding (GO:0005518)* were also among the top 10 most significantly enriched functions.

Differentially expressed proteins were enriched in the biological process category (Table 3-8) for *angiogenesis (GO:0009987)*, *translation elongation (GO:0008152),* and *protein localization (GO:0051179)*. Interestingly, significantly enriched processes also included *fibroblast growth factor receptor signaling (GO:0008543)*, *extracellular matrix organization (GO:0030198)*, *regulation of collagen biosynthetic pathway (GO:0032965)* and *regulation of programmed cell death (GO:0043067)* (Figure 3-8).

Table 3-7: Top 10 BiNGO enriched molecular functions in the proteome

GO ID	GO Description	p-value
5515	protein binding	2.99E-07
3735	structural constituent of ribosome	2.27E-06
5198	structural molecule activity	1.91E-05
3723	RNA binding	5.17E-05
5488	binding	9.40E-05
50840	extracellular matrix binding	3.53E-03
5178	integrin binding	4.05E-03
5093	Rab GDP-dissociation inhibitor activity	4.05E-03
5518	collagen binding	5.81E-03
5515	protein binding	2.99E-07

Table 3-8: Top 10 REVIGO sorted enriched biological processes in the proteome

GO ID	GO Description	log10 p-value
1525	angiogenesis	-4.3958
6414	translational elongation	-7.7545
8104	protein localization	-4.3958
8152	metabolic process	-4.7033
9987	cellular process	-2.6364
22610	biological adhesion	-1.6402
31589	cell-substrate adhesion	-3.1421
32501	multicellular organismal process	-0.4318
32502	developmental process	-0.8356
40011	locomotion	-1.4815

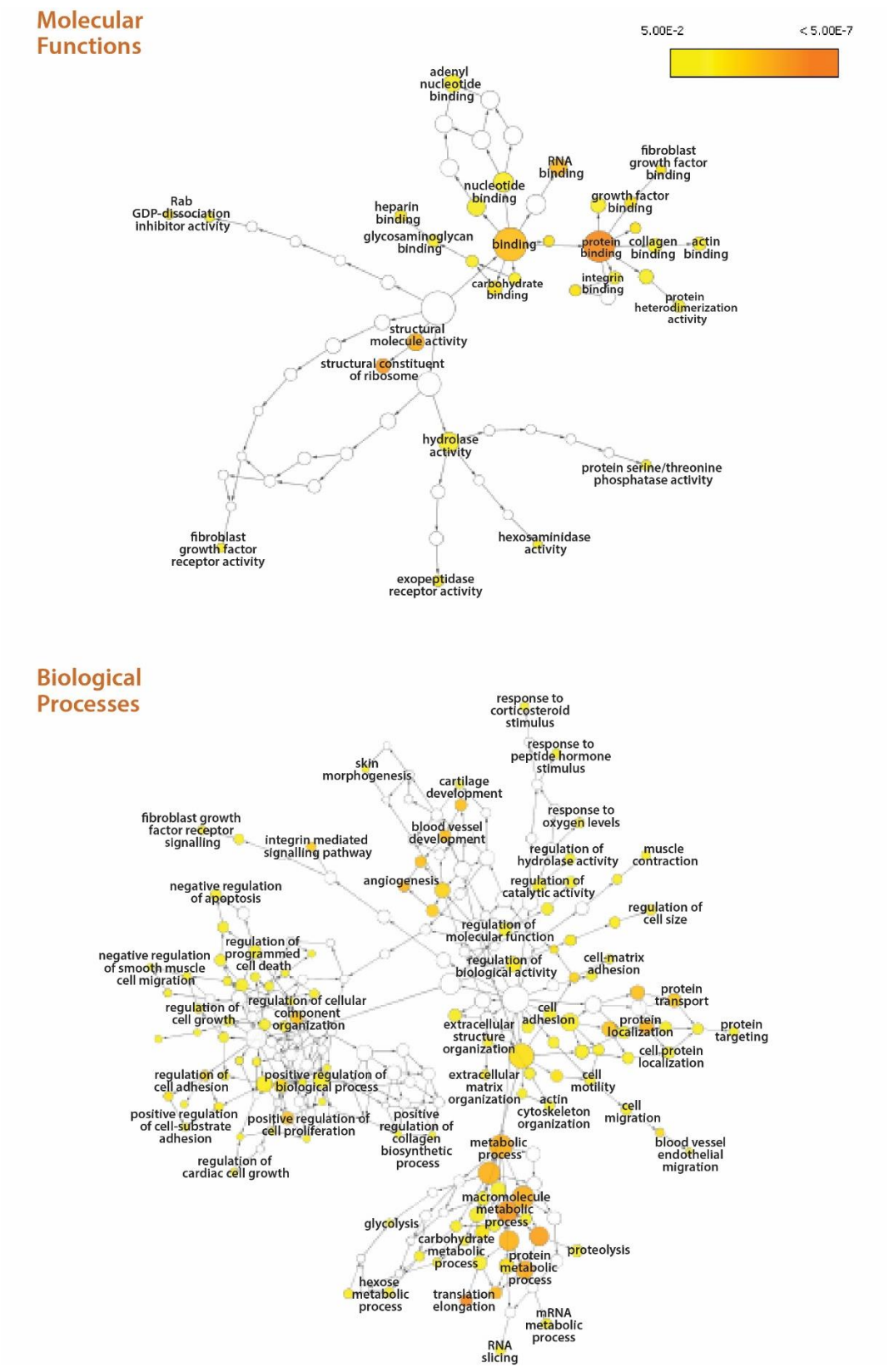

Figure 3-8: BiNGO generated biological processes and molecular function networks for differentially expressed proteins in the proteome of Ac-SDKP treated fibroblasts.

Colour of the nodes is indicative of the p-value for the statistical significance of the enrichment of a GO term while node size is indicative of the number of proteins associated with a GO term.

3.4.3.2. Enriched Reactome pathways in the proteome

The top 10 enriched Reactome pathways in the proteome are listed in Table 3-9.

Table 3-9: Ac-SDKP mediated Reactome pathway enrichment in the proteome

Pathway name	Entities				Reactions	
	found	entities	pValue	FDR	found	ratio
Peptide chain elongation	15	97	0.007	2.2E-11	1.11E-8	0.00187
L13a-mediated translational silencing of Ceruloplasmin expression	16	120	0.008	4.04E-11	1.11E-8	0.02584
GTP hydrolysis and joining of the 60S ribosomal subunit	16	120	0.008	4.04E-11	1.11E-8	0.00374
Eukaryotic Translation Elongation	15	102	0.007	4.39E-11	1.11E-8	0.00439
Formation of a pool of free 40S subunits	15	106	0.007	7.43E-11	1.49E-8	0.03981
Eukaryotic Translation Initiation	16	130	0.009	1.28E-10	1.85E-8	8.94E-04
Cap-dependent Translation Initiation	16	130	0.009	1.28E-10	1.85E-8	0.00926
Nonsense Mediated Decay (NMD) independent of the Exon Junction Complex (EJC)	14	101	0.007	4.21E-10	5.31E-8	0.00114
Nonsense-Mediated Decay (NMD)	15	124	0.009	6.22E-10	6.22E-8	9.75E-04
Eukaryotic Translation Termination	14	106	0.007	3.84e-10	3.45e-08	4.00e-04

Enriched pathways in the proteome included *peptide chain elongation, L13a-mediated translational silencing of Ceruloplasmin expression, GTP hydrolysis and joining of the 60S ribosomal subunit*, and *Eukaryotic Translation Elongation*, and are indicative of active protein transcription and translation.

3.4.3.3. Reactome pathways in the proteome putatively associated with fibrosis

Significantly enriched Reactome pathways putatively involved in the antifibrotic role mediated by Ac-SDKP are listed in Table 3-10. These pathways were selected based on the literature by manually scanning Reactome pathway analysis results. Various signalling pathways including PTK2 signalling, NOTCH4, Raf/MAP, MAPK, and SMAD are likely candidates for Ac-SDKP mediated antifibrotic actions. Importantly, FGFR1 signalling which is the only known receptor for Ac-SDKP was significantly enriched in the proteome.

Table 3-10: Proteome Reactome pathways putatively associated with the antifibrotic role of Ac-SDKP

Reactome Groups	p value	Protein Entities
MET activates PTK2 signalling	8.71E-06	*ITGB1 COL1A1 ITGA2 FN1 LAMC1 PTK2*
Localisation of the PINCH-ILK-PARVIN complex to focal adhesions	3.06E-05	*ITGB1 ILK PARVA*
Signalling by NOTCH4	6.92E-05	*ACTA2 PSMA5 PSMC1 PSME1 PLAT RPS27A RTN4*
ECM proteoglycans	1.76E-04	*ITGB1 COL1A1 SPARC ITGA2 SERPINE1 FN1 LAMC1*
RAF/MAP kinase cascade	3.60E-04	*EEF1A1 PSMA5 EGF PSMC1 PSME1 FN1 TLN1 RPS27A FGF2 PTK2 VCL FGFR1*
Signalling by NOTCH	4.23E-04	*ACTA2 PSMA5 HDAC1 STAT1 EGF PSMC1 PSME1 PLAT RPS27A RTN4*
MAPK1/MAPK3 signalling	4.50E-04	*EEF1A1 PSMA5 EGF PSMC1 PSME1 FN1 TLN1 RPS27A FGF2 PTK2 VCL FGFR1*
Extracellular matrix organisation	0.001	*ITGB1 COL1A1 SPARC MMP1 ITGA2 SERPINE1 FN1 MYH9 LAMC1 COLGALT1 FGF2*
Signalling by FGFR1 in disease	0.002	*STAT1 FGF2 FGFR1*
SMAD2/SMAD3:SMAD4 heterotrimer regulates transcription	0.003	*HDAC1 SERPINE1 RPS27A*

3.5. Discussion

The objective of this section was to employ MS-based discovery proteome and secretome analysis to identify a wider range of proteins regulated by Ac-SDKP in the fibrotic environment and hence further understand the spectrum of its antifibrotic action. The main finding from this section was the identification of an array of proteins and potential pathways which are significantly regulated by Ac-SDKP. Upregulated secretome proteins included collagens I and VI, fibrillin, laminin, decorin, and lumican while downregulated proteins comprised the glycoproteins fibrillin and laminin. ECM proteins and proteoglycans were also enriched in the proteome as evidence by GO and Reactome analysis. Proteins mapping to these pathways included collagens and other proteins of the matrisome, integrins, matrix metalloprotease 1 (MMP-1), secreted protein acidic and rich in cysteine (SPARC), serpine-1 and fibroblast growth factor-2. Importantly, many of the ECM and intracellular proteins have not been previously associated with Ac-SDKP and thus represent novel mechanisms of action of Ac-SDKP.

In the secretome, only 58 differentially expressed proteins were identified, owing to the presence of fetal calf serum proteins in the culture medium of the fibroblasts which likely masked the detection of low abundance proteins (0.01%). Challenges in secretome analysis have been described and the balance between minimising cell stress/death and elimination of serum proteins can be tricky (Stastna and Van Eyk, 2012). Nevertheless, the small number of differentially regulated proteins identified can be thought to represent a snapshot of the most abundant extracellular proteins regulated by Ac-SDKP. Ac-SDKP increased the expression of 23 proteins and decreased the expression of 35 proteins in the secretome. Given the inhibitory function Ac-SDKP both in cell proliferation and fibrosis, it is not surprising that more proteins are downregulated than upregulated (Wdzieczak-Bakala et al., 1990)(Volkov et al., 1996)(Kanasaki et al., 2003).

These proteins grouped mainly to *extracellular matrix organization* and *extracellular structure organization* in their molecular function GO term categorisation and enriched biological GO processes mapped most significantly to *structural molecule activity* and *extracellular matrix structural constituent.* Similarly, the two most enriched Reactome pathways include *ECM proteoglycans* and *extracellular matrix organization.* Considering the role of Ac-SDKP in inhibiting ECM protein deposition, these results are in concordance with known functions of Ac-SDKP (Zhang et al., 2011)(Shibuya et al., 2005).

The 'core matrisome' which regroups ECM and ECM-associated proteins comprises approximately 300 proteins (Yue, 2014)(Hynes and Naba, 2012)(Herrera et al., 2018a). Various key components of the matrisome were identified to be differentially regulated in the secretome including collagens I and VI, fibrillin, laminin, decorin, and lumican. Ac-SDKP inhibited the expression of two collagen I proteins and two collagen VI proteins in the secretome. Collagen I is a fibrillar type of collagen and is known to promote EMT transition in response to TGF-β stimulation through the expression of microRNA-29 (Zeisberg et al., 2001)(Wang et al., 2012). Type VI collagen is part of microfibrillar meshworks which does not form part of major fibrillar systems but is surmised to anchor elements between collagen I and III fibrils in the basement membrane. Ac-SDKP has previously been shown to inhibit collagen I, III and IV but not collagen VI (Xu et al., 2012)(Peng et al., 2012)(Hajem et al., 2013). This is possibly due to the fact that antibodies to collagen VI have not been used in previous studies to investigate collagen modulation by Ac-SKP. However, increased collagen VI expression has been previously described in lung fibrosis (Specks et al., 1995).

Among the matrisome components are a large number of non-collagenous ECM proteins which serve to regulate collagen fibrillogenesis (Yue, 2014). These include small leucine-rich repeat proteoglycans like decorin and lumican and the heparan sulphate proteoglycan agrin which were significantly downregulated by Ac-SDKP treatment in our study. Decorin binds a wide range of matrix structural components, such as collagens, and growth factors (Reed and Iozzo, 2002). Lumican interacts with fibrillar collagens and has been previously linked to pulmonary fibrosis (Chakravarti et al., 1998) (Pilling et al., 2015). Agrin plays a key role in the organisation of the cytoskeleton and interacts with other ECM proteins including laminin (Cotman et al., 1999) (Bezakova and Ruegg, 2003). It is intuitive that an alteration in collagen biosynthesis is likely to be accompanied by a concomitant alteration in the expression of its interacting counterparts.

In our study, Ac-SDKP also lead to a decrease in the expression of other components of the matrisome including the glycoproteins fibrillin and laminin. Fibrillin is an important component of extracellular matrix fibrils which accumulates in fibrosis (Sakai et al., 1986) (Kissin et al., 2002). Fibrillin also bears binding sites for integrin receptors which influence the extracellular microenvironment through the cytoskeleton and by inducing the release and activation of matrix-bound latent TGF-β complexes (Olivieri et al., 2010). Laminin is a major structural component of the basement membrane and plays important roles in fibroblast proliferation and is upregulated

in various forms of fibrosis, including lung fibrosis (Timpl, 1989)(Couchman et al., 1983)(Moriya et al., 2001).

In the proteome, the expression of 114 proteins was found to be affected by Ac-SDKP. Previous MS based techniques to detect Ac-SDKP regulated proteins in the intracellular lung fibroblast environment employed two-dimensional electrophoresis followed by MALDI-TOF/TOF MS and identified 29 differentially regulated proteins (Xiaojun et al., 2016). The GO distribution of the Ac-SDKP differentially expressed proteins in our study was assessed with BiNGO. In the molecular function category, proteins which functioned in *protein binding* and as *structural constituents of ribosomes* were most significantly enriched. Similarly, Xiaojun *et al.* found binding proteins to rank the highest in Ac-SDKP treated rat fibroblast cells (Xiaojun et al., 2016). In the biological process category, proteins involved in *angiogenesis* and *translation initiation* were most enriched. Processes more relevant to fibrosis prevention including *fibroblast growth factor receptor signaling* and *extracellular matrix organization proteins* were also identified.

ECM proteins and proteoglycans were enriched in GO biological processes and Reactome and also formed a network in STRING. These proteins comprised collagens and other proteins of the matrisome, integrins, matrix metalloprotease 1 (MMP-1), secreted protein acidic and rich in cysteine (SPARC), serpine-1 and fibroblast growth factor-2. MMP-1 is a secreted collagenase, involved in the turnover of collagen fibrils in the extracellular environment (Vincenti and Brinckerhoff, 2001). SPARC is a secreted collagen-binding glycoprotein which plays a key role in ECM assembly and molding, and is commonly upregulated in fibrosis, including lung fibrosis (Demopoulos et al., 2002)(Trombetta-eSilva and Bradshaw, 2012)(Sangaletti et al., 2011). Despite seeing a reduction in the levels of MMP-1 and SPARC in the Ac-SDKP proteome, these proteins were not detected in the secretome. This is likely due to the low number of proteins detected in the secretome which resulted in a loss of detection of low abundance proteins. Serpine-1, also known as plasminogen activator inhibitor 1 (PAI-1), is a serine proteinase involved primarily in fibrinolysis but also in the modulation of ECM turnover and cell adhesion (Lijnen, 2005). Various studies have highlighted a critical role for serpine-1 in the development of fibrosis, particularly in lung fibrosis (Eitzman et al., 1996)(Jiang et al., 2017). Interestingly, ACEi have demonstrated an antifibrotic action through an increase in fibrinolysis and ECM degradation mediated by the inhibition of serpine-1 expression (Oikawa et al., 1997). A mechanism for the suppression of serpine-1 by ACEi could thus be through the upregulation of Ac-SDKP.

The integrin-linked kinase (ILK) is an important component of cell to ECM adhesions through interactions with the β1 integrin cytoplasmic domain (Wu, 2004). The focal adhesion protein PINKCH consists of primarily five LIM domains (double-zinc finger motif) and forms a stable complex with ILK and CH-ILKBP/actopaxin/α-parvin (abbreviated parvin)(Wu, 2005). This complex localises to focal adhesions and is regulated by TGF-β1, hence contributing to TGF-β1 mediated effects on cell proliferation (Stanchi et al., 2009)(Jung et al., 2007)(S. M. Kim et al., 2007). It is involved in fibronectin matrix deposition and has hence been implicated in fibrosis including in lung fibrosis (Guo and Wu, 2002)(Kavvadas et al., 2010). Ac-SDKP negatively regulated the localisation of PINCH-ILK-PARVIN pathway in our TGF-β treated fibroblasts. It is interesting to note that Tβ4 has been shown to inhibits the effects of PINCH-1 and ILK and Ac-SDKP is known to share many roles with its precursor (Qiu et al., 2011).

Various signalling pathways were also modulated by Ac-SDKP in the proteome. FGFR signalling was identified among the enriched GO biological processes as well as Reactome analysis. Importantly, FGFR-1 has been implicated in Ac-SDKP mediated endothelial-to-mesenchymal transition (EndMT) and endothelial mitochondrial biogenesis (Li et al., 2017)(Hu et al., 2018). It is believed that Ac-SDKP may bind the FGFR receptor to induce downstream MAP kinase signalling (Li et al., 2017). It is thus possible that Ac-SDKP also binds the FGFR-1 receptor in the WI-38 lung fibroblasts to induce antifibrotic effects. While Ac-SDKP mediated FGFR signalling stimulates MAP4K4 (Li et al., 2017), MAP4K4 expression levels were not found to be different in the proteome. However, this does not indicate a lack of activation of MAP4K4 which could also manifest as an increase in its phosphorylation. Proteins grouping to the Raf/MAP kinase cascade and MAPK1/MAPK3 signalling were nevertheless modulated by Ac-SDKP. Ac-SDKP has been previously shown to inhibit MAPK p44/42 activation in rat mesangial cells (Rhaleb et al., 2001a)(Peng et al., 2012). Proteins of the Notch signalling family were also differentially regulated by Ac-SDKP. Notch signalling has been associated with fibrogenesis across a range of pathologies including pulmonary fibrosis (Nemir et al., 2014)(Dees et al., 2011). An upregulation of Notch signalling is crucial for the myofibroblast differentiation of lung fibroblast (Kavian et al., 2012). Interestingly, some of the beneficial effects of Tβ4 in fibrotic pathological processes have been attributed to Notch signalling suppression (Hong et al., 2017).

We have assessed the effect of Ac-SDKP on the proteome and secretome of TGF-β stimulated fibroblasts. This has not only confirmed previous observations of ECM constituent reduction by Ac-SDKP but also identified various matrisome components which had not been previously

described to be affected by Ac-SDKP. Additional novel mechanisms for antifibrotic actions of the peptide and signalling pathways potentially regulated by Ac-SDKP have been uncovered. Together, these data provide further insight into the molecular actions of Ac-SDKP as well as provide a better understanding of the potential beneficial effects of ACEi and Ac-SDKP therapeutics in fibrotic pathologies.

4. The antifibrotic potential of Ac-SDKP analogues

4.1. Background

Treatment options for fibrotic conditions are scarce and largely non-specific. Although various compounds have been shown to demonstrate *in vitro* and *in vivo* (animal models) efficacy, few many compounds have met success in undergoing clinical trials and being approved for the therapy of fibrosis (Trautwein et al., 2015). The success of the synthetic molecules, pirfenidone and nintedanib in the treatment of idiopathic pulmonary fibrosis is not common and while the precise mechanisms of action of the small molecules is yet to be elucidate, their antifibrotic effects are attributed to the inhibition of pro-fibrotic mediators such as TGF-β, PDGF and interleukins (Distler et al., 2019)(Aimo et al., 2020)(Sgalla et al., 2020). Furthermore, the complex and insidious mechanism of tissue fibrosis makes its treatment particularly challenging and is likely to require combination therapy targeting more than one pathological arm of the fibrotic process. Thus, the rational selection and testing of new compounds for the treatment of fibrosis is warranted.

The role of Ac-SDKP in the prevention and reversal of fibrosis has piqued interest into its therapeutic potential in the management of fibrotic conditions. Ac-SDKP has a short half-life of 80minutes, suggesting that it is constantly being synthesised and degraded in tissues (Rieger et al., 1993). ACEi provide a way of up-regulating Ac-SDKP levels. However, sACE comprises two individual domains, namely, the N and C domains which are both inhibited by currently available ACEi. This may pose a problem in the administration of ACE inhibitors in healthy normotensive patients due to the impairment of the C domain to hydrolyse Ang I and thereby to maintain blood pressure homeostasis. Ac-SDKP is predominantly hydrolysed by the N domain of sACE: studies whereby one of the ACE domains was functionally knocked out via a mutation of the zinc coordinating residue found the N domain to be 40 times more effective at cleaving Ac-SDKP as compared to the C domain (Rousseau-Plasse et al., 1996). The phosphinic peptide inhibitor RXP407 displays three orders of magnitude selectivity for the N domain (Dive et al., 1999). It has been shown to completely inhibit N domain activity without interrupting Angiotensin II (Ang II) formation by the C domain in mice (Junot et al., 2001). Although RXP407 has low bioavailability and cannot be used in therapy, it can be used *in vitro* to predict the effects of N domain-selective ACE inhibition.

Ac-SDKP analogues resistant to ACE hydrolysis provide another way of potentially increasing basal Ac-SDKP levels in fibrosis therapy. In mice with diabetic renal fibrosis, co-treatment with both Ac-SDKP and the ACE inhibitor ramipril further reduced renal fibrosis, as compared to Ac-SDKP or ramipril alone (Castoldi et al., 2013). This additive effect of Ac-SDKP with respect to ACE inhibition suggests that Ac-SDKP administration might not only provide an alternative form of therapy but also additional protective effect against fibrosis as compared to ACE inhibition alone. This is not surprising as chronic ACE inhibition by ACE inhibitors do not result in a massive accumulation of Ac-SDKP. An intermittent reactivation of ACE in between doses of ACE inhibitors as well as an increase in the glomerular filtration of Ac-SDKP by the kidney is thought to be responsible for these observed Ac-SDKP levels (Azizi et al., 1997)(Azizi et al., 1999)(Comte et al., 1997). There is thus merit to combination therapy with ACEi and Ac-SDKP analogues in the management of fibrotic conditions.

Various Ac-SDKP analogues have been previously synthesised; analogues in which tetrapeptide bonds have been replaced by reduced bonds, analogues whereby the L-amino acids were swapped for the corresponding D-amino acid residue and analogues lacking the C-terminal carboxylate moiety. HPLC analysis revealed greater than 97% residual peptide activity for all the analogues with reduced peptide bonds after 24hours incubation with ACE, as compared to no residual activity of the parent compound Ac-SDKP (S. Gaudron et al., 1997)(Thierry et al., 1990)(Ma et al., 2014). Replacing the carboxylate moiety with a carboxamide C-terminus also resulted in protection from hydrolysis but the absence of C-terminal carboxylate group confers no protection (S Gaudron et al., 1997). Finally analogues whereby the D-amino acids were introduced were also resistant to ACE degradation *in vitro* and displayed significantly increased half-lives *in vivo* (Ma et al., 2014)(Zhang et al., 2019).

The *in vitro* effects of the pseudo peptides on haematological cell proliferation have also been investigated. Ac-Serψ(CH_2-NH)Asp-Lys-Pro, Ac-Ser-Aspψ(CH_2-NH)Lys-Pro, Ac-Ser-Asp-Lysψ(CH_2-NH)Pro, and the C-terminus modified peptide (Ac-SDKP-NH_2) significantly reduced the numbers of Colony Forming Unit, CFU-granulocyte/macrophage in the S phase and prevented the mitotic cycling of highly proliferating stem cells (Gaudron et al., 1999).

Further, the Ac-S_DDK_DP analogue in which Asp and Lys were replaced with their D-isomers was tested in cardiac and hepatic fibrosis mice models (Ma et al., 2014)(Zhang et al., 2019). The Ac-S_DDK_DP analogue displayed a prolonged *in vivo* half-life and significantly improved pathological tissue fibrosis in both models through TGF-β/Smad pathway modulation. Analogues were also used to probe the molecular specificity of the inhibitory action of Ac-SDKP on primitive murine

haematopoietic cell cycling. The tri-peptide Ala-Asp-Lys also failed to inhibit the cellular proliferation, but interestingly the tri-peptide Ser-Asp-Lys retained the anti-proliferative ability. Thus the SDK sequence appears to be vital for the prevention of S phase entry into the mitotic cycle (Robinson et al., 1993). However, the molecular specificity of the antifibrotic of Ac-SDKP has not been investigated. This chapter addresses the important question of whether specific fragments of Ac-SDKP can confer antifibrotic activity; this could in turn lead to the design of specific Ac-SDKP analogues which do not impair its anti-proliferative function and do not lead to side effects.

4.2. Study objectives

In order to investigate the antifibrotic potential of Ac-SDKP analogues in a cell line model of fibrosis, the following objectives were identified:

1. investigation of the effects of Ac-SDKP on the TGF-β pathway in a lung fibroblast cell line
2. cleavage site determination of Ac-SDKP analogues by ACE
3. investigation of the contribution of the amino acid residues in the Ac-SDKP sequence towards its antifibrotic effects
4. investigation of the effects of Ac-SDKP in combination with ACE inhibitors in preventing collagen deposition in cells

4.3. Methods

4.3.1. Ac-SDKP analogue design

Ac-SDKP sequences were designed to investigate the functional portion of Ac-SDKP in its antifibrotic role. Sequence tripeptides SDK and DKP in both the acetylated and unacetylated forms were ordered from Biopep Peptide group (Stellenbosch, South Africa) (Table 4-1***, peptides 2-5***). An analogue, previously shown to be resistant to ACE enzymatic cleavage was also used to compare its antifibrotic effect to physiological Ac-SDKP (Gaudron et al., 1999). In the AcSDψKP analogue, the peptide bonds between the Asp-Lys has been converted to the non-hydrolysable CH_2-NH bonds. The Ac-SDKP analogue (Table 4-1***, peptide 6***) was synthesised by Sigma (USA).

Table 4-1: Ac-SDKP sequences and analogues used to investigate the specificity of the antifibrotic effect

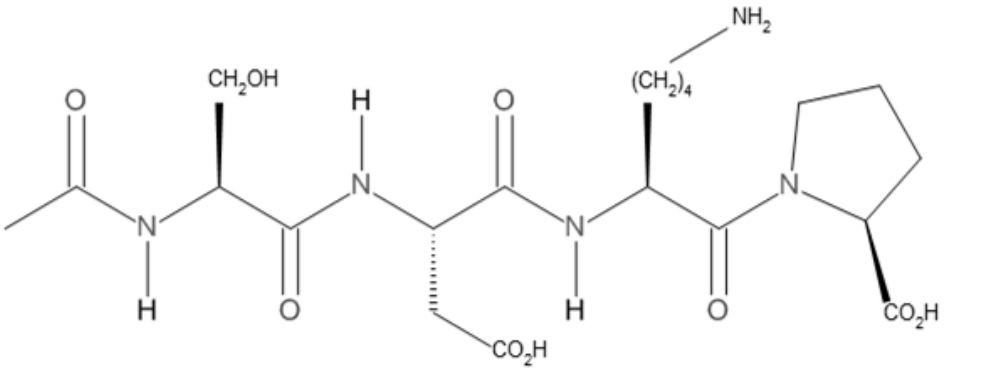

1	**Acetyl**	**Ser**	***(CO-NH)***	**Asp**	***(CO-NH)***	**Lys**	***(CO-NH)***	**Pro**	**Ac-SDKP**
2	Acetyl	Ser		Asp		Lys			**Ac-SDK**
3		Ser		Asp		Lys			**SDK**
4				Asp		Lys		Pro	**DKP**
5	Acetyl			Asp		Lys		Pro	**Ac-DKP**
6	Acetyl	Ser		Asp	***(CH2-NH)***	Lys		Pro	**Ac-SDψKP**

4.3.2. Cell culture

WI-38 lung fibroblasts or CT-1 fibroblasts (ultraviolet-irradiated WI-38 cells) were cultured according to 3.3.1. The fibroblasts were used to assess the effects of Ac-SDKP, ACE inhibitors and Ac-SDKP analogues on the prevention of fibrosis.
Briefly, the cells were reconstituted into 75cm^2 flasks and grown in 10ml of growth medium, lifted using Trypsin-EDTA (Gibco®, USA) and seeded into 6-well plates.

4.3.3. Cell treatment and lysis

Cells were treated with TGF-β (5 ng/ml) or ET-1 (100 ng/ml) for 48 hours in the presence of ascorbic acid (50 µg/ml) for 6 to 48 hours to induce fibrosis. To assess the protective effect of Ac-SDKP, cells in a 25cm^2 flask were lysed in 300µl of Triton lysis buffer (0.05 M HEPES, 0.5 M NaCl, 1% triton X-100, 1 mM PMSF supplemented with 1:1000 Protease Inhibitor Cocktail (Set III, Calbiochem, USA) and Phosphatase Inhibitor Cocktail (PhosSTOP, Roche, Switzerland)). The lysate was centrifuged at 10 000 *g* at 4^{o}C and the supernatant used for western blot analysis.

4.3.4. Sodium dodecyl sulphate polyacrylamide gel electrophoresis

Cell lysates were boiled with Laemmli buffer (60 mM Tris-Cl, 2% SDS, 10% glycerol, 5% 2-mercaptoethanol, 0.01% bromophenol blue, pH 6.8) for 10 minutes. The reduced samples were separated by sodium dodecyl sulphate polyacrylamide gel electrophoresis (SDS-PAGE) (Laemmli, 1970) with the Mini PROTEAN^{TM} III system (BIO-RAD, USA). An 8% resolving gel (0.3% SDS, 125 mM Tris-HCl, pH 8.8) was used for the detection of sACE. A 3% stacking gel (0.3% SDS, 37.5 mM Tris buffer, pH 6.8) was used in and gels were run in Tris-glycine-SDS buffer (pH 8.3) at 25mA per gel.

4.3.5. Western blotting

Following gel electrophoresis, a transfer sandwich was set up using the Mini PROTEAN™ III system (Biorad, USA). Proteins were electrophoretically transferred from gel to Hybond ECL nitrocellulose membrane (GE Healthcare LifeSciences, UK) in cold transfer buffer (20mM Tris-base, 150mM glycine, 20% methanol) at a current of 100V for 1hour. Membranes were incubated for 1hour in blocking buffer (Tris-buffered saline, 0.1% tween-20, 5% skim-milk). Following blocking, membranes were incubated overnight in primary antibody (4G6 rat) dilution (1:100). Primary antibody binding was detected with the corresponding secondary HRP-conjugated

antibody (goat anti-rat) using the Immun-star WesternC™ detection system (BIO-RAD, USA). The chemiluminescence detector (G:BOXChemi, Syngene, USA) was used to detect the light emission produced in the peroxidase catalysis of the oxidation of luminol.

4.3.6. HPLC analysis and progress curves

HPLC of the Ac-SDKP peptides was performed using a Poroshell 120 EC-C18 column (Agilent, USA). To plot progress curves for the hydrolysis of the various Ac-SDKP peptides, 1nM sACE was incubated with 1mM Ac-SDKP at different time points in HEPES assay buffer (50 mM HEPES buffer, 300 mM NaCl, 10 µM ZnSO4, pH6.8) at 37°C. Reactions were stopped by the addition of trifluoroacetic acid (TFA) to a final concentration of 0.1%. Reaction mixtures were analysed by HPLC over a gradient of 2% to 95% ACN (in 0.1 % TFA) on the Agilent 1260 Infinity HPLC (Agilent, USA) at multiple wavelengths simultaneously. The area under the peak for the peptides and their cleavage products was measured using the Agilent 1260 software at λ =214nm.

4.3.7. Hydroxyproline assay

Collagen deposition was assessed as a marker of fibrosis using an assay for hydroxyproline, the major constituent of collagen (Sigma, USA). The hydroxyproline assay kit adapted from a method by Kivirikko *et al.*, was used according to manufacturer's protocol to produce a colorimetric product from the reaction of oxidized hydroxyproline with 4-(Dimethylamino) benzaldehyde (DMAB), which was measured at 560nm (Kivirikko et al., 1967).

4.3.8. Statistical analysis

Data analysis was performed using the statistical software GraphPad PRISM 6.0 (GraphPad software Inc, USA). To compare ratios of treated vs. untreated samples, un-paired, nonparametric, student t-tests were employed with a cut off for statistical significance of $p<0.05$.

4.4. Results

4.4.1. Ac-SDKP inhibits TGF-β/Smad signalling and collagen deposition in lung fibroblasts

4.4.1.1. Ac-SDKP inhibits AngII and ET-1 mediated TGF-β expression

To investigate the effect of that Ac-SDKP on TGF-β activation in our cell line (WI-38 cells), western blots for TGF-β levels were performed. Additionally, the effect of Ac-SDKP on AngII and ET-1 mediated TGF-β signalling was studied.

Treatment of WI-38 cells with AngII and ET-1 induced 1.26 and 1.48-fold increases in TGF-β levels, respectively (Figure 4-1). In both AngII and ET-1 stimulated cells, Ac-SDKP significantly inhibited the increase in TGF-β levels in the cell culture supernatant. This confirmed that WI-38 cells could be used for investigating the antifibrotic actions of Ac-SDKP. Since ET-1 induced a slightly higher upregulation of TGF-β levels, it was used instead of AngII in subsequent experiments.

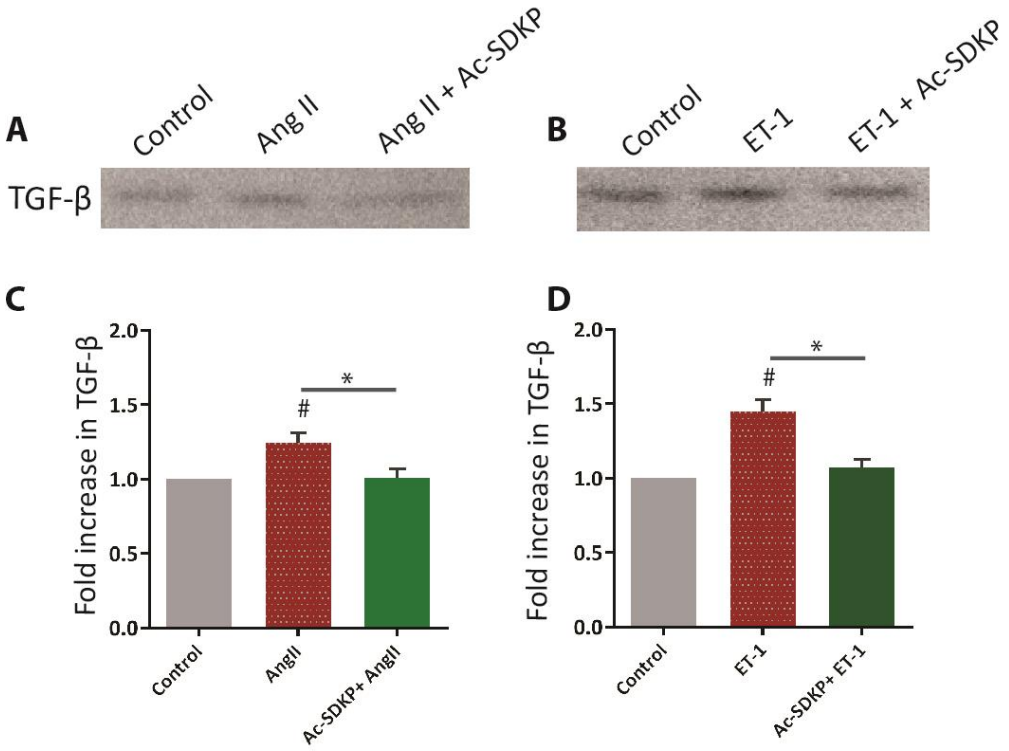

Figure 4-1: Effect of Ac-SDKP on Ang II and ET-1 mediated TGF-β expression
Representative western blot for TGF-β (5 ng/ml) in WI-38 cells treated with **A.** Ang II (100mM) or **B.** ET-1 (100ng/ml) for 48hours in the presence or absence of 100nM Ac-SDKP**.** Densitometry of western blots performed in triplicate for cells treated with **C**. Ang II and **D.** ET-1 for 48hours. Controls represent cells treated with vehicle accordingly. Data is representative of ± standard of the mean (SEM) of triplicates. Significance ($p < 0.05$) is indicated as # for a difference from control or denoted graphically by * with corresponding bars on the graphs**.**

4.4.1.2. Ac-SDKP inhibits TGF-β/Smad3 signalling in WI-38 cells

The binding of TGF-β to its receptor induces Smad2/3 phosphorylation. We investigated whether the inhibition of TGF-β expression by Ac-SDKP causes a reduction in pSmad3 levels. WI-38 cells pre-treated with Ac-SDKP were stimulated with ET-1 for 6hr prior to lysis. Cell lysates were investigated for pSmad3 and Smad3 levels as well as the housekeeping protein GAPDH. Ratios of pSmad3/Smad3, adjusted for GAPDH levels, were determined (Fig 4-2).

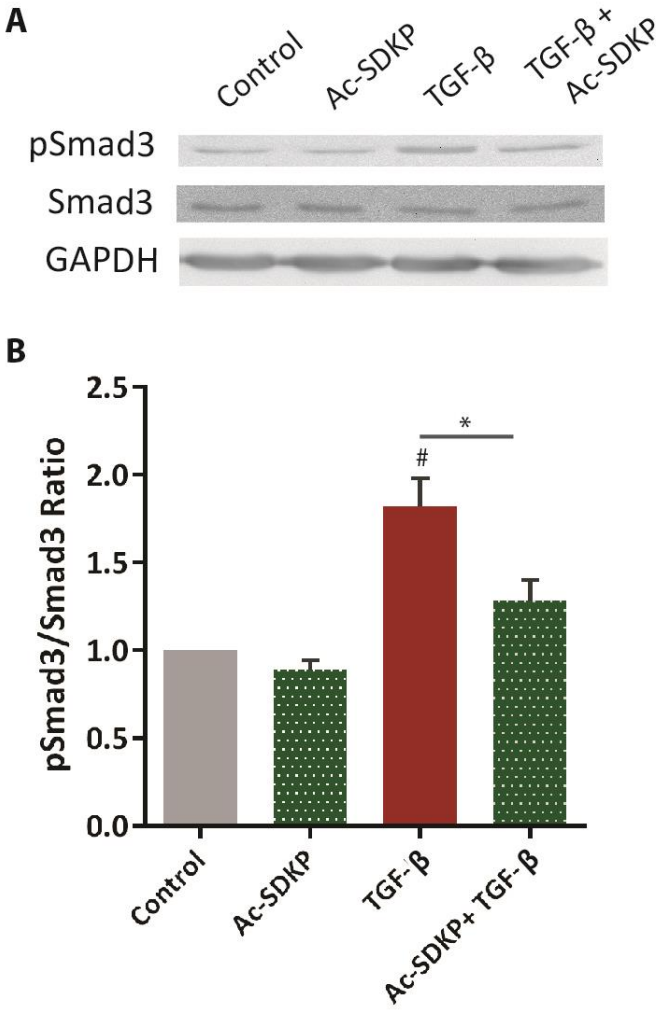

Figure 4-2: The prevention of TGF-β mediated pSmad-3 signalling by Ac-SDKP. Lysates from WI-38 cells pre-treated with 100nM Ac-SDKP for 30mins and incubated with TGF-β (5 ng/ml) for 6hours. **A.** Representative western blots for pSmad-3, Smad-3 and GAPDH on cell lysate. **B.** Densitometry of pSmad-3/Smad-3 ratios adjusted for GAPDH expression. Data is representative of ±SEM of three experimental repeats and each sample blotted n=2 (technical repeat). Significance ($p < 0.05$) is indicated as # for different from control or denoted graphically by * with corresponding bars on the graphs.

The addition of TGF-β to the WI-38 cells induced a 1.8-fold increase in Smad3 phosphorylation ($p < 0.05$). This suggests that TGF-β induces downstream cell signalling in WI-38 cells. Ac-SDKP alone had no effect on pSmad3 phosphorylation in WI-38 cells. However, Ac-SDKP significantly inhibited TGF-β mediated phosphorylation of Smad3. Thus, Ac-SDKP inhibits TGF-β/Smad signalling in WI-38 through the inhibition of TGF-β expression as well as Smad3 phosphorylation.

4.4.1.3. **Ac-SDKP prevents TGF-β mediated collagen accumulation**

TGF-β/ Smad signalling is known to induce the transcription of extracellular matrix components involved in the fibrotic process. Collagen expression by the lung fibroblasts was investigated as a marker of fibrosis. The hydroxyproline (major constituent of collagen) content of the WI-38 cells was measured using a specific assay. The hydroxyproline levels in CT-1 cells (γ- irradiated WI-38 cells) was also measured as the cells grow at a much faster rate and have been shown to have an increased basal expression level of collagen (Namba et al., 1980).

Confluent WI-38 or CT-1 cells were pre-treated with Ac-SDKP or vehicle for 30 mins prior to 48hr incubation with TGF-β. The fold change in the hydroxyproline content of the cells (adjusted using protein content quantification by a Bradford assay) was assessed (Figure 4-3). TGF-β significantly induced collagen expression in WI-38 and CT-1 cells (1.63- and 1.87-fold respectively). In both cell lines, pre-treatment with Ac-SDKP prevented the collagen upregulation measured upon stimulation with TGF-β. Thus, Ac-SDKP leads to a decrease in extracellular matrix components through the inhibition of TGF-β/Smad inhibition.

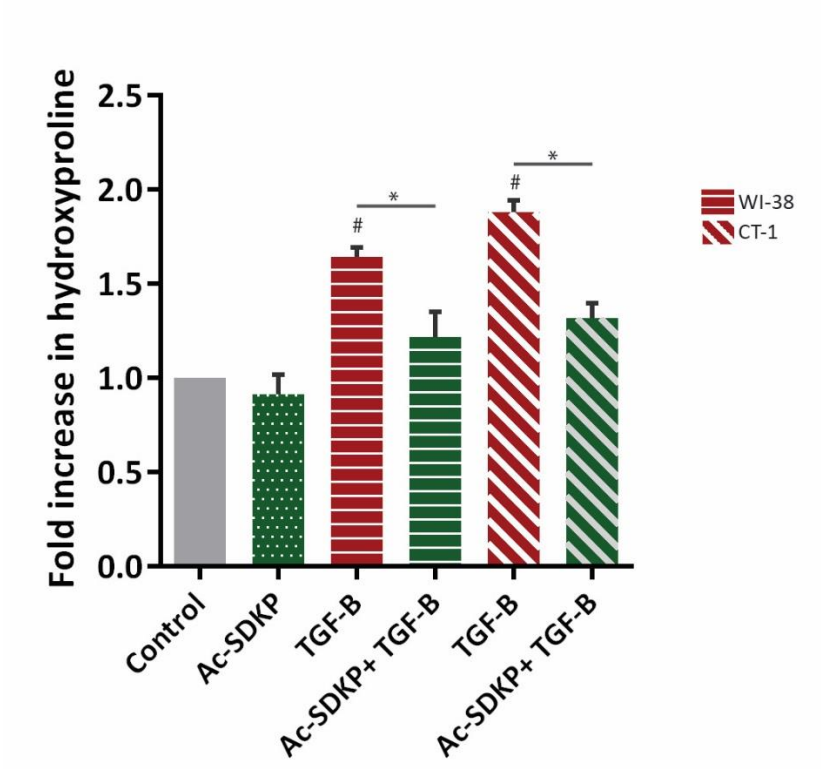

Figure 4-3: Effect of Ac-SDKP on TGF-β mediated cellular collagen levels in WI-38 and CT-1 fibroblasts.

Hydroxyproline content of pre-treated WI-38 or CT-1 cells (100nM Ac-SDKP) prior to the addition of TGF-β (5 ng/ml). The fold increase in hydroxyproline following subtraction of spiked hydroxyproline content is shown. Data is representative of ±SEM of duplicates of two experimental repeats. Significance ($p < 0.05$) is indicated as $^{\#}$ for different from control or denoted graphically by * on the graphs.

4.4.2. Investigating the specificity of the antifibrotic effects of Ac-SDKP

4.4.2.1. The cleavage of Ac-SDKP sequence peptides by ACE

Ac-SDKP is a well-known substrate of ACE and the ability of sACE to cleave the peptides Ac-SDK, SDK, AC-DKP and DKP was probed. The HPLC chromatograms of the hydrolysis of the parent Ac-SDKP by sACE indicated two product peaks labelled (P1 and P2) eluting at 1.9 and 2.8 mins, respectively (Fig 4-4). Both products eluted before the full-length Ac-SDKP which reflects the decrease in hydrophobicity of the shorter fragment peptides.

The Ac-SDKP-derived peptides were incubated with 10nM sACE in a time course experiment and the relative AUC for the uncleaved peptides (S1) were recorded in Fig 4-5. Only Ac-SDKP and Ac-DKP were cleaved by sACE as seen in the progress curves and as evident from P1 and P2 peak products. Interestingly, the efficiency of cleavage of Ac-DKP was lower than that of Ac-SDKP.

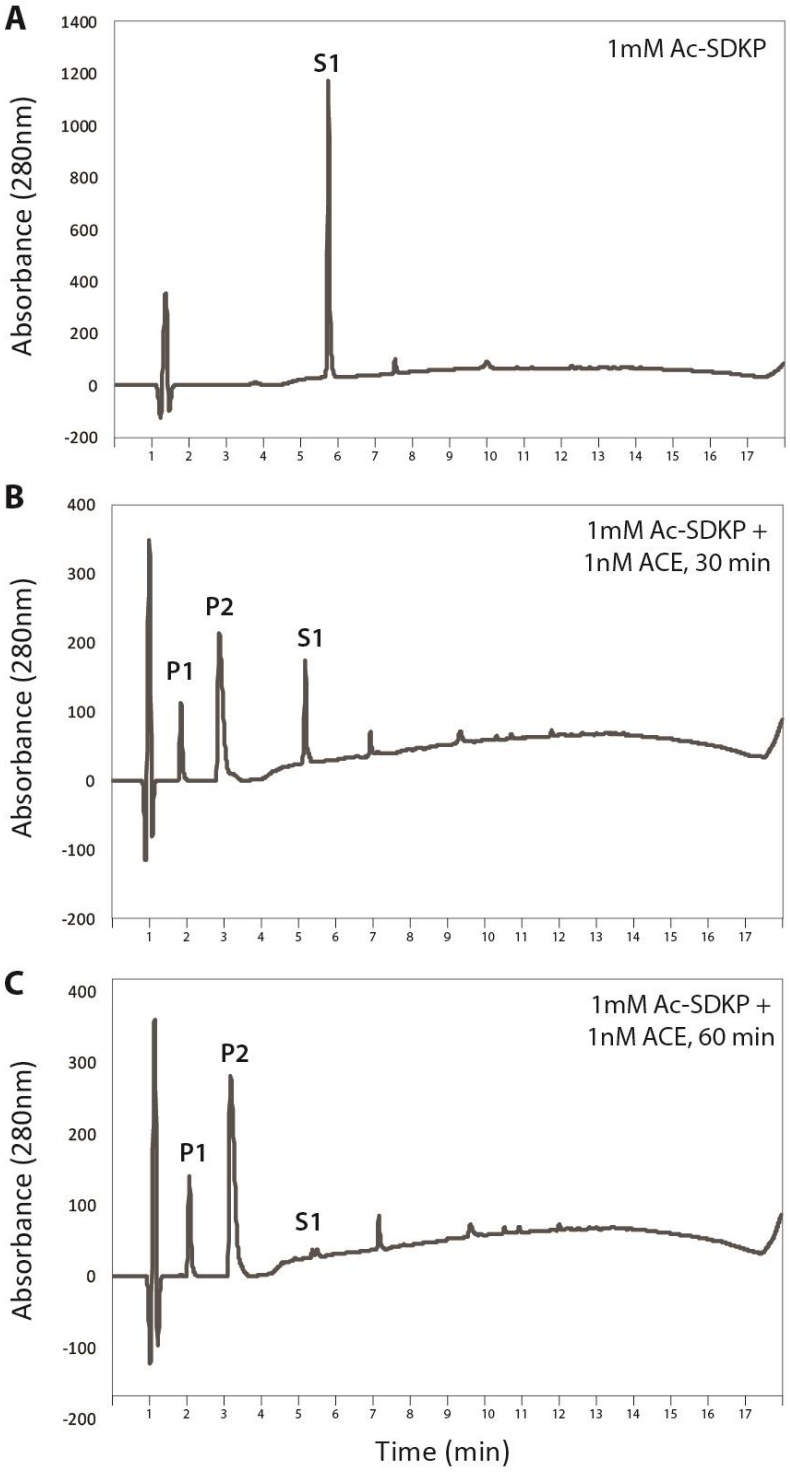

Figure 4-4: Representative chromatograms of Ac-SDKP peptide cleavage by sACE.
HPLC chromatograms of **A.** The substrate, 1mM Ac-SDKP in the absence of sACE **B.** Ac-SDKP incubated with 1nM sACE for 30minutes. **C.** Ac-SDKP incubated with 1nM sACE for 60minutes. The substrate peak is indicated as S1 whilst product peaks is denoted as P1 and P2 respectively.

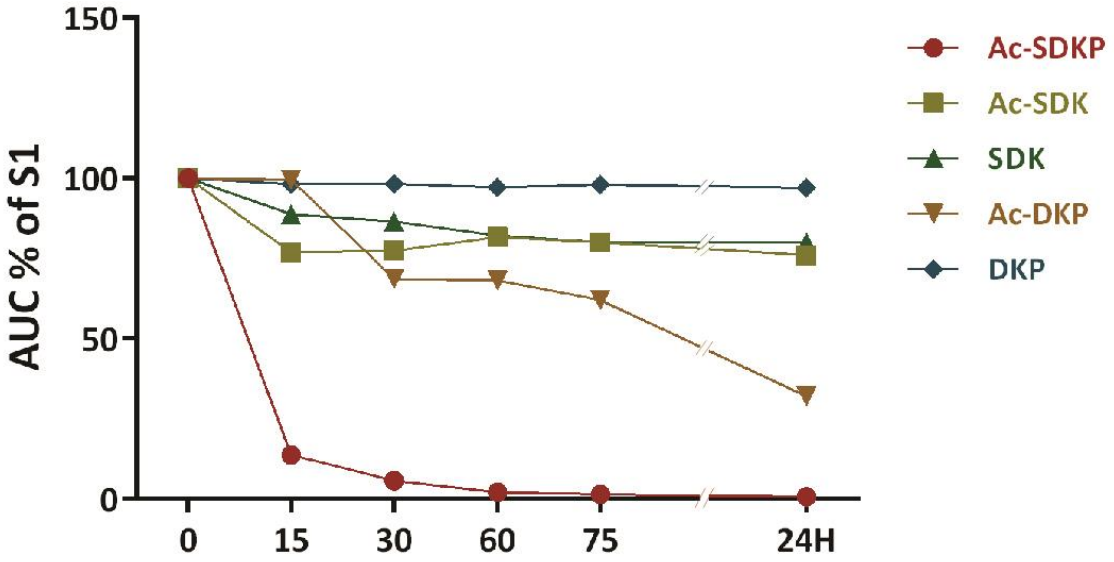

Figure 4-5: Progress curve of the cleavage of Ac-SDKP peptide sequences by sACE.
The % AUC of the substrate peak S1 as indicated in *section 5.4* for the parent peptide Ac-SDKP and the sequence peptides Ac-SDK, SDK, Ac-DKP and DKP are plotted.

4.4.2.2. Ac-SDKP and Ac-DKP inhibit TGF-β expression in WI-38 cells

To determine whether the Ac-SDKP peptides have antifibrotic activity, their effects on ET-1 mediated TGF-β expression was measured in WI-38 cells. Confluent WI-38 cells were pre-treated with 100nM of the different Ac-SDKP peptides for 30mins and subsequently incubated with ET-1 for 48hr. TGF-β levels in concentrated cell culture supernatants were determined by western blotting. Equal amounts of protein were loaded (verified by Ponceau staining) and TGF-β levels were normalised to the untreated control (Figure 4-6). Upon ET-1 stimulation a 1.4-fold increase in TGF-β levels was observed. Only Ac-SDKP and Ac-DKP significantly inhibited the upregulation of TGF-β induced by ET-1. This inhibitory effect appears more marked for Ac-SDKP (although no statistical difference in the Ac-SDKP and Ac-DKP group was observed). It thus appears that the minimal requirement for TGF-β inhibition is the Ac-DKP fragment of Ac-SDKP.

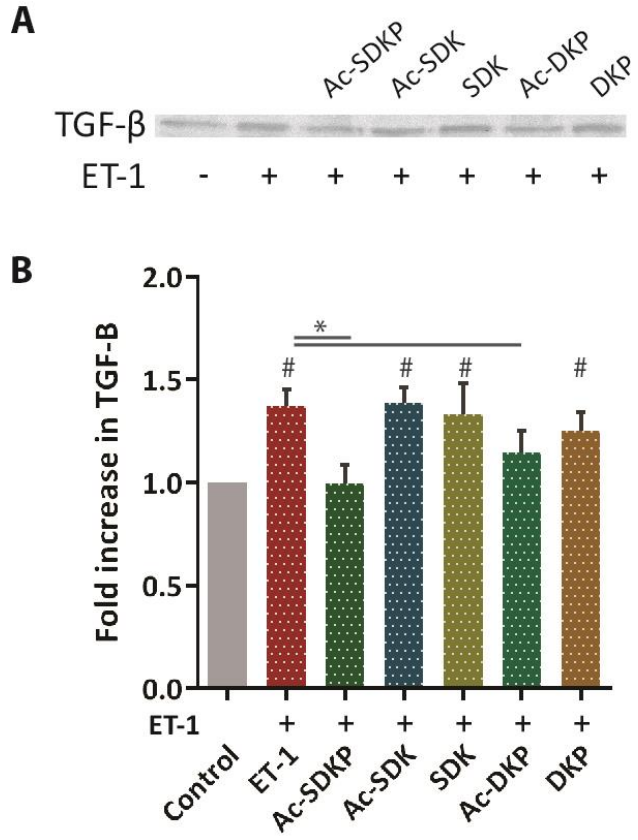

Figure 4-6: Prevention of AngII mediated fibrosis in WI-38 by Ac-SDKP sequence peptides. **A.** Representative western blot for TGF-β in CT-1 cells treated with ET-1 (100 ng/ml) for 48hours in the presence or absence of 100nM of respective Ac-SDKP peptides **B.** Densitometry of western blots performed in duplicate for cells treated with ET-1 for 48hours. Controls represent cells treated with vehicle accordingly. Data is representative of ±SEM of duplicates. Significance ($p < 0.05$) is indicated as # for different from control or denoted graphically by * on the graphs.

4.4.2.3. Ac-SDKP sequence peptides do not inhibit TGF-β-mediated collagen upregulation

The ability of the sequence peptides to inhibit TGF-β mediated collagen accumulation was investigated in CT-1 cells. Confluent CT-1 cells were pre-treated with the respective Ac-SDKP peptide for 30mins and incubated with TGF-β for 48hr. The fold change in the hydroxyproline content measured by the assay (adjusted by protein content measured by a Bradford assay) is plotted (Figure 4-7). As seen previously, TGF-β significantly induced collagen expression in CT-1 cells. Despite the ability of Ac-DKP to inhibit TGF-β expression, a small but not significant inhibition of collagen/hydroxyproline levels was observed indicating a tendency towards an antifibrotic profile for the peptide.

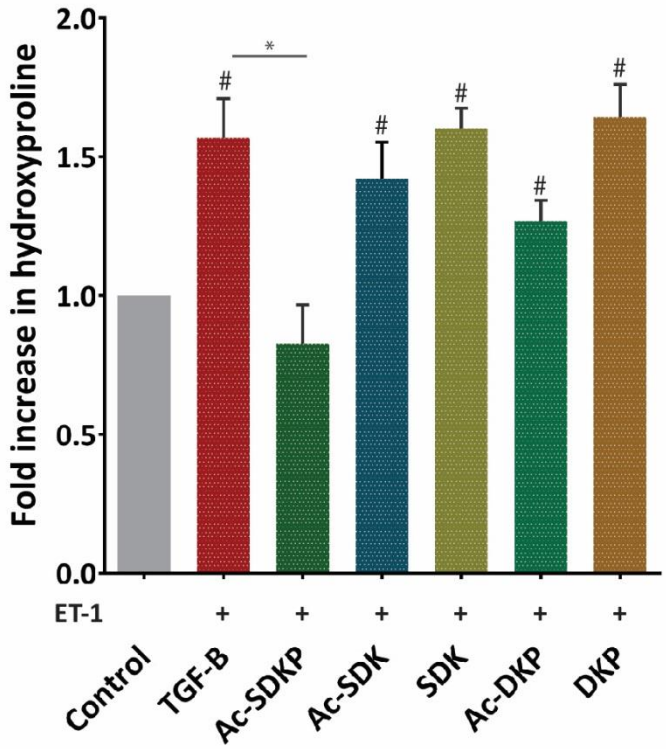

Figure 4-7: Effect of Ac-SDKP sequence peptides on ET-1 mediated collagen levels. Hydroxyproline content of pre-treated CT-1 cells (100nM Ac-SDKP peptides: Ac-SDKP, Ac-SDK, SDK, Ac-DKP, DKP) prior to the addition of ET-1 (100 ng/ml). The fold increase in hydroxyproline following subtraction of spiked hydroxyproline content is shown. Data is representative of ±SEM of duplicates of two experimental repeats. Significance ($p < 0.05$) is indicated as # for different from control or denoted graphically by * on the graphs.

4.4.3. The antifibrotic potential of the Ac-SDψKP analogue

4.4.3.1. Ac- SDψKP resists cleavage by ACE

Ac- SDψKP was previously shown to be uncleaved by ACE. To confirm this finding, Ac-SDψKP was incubated with sACE as seen in *4.4.2.1*. Similarly, the relative AUC for the uncleaved substrate (S1) is plotted in Fig 4-8. No cleavage of Ac-SDψKP was seen at any of the time points, validating its resistance to ACE degradation.

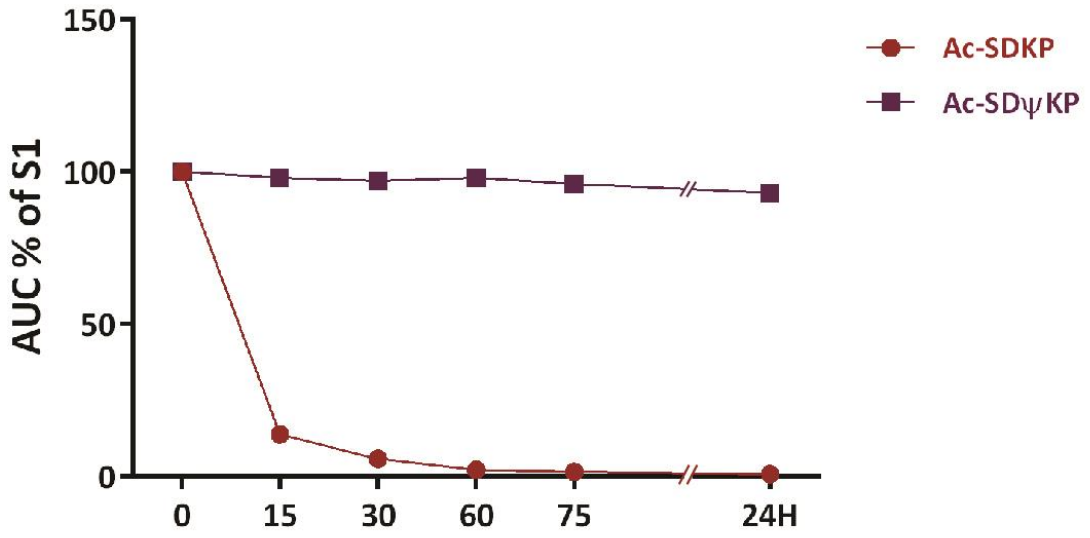

Figure 4-8: Progress curve of the cleavage of Ac-SDψKP peptide bond analogue by sACE.
The integrated peak areas of the substrate as indicated by S1 in *section 4.4* for the parent peptide Ac-SDKP and Ac-SDψKP are plotted.

4.4.3.2. **Ac- SDψKP inhibits the TGF-β/Smad signalling pathway**

The ability for Ac-SDψKP to inhibit the TGF-β/Smad pathway was assessed in a similar fashion to *4.4.1* and *4.4.2*. The comparative effect of Ac-SDψKP pre-treatment on TGF-β levels and downstream pSmad3 activation was measured in WI-38 cells. In ET-1 treated cells, Ac-SDψKP has a comparable effect to Ac-SDKP in preventing TGF-β accumulation in the cell culture supernatant (Fig 4-9 A&B). Similarly, in TGF-β treated cells, Ac-SDψKP also inhibited an increase in Smad3 phosphorylation (Fig 4-9 C&D).

Ac-SDψKP has demonstrated here an antifibrotic potential similar to the physiological Ac-SDKP peptide. Ac-SDψKP showed a tendency towards a better inhibition of the TGF-β signalling than Ac-SDKP; however, the difference was not significant.

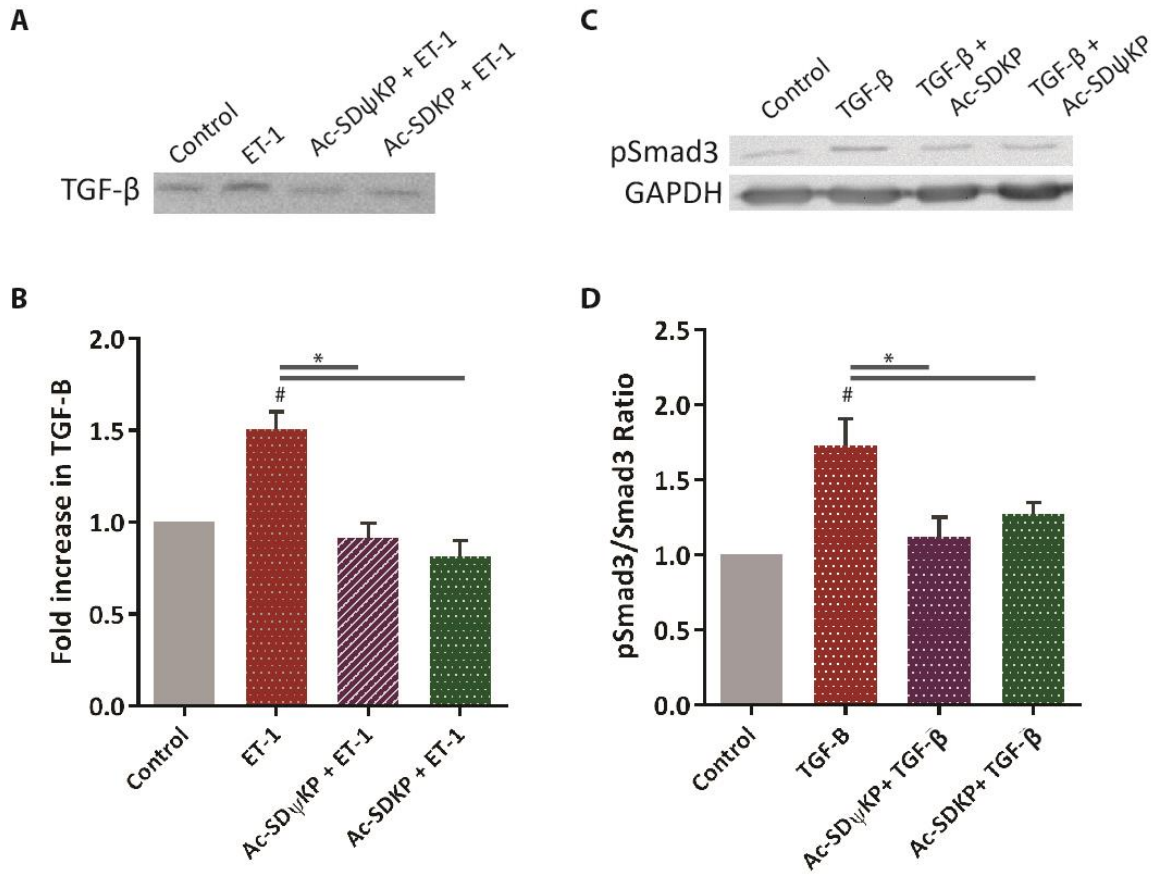

Figure 4-9: Effect of Ac-SDψKP on TGF-β/Smad signalling in WI-38 cells

A. Representative western blot for TGF-β in WI-38 cells treated with Ang II (100mM) for 48hours in the presence or absence of 100nM Ac-SDKP or 100nM Ac-SDψKP **B.** Densitometry of western blots performed in triplicate. **C.** Representative western blots for pSmad-3, Smad-3 and GAPDH on equal protein concentrations of WI-38 lysates treated with TGF-β for 6hours in the presence or absence of 100nM Ac-SDKP or 100nM Ac-SDψKP. **D.** Densitometry of pSmad-3/Smad-3 ratios adjusted for GAPDH expression. Controls represent cells treated with vehicle accordingly. Data is representative of ±SEM of triplicates for TGF-β densitometry and ±SEM of duplicates of two experimental repeats for pSmad-3 and Smad-3. Significance ($p < 0.05$) is indicated by * on the graphs.

4.4.4. Investigating the effect of ACEi in combination with Ac-SDKP on collagen levels

An additive effect for ACEi and exogenous Ac-SDKP has previously been demonstrated in mice models of fibrotic disease (Castoldi et al., 2013). To investigate whether the addition of ACEi could confer increased protection, lisinopril or the N domain-selective ACEi RXP407 were supplemented to Ac-SDKP and Ac-SDψKP treated CT-1 cells.

Ac-SDψKP, lisinopril and RXP407 alone had no effect on the hydroxyproline content of the cells (Figure 4-10). As previously observed, TGF-β induced an increase in the hydroxyproline content of the cells. Ac-SDKP and Ac-SDψKP alone prevented TGF-β mediated increases in hydroxyproline levels. The combination of Ac-SDKP and lisinopril had no additive effect on inhibiting hydroxyproline levels of CT-1 cells. However, the combination of Ac-SDKP and RXP407 demonstrated a greater inhibition of hydroxyproline ($p<0.01$). On the other hand, hydroxyproline inhibition by Ac-SDψKP was not improved by ACEi supplementation, either with lisinopril or RXP407. However, the antifibrotic effect of Ac-SDψKP was comparable to the combination of Ac-SDKP and RXP407.

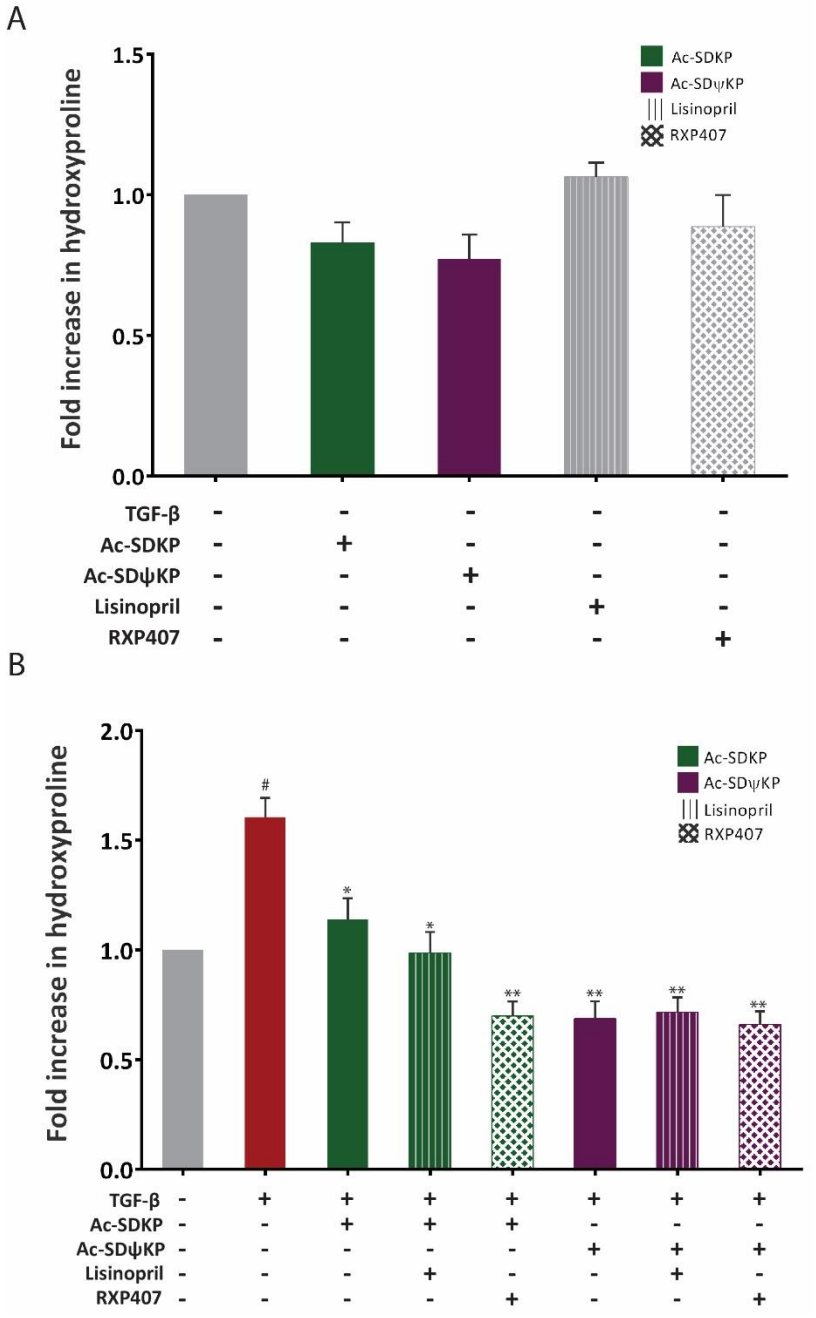

Figure 4-10: Effect of Ac-SDψKP and ACEi on TGF-β mediated cellular collagen levels.

Hydroxyproline content of **A.** unstimulated and **B.** TGF-β (5 ng/ml) pre-treated CT-1 cells (100nM Ac-SDKP, 100nM Ac-SDψKP, 100nM Lis, 100nM, RXP407) prior to the addition of ET-1 for 48hours. The fold increase in hydroxyproline following subtraction of spiked standard is shown. Data is representative of ±SEM of duplicates of two experimental repeats. Significance ($p < 0.05$) is indicated as $^{\#}$ for different from control or denoted * for different from TGF-β treatment alone. ** denotes a significance of $p<0.01$.

4.6. Discussion

There were four key findings from this section of our study. First, the antifibrotic effects of Ac-SDKP were confirmed in a lung fibroblast cell line (WI-38 and its irradiated CT-1 counterpart), demonstrating, for the first time, that this cell line could be used as a model for fibrosis to test the effects of Ac-SDKP, particularly in the prevention of TGF-β mediated Smad phosphorylation and collagen deposition. Second, a large stride was made in identifying the minimal requirement of the Ac-SDKP peptide for its antifibrotic action of Ac-SDKP. The Ac-DKP fragment significantly inhibited TGF-β expression, although this inhibition was less than that of the parent peptide. Importantly, this identified a different minimal requirement to its anti-proliferative ability (SDK fragment identified to be important)(Gaudron et al., 1999). Third, the Ac-SDψKP analogue, shown to be resistant to ACE cleavage, demonstrated an antifibrotic potential. This is the first study to test the effect of this particular Ac-SDKP analogue on fibrosis prevention. Ac-SDψKP significantly inhibited the TGF-β/Smad signalling pathway and collagen expression. The fourth finding was that the combination of ACEi with Ac-SDKP treatment resulted in an increased prevention of collagen expression as compared to Ac-SDKP treatment alone. Importantly, the N domain-selective inhibitor RXP407 demonstrated the most pronounced enhancement of the antifibrotic action of Ac-SDKP.

Fibrosis is driven by an interplay between inflammatory immune cells and fibroblasts, which synthesise ECM components (Kendall and Feghali-Bostwick, 2014). Ac-SDKP largely exerts its beneficial effects through the inhibition of TGF-β/Smad signalling to prevent ECM protein deposition (Peng et al., 2010)(Yang et al., 2004). Ac-SDKP significantly inhibited both AngII and ET-1-mediated TGF-β release in the cell culture supernatant of the lung fibroblasts. Both AngII and ET-1 induce fibrosis through the activation of the TGF-β/Smad cascade (Leask, 2010)(Border and Noble, 1998)(Ruiz-Ortega et al., 2005). Ac-SDKP has previously been shown to inhibit both AngII and ET-1-mediated fibrotic gene expression (González et al., 2014)(Peng et al., 2012). Having established that TGF-β upregulation is induced by AngII and ET-1 in fibroblasts, we next conducted experiments to determine whether Ac-SDKP would inhibit TGF-β-mediated Smad3 signalling. Ac-SDKP significantly inhibited TGF-β-mediated phosphorylation of Smad3, suggesting that Ac-SDKP modulates TGF-β/smad3 signalling in WI-38 cells. This inhibition by Ac-SDKP resulted in a significant reduction in collagen levels in both WI-38 and CT-1 culture supernatants. This result is not unsurprising and confirms the findings of a myriad of studies which has demonstrated the

ability for Ac-SDKP to inhibit both TGF-β and collagen levels in (Xiaojun et al., 2016)(Rhaleb et al., 2013).

The ability of ACE to degrade Ac-SDKP peptides was investigated using HPLC analysis of the peptides incubated with ACE for different time periods. Only the Ac-DKP fragment was cleaved by ACE; however, its hydrolysis was less efficient than that of Ac-SDKP. It is unclear why only the Ac-DKP fragment can be cleaved by ACE. A crystal structure of the KP fragment of Ac-SDKP in the N domain of ACE has provided insight into the binding of the small tetrapeptide to the relatively large ACE catalytic site. This has facilitated the molecular docking of the full-length Ac-SDKP into both the N and C domains of ACE (Masuyer et al., 2015). The docking revealed that the specificity of the interaction of Ac-SDKP with the N domain occurs primarily as a result of bonds formed in the S2 subsite of the enzyme, where the Ac-Ser forms interactions with a conserved histidine of the N domain. However, while we observed that the Ac-DKP fragment was cleaved by ACE, the Ac-SDK peptide was not. It is likely that while interactions in the S2 subsite of the enzyme are important for specificity, interactions with other subsites drive the correct orientation and binding of the full length and tripeptides in the ACE active site.

The effects of Ac-SDKP on haematological stem cell proliferation have also been documented previously (Gaudron et al., 1999). It is plausible that upregulation of Ac-SDKP levels, through the administration of an Ac-SDKP analogue to reduce inflammation and fibrosis, could result in reduced haematological stem cell division. Acute and chronic ACEi therapy increase plasma Ac-SDKP levels approximately 5-fold and higher levels of Ac-SDKP levels are unlikely to arise due to the intermittent reactivation of ACE (Azizi et al., 1996)(Inoue et al., 2011)(Azizi et al., 1997). Thus, the administration of an Ac-SDKP analogue which might increase Ac-SDKP levels beyond a 5-fold increase could potentially lead to adverse effects of haematopoietic stem cell inhibition. Since it had been determined that the minimum requirement of the Ac-SDKP sequence for mitotic cycle progression is the SDK sequence (Gaudron et al., 1999), we sought to investigate the minimum sequence requirement for fibrosis prevention using peptides SDK, DKP, Ac-SDK, and Ac-DKP. The Ac-DKP fragment significantly inhibited the upregulation of TGF-β induced by ET-1 but not to the same extent as the physiological Ac-SDKP peptide. However, this only translated into a small, non-significant inhibition of collagen/ hydroxyproline levels. It is likely that further inhibition of the TGF-β levels are required to further prevent the downstream accumulation of collagen levels. This finding suggests that the minimum requirement for the antifibrotic effect could be the Ac-DKP fragment but that its binding to its receptor is impaired.

Various Ac-SDKP analogues have previously been described, including the Ac-S_DDK_DP analogue in which Asp and Lys were replaced with their D-isomers, which demonstrated antifibrotic effects in cardiac and hepatic fibrosis mice models (Ma et al., 2014)(Zhang et al., 2019). The Ac-SDψKP peptide with a reduced peptide bond was synthesised and as expected, the peptide was resistant to ACE cleavage with 96% of the peptide remaining after 24 h incubation with ACE. We tested the effect of the Ac-SDψKP analogue on the WI-38 fibroblasts and demonstrated that Ac-SDψKP could inhibit TGF-β/ Smad 3 signalling and collagen deposition. Our findings provide a rationale for the testing of this peptide in i*n vivo* models of fibrosis.

Fibrosis typically arises as a result of chronic low-grade inflammation (Wynn, 2008), which disrupts the ECM balance, leading to collagen and ECM protein deposition (Herrera et al., 2018b). The complex aetiology of fibrosing conditions, and their insidious nature, has made their prevention and management particularly challenging (Wilson and Wynn, 2009). Effective therapeutics for the treatment of fibrosis have largely remained elusive. The recognition of Ac-SDKP as an effective and necessary physiological player in the prevention of disseminated fibrosis has uncovered new opportunities for understanding and targeting pathophysiological processes arising during fibrosis (Peng et al., 2007)(Carretero, 2005).

ACEi and Ac-SDKP analogues provide separate but non-redundant ways of preventing fibrosis. ACEi inhibit both the formation of AngII and the cleavage of Ac-SDKP, whereas Ac-SDKP analogues can result in much higher concentrations of the antifibrotic peptide than is achieved by ACEi. We thus investigated whether the addition of ACEi lisinopril or the N domain-selective ACEi RXP407 could result in increased prevention of TGF-β/ Smad 3 signalling. Only, the combination of Ac-SDKP and RXP407 demonstrated a greater inhibition of hydroxyproline as compared to Ac-SDKP alone. This may be due solely to the inhibitory action of the ACEi on the breakdown of Ac-SDKP thus leading a maintenance in its concentrations. This would explain why the exhanced effect was not more effective than the Ac-SDψKP analogue. However, a different situation might be observed in an *in vivo* model where the different mechanisms of action of ACEi, particularly on AngII metabolism come into play.

5. Ac-SDKP and ACEi in the ACE signalling pathway

5.1. Background

Different signalling pathways contribute to the pathological processes that lead to inflammation, and ultimately to fibrosis (Wynn, 2008)(Grynberg et al., 2017)(Ponticos et al., 2009)(Matsuoka et al., 2002). The ACE signalling pathway initially described by the laboratory of Ingrid Flemming revealed the activation of MAPK and JNK signalling, which overlap with pro-inflammatory pathways (Kohlstedt et al., 2002)(Kohlstedt et al., 2004)(Reis et al., 2018).

The ACE cytoplasmic tail bears five serine residues, three of which are located within known kinase sequence motifs. An ACE signal transduction pathway has been described whereby the ACEi and substrate binding to ACE on the cell surface membrane trigger ACE dimerization and CK-2-mediated cytoplasmic tail phosphorylation (Kohlstedt et al., 2004)(Kohlstedt et al., 2006). Through the sequential mutation of the three potential CK-2 phosphorylation targets, Ser1270 has been shown to be the site of phosphorylation that triggers the signalling cascade (Kohlstedt et al., 2002)(Kohlstedt et al., 2004). This cascade leads to the activation of downstream pathways including the c-Jun NH_2-terminal kinase (JNK) and MAPK pathway, as evidenced by JNK and ERK phosphorylation (Kohlstedt et al., 2004)(Reis et al., 2018). Activation of the JNK and MAPK pathways leads to AP-1 induced activation or repression of target genes, including ACE (ACE99 gene), COX-2, β-arrestin 2, and interleukin-1 (Tournier et al., 1997)(Kohlstedt et al., 2005)(Reis et al., 2018).

Ac-SDKP induces the ACE signalling pathway in CHO cells in N or C domain catalytic knockouts of murine ACE (X. Sun et al., 2010). Interestingly, no signalling induction was observed in the fully active conformation of murine ACE. However, it has been shown that the ACE pathway is species-specific, and while there was no signalling response in response to AngI in porcine cells expressing human sACE, a significant activation of JNK was observed upon AngI binding to murine sACE in CHO cells (Kohlstedt et al., 2005). The effect of Ac-SDKP on human sACE signalling remains unknown. Activation of the ACE signalling pathway leads to JNK activation; however, Ac-SDKP inhibits both the JNK and ERK pathways, eventually inhibiting TGF-β-induced collagen expression (Zhang et al., 2011) (Kanasaki et al., 2006).

Different ACE inhibitors can induce different activation profiles in the same cell type (Reis et al., 2018). Captopril, which bears a sulfhydryl group that is associated with additional cardioprotective effects through free radical-scavenging, caused a significantly higher amount of JNK and ERK phosphorylation than ramipril in CHO cells expressing murine ACE (Pasini et al., 2007) (Reis et al., 2018). Next-generation N domain-selective ACE inhibitors have been proposed for the treatment of fibrosis (Douglas et al., 2013). Comparisons between the activation of ACE signalling by an N-selective inhibitor and a non-selective inhibitor would further clarify the suitability of these inhibitors for treating fibrosis.

It is unclear whether the ACE signalling cascade leads to a pro- or an anti-inflammatory response. While COX-2 often leads to inflammatory effects and contributes to pathological processes through the induction of local prostaglandin production, COX-2 inhibitors present a risk factor for atherosclerosis by increasing platelet aggregation, despite the inflammatory nature of the atherosclerotic process (Crofford, 1997)(Mukherjee and Nissen, 2001). It is also plausible that the protective or detrimental effects of the ACE signalling pathway might be tissue- and site-specific. A recent study by Reis *et al.* supports a beneficial, anti-inflammatory effect for the activation of the ACE signalling cascade (Reis et al., 2018). Cellular signalling through ACE upon Ac-SDKP binding could be yet another mechanism by which ACE can exert protective effects.

A direct indication of the degree of activation of the ACE signalling cascade can be obtained by quantifying the levels of phosphorylation at the signalling-specific S1270 site. ACE phosphorylation at this specific site is implicated in the shedding levels of ACE (Kohlstedt et al., 2004). Phosphorylation of ACE by CK2 may modulate enzyme shedding *in vivo* by increasing the stability of the membrane-anchored sACE (Kohlstedt et al., 2004). An assay to quantify ACE Ser1270 phosphorylation would thus provide an indicator of ACE signalling induction.

Phosphorylation and dephosphorylation events are central to most intracellular pathways that distribute signals across the cell (Graves and Krebs, 1999). Approaches such as mass spectrometry provide a unique opportunity to investigate serine/threonine- and tyrosine-phosphorylation sites, especially in the absence of a readily available antibody to a specific phosphorylation site (Pawson and Scott, 2005). Mass spectrometry is a highly sensitive method for the detection and characterisation of protein phosphorylation (Mann et al., 2002)(McLachlin and Chait, 2001). It is increasingly used in the semi-quantitative measurement of protein/peptide phosphorylation, with reproducible results obtained even in label-free quantitative approaches (Piersma et al., 2015)(Y.-T. Wang et al., 2010)(Soderblom et al., 2011).

5.2. Study objectives

The objective of this chapter is to investigate whether Ac-SDKP and the N domain-selective ACEi, RXP407, induce ACE phosphorylation and the downstream cellular signal transduction through the:

1. determination of substrate/inhibitor induced phosphorylation of Ser1270 using a mass spectrometry approach.

2. investigation of the association between ACE and pJNK following treatment with lisinopril, Ac-SDKP, or RXP407 using immunoprecipitation and immunoblotting.

3. analysis of JNK phosphorylation or ACE expression as a result of ACE signalling induction.

5.3. Methods

5.3.1. Cell culture and treatment

5.3.1.1. Cell culture conditions

CHO-K1 cells (American Type Culture Collection-ATCC®CCL-61) transfected with various human sACE constructs (WT-sACE and the C domain knock out, CKO) were reconstituted into 75 cm^2 flasks and grown in 10 ml of growth medium (50% Dulbecco's Modified Eagle Medium (DMEM) (Sigma, USA), 50% HAMS-F12 (Sigma, USA), 20 mM HEPES buffer, pH 7.5, supplemented with 10% foetal calf serum (FCS) [heat-inactivated for 30 min at 56°C]). Cells were grown to 75% confluency, lifted using Trypsin-EDTA (Gibco®, USA) and seeded into 6-well plates. Prior to treatment (see 3.3.2), cellular growth and division was synchronised through serum starvation for 18 hours in 2% FCS medium and 1 hour in Opti-MEM (Gibco®, USA)(Cooper, 2003). All flasks and plates were incubated at 37°C, 5% CO_2 and 80% humidity.

5.3.1.2. Cell treatment with Ac-SDKP or ACEi

Ac-SDKP or inhibitors were added to 85% confluent cells in 6-well plates. One ml of 100 nM inhibitor (lisinopril, RXP407) or 100 nM Ac-SDKP in Opti-MEM was added to the cells and incubated for 5 mins to 24 h. Plain Opti-MEM was used as a control in all experiments. The reaction was stopped by removing the inhibitor or substrate and adding 1 ml of ice-cold 1x phosphate buffered saline (PBS). Extensive washing with 1x PBS was performed to remove all traces of BSA. Cells were then lysed overnight at 4°C in 200 µl of RIPA lysis buffer for subsequent MS analysis, or in 100 µl of Triton buffer (0.05 M HEPES, 0.5 M NaCl, 1% triton X-100, 1 mM PMSF supplemented protease inhibitor cocktail (Set III, Calbiochem, USA)) and phosphatase inhibitor cocktail (PhosSTOP, Roche, Switzerland)) for immunoprecipitations and western blotting. Triton lysates were centrifuged at 10000 *g* at 4°C and the supernatants were retained. Supernatants were either used immediately or stored at -80°C for western blot analysis. For in-gel tryptic digest of proteins, samples were lysed overnight in 250 µl of Laemmli buffer and boiled for 15 minutes. Lysates were stored at -80°C.

5.3.2. Western blotting and immunoprecipitation

5.3.2.1. SDS-PAGE gel electrophoresis

SDS-PAGE gels were carried out as per section 4.3.4.

5.3.2.2. Immunoprecipitation (IP)

IP of ACE, JNK, and p-JNK was performed using specific monoclonal antibodies (Bonifacino et al., 1999). The ACE 9B9 antibody was obtained from our collaborator, while the JNK and p-JNK antibodies were ordered from Cell Signalling Technology (USA) (Gordon et al., 2010). Briefly, 200 µl of cell lysates were pre-cleared with 20 µl of 50% magnetic protein-G Dynabead slurry (Thermofischer, USA). Lysates were thereafter incubated at 4°C with gentle rotation overnight with a 1/100 antibody: sample ratio. Following antibody binding, 25 µl of Protein-G Dynabeads was added to the mixture and incubated at 4°C for 3 hours with gentle rotation. After binding, the supernatants were removed by precipitating the magnetic beads with a strong magnet and washing 3 times with 250 µl of lysis buffer. The elution of the antigen and antibody was performed by boiling the beads with 30 µl of Laemmli buffer for 5 minutes. The detection of immunoprecipitated p-JNK and co-immunoprecipitated ACE and pJNK was carried out by western blotting using ACE and JNK antibodies, respectively.

5.3.2.3. Western blotting

Western blots were performed according to section 4.3.5. The 4G6 monoclonal antibody (a gift from our collaborator) was used for the detection of ACE (Balyasnikova et al., 2005). Antibodies for GAPDH, pJNK, and JNK were obtained from Cell Signalling Technology. Densitometry analysis was performed on western blot images using Image J (NIH).

5.3.3. Mass spectrometric detection of phosphorylated ACE at S1270

5.3.3.1. FASP

FASP of cell lysates for discovery and targeted MS analysis was performed as per section 3.3.3.3 using 200 µg of sACE-CHO cell lysate.

5.3.3.2. In-gel protein digestion and mass spectrometry analysis

An in-gel digestion method was adapted from Shevchenko *et al*. for the tryptic digest of sACE-CHO cell lysate (Shevchenko et al., 1996). Following 1-D reducing SDS-PAGE, proteins were visualised and fixed by staining with Coomassie staining solution (0.25% Coomassie brilliant blue, 50% methanol, 10% acetic acid) and destained overnight (25% ethanol, 10% acetic acid). Bands of interest (size range of ≈ 150-250 kD) were excised and diced into 1 mm^2 pieces, then destained with 200 mM ammonium bicarbonate (NH_4CO_3)/acetonitrile (ACN) (50:50) and vortexed until transparent. Samples were dehydrated with 100% ACN and dried in a Savant SpeedyVac (ThermoScientific, USA). Reduction and alkylation of cysteine residues was performed by incubating with 200 µl of 10 mM dithiothreitol (DTT) in 25 mM NH_4HCO_3 at 56°C for 1 hour, followed by incubating with 200 µl of 55 mM iodoacetamide (Sigma, USA) in 25 mM NH_4HCO_3 in the dark for 45 minutes at room temperature. Tryptic digest was performed by rehydrating the gel pieces in trypsin solution at a trypsin to protein ratio of 1:50 (New England Biolabs, USA). The gel pieces were covered in 25 mM NH_4HCO_3 and samples were incubated overnight in a wet chamber to allow diffusion of the trypsin into the gel pieces.

5.3.3.3. Sample desalting

Desalting of tryptic peptides was performed according to 3.3.5.

5.3.3.4. Phosphopeptide enrichment by Fe-IMAC

To perform phospho-enrichment, desalted tryptic peptides were reconstituted in 0.5 ml of Fe-IMAC solvent A (30% ACN, 0.07% (v/v) TFA) and injected on a 4 mM iron (Fe)-IMAC column (Thermo Fisher Scientific, USA) coupled with an Agilent 1260 Infinity HPLC system (Agilent, USA). The column was charged with iron according to the manufacturer's instructions and prepared as described by Ruprecht *et al* (Ruprecht et al., 2017). Briefly, the column was rinsed with 20 mM FA, charged with 25 mM $FeCl_3$ in 100 mM acetic acid and washed extensively with 20 mM FA to

remove unbound iron ions. The sample was loaded onto the column at a rate of 0.1 ml/min for 5 minutes and eluted with a non-linear 0% to 50% Fe-IMAC in solvent B (0.5% (v/v) NH_4OH). The flow-through and phospho-enriched fractions were collected with the guidance of the UV signal (280 nm) and dried in a vacuum centrifuge prior to a second round of desalting as described in 3.3.5.

5.3.3.5. **Mass spectrometry**

Both discovery and targeted MS analysis was carried out on the Q-Exactive™ Hybrid Quadrupole-Orbitrap Mass Spectrometer coupled to a Dionex UltiMate 3500 RSLC nano-LC system according to 3.3.4. For targeted MS, elution was carried out using a 140-minute linear gradient of acetonitrile/0.1% formic acid at a constant flow rate of 300 nl/min. The Q-Exactive was operated using the PRM method, with an isolation window of 4.0 m/z and an isolation list that was developed using Skyline (MacLean et al., 2010) to specifically target the cytoplasmic tail of ACE, detecting the doubly phosphorylated serine peptide (H**S**HGPQFG**S**EVELR (870.35 *m/z*) and singly phosphorylated peptides (H**S**HGPQFGSEVELR, HSHGPQFG**S**EVELR (830.36 *m/z*)), as well as the non-phosphorylated cytoplasmic tail peptide (HSHGPQFGSEVELR, (790.38 *m/z*)). Fragmentation of these selected peptides was performed by via high-energy collision dissociation with a normalized collision energy (NCE) of 27. The abundance threshold for targeted ion selection was 1.7×10^4 and a charge exclusion of z=1 and z>4 ions was selected. Chromatograms of both parent and fragment ion transitions were subsequently analysed in Skyline. For discovery MS analysis, raw data was analysed in MaxQuant as described in section 3.3.5.

5.3.4. Statistical analysis

Data analysis was performed using the statistical software GraphPad PRISM 6.0 (GraphPad software Inc, USA). Un-paired, nonparametric Student's t-tests were employed for the comparison of treated vs. untreated samples, with a cut off for statistical significance of $p<0.05$.

5.4. Results

5.4.1. ACE S1270 phosphorylation by lisinopril

5.4.1.1. Mass spectrometric detection of S1270 phosphorylation

A direct quantification of the induction of the ACE signal cascade requires the quantification of phosphorylation levels at the implicated serine residue. We attempted to optimise the quantification of various modified variants of the cytoplasmic tail peptide during several MS experiments. CHO cells expressing s-ACE and incubated for 7minutes with lisinopril were used for the MS detection of phospho-Ser1270. Two sample preparation methods were used: FASP and in-gel tryptic digest. A targeted method was developed for targeting the phosphorylated cytoplasmic tail of ACE for detection of the doubly phosphorylated serine peptide (H**S**HGPQFG**S**EVELR (870.35 *m/z*) and singly phosphorylated peptides (H**S**HGPQFGSEVELR, HSHGPQFG**S**EVELR (830.36 *m/z*)), as well as the non-phosphorylated cytoplasmic tail peptide (HSHGPQFGSEVELR, (790.38 *m/z*)).

Neither the unphosphorylated nor the phosphorylated versions of the cytoplasmic tail peptide of interest could be detected in discovery MS (data not shown). However, targeted MS is capable of extremely sensitive detection of target peptides and it does not rely on the chance inclusion of the target peptide in a top N method. Targeted MS is an effective tool for measuring low-abundance or otherwise elusive peptides in a complex mixture.

In targeted MS analysis of samples prepared by FASP and in-gel tryptic digests, a very low signal for the phosphorylated peptides was detected. A representative chromatogram is depicted in Figure 5-1. The unphosphorylated peptide of interest was identified across all the samples with both sample preparation methods. However, due to the low intensity and lack of multiple co-eluting fragment ions for the modified peptide, no confident quantification of the phospho Ser1270 peptide could be performed. This highlighted the need for alternative strategies to detect these phosphorylated peptides.

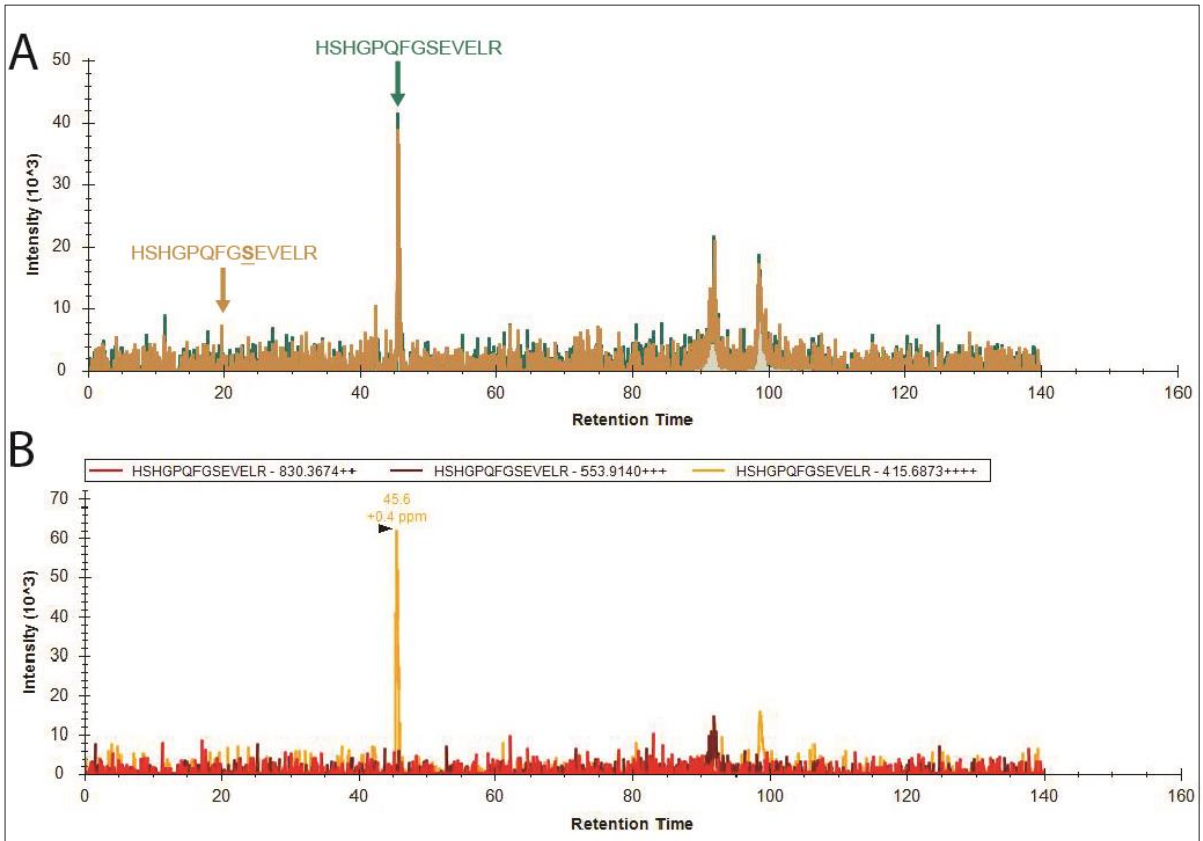

Figure 5-1: Mass spectra chromatograms from 7-minute lisinopril treatment of sACE-expressing cells **A.** Skyline-generated representative extracted ion chromatograms of the unmodified and modified HSHGPQFGSEVELR peptide. **B.** Skyline chromatograms of the +2, +3 and +4 charged phosphorylated HSHGPQFGSEVELR peptide at Ser1270. Only the +4 peptide was detected above background levels.

5.4.1.2. **Phosphopeptide enrichment for phospho S1270 detection**

Due to the substoichiometric nature of phosphorylation events (Steen et al., 2006), enrichment of phosphorylated peptides was performed on an Fe-IMAC column to improve the detection of the phosphopeptides of interest. A definite peak at 8.3 minutes was observed corresponding to phosphorylated peptides that had bound to the positively charged Fe+ ions of the column (Figure 5-2). Unphosphorylated peptides eluted after 1 minute with the solvent. Both the unphosphorylated and the phosphorylated fractions were collected for LC-MS/MS analysis.

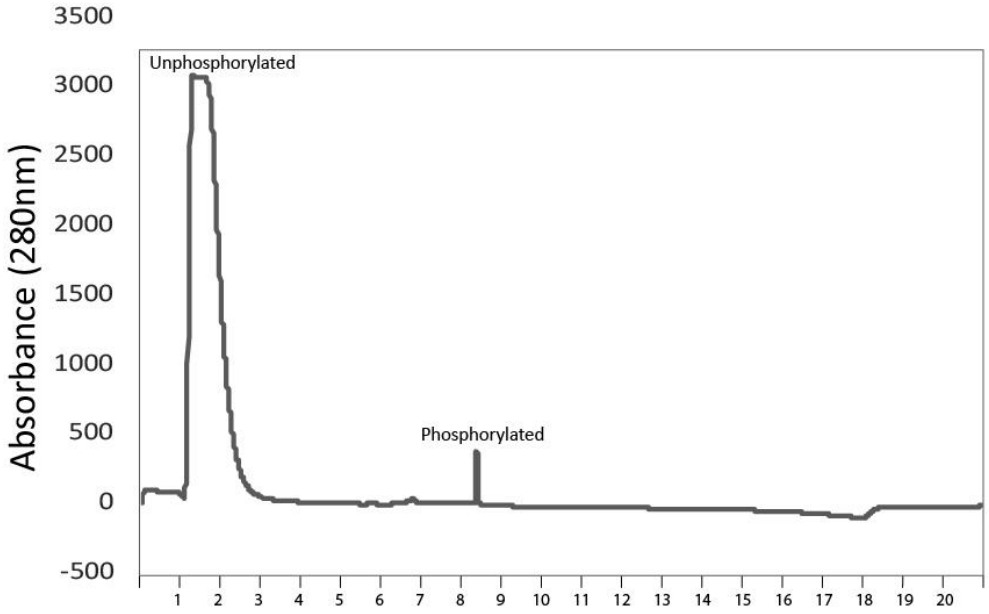

Figure 5-2: Representative chromatogram of Fe-IMAC phospho peptide enrichment.
HPLC chromatograms of the large unphosphorylated peptide peak co-eluting with the buffer at 1 minute, and the small phosphorylated peptide peak eluting at 8.3 minutes.

5.4.1.3. **Targeted MS of phospho-peptide pool**

Following peptide enrichment, both the phosphorylated and unphosphorylated fractions were analysed in a targeted PRM-MS experiment. The chromatograms of the different ion transitions were analysed in skyline and the corresponding peak area data was analysed (Figure 5-3).

The doubly phosphorylated peptide was not detected but both the singly phosphorylated peptides at both serine sites were detected. The detection of the b9 ions for the HSHGPQFGSEVELR peptide of interest allowed for the distinction between the singly phosphorylated peptides. However, while a number of co-eluting fragment ions were identified for the unmodified peptide, this was not the case for the phosphorylated peptide. The predominant ion was the b2 ion for the Ser1270 phospho site, and so while the Ser1270 phosphopeptide could be identified, accurate quantification could not be performed.

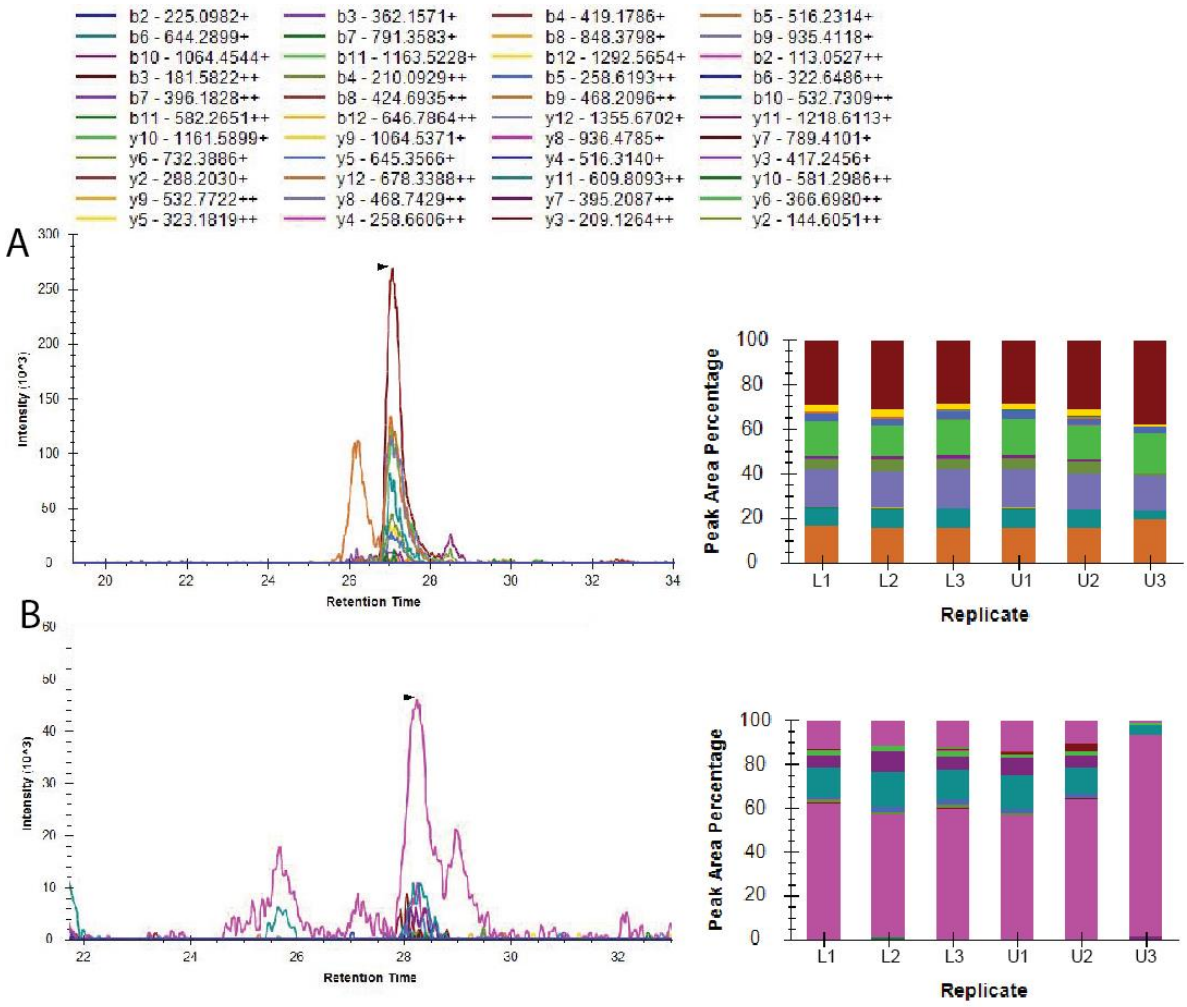

Figure 5-3: Extracted ion chromatograms and peak area proportions following 7-minute treatment of sACE-expressing cells with control (U) and lisinopril (L).

A) Representative extracted ion chromatogram of the unmodified HSHGPQFGSEVELR peptide with the observed fragment ions in each of the replicates of the treated and untreated cell lysates. B) Representative chromatogram depicting fragment ion profile of the Ser1270 phosphorylated HSHGPQFGSEVELR peptide, showing dominance of the b2 ion.

5.4.2. Association between ACE and pJNK upon ACEi and Ac-SDKP treatment

An association between ACE and pJNK occurs upon the activation of the ACE signalling cascade. To assess whether ACEi or Ac-SDKP induce sACE and pJNK association, co-immunoprecipitations were performed using specific antibodies, and signal-induced associations were detected by western blotting against sACE and pJNK. The cell lysates were normalised to the samples with the lowest total protein concentration prior to immunoprecipitation. Associations between pJNK and ACE were visualised by the detection of ACE in the JNK antibody immuno-precipitate, and the corresponding detection of pJNK in the ACE antibody (9B9) precipitate (Figure 5-4). Importantly, 9B9 resulted in the immunoprecipitation of pJNK in the CHO-sACE lysate treated with ACEi and Ac-SDKP, but not in the control, indicating a lack of association in the absence of inhibitor/substrate binding to ACE.

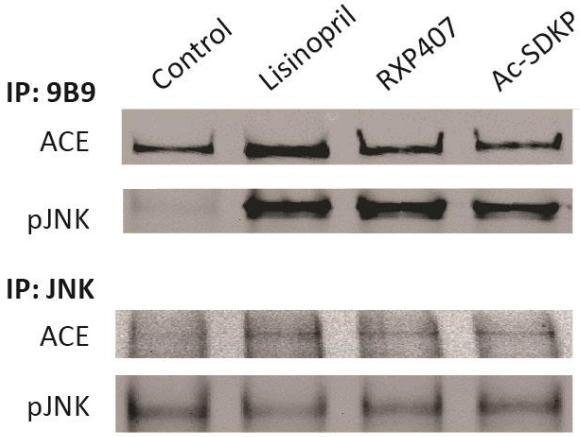

Figure 5-4: Co-immunoprecipitation of sACE and pJNK after treatment with lisinopril, RXP407 and Ac-SDKP.
Western blot of the immunoprecipitation of sACE and pJNK in CHO-sACE cell lysis after a 7-minute treatment with lisinopril. Bands corresponding to the correct size of sACE (≈170 kDa) and pJNK (54 kDa) were detected upon blotting with both sACE- and JNK-specific antibodies.

5.4.3. Immuno-quantitation of pJNK induction by ACEi and Ac-SDKP

5.4.3.1. Dose response of pJNK to Ac-SDKP

A range of Ac-SDKP concentrations were used to determine the optimal concentration of Ac-SDKP that induces pJNK phosphorylation in sACE-CHO cells. Samples were immunoprecipitated using an antibody specific to JNK and western blotting was used to probe for total JNK and induced pJNK levels. A 100 nM concentration of Ac-SDKP resulted in the maximum pJNK/tJNK induction and was therefore used in subsequent experiments (Figure 5-5).

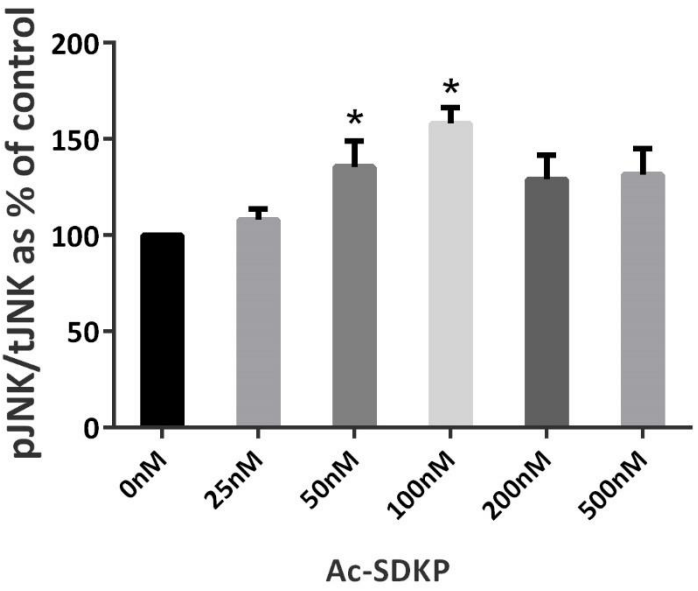

Figure 5-5: The dose-response of pJNK induction upon Ac-SDKP treatment.
Densitometry of immunoprecipitation after treatment with various concentrations of Ac-SDKP for 7 min, probed with a JNK-specific antibody. Western blotting was performed using both pJNK and JNK antibodies and the ratios of the pJNK densitometry to tJNK was calculated as a percentage of the control. Data is the average ±SEM of two experiments in duplicate and significance is indicated by an asterisk (*) ($p < 0.05$).

5.4.3.2. Immuno-quantitation of pJNK association with ACE

IPs were performed with the specific monoclonal antibody 9B9 on CHO-sACE cells to determine whether lisinopril and Ac-SDKP induce an increase in the association between sACE and pJNK on the intracellular side of the membrane. Treatment with lisinopril as well as Ac-SDKP resulted in significant pJNK association with ACE, suggesting that activation of the JNK pathway is initiated upon binding of both the substrate and inhibitor (Figure 5-6). Notably, RXP407 treatment resulted in a significantly lower increase in pJNK association with ACE than lisinopril or Ac-SDKP.

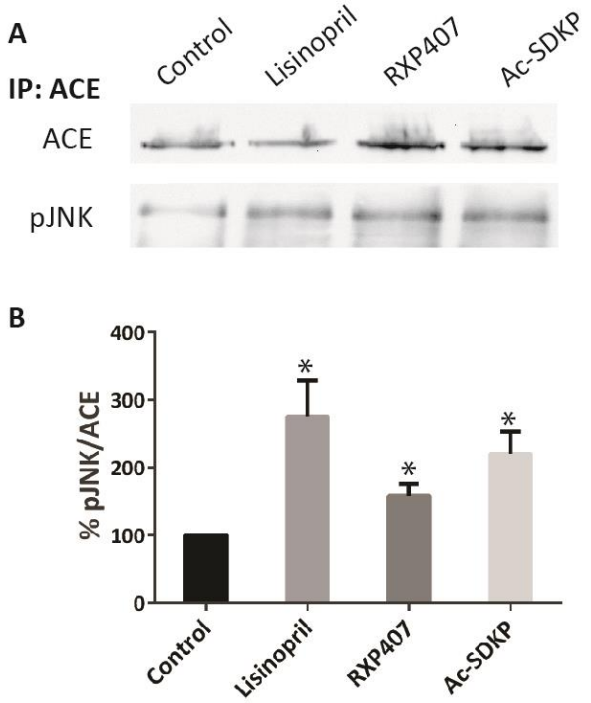

Figure 5-6: Increased co-immunoprecipitation of pJNK with sACE on treatment with ACEi and Ac-SDKP.

sACE and associated pJNK was co-immunoprecipitated from CHO-sACE lysates with the ACE 9B9 antibody following treatment with 200 nM lisinopril, RXP407, or 100 nM Ac-SDKP for 7 minutes. **A)** Representative western blot for sACE and pJNK **B)** Densitometry analysis of pJNK/ACE ratios over untreated samples. Data represents average ±SEM of two experiments, each in duplicate. Significance is indicated by * $p < 0.05$; ** $p < 0.01$.

5.4.3.3. Immuno-quantitation of cytosolic pJNK levels

To confirm that the observed pJNK levels associated with ACE translated into increased JNK pathway activation, the cytosolic ratio of pJNK/JNK was investigated. A JNK antibody was used for the IP and the levels of pJNK and JNK were measured by western blotting and densitometry (Figure 5-7).

Both ACEi and Ac-SDKP induced an increase in the p-JNK/JNK ratio, indicative of activation of the JNK signalling cascade upon binding of substrate and inhibitor. The pattern of increased activation by lisinopril as compared to RXP407 was observed as in 5.4.3.2.

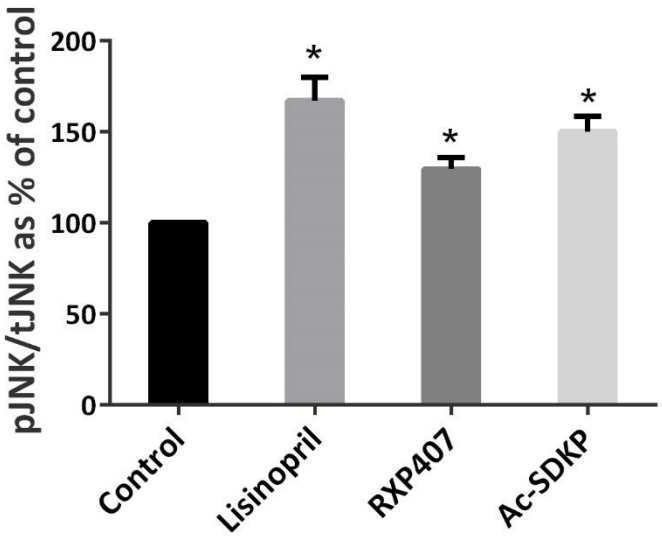

Figure 5-7: Increased co-immunoprecipitation of pJNK with JNK on treatment with ACEi and Ac-SDKP.
Densitometry of JNK and pJNK levels from CHO-sACE lysates following treatment with 200 nM lisinopril/RXP407 or 100 nM Ac-SDKP for 7 minutes and measured by western blotting. Data is representative of mean ±SEM of two experimental experiments blotted n=2 each. Significance is indicated by * ($p < 0.05$).

5.4.4. Effect of Ac-SDKP and inhibitors on ACE expression levels in sACE-CHO cells

The downstream effect of ACE signaling pathway activation is an increase in ACE expression after 12-24 hours of treatment (Kohlstedt et al., 2005)(X. Sun et al., 2010). The effects of ACEi and Ac-SDKP were investigated in sACE-expressing cells at various time points (8 hours, 12 hours, and 24 hours) following treatment. In the present study, the levels of ACE expression induced by inhibitors and Ac-SDKP were not significantly different than those of the untreated controls at the different incubation times, except for lisinopril treatment at 8 hours that showed increased ACE expression (Figure 5-8).

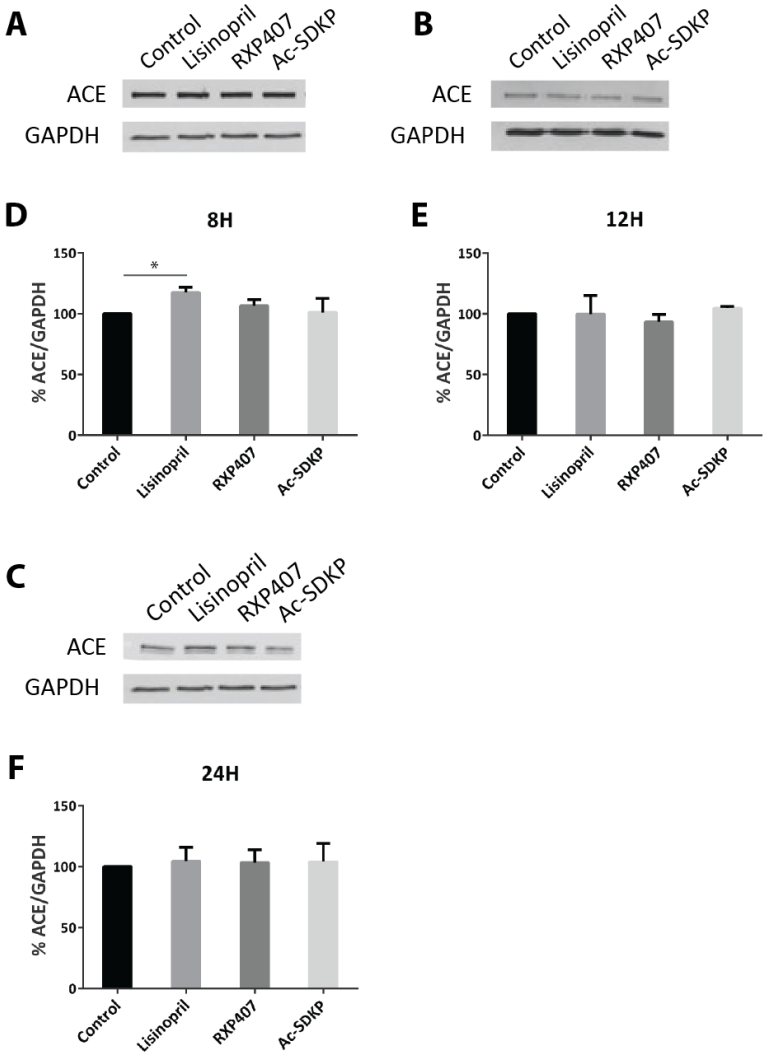

Figure 5-8: sACE expression post lisinopril, Ac-SDKP, or RXP407 treatment.
sACE-CHO cells were treated with 100 nM lisinopril, RXP407 or Ac-SDKP for 8-24 hours prior to lysis. Representative western blots of sACE and GAPDH after A) 8H B) 12H and C)24H treatments are depicted. Densitometry of sACE/GAPDH ratio bands as a percentage of vehicle treated samples for D) 8H, E) 12H, and F) 24H lysates are shown. Data represents the mean ±SEM of 3 experiments and significance is denoted by an asterisk (*) for $p < 0.05$.

5.4.5. Effect of Ac-SDKP and inhibitors on ACE expression in CHO cells expressing sACE with inactivated C domain

Ac-SDKP (at a 10 µM concentration) increased the expression of ACE after 24 h in N or C domain knock-out mutants of murine ACE (X. Sun et al., 2010). To investigate whether Ac-SDKP can induce ACE expression in a knock-out mutant of sACE, a CKO-CHO (transfected by Dr Kate Larmuth) cell line was used, where the zinc coordinating amino acid residues were mutated in the C domain to obtain a C domain catalytical knock-out. We investigated and quantified the effect of a range of concentrations of Ac-SDKP on ACE expression in CKO-CHO cells by western blotting and densitometry (Figure 5-9). GAPDH was used to control for differences in protein loading levels. A slight but not significant increase in ACE expression was observed at 24 h when 1 and 10 µM Ac-SDKP were added.

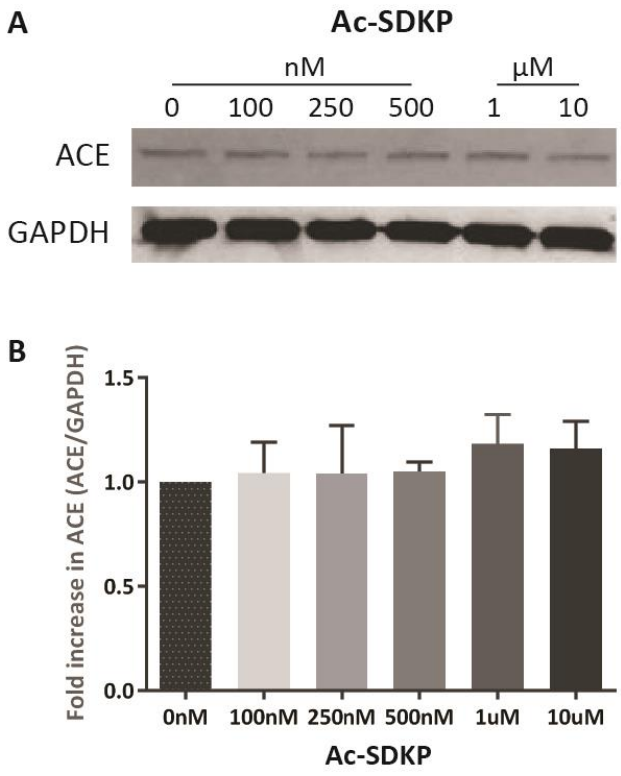

Figure 5-9: sACE levels induced by Ac-SDKP treatment in CKO-CHO cells.
CKO-CHO cells were treated with 100 nM-10 µM Ac-SDKP for 24 hours prior to lysis. A) Representative western blot of sACE and GAPDH after 24 h treatment. B) Densitometry of sACE bands as a percentage of vehicle treated samples. Data represents the mean ±SEM of 3 experiments.

5.5. Discussion

The ACE signalling pathway, activated by the phosphorylation of Ser1270 on the cytoplasmic portion of the membrane-bound protein, can be triggered both by inhibitor and substrate binding to ACE (Sun et al., 2010). We investigated for the first time whether Ac-SDKP and the N domain-selective ACEi RXP407 trigger the ACE signalling pathway via human sACE. The first major finding from this chapter was that Ac-SDKP as well as RXP407 could induce signalling via binding to ACE, thus identifying a potential novel mechanism of action for the antifibrotic Ac-SDKP. A limitation of this study was that a quantification of the phosphorylation level could not be obtained. The second important finding was that Ac-SDKP and ACEi did not result in an increase in ACE expression. This is in line with their well-documented anti-inflammatory and antifibrotic effects as ACE expression leads to the formation of the pro-inflammatory AngII.

The first step of the ACE signalling pathway involves the dimerization and CK-2-mediated phosphorylation of Ser1270 (Kohlstedt et al., 2006). This phosphorylation event has been linked to the shedding of ACE, with an accumulation of soluble ACE observed in the supernatant of human umbilical vein endothelial cells (HUVECs) transfected with non-phosphorylated forms of ACE (Ser1270 mutated to Ala1270) (Kohlstedt et al., 2002). This was indirectly confirmed by Barauna et al., who demonstrated that ACE can act as a mechano-sensor, able to sense shear stress, and is capable of regulating its own levels through a reduction in Ser1270 phosphorylation, JNK activation, and ACE expression levels (Moskowitz, 2002)(Barauna et al., 2011). In an attempt to quantify the degree of phosphorylation of Ser1270, and thus the ACE signalling response upon treatment with Ac-SDKP and RXP407, we performed MS analysis of cell lysates of untreated and treated sACE-CHO cells. The initial discovery MS analysis failed to detect both the modified and unmodified variants of the peptide of interest. This was not surprising as discovery MS analysis does not necessarily provide full coverage of the protein sequence. Instead, the abundance of the protein in question as well as the ability of each specific peptide to ‘fly’ in the MS, as well as the complexities of the background matrix all affect the visibility of a particular peptide in discovery MS. As a result, regions/peptides of interest are routinely missing in discovery MS experiments (McLachlin and Chait, 2001). A targeted approach was thus adopted to localize and quantify the Ser1270 phosphorylation in an unenriched sample. Whilst this approach allowed the detection of the unmodified peptide, its phosphorylated counterpart could not be detected.

This is likely due to the sub-stoichiometric nature of phosphorylation modifications - since the phosphopeptide is present at far lower concentrations than the unphosphorylated one, its detection presents a challenge (Wu et al., 2011). The phospho-proteome represents approximately 1% of the total proteome. Further, negatively charged modifications including phosphorylation can interfere with proteolytic digestion by trypsin, further affecting the visibility of phosphopeptides (Benore-Parsons et al., 1989).

To circumvent these challenges in phosphopeptide detection, two fractionation strategies were used to reduce the complexity of the sample. Optimisation of the phosphopeptide detection was performed on the Q-Exactive using lisinopril as a positive control. An in-gel digestion strategy, whereby a gel piece in the molecular weight region corresponding to the size of sACE, was excised and digested. The unmodified peptide was detected with several co-eluting fragment ions and a good signal: noise ratio, but the pSer1270 HSHGPQFG**S**EVELR variant had poor signal. Gel-based tryptic digests may result in incomplete digestion of proteins embedded in the polyacrylamide gel matrix, as well as during the extraction of digested peptides from the matrix (Gundry et al., 2009). An Fe-IMAC HPLC column was subsequently used for the enrichment of phosphopeptides. The strength of this technique lies in the linear efficiency of the enriched product with the quantity of starting material, and the negligible levels of incomplete phosphopeptide binding or elution from the column (Ruprecht et al., 2017). This strategy allowed for the detection of the phosphorylated Ser1270 peptide. While the detection of the b9 ion for the HSHGPQFG**S**EVELR peptide confirmed the presence of the phosphorylated site of interest, the majority fragment ion observed was the b2 ion, which does not discriminate between the two potential serine phosphorylated sites on the peptide. The fragment ions co-eluting with b2 for the phosphopeptide had low intensity, so that accurate quantification of the phospho-Ser1270 levels in comparison to the unmodified peptide could not be performed. The detection of predominantly triply and quadruply charged precursors may point to the cause of the low abundance of this peptide despite enrichment strategies. Tryptic peptides often acquire higher charged states following ESI, and this is emphasised with phosphopeptides. If the precursor was multiply charged (>4+), the resulting fragment ions may have been multiply charged (>2+) and these may have been excluded during discovery MS. Another limitation of the approach used is the cell construct used for the inhibitor treatment. The sACE-CHO cells over-expresses sACE, so the ratio of phosphorylated to unphosphorylated sACE is unknown, as is the maximal phosphorylation level of this peptide.

We also investigated the effect of the N domain-selective RXP407 compared to that of lisinopril on ACE signalling. While the effects of ramipril, captopril, and enalapril on the ACE signalling pathway have been investigated, our group has been the first to test the effects of lisinopril and a domain-selective inhibitor on ACE signalling (Tournier et al., 1997)(Kohlstedt et al., 2005)(Reis et al., 2018)(Sun et al., 2010). Both lisinopril and RXP407 lead to the activation of the ACE signalling cascade. Interestingly, lisinopril induced a small but significant increase in ACE expression at a single 8 h time point, while RXP407 did not cause any upregulation of ACE expression. Although ramipril induces ACE signalling, captopril failed to induce ACE expression. It is thus entirely plausible that lisinopril and RXP407 have minimal effects on ACE expression through their binding to ACE on the cell surface membrane. This could also be due to the absence of the native promoter for ACE; therefore *in vivo* confirmation of these results are warranted.

Ac-SDKP is well established in its role as an antifibrotic agent, and as an inhibitor of TGF-β/Smad signalling (Peng et al., 2001)(Cavasin et al., 2007). This effect was confirmed in our experiments on a fibroblast cell line (Chapter 4). Non-canonical TGF-β signalling can activate non-Smad pathways, including the JNK and MAPK pathways, leading to stress fibre formation as well as epithelial-to-mesenchymal differentiation (Derynck et al., 1998). Ac-SDKP inhibits both MAPK and JNK phosphorylation, decreasing collagen and extracellular matrix deposition (Rhaleb et al., 2001)(Peng et al., 2012)(Zhang et al., 2011). Conversely, Ac-SDKP induced JNK phosphorylation in the ACE signalling pathway in murine sACE (Sun et al., 2010). We therefore conducted experiments to determine whether Ac-SDKP activated JNK when bound to human sACE. In the present study, Ac-SDKP also activated ACE outside-in signalling, as evidenced by an increased association of pJNK with ACE compared to that of the control, suggesting that the ACE signalling pathway is activated upon Ac-SDKP binding to ACE. This resulted in an increase in circulating pJNK levels in sACE-CHO cells. However, no concomitant increase in ACE expression was detected in either the sACE-CHO or the CKO-CHO cell line. This contrasts with Sun., *et al* who observed increased mACE expression in C domain knock out mutants of murine ACE, despite the absence of the native ACE promoter. This again highlights the species-specific nature of the ACE signalling pathway, which has broader implications for models based on murine cells.

While initial experiments of the ACE signalling pathway suggested a pro-inflammatory response profile, captopril treatment lead to a reduction in cyclooxygenase 2, IL-1β, and

arrestin-2 expression levels, which supports a protective role for the ACE pathway in inflammation and fibrosis (Reis et al., 2018). Ac-SDKP inhibits IL-1β-mediated increases in MMP activity and expression in cardiac fibroblasts, leading to an increase in TIMP-1 and TIMP-2 expression (Rhaleb et al., 2013).

The RAAS is inextricably linked to inflammation, and Ac-SDKP may therefore exert beneficial effects through the inhibition of IL-1β levels. The observed activation of ACE signalling by Ac-SDKP could lead to a decrease in the expression of inflammatory mediators. While the potential anti-inflammatory effects mediated by the ACE signalling pathway through Ac-SDKP and ACEi are likely to be environment- and cell- specific, the proposed mechanism of this protective effect (Figure 5-10) outline a plausible mechanism of action for both Ac-SDKP and ACEi.

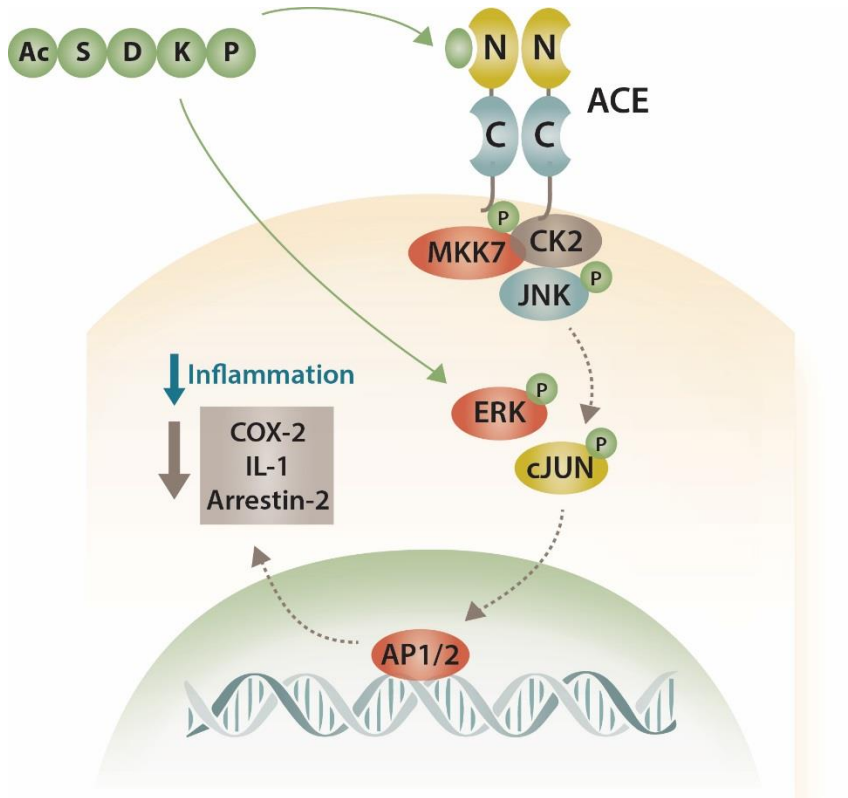

Figure 5-10: Potential targets of Ac-SDKP-mediated ACE signalling cascade.
Ac-SDKP has been shown in our study through binding to sACE to induce JNK signalling and in previous studies to cause ERK phosphorylation through binding to ACE. This is proposed to lead to a decrease in inflammatory and fibrotic mediators such as COX-2 and IL-1. MKK7: Map kinase kinase 7, CK2: Casein Kinase 2, AP1: Apoprotein 1, COX-2: Cyclooxygenase 2, IL-1: Interleukin 1.

6. Conclusions, limitations and future directions

6.1. Conclusions

The incidence of constrictive pericarditis, a fibrotic complication of tuberculous pericarditis, has highlighted the need for studies into the pathological mechanisms of fibrosis in the pericardial environment (Naicker and Ntsekhe, 2020). The overarching aim of this thesis is to study and gain further insight into the molecular mechanisms and mediators involved in the development of fibrosis, particularly in TB pericarditis. In Chapter 2, the roles played by Ac-SDKP, ACE, POP and Gal-3 in the pathophysiology of constrictive TB pericarditis were investigated. The levels of Ac-SDKP and Gal-3 in TB+ and TB- pericardial fluid were quantified. Notably, Ac-SDKP levels were decreased in TB+ pericardial fluid; however, there was no significant change in the levels of profibrotic Gal-3. The physiological importance of Ac-SDKP has been highlighted in the disseminated organ fibrosis occurring as a result of POP inhibitor administration (Carretero, 2005). This points to a potent effect of the tetrapeptide in its immediate environment and hence, its absence constitutes a highly plausible factor for pericardial fibrosis progression. Importantly, we investigated the Ac-SDKP metabolism through the quantification of the enzymatic activities of i) its rate limiting synthesising enzyme POP, and ii) its predominant degrading enzyme ACE. This uncovered a potential mechanism for reduced Ac-SDKP levels in TB pericardial fluid. An increase in ACE activity, arising from an immune/inflammatory response to the presence of *M.tb* in the pericardium, results in increased cleavage of Ac-SDKP. The rate limiting enzyme involved in Ac-SDKP formation, notably POP, was also present in pericardial fluid suggesting the local production of Ac-SDKP.

The precise molecular effects of Ac-SDKP is unknown and in Chapter 3 MS-based discovery proteomics was used to interrogate intracellular and extracellular proteins that are regulated by the tetrapeptide. We observed that Ac-SDKP was capable of inducing a range of cellular and extracellular dysregulations. In the secretome, Ac-SDKP inhibited the expression of various ECM constituents including both collagens and non-collagenous proteins. This study is the first to demonstrate the inhibitory action of Ac-SDKP on collagen VI, lumican and decorin. Additionally, fibrogenic players, modulated by Ac-SDKP in the intracellular space including SPARC, serpine-1 and fibroblast growth factor-2, were identified. Ac-SDKP is likely to induce its effects by binding to the FGFR-1 receptor as suggested in previous studies (Li et al., 2017)(Hu

et al., 2018). Further novel mechanisms of action for Ac-SDKP, including the PINCH-ILK-PARVIN complex mediated focal adhesion and Notch signalling, were identified.

Fibrosis is increasingly recognised as a significant contributor to morbidity and mortality across a myriad of disease aetiologies. However, treatment strategies which specifically target the pathological processes occurring in fibrosis, are scarce. In Chapter 4, the antifibrotic potential of Ac-SDKP analogues and ACEi was assessed. In WI-38 human fibroblasts, Ac-SDKP significantly inhibited TGF-β expression, Smad phosphorylation and a downstream reduction in collagen levels. Previous studies revealed that SDK is the minimum requirement for the anti-proliferative effects of Ac-SDKP (Robinson et al., 1993). Thus the effect of peptides SDK, DKP, Ac-SDK, and Ac-DKP on fibrosis prevention were tested. Only the Ac-DKP fragment moderately inhibited TGF-β expression and could be slowly cleaved by ACE. We also demonstrated that the Ac-SDψKP peptide could inhibit TGF-β/ Smad 3 signalling and collagen deposition. In addition, the Ac-SDKP physiological peptide, but not Ac-SDψKP in combination with ACEi, demonstrated a greater inhibition of hydroxyproline as compared to Ac-SDKP alone.

In Chapter 5, we investigated the effects of Ac-SDKP, lisinopril and RXP407 on the ACE-signalling cascade. Ac-SDKP and ACE inhibitors are known to induce anti-inflammatory and antifibrotic effects. However, earlier reports of ACE-signalling pointed to a pro-inflammatory profile of ACE-cascade signalling with a downstream increase in AP1 mediated COX-2 and ACE expression (Kohlstedt et al., 2005). Interestingly, Ac-SDKP is known to inhibit the JNK pathway leading to a reduction in differentiation, proliferation, inflammation and apoptosis (Zhang et al., 2011). It was thus of interest to determine whether Ac-SDKP and the ACE inhibitors could potentiate JNK activation in a different pathway to induce the expression of ACE. Ac-SDKP and RXP407 induced JNK phosphorylation but not ACE expression, a finding in support of their anti-inflammatory and antifibrotic profiles.

The treatment of fibrotic conditions, including fibrosing pericarditis, remains a major challenge. This study has added to the understanding of the antifibrotic action of Ac-SDKP and has confirmed its altered metabolism in the TB pericardium. These findings provide rationale for the investigation of ACEi therapeutics, specifically N domain ACEi as well as Ac-SDKP analogues, in fibrosing conditions. This study also paves the way for *in vivo* studies investigating the efficacy of ACEi in TB pericarditis.

6.2. Limitations

Considering the evidence that Ac-SDKP may play a central role in prevention or reduction in pericardial fibrosis we hypothesized that low levels of Ac-SDKP in patients with TB pericarditis would contribute to the pathophysiology of pericardial fibrosis. Although a disrupted Ac-SDKP metabolism was demonstrated in our study, a major limitation was that these levels have not been directly correlated with phenotypic evidence of pericardial fibrosis. Cardiac magnetic resonance (CMR) imaging, the gold standard for the non-invasive diagnosis of constriction, could be employed for the visualisation of pericardial thickening as it allows for high-resolution imaging though its multiple modalities (Srichai, 2011)(Ariyarajah et al., 2009). This was piloted in our study on a small subset of patients (12 patients) by performing CMR analysis at 6- or 12-months post pericardiocentesis (see Appendix 1). High mortality rates associated with HIV and TB pericarditis co-infection prevented CMR analysis 12 months post pericardiocentesis in many patients which lead to a much smaller than intended sample size of patients who were followed up. Thus, the study was amended to allow for follow up at 6 months. This inherently induces a bias as it is possible that patients who passed away prior to a 12 month follow up may have had the most advanced form of the disease and presented with the more pronounced fibrosis. This potentially explains why only one patient in our study population had a pericardium of greater than 4 mm thickness on CMR (4.5mm). Thus, future studies should allow for multiple and long term CMR imaging events to visualise the onset and progression of pericardial abnormalities and correlate these findings to Ac-SDKP and ACE levels.

In order to further map out the effects of Ac-SDKP on fibroblasts, a discovery mass spectrometric approach was used. A major limitation in our secretomic analysis is the presence serum proteins in the sample used. Hence, the 355 differentially expressed proteins observed are likely to represent only a portion of the proteins regulated by Ac-SDKP. Thus, low abundance proteins or proteins displaying a very small fold change are likely to have been missed on our study. In the future, the depletion of serum proteins or the study of exosomal vesicle proteins may provide further insight into the secretome modulation by Ac-SDKP.

Finally, the quantification of the initial signalling response induced through the binding of Ac-SDKP and the ACEi to ACE could be improved in future studies. Targeted MS was used to identify the unphosphorylated and phosphorylated peptide bearing the Ser1270 residue whereby the cascade is initiated. Although the phosphorylated peptide of interest was

detected, it was not in sufficiently high abundance to distinguish between a different Ser phosphorylation site on the peptide. Thus, the degree to which the ACE signalling cascade is induced could not be quantified. The synthesis of a labelled unmodified and modified HSHGPQFG**S**EVELR peptide could aid in the detection of its physiological counterpart. This would overcome the low abundance issue of the pSer1270 peptide as well as aid in the distinction between the two phosphorylation sites. This would also be the first step in mapping the entire ACE signalling pathway activated by Ac-SDKP and ACEi in order to fully understand its physiological importance.

6.3. Future Directions

The need for novel and better biomarkers to improve diagnosis and therapy as well as to monitor responses to therapy across a large spectrum of pathologies has been increasingly recognised (Rifai et al., 2006)(Williams et al., 2012)(Butler, 2008). The identification of a predictive biomarker for high risk TB pericarditis patients for constriction would aid in the pre-emptive management of the complication, thus potentially reducing the need for pericardiectomies. This study has identified Ac-SDP and ACE dysregulation in the TB pericardial environment. Future work to correlate the decreased Ac-SDKP levels with the occurrence of pathophysiological fibrotic changes in the pericardium is warranted. Interestingly, our observation of heightened ACE activity has raised questions as to whether ACEi can be implemented in the management of TB pericarditis to prevent the development of fibrosing pericarditis. Whilst a mouse model of TB pericarditis is currently not available, future studies can investigate whether ACEi can penetrate the pericardium and whether they affect local AngII and Ac-SDKP levels in patients undergoing open heart surgery who are on ACEi therapy.

The antifibrotic effects of Ac-SDKP have been demonstrated in a wide range of studies. However, the precise molecular machinery triggered by Ac-SDKP binding to fibroblast cells is unknown. We identified of a myriad of proteins and signalling pathways modulated by Ac-SDKP including matrisomal proteins and inflammatory and fibrotic glycoproteins. Future studies to validate these mechanisms are warranted. Moreover, phospho-proteomic studies can shed further light on signalling pathways activated or repressed in the antifibrotic action of Ac-SDKP.

Lastly, ACEi and Ac-SDKP analogues have been identified as non-redundant options in the therapeutic management of fibrotic conditions. A mild antifibrotic action of Ac-SDKP for the

Ac-DKP peptide has been identified in this study. In the future, the antifibrotic effect and anti-proliferative effects of a synthesised Ac-ADKP peptide for instance could be investigated to determine whether the stability of the Ac-DKP fragment can be improved whilst maintaining its specificity of action. Further, the Ac-SDψKP analogue displayed a similar *in vitro* antifibrotic effect as Ac-SDKP. Future *in vivo* work needs to be performed as a different picture may emerge in more complex environments where the half-life of the Ac-SDψKP analogue is likely to be much longer than that of the physiological peptide, hence potentiating its protective effects. Finally, future studies are warranted on the combination of the Ac-SDψKP analogue with the N domain-selective RXP407 in an *in vivo* model of fibrosis.

7. Appendix

Appendix 1: CMR analysis

Our study design involving TB pericarditis patients thus included a clinical follow up of patients with the aim of correlating molecular findings with imaging findings consistent with pericardial inflammation or fibrosis. Follow up of enrolled patients with known/suspected TB pericarditis was done between January 2014 and December 2018 at Groote Schuur Hospital, Observatory, Cape Town. A CMR was performed at 6 to 12 months post pericardiocentesis. A standard CMR protocol used at the Groote Schuur Hospital was employed for imaging the pericardium. Written, informed and voluntary consent was provided by all patients participating in the study. CMR analysis, to extract relevant cardiac and pericardial measurement and to describe pericardial features, was performed by Stephen Jermy from Prof Ntobeko Ntusi's group. Documented CMR parameters were thereafter analysed and features of pericardial inflammation and fibrosis were probed according to Table 3-1 (Petersen et al., 2017).

Table 8-1: CMR features of constrictive pericarditis

Feature	**Evidenced by**
Thickened Pericardium	T1 and T2 weighted images and LGE images
Atrial enlargement	Right atrial (RA) and left atrial (LA) area
Dilated Superior Vena Cava (SVC)	SVC measurement
Dilated Inferior Vena Cava (IVC)	IVC measurement
Presence of Effusion	Absent or present
Abnormal Pericardial presentation	Late Gadolinium Enhancement images

Features of fibrosis were investigated in 6-12 month follow ups CMRs, on a subset of TB+ patients. It is unfortunate that a proportion of TB+ patients enrolled in the study were lost to follow up; either as a result of death or from loss to follow up. These circumstances lead to the need for earlier (6 month) follow ups in a subset of patients.

From 16 patients who were followed up with CMR, only one demonstrated pericardial thickening (beyond 4mm)(see Table 8-3). Whilst a thickened pericardium is typically the hallmark of pericardial fibrosis, it is not always present in constriction (Napolitano et al., 2009).

Four patients had a pericardial effusion 6-12 months post pericardiocentesis. Patient CMR6 had a pronounced effusion ranging from 13-19 cm likely manifesting as ECP whereby the presence of the effusion results in constrictive disease in the absence of pericardial thickening. Finally, atrial enlargement was commonly observed in the patients. It is possible that these represent early features of fibrosing pericarditis which would later be accompanied by more pronounced pericardial thickening.

Table 8-3: CMR features of fibrosing pericarditis in follow up TB+ patients.
Cells highlighted in red represent abnormal findings whereas cells highlighted in orange represent values approaching the abnormal range. (LA: left atrium, RA: right atrium, SVC: superior vena cava, IVC: inferior vena cava.)

CMR Identifier	Pericardial thickness (<4mm)	Atrial Enlargement		Dilated Vena Cava		Presence of Effusion
		LA area ≤ 20cm^2	RA area ≤ 18cm^2	SVC 8-20mm	IVC 12-23mm	
CMR1	3.5	20	25	19	21	No
CMR2	3.2	18	19	17	15	No
CMR3	3.5	27	26	18	14	No
CMR4	3.5	20	22	20	15	No
CMR5	4.5	25	17	19	18	No
CMR6	3	21	18	14	13	Yes
CMR7	2.9	16	28	16	16	No
CMR8	3	13	14	13	11	No
CMR9	2.8	21	20	18	12	No
CMR10	2.8	25	24	15	15	No
CMR11	2.8	27	32	19	19	Yes
CMR12	NA	13	13	17	12	No
CMR13	2.7	24	19	14	14	No
CMR14	3	22	24	15	13	No
CMR15	3.5	37	29	18	23	Yes
CMR16	3.4	39	19	21	17	Yes

Appendix 2: Standard Curves

Ac-SDKP Standard Curve

An Ac-SDKP standard curve was generated to determine Ac-SDKP concentrations using the Ac-SDKP standards provided in the ELISA kit. A sigmoidal curve was plotted according to manufacturer's instructions.

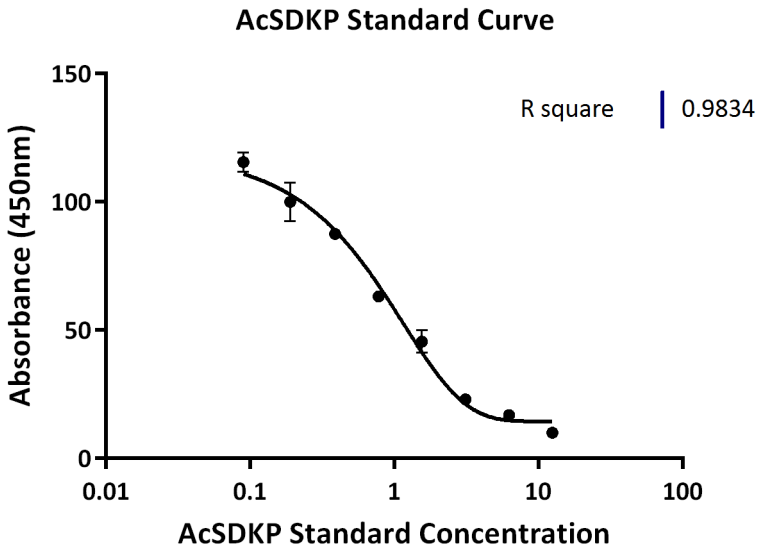

Galectin-3 Standard Curve

A Gal-3 standard curve was generated to determine Gal-3 concentrations using the Gal-3 standards provided in the ELISA kit. A linear regression was plotted according to manufacturer's instructions.

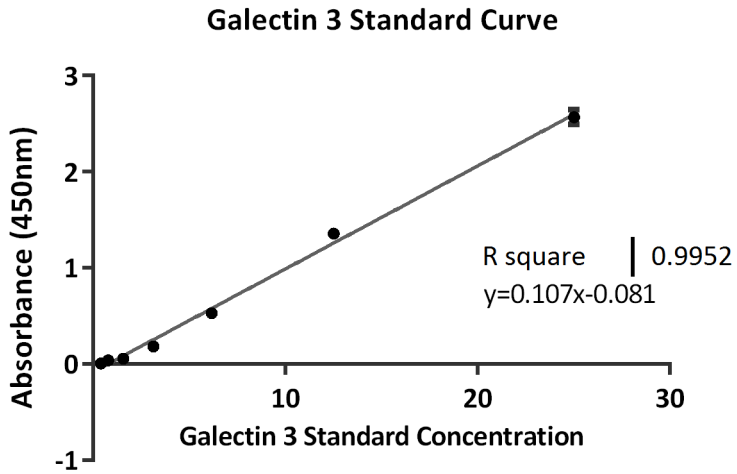

HL Standard Curve

An HL product standard curve was generated to determine ACE activity using the synthetic ZFHL substrate.

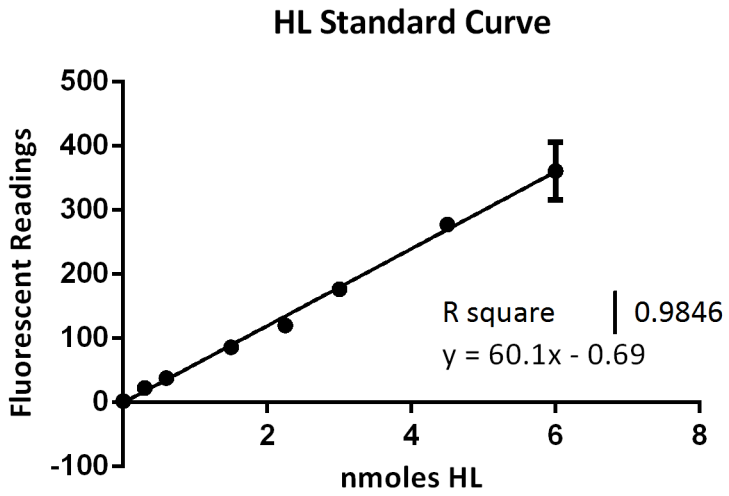

AMC Standard Curve

An AMC product standard curve was generated to determine POP activity using the synthetic Z-Gly-Pro-AMC substrate.

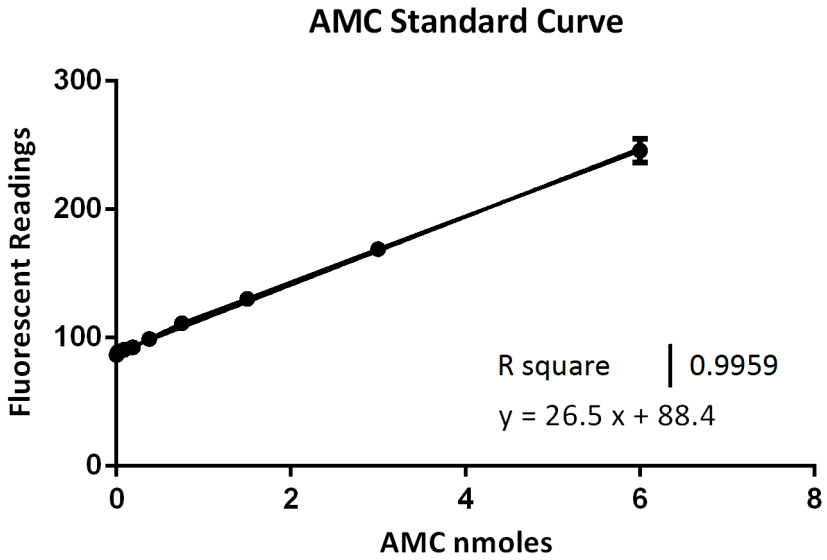

Hydroxyproline Standard Curve

A hydroxyproline standard curve was used to determine cellular hydroxyproline levels using the standards provided in the kit.

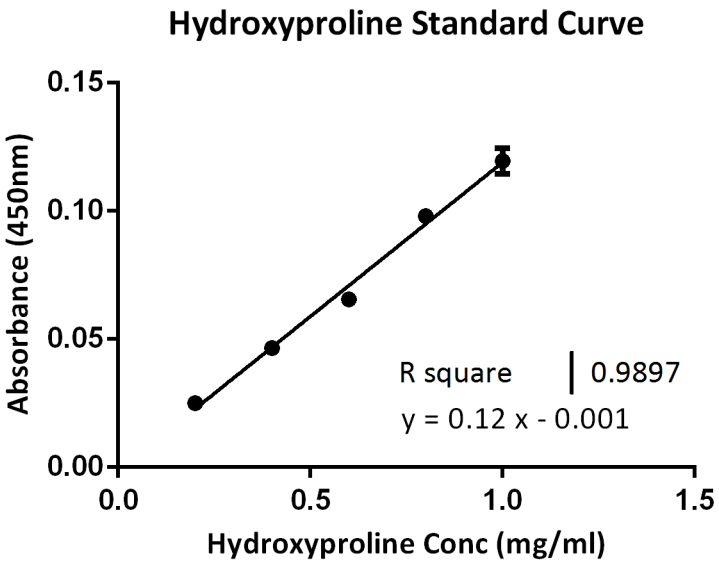

Appendix 3: Western Blotting

SDS-PAGE resolving gels

0.3 % SDS, 1.125 M Tris, pH 8.8

SDS-PAGE 3% stacking gels

0.3 % SDS, 0.375 M Tris, pH 6.8

Transfer Buffer

20 mM Tris, 150 mM glycine, 20 % methanol

Blocking buffer

5% (w/v) skim milk, 0.1% (v/v) Tween-20, 0.2 M NaCl, 0.05 M Tris (pH7.4)

TBS-T

0.1% (v/v) Tween-20, 0.2 M NaCl, 0.05 M Tris (pH7.4)

Laemmli Buffer

20 % glycerol, 6 % SDS, 125 mM Tris, 5 % β-mercaptoethanol, bromophenol blue, pH 6.8

Appendix 4: MS Results

Table 8-4: BiNGO Enriched molecular functions in the secretome

GO ID	GO description	p value	corrected p-value	cluster frequency	total frequency	Genes
32501	multicellular organismal process	5.77E-09	5.96E-06	37/54 68.5%	1784/5957 29.9%	FBN2 ECM1 HSP90AB1 C1S LTBP4 PARK7 LAMC1 EFEMP2 LGALS1 PRDX1 LMNA ANXA1 TPI1 TPM4 ANXA2 HSPA5 LUM ANXA5 FN1 HSPG2 YWHAZ DCN NME1 DKK3 FKBP1A COL1A1 TUBB2A COL1A2 ANGPTL2 COL6A3 TAGLN2 PTX3 TLN1 PFN1 AGRN NES VCL
30198	extracellular matrix organization	1.59E-08	7.45E-06	9/54 16.6%	71/5957 1.1%	CST3 FKBP1A COL1A1 COL1A2 ANXA2 LUM COL6A2 LAMC1 DCN
43062	extracellular structure organization	2.17E-08	7.45E-06	10/54 18.5%	100/5957 1.6%	CST3 FKBP1A COL1A1 COL1A2 ANXA2 LUM COL6A2 LAMC1 AGRN DCN
7275	multicellular organismal development	1.91E-07	4.93E-05	30/54 55.5%	1356/5957 22.7%	FBN2 ECM1 HSP90AB1 C1S LTBP4 LAMC1 LGALS1 PRDX1 LMNA ANXA1 TPI1 ANXA2 HSPA5 FN1 HSPG2 DCN NME1 DKK3 FKBP1A COL1A1 TUBB2A COL1A2 ANGPTL2 COL6A3 TAGLN2 PTX3 PFN1 AGRN NES VCL
32502	developmental process	1.81E-06	3.11E-04	30/54 55.5%	1496/5957 25.1%	FBN2 ECM1 HSP90AB1 C1S LTBP4 LAMC1 LGALS1 PRDX1 LMNA ANXA1 TPI1 ANXA2 HSPA5 FN1 HSPG2 DCN NME1 DKK3 FKBP1A COL1A1 TUBB2A COL1A2 ANGPTL2 COL6A3 TAGLN2

						PTX3 PFN1 AGRN NES VCL
48731	system development	1.53E-06	3.11E-04	26/54 48.1%	1146/5957 19.2%	ECM1 HSP90AB1 C1S LAMC1 LGALS1 PRDX1 LMNA ANXA1 ANXA2 HSPA5 FN1 HSPG2 DCN NME1 DKK3 FKBP1A COL1A1 TUBB2A COL1A2 COL6A3 TAGLN2 PTX3 PFN1 AGRN NES VCL
48856	anatomical structure development	2.43E-06	3.58E-04	27/54 50.0%	1256/5957 21.0%	FBN2 ECM1 HSP90AB1 C1S LAMC1 LGALS1 PRDX1 LMNA ANXA1 ANXA2 HSPA5 FN1 HSPG2 DCN NME1 DKK3 FKBP1A COL1A1 TUBB2A COL1A2 COL6A3 TAGLN2 PTX3 PFN1 AGRN NES VCL
48513	organ development	1.14E-05	1.47E-03	21/54 38.8%	873/5957 14.6%	ECM1 HSP90AB1 ANXA1 ANXA2 HSPA5 FN1 LAMC1 HSPG2 DCN NME1 DKK3 FKBP1A COL1A1 COL1A2 LMNA COL6A3 TAGLN2 PTX3 PFN1 AGRN VCL
16043	cellular component organization	1.54E-05	1.76E-03	28/54 51.8%	1467/5957 24.6%	VCP LAMC1 CST3 TUBA1B LMNA PTRF HSPA8 ANXA2 LUM ANXA5 FN1 ACTN4 YWHAZ DCN NME1 FKBP1A COL1A1 TUBB2A COL1A2 COL6A2 FSCN1 ANGPTL2 PTX3 TLN1 PFN1 AGRN VCL PLEC
51346	negative regulation of hydrolase activity	1.99E-05	2.06E-03	5/54 9.2%	36/5957 0.6%	CST3 FKBP1A ECM1 HSPA5 ANGPTL2
6950	response to stress	2.37E-05	2.22E-03	21/54 38.8%	915/5957 15.3%	HSPA8 VCP HSP90AB1 ANXA1 TPM4 C1S HSPA5 ANXA5 FN1 PARK7 ACTN4 YWHAZ DCN

						CST3 COL1A1 EFEMP2 LGALS1 PRDX1 ANGPTL2 PTX3 PFN1
30199	collagen fibril organization	3.51E-05	3.02E-03	4/54 7.4%	20/5957 0.3%	COL1A1 COL1A2 ANXA2 LUM
42221	response to chemical stimulus	8.14E-05	6.46E-03	19/54 35.1%	837/5957 14.0%	HSPA8 VCP HSP90AB1 TPM4 C1S HSPA5 ANXA5 PARK7 ACTN4 YWHAZ DCN NME1 COL1A1 LGALS1 COL6A2 PRDX1 ANGPTL2 PFN1 NES
61061	muscle structure development	2.04E-04	1.51E-02	7/54 12.9%	134/5957 2.2%	FKBP1A LGALS1 LMNA COL6A3 TAGLN2 AGRN DCN
31340	positive regulation of vesicle fusion	3.57E-04	2.45E-02	2/54 3.7%	3/5957 0.0%	ANXA1 ANXA2
7517	muscle organ development	3.94E-04	2.54E-02	6/54 11.1%	106/5957 1.7%	FKBP1A LMNA COL6A3 TAGLN2 AGRN DCN
34329	cell junction assembly	4.92E-04	2.83E-02	4/54 7.4%	40/5957 0.6%	LAMC1 TLN1 VCL PLEC
22607	cellular component assembly	6.01E-04	2.83E-02	14/54 25.9%	589/5957 9.8%	VCP ANXA5 LAMC1 ACTN4 FKBP1A TUBA1B TUBB2A FSCN1 ANGPTL2 TLN1 AGRN PTRF VCL PLEC
10466	negative regulation of peptidase activity	6.10E-04	2.83E-02	3/54 5.5%	18/5957 0.3%	CST3 ECM1 HSPA5
18149	peptide cross-linking	6.10E-04	2.83E-02	3/54 5.5%	18/5957 0.3%	ANXA1 FN1 DCN
31338	regulation of vesicle fusion	6.30E-04	2.83E-02	2/54 3.7%	4/5957 0.0%	ANXA1 ANXA2
43589	skin morphogenesis	6.30E-04	2.83E-02	2/54 3.7%	4/5957 0.0%	COL1A1 COL1A2
9888	tissue development	5.02E-04	2.83E-02	11/54 20.3%	378/5957 6.3%	FKBP1A COL1A1 ECM1 ANXA1 COL1A2 LMNA LAMC1 PFN1 AGRN DCN VCL
6984	ER-nucleus signalling pathway	7.13E-04	3.06E-02	3/54 5.5%	19/5957 0.3%	VCP HSPA5 LMNA
9653	anatomical structure morphogenesis	8.24E-04	3.40E-02	14/54 25.9%	608/5957 10.2%	FBN2 ANXA2 HSPA5 FN1 LAMC1 HSPG2 DCN DKK3 FKBP1A

						COL1A1 COL1A2 PTX3 PFN1 VCL
6986	response to unfolded protein	8.95E-04	3.55E-02	4/54 7.4%	47/5957 0.7%	HSPA8 VCP HSP90AB1 HSPA5
51591	response to cAMP	1.23E-03	4.71E-02	3/54 5.5%	23/5957 0.3%	COL1A1 C1S NME1
34330	cell junction organization	1.30E-03	4.71E-02	4/54 7.4%	52/5957 0.8%	LAMC1 TLN1 VCL PLEC
50896	response to stimulus	1.32E-03	4.71E-02	25/54 46.2%	1574/5957 26.4%	VCP HSP90AB1 C1S PARK7 ENO1 CST3 EFEMP2 LGALS1 PRDX1 HSPA8 ANXA1 TPM4 HSPA5 ANXA5 FN1 ACTN4 YWHAZ DCN NME1 COL1A1 COL6A2 ANGPTL2 PTX3 PFN1 NES

Table 8-5: BiNGO Enriched biological processes in the secretome

GO ID	GO description	p value	corrected p-value	cluster frequency	total frequency	Genes
5198	structural molecule activity	2.52E-11	5.52E-09	20/55 36.3%	384/6246 6.1%	FBN2 ANXA1 TPM4 LUM RPL12 FN1 LAMC1 COL1A1 TUBA1B EFEMP2 TUBB2A COL1A2 COL6A2 LMNA VIM TLN1 AGRN NES VCL PLEC
5201	extracellular matrix structural constituent	8.62E-09	9.43E-07	8/55 14.5%	50/6246 0.8%	FBN2 COL1A1 EFEMP2 COL1A2 LUM COL6A2 FN1 LAMC1
4859	phospholipase inhibitor activity	3.51E-05	2.56E-03	3/55 5.4%	8/6246 0.1%	ANXA1 ANXA2 ANXA5
50840	extracellular matrix binding	5.02E-05	2.75E-03	4/55 7.2%	24/6246 0.3%	ECM1 LGALS1 AGRN DCN
5509	calcium ion binding	8.95E-05	3.17E-03	11/55 20.0%	322/6246 5.1%	FBN2 EFEMP2 ANXA1 TPM4 ANXA2 C1S HSPA5 ANXA5 LTBP4 SVEP1 ACTN4
30674	protein binding, bridging	1.00E-04	3.17E-03	5/55 9.0%	54/6246 0.8%	ANXA1 COL1A2 HSPA5 COL6A2 FSCN1
55102	lipase inhibitor activity	1.01E-04	3.17E-03	3/55 5.4%	11/6246 0.1%	ANXA1 ANXA2 ANXA5
43236	laminin binding	1.34E-04	3.68E-03	3/55 5.4%	12/6246 0.1%	ECM1 LGALS1 AGRN
5544	calcium-dependent phospholipid binding	2.73E-04	6.64E-03	3/55 5.4%	15/6246 0.2%	ANXA1 ANXA2 ANXA5
4857	enzyme inhibitor activity	3.49E-04	7.64E-03	7/55 12.7%	153/6246 2.4%	CST3 ANXA1 ANXA2 HSPA5 ANXA5 ANGPTL2 COL6A3
5515	protein binding	1.24E-03	2.47E-02	47/55 85.4%	4151/6246 66.4%	ECM1 VCP HSP90AB1 LTBP4 PARK7 LAMC1 ENO1 CST3 TUBA1B UCHL1 EFEMP2 LGALS1 PRDX1 LMNA FLNC PTRF HSPA8 ANXA1 TPI1 TPM4 ANXA2 HSPA5 LUM ANXA5 FN1 ACTN4 PDIA6 HSPG2 YWHAZ DCN NME1 FKBP1A COL1A1 TUBB2A PKM COL1A2 COL6A2 HNRNPA2B1 FSCN1 ANGPTL2 TAGLN2 VIM TLN1 PFN1 AGRN VCL PLEC
5518	collagen binding	1.81E-03	3.22E-02	3/55 5.4%	28/6246 0.4%	LUM FN1 DCN
5200	structural constituent of cytoskeleton	2.06E-03	3.22E-02	4/55 7.2%	62/6246 0.9%	TUBA1B VIM TLN1 AGRN

51920	peroxiredoxin activity	2.06E-03	3.22E-02	2/55 3.6%	8/6246 0.1%	PRDX1 PARK7
3779	actin binding	2.65E-03	3.70E-02	7/55 12.7%	216/6246 3.4%	TPM4 FSCN1 ACTN4 FLNC TLN1 PFN1 PLEC
8092	cytoskeletal protein binding	2.70E-03	3.70E-02	9/55 16.3%	342/6246 5.4%	TPM4 ANXA2 FSCN1 ACTN4 FLNC TLN1 PFN1 NME1 PLEC
48407	platelet-derived growth factor binding	3.27E-03	4.22E-02	2/55 3.6%	10/6246 0.1%	COL1A1 COL1A2

Table 8-6: BinGO Enriched biological pathways in the proteome

6414	translational elongation	6.0918E-12	9.2900E-9	12/107 11.2%	96/14296 0.6%	EEF1A1 RPS15A RPL18A RPL10 RPL23 RPL13A RPL15 RPS2 RPL8 RPS27A RPL9 RPL19
43170	macromolecule metabolic process	3.4049E-9	2.5962E-6	59/107 55.1%	4014/14296 28.0%	PYGB ILK PLAT PPP2R2A RPL8 RPL9 FGF2 MYLK RPL18A SCP2 SCRN1 ANPEP CCN2 CCN1 EIF5A PRMT5 MMP1 RPL23 RPL13A MOGS OXSR1 EEF1A1 PSMA5 UGDH PSME1 MYH9 PTMA DDX5 RPL10 HDAC1 SRSF1 GNS HSP90B1 DPP4 RPS15A PCBP1 RPL15 RPS2 RPS27A RPL19 CTSA ST13 STAT1 EGF FN1 PTK2 COL1A1 HNRNPL HNRNPK PSMC1 DNAJA2 HNRNPD BAX TPP1 RBMX FGFR2 HSPA1B RAN FGFR1
19538	protein metabolic process	8.5302E-9	4.3362E-6	45/107 42.0%	2609/14296 18.2%	RPL10 HDAC1 ILK PLAT PPP2R2A RPL8 RPL9 FGF2 MYLK HSP90B1 DPP4 RPS15A RPL18A SCP2 SCRN1 ANPEP RPL15 RPS2 CCN1 RPS27A RPL19 CTSA EIF5A PRMT5 ST13 MMP1 STAT1 EGF RPL23 FN1 RPL13A MOGS OXSR1 PTK2 EEF1A1 PSMA5 PSMC1 DNAJA2 PSME1 MYH9 BAX TPP1 FGFR2 HSPA1B FGFR1
44267	cellular protein metabolic process	3.7986E-8	1.4482E-5	39/107 36.4%	2151/14296 15.0%	RPL10 HDAC1 ILK PLAT PPP2R2A RPL8 RPL9 FGF2 MYLK HSP90B1 RPS15A RPL18A SCP2 RPL15 RPS2 CCN1 RPS27A RPL19 EIF5A PRMT5 ST13 STAT1 EGF RPL23 FN1 RPL13A MOGS OXSR1 PTK2 EEF1A1 PSMA5 PSMC1 DNAJA2 PSME1 MYH9 BAX FGFR2 HSPA1B FGFR1
44238	primary metabolic process	5.8687E-8	1.7740E-5	67/107 62.6%	5284/14296 36.9%	PYGB HEXA ILK PLAT PPP2R2A ENO1 RPL8 RPL9 FGF2 MYLK RPL18A SCP2 SCRN1 ANPEP CCN2 CCN1 PGM1 EIF5A PRMT5 MMP1 RPL23 RPL13A MOGS OXSR1 APRT EEF1A1 PSMA5 UGDH PKM

						DDAH2 PSME1 MYH9 PTMA DDX5 RPL10 HDAC1 SRSF1 GNS HSP90B1 DPP4 RPS15A PCBP1 RPL15 RPS2 RPS27A RPL19 CTSA GOT1 ST13 STAT1 EGF FN1 PTK2 HNRNPL HNRNPK PSMC1 DNAJA2 HNRNPD BAX TPP1 GALM PFKM RBMX FGFR2 HSPA1B RAN FGFR1
8152	metabolic process	6.9796E-8	1.7740E-5	72/107 67.2%	5955/14296 41.6%	PYGB HEXA ILK PLAT PPP2R2A ENO1 RPL8 RPL9 FGF2 MYLK RPL18A LAMP1 SCP2 NAGLU SCRN1 ANPEP CCN2 CCN1 PGM1 EIF5A PRMT5 MMP1 RPL23 RPL13A MOGS OXSR1 APRT EEF1A1 PSMA5 UGDH PKM PPA2 DDAH2 PSME1 MYH9 PTMA DDX5 RPL10 HDAC1 SRSF1 GNS HSP90B1 DPP4 RPS15A PCBP1 RPL15 RPS2 RPS27A RPL19 CTSA CYB5B GOT1 ST13 STAT1 EGF FN1 PTK2 COL1A1 HNRNPL HNRNPK PSMC1 DNAJA2 HNRNPD BAX TPP1 GALM PFKM RBMX FGFR2 HSPA1B RAN FGFR1
44237	cellular metabolic process	1.1440E-7	2.4923E-5	64/107 59.8%	4987/14296 34.8%	PYGB ILK PLAT PPP2R2A ENO1 RPL8 RPL9 FGF2 MYLK RPL18A LAMP1 SCP2 ANPEP CCN2 CCN1 PGM1 EIF5A PRMT5 RPL23 RPL13A MOGS OXSR1 APRT EEF1A1 PSMA5 UGDH PKM PPA2 DDAH2 PSME1 MYH9 PTMA DDX5 RPL10 HDAC1 SRSF1 HSP90B1 RPS15A PCBP1 RPL15 RPS2 RPS27A RPL19 CYB5B GOT1 ST13 STAT1 EGF FN1 PTK2 HNRNPL HNRNPK PSMC1 DNAJA2 HNRNPD BAX TPP1 GALM PFKM RBMX FGFR2 HSPA1B RAN FGFR1
44260	cellular macromolecule metabolic process	1.6047E-7	3.0589E-5	51/107 47.6%	3506/14296 24.5%	PYGB ILK PLAT PPP2R2A RPL8 RPL9 FGF2 MYLK RPL18A SCP2 CCN2 CCN1 EIF5A PRMT5 RPL23 RPL13A MOGS OXSR1 EEF1A1 PSMA5 PSME1 MYH9 PTMA DDX5 RPL10 HDAC1 SRSF1 HSP90B1 RPS15A PCBP1 RPL15 RPS2 RPS27A RPL19 ST13 STAT1 EGF FN1 PTK2 HNRNPL HNRNPK PSMC1 DNAJA2 HNRNPD BAX TPP1 RBMX FGFR2 HSPA1B RAN FGFR1
1525	angiogenesis	1.9952E-7	3.3271E-5	10/107 9.3%	152/14296 1.0%	EGF ANPEP FN1 MYH9 CCN2 CCN1 FGF2 RTN4 PTK2 FGFR1
6412	translation	2.3845E-7	3.3271E-5	13/107 12.1%	289/14296 2.0%	EIF5A RPL10 RPL23 RPL13A RPL8 RPL9 EEF1A1 RPS15A RPL18A RPL15 RPS2 RPS27A RPL19

8104	protein localization	2.399 9E-7	3.3271E-5	23/107 21.4%	920/14296 6.4%	CTSA EIF5A GOT1 GDI1 EGF RPL23 ITGA2 GDI2 AP1B1 AP3B1 ACTN4 FGF2 HSP90B1 COL1A1 SNX18 LMAN2 MYH9 TPP1 CCN1 TLN1 SEC22B VCL RAN
1568	blood vessel development	6.669 1E-7	8.4753E-5	12/107 11.2%	265/14296 1.8%	COL1A1 EGF ANPEP FN1 MYH9 PLAT CCN2 CCN1 FGF2 RTN4 PTK2 FGFR1
48514	blood vessel morphogenesis	7.582 7E-7	8.8950E-5	11/107 10.2%	220/14296 1.5%	EGF ANPEP FN1 MYH9 PLAT CCN2 CCN1 FGF2 RTN4 PTK2 FGFR1
45184	establishment of protein localization	8.576 9E-7	9.2894E-5	20/107 18.6%	766/14296 5.3%	CTSA EIF5A GOT1 GDI1 RPL23 ITGA2 GDI2 AP1B1 AP3B1 ACTN4 FGF2 HSP90B1 COL1A1 SNX18 LMAN2 MYH9 TPP1 CCN1 SEC22B RAN
1944	vasculature development	9.137 1E-7	9.2894E-5	12/107 11.2%	273/14296 1.9%	COL1A1 EGF ANPEP FN1 MYH9 PLAT CCN2 CCN1 FGF2 RTN4 PTK2 FGFR1
8284	positive regulation of cell proliferation	1.588 0E-6	1.5135E-4	15/107 14.0%	459/14296 3.2%	EIF5A HDAC1 STAT1 EGF ITGA2 ILK LAMC1 FGF2 DPP4 RPS15A DNAJA2 CCN2 CCN1 FGFR2 FGFR1
33036	macromolecule localization	1.727 7E-6	1.5499E-4	24/107 22.4%	1110/1429 6 7.7%	CTSA EIF5A GOT1 GDI1 EGF RPL23 ITGA2 GDI2 AP1B1 AP3B1 ACTN4 FGF2 HSP90B1 COL1A1 SNX18 SCP2 LMAN2 MYH9 TPP1 CCN1 TLN1 SEC22B VCL RAN
51128	regulation of cellular component organization	2.360 6E-6	1.9999E-4	16/107 14.9%	538/14296 3.7%	EIF5A PRMT5 EGF ITGA2 SERPINE1 FN1 ILK ACTN4 ARPC5 RTN4 PTK2 DPP4 MYH9 TPP1 GAL1 HSPA1B
15031	protein transport	2.892 2E-6	2.3214E-4	19/107 17.7%	755/14296 5.2%	CTSA EIF5A GOT1 GDI1 RPL23 GDI2 AP1B1 AP3B1 ACTN4 FGF2 HSP90B1 COL1A1 SNX18 LMAN2 MYH9 TPP1 CCN1 SEC22B RAN
7229	integrin-mediated signaling pathway	4.063 7E-6	3.0986E-4	6/107 5.6%	57/14296 0.3%	ITGB1 ITGA2 ILK MYH9 CCN2 PTK2
48646	anatomical structure formation involved in morphogenesis	4.412 2E-6	3.2041E-4	13/107 12.1%	375/14296 2.6%	EGF FN1 ILK FGF2 RTN4 PTK2 COL1A1 ACTC1 ANPEP MYH9 CCN2 CCN1 FGFR1
9653	anatomical structure morphogenesis	8.489 4E-6	5.8847E-4	24/107 22.4%	1217/1429 6 8.5%	EIF4A1 EGF ITGA2 SERPINE1 FN1 ILK PLAT LAMC1 FGF2 RTN4 PTK2 COL1A1 ACTA2 UGDH ACTC1 SCP2 ANPEP MYH9 BAX TPP1 CCN2 CCN1 VCL FGFR1
31589	cell-substrate adhesion	9.133 5E-6	6.0559E-4	7/107 6.5%	99/14296 0.6%	ITGB1 ITGA2 FN1 ILK CCN2 LAMC1 VCL
30155	regulation of cell adhesion	1.498 5E-5	9.5217E-4	8/107 7.4%	148/14296 1.0%	DPP4 COL1A1 ITGA2 SERPINE1 ILK CCN1 EDIL3 GAL1
43542	endothelial cell migration	3.324 2E-5	2.0278E-3	4/107 3.7%	25/14296 0.1%	DPP4 MYH9 FGF2 PTK2

9987	cellular process	3.5825E-5	2.1013E-3	89/10783.1%	9360/142966 65.4%	ITGB1 LGALS3BP PYGB SERPINE1 ILK PLAT PPP2R2A ENO1 LAMC1 RPL8 RPL9 FGF2 MYLK ACTR1A RPL18A LAMP1 SCP2 SCRN1 ANPEP FLOT2 CCN2 CCN1 EDIL3 PGM1 GAL1 EIF5A PRMT5 RPL23 ITGA2 AP1B1 RPL13A MOGS AP3B1 ACTN4 OXSR1 APRT EEF1A1 PSMA5 UGDH PKM PPA2 DDAH2 PSME1 MYH9 TLN1 SEC22B PTMA VCL DYNC1I2 DDX5 RPL10 HDAC1 SRSF1 RTN4 HSP90B1 DPP4 RPS15A PCBP1 RPL15 RPS2 RPS27A RPL19 CTSA CYB5B GOT1 ST13 STAT1 EGF FN1 PARVA ARPC5 PTK2 COL1A1 HNRNPL SNX18 HNRNPK ACTC1 PSMC1 DNAJA2 HNRNPD BAX TPP1 GALM PFKM RBMX FGFR2 HSPA1B RAN FGFR1
10467	gene expression	4.6626E-5	2.5645E-3	23/10721.4%	1260/142966 8.8%	EIF5A PRMT5 DDX5 RPL10 STAT1 RPL23 SRSF1 RPL13A RPL8 RPL9 EEF1A1 HNRNPL HNRNPK RPS15A RPL18A PCBP1 HNRNPD RPL15 RPS2 RPS27A PTMA RBMX RPL19
34446	substrate adhesion-dependent cell spreading	4.7086E-5	2.5645E-3	3/1072.8%	10/142960.0%	FN1 ILK LAMC1
10810	regulation of cell-substrate adhesion	5.0514E-5	2.6459E-3	5/1074.6%	54/142960.3%	COL1A1 ILK CCN1 EDIL3 GAL1
6928	cellular component movement	5.2493E-5	2.6459E-3	13/10712.1%	474/142963.3%	ITGB1 ITGA2 FN1 PLAT ARPC5 LAMC1 FGF2 PTK2 DPP4 MYH9 CCN2 TLN1 VCL
42127	regulation of cell proliferation	5.3786E-5	2.6459E-3	18/10716.8%	848/142965.9%	EIF5A SPARC HDAC1 STAT1 EGF ITGA2 SERPINE1 ILK LAMC1 FGF2 DPP4 RPS15A DNAJA2 CCN2 CCN1 FGFR2 HSPA1B FGFR1
9059	macromolecule biosynthetic process	9.1850E-5	4.3772E-3	20/10718.6%	1052/142966 7.3%	EIF5A RPL10 STAT1 EGF RPL23 RPL13A MOGS RPL8 RPL9 EEF1A1 COL1A1 UGDH RPS15A RPL18A CCN2 RPL15 RPS2 RPS27A PTMA RPL19
8543	fibroblast growth factor receptor signaling pathway	1.0269E-4	4.7456E-3	4/1073.7%	33/142960.2%	CCN2 FGF2 FGFR2 FGFR1
30198	extracellular matrix organization	1.2126E-4	5.4387E-3	6/1075.6%	103/142960.7%	COL1A1 ILK CCN2 LAMC1 CCN1 PTK2
90066	regulation of anatomical structure size	1.3092E-4	5.7042E-3	10/1079.3%	317/142962.2%	ACTA2 DDX5 ILK ENO1 ARPC5 FGF2 RTN4 FGFR2 HSPA1B FGFR1

65008	regulation of biological quality	1.4029E-4	5.9428E-3	25/10723.3%	1541/142966 10.7%	DDX5 HDAC1 SERPINE1 ILK PLAT ENO1 FGF2 RTN4 HSP90B1 CCN1 GOT1 ITGA2 FN1 AP3B1 ARPC5 PTK2 ACTA2 MYH9 BAX TPP1 TLN1 PFKM FGFR2 HSPA1B FGFR1
45785	positive regulation of cell adhesion	1.6424E-4	6.7695E-3	5/1074.6%	69/142960.4%	ITGA2 ILK CCN1 EDIL3 GAL1
51271	negative regulation of cellular component movement	2.0088E-4	8.0615E-3	5/1074.6%	72/142960.5%	SERPINE1 ILK ACTN4 FGF2 VCL
8361	regulation of cell size	2.3704E-4	9.2690E-3	8/1077.4%	219/142961.5%	DDX5 ILK ENO1 FGF2 RTN4 FGFR2 HSPA1B FGFR1
16477	cell migration	2.5702E-4	9.7988E-3	9/1078.4%	281/142961.9%	DPP4 ITGB1 FN1 MYH9 PLAT CCN2 LAMC1 FGF2 PTK2
48522	positive regulation of cellular process	2.6785E-4	9.8342E-3	29/10727.1%	2003/142966 14.0%	DDX5 HDAC1 SERPINE1 ILK LAMC1 FGF2 RTN4 DPP4 RPS15A CCN2 CCN1 EDIL3 GAL1 EIF5A GOT1 STAT1 EGF ITGA2 AP3B1 ACTN4 PSMA5 PSMC1 DNAJA2 PSME1 BAX PFKM FGFR2 RAN FGFR1
32535	regulation of cellular component size	2.7084E-4	9.8342E-3	9/1078.4%	283/142961.9%	DDX5 ILK ENO1 ARPC5 FGF2 RTN4 FGFR2 HSPA1B FGFR1
51179	localization	3.1737E-4	1.1036E-2	38/10735.5%	2983/142966 20.8%	ITGB1 DYNC1I2 GDI1 GDI2 PLAT LAMC1 FGF2 HSP90B1 DPP4 ACTR1A SCP2 SCRN1 LMAN2 CCN2 CCN1 CTSA EIF5A CYB5B TMED9 GOT1 EGF RPL23 ITGA2 AP1B1 FN1 AP3B1 ACTN4 PTK2 COL1A1 SNX18 ACTC1 MYH9 BAX TPP1 TLN1 SEC22B VCL RAN
51641	cellular localization	3.1841E-4	1.1036E-2	18/10716.8%	977/142966.8%	CTSA EIF5A EGF RPL23 AP1B1 AP3B1 FGF2 PTK2 ACTC1 SCRN1 MYH9 TPP1 CCN2 CCN1 TLN1 SEC22B VCL RAN
34613	cellular protein localization	3.9381E-4	1.3346E-2	11/10710.2%	433/142963.0%	CTSA EIF5A EGF RPL23 AP1B1 TPP1 AP3B1 CCN1 FGF2 VCL RAN
70727	cellular macromolecule localization	4.1741E-4	1.3517E-2	11/10710.2%	436/142963.0%	CTSA EIF5A EGF RPL23 AP1B1 TPP1 AP3B1 CCN1 FGF2 VCL RAN
14910	regulation of smooth muscle cell migration	4.2358E-4	1.3517E-2	3/1072.8%	20/142960.1%	ITGA2 SERPINE1 ILK
22603	regulation of anatomical structure morphogenesis	4.2545E-4	1.3517E-2	9/1078.4%	301/142962.1%	SERPINE1 FN1 ILK MYH9 BAX FGF2 RTN4 PTK2 FGFR1
7160	cell-matrix adhesion	4.3609E-4	1.3572E-2	5/1074.6%	85/142960.5%	ITGB1 ITGA2 ILK CCN2 VCL
19318	hexose metabolic process	4.7610E-4	1.4521E-2	7/1076.5%	185/142961.2%	PYGB UGDH PKM GALM ENO1 PFKM PGM1

48638	regulation of developmental growth	5.2421E-4	1.5675E-2	4/107 3.7%	50/14296 0.3%	ILK FGF2 RTN4 FGFR1
43589	skin morphogenesis	5.4689E-4	1.6039E-2	2/107 1.8%	5/14296 0.0%	COL1A1 ITGA2
51674	localization of cell	5.7738E-4	1.6306E-2	9/107 8.4%	314/14296 2.1%	DPP4 ITGB1 FN1 MYH9 PLAT CCN2 LAMC1 FGF2 PTK2
48870	cell motility	5.7738E-4	1.6306E-2	9/107 8.4%	314/14296 2.1%	DPP4 ITGB1 FN1 MYH9 PLAT CCN2 LAMC1 FGF2 PTK2
34645	cellular macromolecule biosynthetic process	6.0563E-4	1.6793E-2	18/107 16.8%	1031/14296 7.2%	EIF5A RPL10 STAT1 EGF RPL23 RPL13A MOGS RPL8 RPL9 EEF1A1 RPS15A RPL18A CCN2 RPL15 RPS2 RPS27A PTMA RPL19
60548	negative regulation of cell death	6.6654E-4	1.8151E-2	10/107 9.3%	389/14296 2.7%	EIF5A DDAH2 HDAC1 SERPINE1 ILK BAX FGF2 HSPA1B HSP90B1 FGFR1
6006	glucose metabolic process	7.9353E-4	2.1230E-2	6/107 5.6%	146/14296 1.0%	PYGB UGDH PKM ENO1 PFKM PGM1
7155	cell adhesion	8.2970E-4	2.1740E-2	14/107 13.0%	711/14296 4.9%	ITGB1 LGALS3BP ITGA2 FN1 ILK PARVA LAMC1 DPP4 FLOT2 MYH9 CCN2 CCN1 EDIL3 VCL
22610	biological adhesion	8.4110E-4	2.1740E-2	14/107 13.0%	712/14296 4.9%	ITGB1 LGALS3BP ITGA2 FN1 ILK PARVA LAMC1 DPP4 FLOT2 MYH9 CCN2 CCN1 EDIL3 VCL
6936	muscle contraction	1.0473E-3	2.6599E-2	6/107 5.6%	154/14296 1.0%	ACTA2 ACTC1 TPM2 TLN1 VCL MYLK
1558	regulation of cell growth	1.0639E-3	2.6599E-2	7/107 6.5%	212/14296 1.4%	ILK ENO1 CCN2 CCN1 FGF2 RTN4 HSPA1B
31960	response to corticosteroid stimulus	1.0930E-3	2.6682E-2	5/107 4.6%	104/14296 0.7%	COL1A1 GOT1 SERPINE1 PLAT CCN2
50790	regulation of catalytic activity	1.1266E-3	2.6682E-2	16/107 14.9%	907/14296 6.3%	GDI1 STAT1 EGF TPM2 ITGA2 SERPINE1 GDI2 ILK FGF2 HSP90B1 PSMA5 PSMC1 PSME1 BAX TPP1 CCN2
14912	negative regulation of smooth muscle cell migration	1.1373E-3	2.6682E-2	2/107 1.8%	7/14296 0.0%	SERPINE1 ILK
46668	regulation of retinal cell programmed cell death	1.1373E-3	2.6682E-2	2/107 1.8%	7/14296 0.0%	BAX FGF2
5996	monosaccharide metabolic process	1.1858E-3	2.7212E-2	7/107 6.5%	216/14296 1.5%	PYGB UGDH PKM GALM ENO1 PFKM PGM1
70482	response to oxygen levels	1.1955E-3	2.7212E-2	6/107 5.6%	158/14296 1.1%	DPP4 ITGA2 PLAT CCN2 ACTN4 HSP90B1
16052	carbohydrate catabolic process	1.2413E-3	2.7581E-2	5/107 4.6%	107/14296 0.7%	PYGB PKM ENO1 GNS PFKM
9056	catabolic process	1.2500E-3	2.7581E-2	17/107 15.8%	1006/14296 7.0%	PYGB GOT1 ENO1 GNS HSP90B1 PSMA5 PKM LAMP1 DDAH2 PSMC1 PSME1 HNRNPD MYH9 BAX TPP1 PFKM HSPA1B

43062	extracellular structure organization	1.2754E-3	2.7581E-2	6/107 5.6%	160/14296 1.1%	COL1A1 ILK CCN2 LAMC1 CCN1 PTK2
7169	transmembrane receptor protein tyrosine kinase signaling pathway	1.2841E-3	2.7581E-2	7/107 6.5%	219/14296 1.5%	EGF PLAT CCN2 FGF2 PTK2 FGFR2 FGFR1
48518	positive regulation of biological process	1.3338E-3	2.8201E-2	29/107 27.1%	2207/14296 15.4%	DDX5 HDAC1 SERPINE1 ILK LAMC1 FGF2 RTN4 DPP4 RPS15A CCN2 CCN1 EDIL3 GAL1 EIF5A GOT1 STAT1 EGF ITGA2 AP3B1 ACTN4 PSMA5 PSMC1 DNAJA2 PSME1 BAX PFKM FGFR2 RAN FGFR1
9057	macromolecule catabolic process	1.3499E-3	2.8201E-2	11/107 10.2%	503/14296 3.5%	PSMA5 PYGB PSMC1 PSME1 HNRNPD MYH9 BAX TPP1 GNS HSPA1B HSP90B1
9058	biosynthetic process	1.3980E-3	2.8494E-2	25/107 23.3%	1795/14296 12.5%	RPL10 RPL8 RPL9 FGF2 RPS15A RPL18A SCP2 CCN2 RPL15 RPS2 RPS27A RPL19 EIF5A GOT1 STAT1 EGF RPL23 RPL13A MOGS APRT EEF1A1 COL1A1 UGDH DDAH2 PTMA
8380	RNA splicing	1.4013E-3	2.8494E-2	8/107 7.4%	287/14296 2.0%	HNRNPL PRMT5 DDX5 HNRNPK PCBP1 SRSF1 HNRNPD RBMX
40008	regulation of growth	1.4818E-3	2.9733E-2	9/107 8.4%	359/14296 2.5%	ILK ENO1 CCN2 CCN1 FGF2 RTN4 PTK2 HSPA1B FGFR1
60045	positive regulation of cardiac muscle cell proliferation	1.5089E-3	2.9885E-2	2/107 1.8%	8/14296 0.0%	FGF2 FGFR1
46620	regulation of organ growth	1.5732E-3	3.0557E-2	3/107 2.8%	31/14296 0.2%	FGF2 PTK2 FGFR1
30336	negative regulation of cell migration	1.5830E-3	3.0557E-2	4/107 3.7%	67/14296 0.4%	SERPINE1 ILK FGF2 VCL
6886	intracellular protein transport	1.6296E-3	3.0811E-2	9/107 8.4%	364/14296 2.5%	CTSA EIF5A RPL23 AP1B1 TPP1 AP3B1 CCN1 FGF2 RAN
3012	muscle system process	1.6365E-3	3.0811E-2	6/107 5.6%	168/14296 1.1%	ACTA2 ACTC1 TPM2 TLN1 VCL MYLK
40011	locomotion	1.6893E-3	3.1416E-2	10/107 9.3%	440/14296 3.0%	DPP4 ITGB1 FN1 MYH9 PLAT CCN2 LAMC1 CCN1 FGF2 PTK2
10811	positive regulation of cell-substrate adhesion	1.7266E-3	3.1724E-2	3/107 2.8%	32/14296 0.2%	ILK CCN1 EDIL3
16071	mRNA metabolic process	1.7890E-3	3.2241E-2	9/107 8.4%	369/14296 2.5%	HNRNPL PRMT5 DDX5 HNRNPK PCBP1 SRSF1 HNRNPD RBMX HSPA1B
5975	carbohydrate metabolic process	1.8114E-3	3.2241E-2	11/107 10.2%	522/14296 3.6%	PYGB UGDH PKM GOT1 HEXA MOGS GALM ENO1 GNS PFKM PGM1

43067	regulation of programmed cell death	1.8182E-3	3.2241E-2	15/107 14.0%	860/14296 6.0%	EIF5A HDAC1 STAT1 SERPINE1 ILK ACTN4 FGF2 RTN4 HSP90B1 DDAH2 BAX CCN2 GAL1 HSPA1B FGFR1
30036	actin cytoskeleton organization	1.9216E-3	3.2354E-2	7/107 6.5%	235/14296 1.6%	ACTC1 MYH9 PARVA ACTN4 ARPC5 TLN1 HSP90B1
51649	establishment of localization in cell	1.9240E-3	3.2354E-2	15/107 14.0%	865/14296 6.0%	CTSA EIF5A RPL23 AP1B1 AP3B1 FGF2 PTK2 ACTC1 SCRN1 MYH9 TPP1 CCN2 CCN1 SEC22B RAN
7010	cytoskeleton organization	1.9287E-3	3.2354E-2	10/107 9.3%	448/14296 3.1%	ACTC1 MYH9 BAX PARVA ACTN4 ARPC5 TLN1 PTK2 RAN HSP90B1
21936	regulation of granule cell precursor proliferation	1.9306E-3	3.2354E-2	2/107 1.8%	9/14296 0.0%	EGF FGF2
21940	positive regulation of granule cell precursor proliferation	1.9306E-3	3.2354E-2	2/107 1.8%	9/14296 0.0%	EGF FGF2
10941	regulation of cell death	1.9677E-3	3.2617E-2	15/107 14.0%	867/14296 6.0%	EIF5A HDAC1 STAT1 SERPINE1 ILK ACTN4 FGF2 RTN4 HSP90B1 DDAH2 BAX CCN2 GAL1 HSPA1B FGFR1
51336	regulation of hydrolase activity	1.9966E-3	3.2740E-2	9/107 8.4%	375/14296 2.6%	GDI1 STAT1 TPM2 ITGA2 SERPINE1 GDI2 BAX CCN2 HSP90B1
43066	negative regulation of apoptosis	2.0330E-3	3.2983E-2	9/107 8.4%	376/14296 2.6%	EIF5A DDAH2 HDAC1 SERPINE1 ILK BAX HSPA1B HSP90B1 FGFR1
40013	negative regulation of locomotion	2.0649E-3	3.3147E-2	4/107 3.7%	72/14296 0.5%	SERPINE1 ILK FGF2 VCL
51270	regulation of cellular component movement	2.1139E-3	3.3496E-2	7/107 6.5%	239/14296 1.6%	ITGA2 SERPINE1 ILK ACTN4 FGF2 VCL RTN4
51129	negative regulation of cellular component organization	2.1306E-3	3.3496E-2	6/107 5.6%	177/14296 1.2%	DPP4 TPP1 RTN4 PTK2 GAL1 HSPA1B
44262	cellular carbohydrate metabolic process	2.1840E-3	3.3986E-2	9/107 8.4%	380/14296 2.6%	PYGB UGDH PKM GOT1 MOGS GALM ENO1 PFKM PGM1
43069	negative regulation of programmed cell death	2.2231E-3	3.4059E-2	9/107 8.4%	381/14296 2.6%	EIF5A DDAH2 HDAC1 SERPINE1 ILK BAX HSPA1B HSP90B1 FGFR1
65009	regulation of molecular function	2.2334E-3	3.4059E-2	17/107 15.8%	1062/14296 7.4%	GDI1 STAT1 EGF TPM2 ITGA2 SERPINE1 GDI2 ILK ACTN4 FGF2 HSP90B1 PSMA5 PSMC1 PSME1 BAX TPP1 CCN2

10453	regulation of cell fate commitment	2.4015E-3	3.5905E-2	2/107 1.8%	10/14296 0.0%	FGF2 FGFR1
42659	regulation of cell fate specification	2.4015E-3	3.5905E-2	2/107 1.8%	10/14296 0.0%	FGF2 FGFR1
45926	negative regulation of growth	2.5502E-3	3.7757E-2	5/107 4.6%	126/14296 0.8%	ENO1 FGF2 RTN4 PTK2 HSPA1B
51216	cartilage development	2.6399E-3	3.8709E-2	4/107 3.7%	77/14296 0.5%	COL1A1 CCN2 FGF2 FGFR1
30029	actin filament-based process	2.7203E-3	3.9281E-2	7/107 6.5%	250/14296 1.7%	ACTC1 MYH9 PARVA ACTN4 ARPC5 TLN1 HSP90B1
31344	regulation of cell projection organization	2.7303E-3	3.9281E-2	5/107 4.6%	128/14296 0.8%	ITGA2 ILK RTN4 PTK2 GAL1
43434	response to peptide hormone stimulus	2.8036E-3	3.9772E-2	6/107 5.6%	187/14296 1.3%	COL1A1 GOT1 STAT1 PLAT CCN2 CCN1
43085	positive regulation of catalytic activity	2.8361E-3	3.9772E-2	11/107 10.2%	553/14296 3.8%	PSMA5 STAT1 EGF ITGA2 PSMC1 PSME1 ILK BAX TPP1 CCN2 FGF2
45807	positive regulation of endocytosis	2.8427E-3	3.9772E-2	3/107 2.8%	38/14296 0.2%	ITGA2 SERPINE1 ACTN4
44093	positive regulation of molecular function	2.8965E-3	3.9873E-2	12/107 11.2%	638/14296 4.4%	PSMA5 STAT1 EGF ITGA2 PSMC1 PSME1 ILK BAX TPP1 CCN2 ACTN4 FGF2
33628	regulation of cell adhesion mediated by integrin	2.9208E-3	3.9873E-2	2/107 1.8%	11/14296 0.0%	DPP4 SERPINE1
44249	cellular biosynthetic process	2.9284E-3	3.9873E-2	23/107 21.4%	1685/14296 11.7%	EIF5A GOT1 RPL10 STAT1 EGF RPL23 RPL13A MOGS RPL8 RPL9 FGF2 APRT EEF1A1 UGDH RPS15A RPL18A DDAH2 CCN2 RPL15 RPS2 RPS27A PTMA RPL19
31345	negative regulation of cell projection organization	3.0630E-3	4.1337E-2	3/107 2.8%	39/14296 0.2%	RTN4 PTK2 GAL1
6508	proteolysis	3.1096E-3	4.1597E-2	13/107 12.1%	730/14296 5.1%	CTSA MMP1 PLAT HSP90B1 DPP4 PSMA5 SCRN1 ANPEP PSMC1 PSME1 MYH9 BAX TPP1
44419	interspecies interaction between organisms	3.1536E-3	4.1706E-2	8/107 7.4%	327/14296 2.2%	ITGB1 HNRNPK MMP1 HDAC1 STAT1 ANPEP ITGA2 RAN
44275	cellular carbohydrate catabolic process	3.1724E-3	4.1706E-2	4/107 3.7%	81/14296 0.5%	PYGB PKM ENO1 PFKM

22607	cellular component assembly	3.2292E-3	4.2090E-2	15/107 14.0%	913/14296 6.3%	PRMT5 SRSF1 ILK PARVA ACTN4 LAMC1 PTK2 HSP90B1 ACTC1 SCP2 BAX TPP1 TLN1 PFKM VCL
32967	positive regulation of collagen biosynthetic process	3.4879E-3	4.4326E-2	2/107 1.8%	12/14296 0.0%	ITGA2 CCN2
10714	positive regulation of collagen metabolic process	3.4879E-3	4.4326E-2	2/107 1.8%	12/14296 0.0%	ITGA2 CCN2
43534	blood vessel endothelial cell migration	3.4879E-3	4.4326E-2	2/107 1.8%	12/14296 0.0%	MYH9 FGF2
51272	positive regulation of cellular component movement	3.6569E-3	4.6089E-2	5/107 4.6%	137/14296 0.9%	ITGA2 SERPINE1 ILK ACTN4 FGF2
6096	glycolysis	3.7857E-3	4.7321E-2	3/107 2.8%	42/14296 0.2%	PKM ENO1 PFKM
6605	protein targeting	3.9989E-3	4.8872E-2	6/107 5.6%	201/14296 1.4%	EIF5A RPL23 AP3B1 CCN1 FGF2 RAN
46907	intracellular transport	4.0447E-3	4.8872E-2	12/107 11.2%	665/14296 4.6%	CTSA EIF5A ACTC1 RPL23 AP1B1 MYH9 TPP1 AP3B1 CCN1 SEC22B FGF2 RAN
60043	regulation of cardiac muscle cell proliferation	4.1020E-3	4.8872E-2	2/107 1.8%	13/14296 0.0%	FGF2 FGFR1
10977	negative regulation of neuron projection development	4.1020E-3	4.8872E-2	2/107 1.8%	13/14296 0.0%	RTN4 GAL1
55021	regulation of cardiac muscle tissue growth	4.1020E-3	4.8872E-2	2/107 1.8%	13/14296 0.0%	FGF2 FGFR1
55024	regulation of cardiac muscle tissue development	4.1020E-3	4.8872E-2	2/107 1.8%	13/14296 0.0%	FGF2 FGFR1

Table 8- 7: BiNGO Enriched molecular functions in the proteome

5515	protein binding	4.8671E-10	1.7035E-7	87/107 81.3%	8118/15435 52.5%	ITGB1 LGALS3BP EIF4A1 PYGB SPARC GDI1 SERPINE1 HEXA GDI2 ILK PLAT PPP2R2A ENO1 LAMC1 FGF2 MYLK TXNDC17 ACTR1A RPL18A SCP2 FLOT2 CCN2 CCN1 EDIL3 GAL1 EIF5A GSTK1 PRMT5 RPL23 TPM2 ITGA2 AP1B1 AP3B1 ACTN4 OXSR1 RANGAP1 APRT EEF1A1 PSMA5 ACTA2 PKM DDAH2 MYH9 TLN1 SEC22B VCL DYNC1I2 DDX5 TAGLN HDAC1 SRSF1 TWF2 KLC1 GNS RTN4 HSP90B1 DPP4 RPS15A PCBP1 RPS2 CTSA FARP1 ST13 STAT1 EGF FN1 PARVA ARPC5 DEK PTK2 COL1A1 HNRNPL NSFL1C SNX18 HNRNPK ACTC1 PSMC1 DNAJA2 HNRNPD BAX TPP1 PFKM RBMX FGFR2 HSPA1B RAN FGFR1
3735	structural constituent of ribosome	1.0618E-8	1.8582E-6	11/107 10.2%	156/15435 1.0%	RPS15A RPL18A RPL10 RPL23 RPL13A RPL15 RPS2 RPL8 RPS27A RPL9 RPL19
5198	structural molecule activity	1.6193E-7	1.8892E-5	18/107 16.8%	604/15435 3.9%	RPL10 RPL23 TPM2 FN1 RPL13A ARPC5 LAMC1 RPL8 RPL9 COL1A1 RPS15A RPL18A RPL15 RPS2 TLN1 RPS27A VCL RPL19
3723	RNA binding	6.0103E-7	5.2590E-5	19/107 17.7%	733/15435 4.7%	EIF5A EIF4A1 DDX5 RPL10 RPL23 SRSF1 RPL8 RPL9 HSP90B1 HNRNPL HNRNPK RPS15A RPL18A PCBP1 HNRNPD RPL15 RPS2 RBMX RPL19
5488	binding	1.0496E-6	7.3470E-5	103/107 96.2%	12362/15435 80.0%	EIF4A1 SPARC SERPINE1 PLAT PPP2R2A ENO1 RPL8 RPL9 FGF2 MYLK TXNDC17 RPL18A SCP2 ANPEP CCN2 CCN1 GSTK1 RPL23 TPM2 AP1B1 ACTN4 EEF1A1 PPA2 TLN1 VCL DDX5 TWF2 KLC1 GNS RTN4 HSP90B1 DPP4 PCBP1 CTSA APA1 GOT1 ST13 FN1 PARVA ARPC5 PTK2 COL1A1 HNRNPL NSFL1C HNRNPK HNRNPD TPP1 FGFR2 FGFR1 ITGB1 LGALS3BP PYGB GDI1 HEXA GDI2 ILK LAMC1 ACTR1A FLOT2 EDIL3 PGM1 GAL1 EIF5A PRMT5 MMP1 ITGA2 AP3B1 OXSR1 RANGAP1

						APRT PSMA5 ACTA2 UGDH PKM DDAH2 MYH9 SEC22B DYNC1I2 TAGLN RPL10 HDAC1 SRSF1 RPS15A LMAN2 RPL15 RPS2 RPS27A RPL19 CYB5B FARP1 STAT1 EGF DEK SNX18 ACTC1 PSMC1 DNAJA2 BAX GALM PFKM RBMX HSPA1B RAN
30246	carbohydrate binding	4.4207E-5	2.2779E-3	11/107 10.2%	364/15435 2.3%	PYGB LMAN2 FN1 GALM CCN2 CCN1 FGF2 PFKM FGFR2 GAL1 FGFR1
5093	Rab GDP-dissociation inhibitor activity	4.7611E-5	2.2779E-3	2/107 1.8%	2/15435 0.0%	GDI1 GDI2
50840	extracellular matrix binding	5.2066E-5	2.2779E-3	4/107 3.7%	30/15435 0.1%	SPARC ITGA2 CCN1 GAL1
5178	integrin binding	7.4415E-5	2.8939E-3	5/107 4.6%	63/15435 0.4%	ITGA2 ILK CCN2 ACTN4 EDIL3
19838	growth factor binding	9.3782E-5	3.2824E-3	6/107 5.6%	106/15435 0.6%	COL1A1 CCN2 RPS2 CCN1 FGFR2 FGFR1
8201	heparin binding	1.2105E-4	3.7343E-3	6/107 5.6%	111/15435 0.7%	FN1 CCN2 CCN1 FGF2 FGFR2 FGFR1
5518	collagen binding	1.3439E-4	3.7343E-3	4/107 3.7%	38/15435 0.2%	DPP4 SPARC ITGA2 FN1
17134	fibroblast growth factor binding	1.3870E-4	3.7343E-3	3/107 2.8%	15/15435 0.0%	RPS2 FGFR2 FGFR1
8238	exopeptidase activity	2.4576E-4	6.1441E-3	5/107 4.6%	81/15435 0.5%	DPP4 CTSA SCRN1 ANPEP TPP1
3779	actin binding	4.0909E-4	9.5454E-3	9/107 8.4%	323/15435 2.0%	TAGLN TPM2 TWF2 MYH9 PARVA ACTN4 ARPC5 TLN1 MYLK
5007	fibroblast growth factor receptor activity	4.6966E-4	1.0274E-2	2/107 1.8%	5/15435 0.0%	FGFR2 FGFR1
5539	glycosaminoglycan binding	5.7289E-4	1.1795E-2	6/107 5.6%	148/15435 0.9%	FN1 CCN2 CCN1 FGF2 FGFR2 FGFR1
5092	GDP-dissociation inhibitor activity	7.0130E-4	1.3636E-2	2/107 1.8%	6/15435 0.0%	GDI1 GDI2
8092	cytoskeletal protein binding	7.7695E-4	1.4312E-2	11/107 10.2%	507/15435 3.2%	FARP1 TAGLN ACTC1 TPM2 TWF2 MYH9 PARVA ACTN4 ARPC5 TLN1 MYLK
42802	identical protein binding	8.9821E-4	1.5107E-2	13/107 12.1%	685/15435 4.4%	ITGB1 GSTK1 PYGB HDAC1 ITGA2 ACTN4 OXSR1 DPP4 COL1A1 MYH9 BAX PFKM GAL1
30247	polysaccharide binding	9.4956E-4	1.5107E-2	6/107 5.6%	163/15435 1.0%	FN1 CCN2 CCN1 FGF2 FGFR2 FGFR1
1871	pattern binding	9.4956E-4	1.5107E-2	6/107 5.6%	163/15435 1.0%	FN1 CCN2 CCN1 FGF2 FGFR2 FGFR1
16787	hydrolase activity	1.1007E-3	1.6750E-2	28/107 26.1%	2240/15435 14.5%	EIF4A1 DYNC1I2 DDX5 HDAC1 HEXA PLAT PPP2R2A ENO1 KLC1 GNS DPP4 SCP2 NAGLU SCRN1 ANPEP CCN1 CTSA MMP1 MOGS EEF1A1

						PSMA5 ACTC1 PPA2 DDAH2 PSMC1 MYH9 TPP1 RAN
166	nucleotide binding	1.2128E-3	1.7687E-2	28/107 26.1%	2254/15435 14.6%	EIF4A1 DDX5 SRSF1 TWF2 ILK MYLK HSP90B1 ACTR1A RPL23 OXSR1 PTK2 APRT EEF1A1 HNRNPL ACTA2 UGDH PKM ACTC1 PSMC1 DNAJA2 HNRNPD MYH9 PFKM RBMX FGFR2 HSPA1B RAN FGFR1
32403	protein complex binding	1.3391E-3	1.8748E-2	7/107 6.5%	238/15435 1.5%	ITGA2 ILK CCN2 ACTN4 TLN1 EDIL3 RTN4
46983	protein dimerization activity	2.2144E-3	2.9809E-2	11/107 10.2%	578/15435 3.7%	DPP4 ITGB1 PYGB SCP2 ITGA2 HEXA MYH9 BAX ACTN4 CCN1 GAL1
32559	adenyl ribonucleotide binding	3.0420E-3	3.9434E-2	20/107 18.6%	1496/15435 9.6%	EIF4A1 DDX5 TWF2 ILK OXSR1 PTK2 MYLK HSP90B1 APRT ACTA2 ACTR1A PKM ACTC1 PSMC1 DNAJA2 MYH9 PFKM FGFR2 HSPA1B FGFR1
4722	protein serine/threonine phosphatase activity	3.2679E-3	4.0849E-2	3/107 2.8%	43/15435 0.2%	SCP2 PPP2R2A CCN1
1882	nucleoside binding	3.4966E-3	4.1218E-2	21/107 19.6%	1623/15435 10.5%	EIF4A1 DDX5 TWF2 ILK ACTN4 OXSR1 PTK2 MYLK HSP90B1 APRT ACTA2 ACTR1A PKM ACTC1 PSMC1 DNAJA2 MYH9 PFKM FGFR2 HSPA1B FGFR1
15929	hexosaminidase activity	3.5330E-3	4.1218E-2	2/107 1.8%	13/15435 0.0%	NAGLU HEXA
46982	protein heterodimerization activity	3.8334E-3	4.3280E-2	6/107 5.6%	215/15435 1.3%	ITGB1 SCP2 ITGA2 HEXA BAX CCN1

8. References

A. Molteni, P.V., J.E. Moulder, E.F. Cohen, W.F. Ward, B.L. Fish, J.M. Taylor, L.F. Wolfe, L. Brizio-Molteni, 2000. Control of radiation-induced pneumopathy and lung fibrosis by angiotensin-converting enzyme inhibitors and an angiotensin II type 1 receptor blocker. International Journal of Radiation Biology 76, 523–532. https://doi.org/10.1080/095530000138538

Acharya, K.R., Sturrock, E.D., Riordan, J.F., Ehlers, M.R., 2003. Ace revisited: a new target for structure-based drug design. Nature Reviews Drug Discovery 2, 891.

Aebersold, R., Mann, M., 2016. Mass-spectrometric exploration of proteome structure and function. Nature 537, 347–355. https://doi.org/10.1038/nature19949

Aebersold, R., Mann, M., 2003. Mass spectrometry-based proteomics. Nature 422, 198.

Afanasyeva, M., Georgakopoulos, D., Fairweather, D., Caturegli, P., Kass, D.A., Rose, N.R., 2004. Novel Model of Constrictive Pericarditis Associated With Autoimmune Heart Disease in Interferon-γ–Knockout Mice. Circulation 110, 2910–2917. https://doi.org/10.1161/01.CIR.0000147538.92263.3A

Agostoni, A., Cicardi, M., Cugno, M., Zingale, L.C., Gioffré, D., Nussberger, J., 1999. Angioedema due to angiotensin-converting enzyme inhibitors. Immunopharmacology 44, 21–25.

Ahmad, N., Gabius, H.-J., André, S., Kaltner, H., Sabesan, S., Roy, R., Liu, B., Macaluso, F., Brewer, C.F., 2004. Galectin-3 Precipitates as a Pentamer with Synthetic Multivalent Carbohydrates and Forms Heterogeneous Cross-linked Complexes. J. Biol. Chem. 279, 10841–10847. https://doi.org/10.1074/jbc.M312834200

Aidoudi, S., Guigon, M., Lebeurier, I., Caen, J.P., Han, Z.C., 1996. In vivo effect of platelet factor 4 (PF4) and tetrapeptide AcSDKP on haemopoiesis of mice treated with 5-fluorouracil. British Journal of Haematology 94, 443–448. https://doi.org/10.1046/j.1365-2141.1996.d01-1821.x

Aimo, A., Cerbai, E., Bartolucci, G., Adamo, L., Barison, A., Lo Surdo, G., Biagini, S., Passino, C., Emdin, M., 2020. Pirfenidone is a cardioprotective drug: Mechanisms of action and preclinical evidence. Pharmacological Research 155, 104694. https://doi.org/10.1016/j.phrs.2020.104694

Ainslie, G.M., Benatar, S.R., 1985. Serum Angiotensin Converting Enzyme in Sarcoidosis: Sensitivity and Specificity in Diagnosis: Correlations with Disease Activity, Duration, Extra-thoracic Involvement, Radiographic Type and Therapy. QJM 55, 253–270.

Akahani, S., Nangia-Makker, P., Inohara, H., Kim, H.-R.C., Raz, A., 1997. Galectin-3: A Novel Antiapoptotic Molecule with A Functional BH1 (NWGR) Domain of Bcl-2 Family. Cancer Res 57, 5272–5276.

Akhurst, R.J., 2002. TGF-β antagonists: Why suppress a tumor suppressor? Journal of Clinical Investigation 109, 1533–1536. https://doi.org/10.1172/JCI15970

Araujo, M.C., Melo, R.L., Cesari, M.H., Juliano, M.A., Juliano, L., Carmona, A.K., 2000. Peptidase specificity characterization of C- and N-terminal catalytic sites of angiotensin I-converting enzyme. Biochemistry 39, 8519–8525.

Ariyarajah, V., Jassal, D.S., Kirkpatrick, I., Kwong, R.Y., 2009. The Utility of Cardiovascular Magnetic Resonance in Constrictive Pericardial Disease. Cardiol Rev 17, 77–82. https://doi.org/10.1097/CRD.0b013e318197e950

Azizi, M., Ezan, E., Nicolet, L., Grognet, J.M., Ménard, J., 1997. High plasma level of N-acetyl-seryl-aspartyl-lysyl-proline: a new marker of chronic angiotensin-converting enzyme inhibition. Hypertension 30, 1015–1019.

Azizi, M., Ezan, E., Reny, J.-L., Wdzieczak-Bakala, J., Gerineau, V., Ménard, J., 1999. Renal and Metabolic Clearance of N-Acetyl-Seryl-Aspartyl-Lysyl-Proline (AcSDKP) During Angiotensin-Converting Enzyme Inhibition in Humans. Hypertension 33, 879–886. https://doi.org/10.1161/01.HYP.33.3.879

Azizi, M., Junot, C., Ezan, E., Ménard, J., 2001. Angiotensin I-Converting Enzyme And Metabolism Of The Haematological Peptide N-Acetyl-Seryl-Aspartyl-Lysyl-Proline. Clinical and Experimental Pharmacology and Physiology 28, 1066–1069. https://doi.org/10.1046/j.1440-1681.2001.03560.x

Azizi, M., Rousseau, A., Ezan, E., Guyene, T.-T., Michelet, S., Grognet, J.-M., Lenfant, M., Corvol, P., Ménard, J., 1996. Acute angiotensin-converting enzyme inhibition increases the plasma level of the natural stem cell regulator N-acetyl-seryl-aspartyl-lysyl-proline. Journal of Clinical Investigation 97, 839.

Bailey, G.L., Hampers, C.L., Hager, E.B., Merrill, J.P., 1968. Uremic pericarditis. Clinical features and management. Circulation 38, 582–591. https://doi.org/10.1161/01.CIR.38.3.582

Balyasnikova, I.V., Metzger, R., Sun, Z.-L., Berestetskaya, Y.V., Albrecht, R.F., Danilov, S.M., 2005. Development and characterization of rat monoclonal antibodies to denatured mouse angiotensin-converting enzyme. Tissue Antigens 65, 240–251.

Barauna, V.G., Campos, L.C.G., Miyakawa, A.A., Krieger, J.E., 2011. ACE as a Mechanosensor to Shear Stress Influences the Control of Its Own Regulation via Phosphorylation of Cytoplasmic Ser1270. PLoS ONE 6, e22803. https://doi.org/10.1371/journal.pone.0022803

Bataller, R., Schwabe, R.F., Choi, Y.H., Yang, L., Paik, Y.H., Lindquist, J., Qian, T., Schoonhoven, R., Hagedorn, C.H., Lemasters, J.J., Brenner, D.A., 2003. NADPH oxidase signal transduces angiotensin II in hepatic stellate cells and is critical in hepatic fibrosis. J. Clin. Invest. 112, 1383–1394. https://doi.org/10.1172/JCI18212

Benore-Parsons, M., Seidah, N.G., Wennogle, L.P., 1989. Substrate phosphorylation can inhibit proteolysis by trypsin-like enzymes. Arch. Biochem. Biophys. 272, 274–280. https://doi.org/10.1016/0003-9861(89)90220-8

Bernstein, K.E., Khan, Z., Giani, J.F., Cao, D.-Y., Bernstein, E.A., Shen, X.Z., 2018. Angiotensin-converting enzyme in innate and adaptive immunity. Nature Reviews Nephrology 14, 325–336. https://doi.org/10.1038/nrneph.2018.15

Berridge, M.J., 1995. Calcium signalling and cell proliferation. BioEssays 17, 491–500. https://doi.org/10.1002/bies.950170605

Berridge, M.J., Lipp, P., Bootman, M.D., 2000. The versatility and universality of calcium signalling. Nat Rev Mol Cell Biol 1, 11–21. https://doi.org/10.1038/35036035

Bezakova, G., Ruegg, M.A., 2003. New insights into the roles of agrin. Nature Reviews Molecular Cell Biology 4, 295–309. https://doi.org/10.1038/nrm1074

Birdsall, B., Feeney, J., Burdett, I.D.J., Bawumia, S., Barboni, E.A.M., Hughes, R.C., 2001. NMR Solution Studies of Hamster Galectin-3 and Electron Microscopic Visualization of Surface-Adsorbed Complexes: Evidence for Interactions between the N- and C-Terminal Domains. Biochemistry 40, 4859–4866. https://doi.org/10.1021/bi002907f

Blenis, J., 1993. Signal transduction via the MAP kinases: proceed at your own RSK. PNAS 90, 5889–5892.

Bogden, A.E., Moreau, J.-P., Gamba-Vitalo, C., Deschamps de Paillette, E., Tubiana, M., Frindel, E., Carde, P., 1998. Goralatide (AcSDKP), a negative growth regulator, protects the stem cell compartment during chemotherapy, enhancing the myelopoietic response to GM-CSF. International Journal of Cancer 76, 38–46. https://doi.org/10.1002/(SICI)1097-0215(19980330)76:1<38::AID-IJC8>3.0.CO;2-Z

Bonifacino, J.S., Dell'Angelica, E.C., Springer, T.A., 1999. Immunoprecipitation. Current protocols in protein science 18, 9–8.

Bonnet, D., Lemoine, F.M., Pontvert-Delucq, S., Baillou, C., Najman, A., Guigon, M., 1993. Direct and reversible inhibitory effect of the tetrapeptide acetyl-N- Ser-Asp-Lys-Pro (Seraspenide) on the growth of human CD34+ subpopulations in response to growth factors. Blood 82, 3307–3314.

Border, W.A., Noble, N.A., 1998. Interactions of transforming growth factor-β and angiotensin II in renal fibrosis. Hypertension 31, 181–188.

Bornfeldt, K.E., Raines, E.W., Graves, L.M., Skinner, M.P., Krebs, E.G., Ross, R., 1995. Platelet-derived Growth Factor. Annals of the New York Academy of Sciences 766, 416–430. https://doi.org/10.1111/j.1749-6632.1995.tb26691.x

Botti, R.E., Driscol, T.E., Pearson, O.H., Smith, J.C., 1968. Radiation myocardial fibrosis simulating constrictive pericarditis. A review of the literature and a case report. Cancer 22, 1254–1261. https://doi.org/10.1002/1097-0142(196811)22:6<1254::AID-CNCR2820220624>3.0.CO;2-9

Branton, M.H., Kopp, J.B., 1999. TGF-β and fibrosis. Microbes and Infection 1, 1349–1365. https://doi.org/10.1016/S1286-4579(99)00250-6

Brice, E.A.W., Friedlander, W., Bateman, E.D., Kirsch, B.E., 1995. Serum Angiotensin-Converting Enzyme Activity, Concentration, and Specific Activity in Granulomatous Interstitial Lung Disease, Tuberculosis, and COPD. CHEST 107, 706–710. https://doi.org/10.1378/chest.107.3.706

Brilla, C.G., Funck, R.C., Rupp, H., 2000. Lisinopril-Mediated Regression of Myocardial Fibrosis in Patients With Hypertensive Heart Disease. Circulation 102, 1388–1393. https://doi.org/10.1161/01.CIR.102.12.1388

Brilla, C.G., Reams, G.P., Maisch, B., Weber, K.T., 1993. Renin-angiotensin system and myocardial fibrosis in hypertension: regulation of the myocardial collagen matrix. Eur Heart J 14 Suppl J, 57–61.

Brown, L., Duce, B., Miric, G., Sernia, C., 1999. Reversal of cardiac fibrosis in deoxycorticosterone acetate-salt hypertensive rats by inhibition of the renin-angiotensin system. J. Am. Soc. Nephrol. 10 Suppl 11, S143-148.

Browne, P., O'Cuinn, G., 1983. An evaluation of the role of a pyroglutamyl peptidase, a post-proline cleaving enzyme and a post-proline dipeptidyl amino peptidase, each purified

from the soluble fraction of guinea-pig brain, in the degradation of thyroliberin in vitro. Eur. J. Biochem. 137, 75–87.

Burgess, L.J., Reuter, H., Carstens, M.E., Taljaard, J.J.F., Doubell, A.F., 2002. THe use of adenosine deaminase and interferon-γ as diagnostic tools for tuberculous pericarditis*. Chest 122, 900–905. https://doi.org/10.1378/chest.122.3.900

Butler, D., 2008. Translational research: Crossing the valley of death [WWW Document]. Nature. https://doi.org/10.1038/453840a

Byers, R.J., Marshall, D. a. S., Freemont, A.J., 1997. Pericardial involvement in systemic sclerosis. Annals of the Rheumatic Diseases 56, 393–394. https://doi.org/10.1136/ard.56.6.393

Caldwell, P.R., Seegal, B.C., Hsu, K.C., Das, M., Soffer, R.L., others, 1976. Angiotensin-converting enzyme: vascular endothelial localization. Science (New York, NY) 191, 1050.

Calvier, L., Miana, M., Reboul, P., Cachofeiro, V., Martinez-Martinez, E., de Boer, R.A., Poirier, F., Lacolley, P., Zannad, F., Rossignol, P., López-Andrés, N., 2013. Galectin-3 mediates aldosterone-induced vascular fibrosis. Arterioscler Thromb Vasc Biol 33, 67–75. https://doi.org/10.1161/ATVBAHA.112.300569

Caprioli, R.M., Farmer, T.B., Gile, J., 1997. Molecular imaging of biological samples: localization of peptides and proteins using MALDI-TOF MS. Analytical chemistry 69, 4751–4760.

Carde, P., Chastang, C., Goncalves, E., Mathieu-Tubiana, N., Vuillemin, E., Delwail, V., Corbion, O., Vekhoff, A., Isnard, F., Ferrero, J.M., 1992. [Seraspenide (acetylSDKP): phase I-II trial study of inhibitor of hematopoiesis protects against toxicity of aracytine and ifosfamide monochemotherapies]. C R Acad Sci III 315, 545–550.

Carretero, O.A., 2005. Novel mechanism of action of ACE and its inhibitors. Am J Physiol Heart Circ Physiol 289, H1796–H1797. https://doi.org/10.1152/ajpheart.00781.2005

Cashman, J.D., Eaves, A.C., Eaves, C.J., 1994. The tetrapeptide AcSDKP specifically blocks the cycling of primitive normal but not leukemic progenitors in long-term culture: evidence for an indirect mechanism. Blood 84, 1534–1542.

Castoldi, G., di Gioia, C.R.T., Bombardi, C., Perego, C., Perego, L., Mancini, M., Leopizzi, M., Corradi, B., Perlini, S., Zerbini, G., Stella, A., 2009. Prevention of myocardial fibrosis by N-acetyl-seryl-aspartyl-lysyl-proline in diabetic rats. Clin. Sci. 118, 211–220. https://doi.org/10.1042/CS20090234

Castoldi, G., di Gioia, C.R.T., Bombardi, C., Preziuso, C., Leopizzi, M., Maestroni, S., Corradi, B., Zerbini, G., Stella, A., 2013. Renal Antifibrotic Effect of N-Acetyl-Seryl-Aspartyl-Lysyl-Proline in Diabetic Rats. American Journal of Nephrology 37, 65–73. https://doi.org/10.1159/000346116

Castoldi, G., Di Gioia, C.R.T., Bombardi, C., Perego, C., Perego, L., Mancini, M., Leopizzi, M., Corradi, B., Perlini, S., Zerbini, G., Stella, A., 2010. Prevention of myocardial fibrosis by N -acetyl-seryl-aspartyl-lysyl-proline in diabetic rats. Clinical Science 118, 211–220. https://doi.org/10.1042/CS20090234

Cavasin, M.A., Liao, T.-D., Yang, X.-P., Yang, J.J., Carretero, O.A., 2007. Decreased Endogenous Levels of Ac-SDKP Promote Organ Fibrosis. Hypertension 50, 130–136. https://doi.org/10.1161/HYPERTENSIONAHA.106.084103

Cavasin, M.A., Rhaleb, N.-E., Yang, X.-P., Carretero, O.A., 2004. Prolyl Oligopeptidase Is Involved in Release of the Antifibrotic Peptide Ac-SDKP. Hypertension 43, 1140–1145. https://doi.org/10.1161/01.HYP.0000126172.01673.84

Chakravarti, S., Magnuson, T., Lass, J.H., Jepsen, K.J., LaMantia, C., Carroll, H., 1998. Lumican Regulates Collagen Fibril Assembly: Skin Fragility and Corneal Opacity in the Absence of Lumican. J Cell Biol 141, 1277–1286. https://doi.org/10.1083/jcb.141.5.1277

Chan, G.C., Wu, H.J., Chan, K.W., Yiu, W.H., Zou, A., Huang, X.R., Lan, H.Y., Lai, K.N., Tang, S.C., 2018. N-acetyl-seryl-aspartyl-lysyl-proline mediates the anti-fibrotic properties of captopril in unilateral ureteric obstructed BALB/C mice. Nephrology 23, 297–307.

Chan, G.C., Yiu, W.H., Wu, H.J., Wong, D.W., Lin, M., Huang, X.R., Lan, H.Y., Tang, S.C., 2015. N-acetyl-seryl-aspartyl-lysyl-proline alleviates renal fibrosis induced by unilateral ureteric obstruction in BALB/C mice. Mediators of inflammation 2015.

Chen, M.M., Lam, A., Abraham, J.A., Schreiner, G.F., Joly, A.H., 2000. CTGF Expression is Induced by TGF- β in Cardiac Fibroblasts and Cardiac Myocytes: a Potential Role in Heart Fibrosis. Journal of Molecular and Cellular Cardiology 32, 1805–1819. https://doi.org/10.1006/jmcc.2000.1215

Chen, Y., Sun, F., Zhang, Y., Song, G., Qiao, W., Zhou, K., Ren, S., Zhao, Q., Ren, W., 2020. Comprehensive molecular characterization of circRNA-associated ceRNA network in constrictive pericarditis. Ann Transl Med 8. https://doi.org/10.21037/atm-20-2912

Cohen, M.V., Greenberg, M.A., 1979. Constrictive pericarditis: early and late complication of cardiac surgery. Am. J. Cardiol. 43, 657–661. https://doi.org/10.1016/0002-9149(79)90028-6

Comte, L., Lorgeot, V., Volkov, L., Allegraud, A., Aldigier, J.-C., Praloran, V., 1997. Effects of the angiotensin-converting enzyme inhibitor enalapril on blood haematopoietic progenitors and Acetyl-N-Ser-Asp-Lys-Pro concentrations. European Journal of Clinical Investigation 27, 788–790. https://doi.org/10.1046/j.1365-2362.1997.1980737.x

Cooper, S., 2003. Reappraisal of serum starvation, the restriction point, G0, and G1 phase arrest points. FASEB J 17, 333–340. https://doi.org/10.1096/fj.02-0352rev

Corbett, E.L., Watt, C.J., Walker, N., Maher, D., Williams, B.G., Raviglione, M.C., Dye, C., 2003. The growing burden of tuberculosis: global trends and interactions with the HIV epidemic. Archives of internal medicine 163, 1009.

Cotman, S.L., Halfter, W., Cole, G.J., 1999. Identification of Extracellular Matrix Ligands for the Heparan Sulfate Proteoglycan Agrin. Experimental Cell Research 249, 54–64. https://doi.org/10.1006/excr.1999.4463

Couchman, J.R., Höök, M., Rees, D.A., Timpl, R., 1983. Adhesion, growth, and matrix production by fibroblasts on laminin substrates. J Cell Biol 96, 177–183. https://doi.org/10.1083/jcb.96.1.177

Cox, J., Mann, M., 2008. MaxQuant enables high peptide identification rates, individualized p.p.b.-range mass accuracies and proteome-wide protein quantification. Nat. Biotechnol. 26, 1367–1372. https://doi.org/10.1038/nbt.1511

Crockford, D., Turjman, N., Allan, C., Angel, J., 2010. Thymosin β4: structure, function, and biological properties supporting current and future clinical applications. Annals of the New York Academy of Sciences 1194, 179–189. https://doi.org/10.1111/j.1749-6632.2010.05492.x

Crofford, L.J., 1997. COX-1 and COX-2 tissue expression: implications and predictions. The Journal of rheumatology. Supplement 49, 15–19.

Croft, D., O'Kelly, G., Wu, G., Haw, R., Gillespie, M., Matthews, L., Caudy, M., Garapati, P., Gopinath, G., Jassal, B., Jupe, S., Kalatskaya, I., Mahajan, S., May, B., Ndegwa, N., Schmidt, E., Shamovsky, V., Yung, C., Birney, E., Hermjakob, H., D'Eustachio, P., Stein, L., 2011. Reactome: a database of reactions, pathways and biological processes. Nucleic Acids Res 39, D691–D697. https://doi.org/10.1093/nar/gkq1018

Cushman, D.W., Ondetti, M.A., 1991. History of the design of captopril and related inhibitors of angiotensin converting enzyme. Hypertension 17, 589–592.

Daley, C.L., Small, P.M., Schecter, G.F., Schoolnik, G.K., McAdam, R.A., Jacobs, W.R., Hopewell, P.C., 1992. An Outbreak of Tuberculosis with Accelerated Progression among Persons Infected with the Human Immunodeficiency Virus. New England Journal of Medicine 326, 231–235. https://doi.org/10.1056/NEJM199201233260404

De Boer, R.A., Yu, L., Van Veldhuisen, D.J., 2010. Galectin-3 in cardiac remodeling and heart failure. Current heart failure reports 7, 1–8.

de Gouveia, R.H., Santos, C., Santi, R., Nesi, G., 2016. Lessons from the past: Uremic pericarditis. Cor et Vasa. https://doi.org/10.1016/j.crvasa.2016.09.001

Dees, C., Tomcik, M., Zerr, P., Akhmetshina, A., Horn, A., Palumbo, K., Beyer, C., Zwerina, J., Distler, O., Schett, G., Distler, J.H.W., 2011. Notch signalling regulates fibroblast activation and collagen release in systemic sclerosis. Annals of the Rheumatic Diseases 70, 1304–1310. https://doi.org/10.1136/ard.2010.134742

D'Elia, E., Ferrazzi, P., Imazio, M., Simon, C., Pentiricci, S., Stamerra, C.A., Iacovoni, A., Gori, M., Duino, V., Senni, M., Brucato, A.L., 2019. Constrictive pericarditis: a common pathophysiology for different macroscopic anatomies. Journal of Cardiovascular Medicine 20, 725–726. https://doi.org/10.2459/JCM.0000000000000844

Demopoulos, K., Arvanitis, D.A., Vassilakis, D.A., Siafakas, N.M., Spandidos, D.A., 2002. MYCL1, FHIT, SPARC, p16(INK4) and TP53 genes associated to lung cancer in idiopathic pulmonary fibrosis. J. Cell. Mol. Med. 6, 215–222. https://doi.org/10.1111/j.1582-4934.2002.tb00188.x

Deng, H., Xu, H., Zhang, X., Sun, Y., Wang, R., Brann, D., Yang, F., 2016. Protective effect of Ac-SDKP on alveolar epithelial cells through inhibition of EMT via TGF-β1/ROCK1 pathway in silicosis in rat. Toxicology and applied pharmacology 294, 1–10.

Depboylu, B.C., Mootoosamy, P., Vistarini, N., Testuz, A., El-Hamamsy, I., Cikirikcioglu, M., 2017. Surgical Treatment of Constrictive Pericarditis. Tex Heart Inst J 44, 101–106. https://doi.org/10.14503/THIJ-16-5772

Diegelmann, R., F., 2004. Wound healing: an overview of acute, fibrotic and delayed healing. Frontiers in Bioscience 9, 283. https://doi.org/10.2741/1184

Diet Frank, Pratt Richard E., Berry Gerald J., Momose Naoko, Gibbons Gary H., Dzau Victor J., 1996. Increased Accumulation of Tissue ACE in Human Atherosclerotic Coronary Artery Disease. Circulation 94, 2756–2767. https://doi.org/10.1161/01.CIR.94.11.2756

Dijke, P. ten, Hill, C.S., 2004. New insights into TGF-β–Smad signalling. Trends in Biochemical Sciences 29, 265–273. https://doi.org/10.1016/j.tibs.2004.03.008

Distler, O., Volkmann, E.R., Hoffmann-Vold, A.M., Maher, T.M., 2019. Current and future perspectives on management of systemic sclerosis-associated interstitial lung disease. Expert Rev Clin Immunol 15, 1009–1017. https://doi.org/10.1080/1744666X.2020.1668269

Dive, V., Cotton, J., Yiotakis, A., Michaud, A., Vassiliou, S., Jiracek, J., Vazeux, G., Chauvet, M.T., Cuniasse, P., Corvol, P., 1999. RXP 407, a phosphinic peptide, is a potent inhibitor of angiotensin I converting enzyme able to differentiate between its two active sites. Proceedings of the National Academy of Sciences 96, 4330–4335.

Doi, S., Zou, Y., Togao, O., Pastor, J.V., John, G.B., Wang, L., Shiizaki, K., Gotschall, R., Schiavi, S., Yorioka, N., 2011. Klotho inhibits transforming growth factor-β1 (TGF-β1) signaling and suppresses renal fibrosis and cancer metastasis in mice. Journal of Biological Chemistry 286, 8655–8665.

Dorfman, T.A., Aqel, R., 2009. Regional pericarditis: a review of the pericardial manifestations of acute myocardial infarction. Clin Cardiol 32, 115–120. https://doi.org/10.1002/clc.20444

Douglas, R.G., Ehlers, M.R., Sturrock, E.D., 2013. Antifibrotic peptide N-acetyl-Ser-Asp-Lys-Pro (Ac-SDKP): Opportunities for angiotensin-converting enzyme inhibitor design. Clinical and Experimental Pharmacology and Physiology 40, 535–541. https://doi.org/10.1111/1440-1681.12062

Dumic, J., Dabelic, S., Flögel, M., 2006. Galectin-3: an open-ended story. Biochim. Biophys. Acta 1760, 616–635. https://doi.org/10.1016/j.bbagen.2005.12.020

Ehlers, M.R., Fox, E.A., Strydom, D.J., Riordan, J.F., 1989. Molecular cloning of human testicular angiotensin-converting enzyme: the testis isozyme is identical to the C-terminal half of endothelial angiotensin-converting enzyme. PNAS 86, 7741–7745.

Ehlers, M.R.W., Schwager, S.L.U., Scholle, R.R., Manji, G.A., Brandt, W.F., Riordan, J.F., 1996. Proteolytic Release of Membrane-Bound Angiotensin-Converting Enzyme: Role of the Juxtamembrane Stalk Sequence†. Biochemistry 35, 9549–9559. https://doi.org/10.1021/bi9602425

Eitzman, D.T., McCoy, R.D., Zheng, X., Fay, W.P., Shen, T., Ginsburg, D., Simon, R.H., 1996. Bleomycin-induced pulmonary fibrosis in transgenic mice that either lack or overexpress the murine plasminogen activator inhibitor-1 gene. J Clin Invest 97, 232–237. https://doi.org/10.1172/JCI118396

Elad-Sfadia, G., Haklai, R., Balan, E., Kloog, Y., 2004. Galectin-3 Augments K-Ras Activation and Triggers a Ras Signal That Attenuates ERK but Not Phosphoinositide 3-Kinase Activity. J. Biol. Chem. 279, 34922–34930. https://doi.org/10.1074/jbc.M312697200

Ellman, G.L., Courtney, K.D., Featherstone, R.M., 1961. A new and rapid colorimetric determination of acetylcholinesterase activity. Biochemical pharmacology 7, 88–95.

Engvall, E., Perlmann, P., 1971. Enzyme-linked immunosorbent assay (ELISA) quantitative assay of immunoglobulin G. Immunochemistry 8, 871–874.

Fairweather, D., Frisancho-Kiss, S., Yusung, S.A., Barrett, M.A., Davis, S.E., Gatewood, S.J.L., Njoku, D.B., Rose, N.R., 2004. Interferon-gamma protects against chronic viral myocarditis by reducing mast cell degranulation, fibrosis, and the profibrotic cytokines transforming growth factor-beta 1, interleukin-1 beta, and interleukin-4 in the heart. Am. J. Pathol. 165, 1883–1894. https://doi.org/10.1016/S0002-9440(10)63241-5

Fernandes, F., Melo, D.T.P. de, Ramires, F.J.A., Sabino, E.C., Moreira, C.H.V., Benvenutti, L.A., Hotta, V.T., Sayegh, A.L.C., Souza, F.R. de, Dias, R.R., Mady, C., 2020. Galectin-3 Levels in Patients with Chronic Constrictive Pericarditis. Arq. Bras. Cardiol. 114, 683–689. https://doi.org/10.36660/abc.20190152

Fowler NO, 1991. TUberculous pericarditis. JAMA 266, 99–03. https://doi.org/10.1001/jama.1991.03470010103039

Fox, A.J., Lalloo, U.G., Belvisi, M.G., Bernareggi, M., Chung, K.F., Barnes, P.J., 1996. Bradykinin–evoked sensitization of airway sensory nerves: A mechanism for ACE–inhibitor cough. Nature Medicine 2, 814–817. https://doi.org/10.1038/nm0796-814

Frantz, C., Stewart, K.M., Weaver, V.M., 2010. The extracellular matrix at a glance. J Cell Sci 123, 4195–4200. https://doi.org/10.1242/jcs.023820

Frindel, E., Guigon, M., 1977. Inhibition of CFU entry into cycle by a bone marrow extract. Exp. Hematol. 5, 74–76.

Fuchs, S., Xiao, H.D., Hubert, C., Michaud, A., Campbell, D.J., Adams, J.W., Capecchi, M.R., Corvol, P., Bernstein, K.E., 2008. Angiotensin-Converting Enzyme C-Terminal Catalytic Domain Is the Main Site of Angiotensin I Cleavage In Vivo. Hypertension 51, 267–274. https://doi.org/10.1161/HYPERTENSIONAHA.107.097865

Gao, R., Kanasaki, K., Li, J., Kitada, M., Okazaki, T., Koya, D., 2019. βklotho is essential for the anti-endothelial mesenchymal transition effects of N-acetyl-seryl-aspartyl-lysyl-proline. FEBS open bio 9, 1029–1038.

Gao, X., Xu, H., Zhang, B., Tao, T., Liu, Y., Xu, D., Cai, W., Wei, Z., Li, Shifeng, Zhang, H., Mao, N., Zhang, G., Li, D., Jin, F., Li, Shumin, Zhang, L., Liu, H., Hao, X., Yang, F., 2019. Interaction of N-acetyl-seryl-aspartyl-lysyl-proline with the angiotensin-converting enzyme 2–angiotensin-(1–7)–Mas axis attenuates pulmonary fibrosis in silicotic rats. Experimental Physiology 104, 1562–1574. https://doi.org/10.1113/EP087515

Gaudino, M., Anselmi, A., Pavone, N., Massetti, M., 2013. Constrictive Pericarditis After Cardiac Surgery. The Annals of Thoracic Surgery 95, 731–736. https://doi.org/10.1016/j.athoracsur.2012.08.059

Gaudron, S., Adeline, M.T., Potier, P., Thierry, J., 1997. NAcSDKP analogues resistant to angiotensin-converting enzyme [WWW Document]. URL http://www.ncbi.nlm.nih.gov/pubmed/9397177 (accessed 2.14.19).

Gaudron, S, Adeline, M.T., Potier, P., Thierry, J., 1997. NAcSDKP analogues resistant to angiotensin-converting enzyme. J. Med. Chem. 40, 3963–3968. https://doi.org/10.1021/jm9701132

Gaudron, S., Grillon, C., Thierry, J., Riches, A., Wierenga, P.K., Wdzieczak-Bakala, J., 1999. In Vitro Effect of Acetyl-N-Ser-Asp-Lys-Pro (AcSDKP) Analogs Resistant to Angiotensin I-Converting Enzyme on Hematopoietic Stem Cell and Progenitor Cell Proliferation. STEM CELLS 17, 100–106. https://doi.org/10.1002/stem.170100

Geest, R.J.V., Lesnik-Oberstein, S.Y., Tan, H.S., Mura, M., Goldschmeding, R., Noorden, C.J.F.V., Klaassen, I., Schlingemann, R.O., 2012. A shift in the balance of vascular endothelial growth factor and connective tissue growth factor by bevacizumab causes the angiofibrotic switch in proliferative diabetic retinopathy. British Journal of Ophthalmology bjophthalmol-2011-301005. https://doi.org/10.1136/bjophthalmol-2011-301005

Goldstein, J.A., 2004. Cardiac tamponade, constrictive pericarditis, and restrictive cardiomyopathy. Current Problems in Cardiology 29, 503–567. https://doi.org/10.1016/j.cpcardiol.2004.03.002

Gomes, R.A. da S., Teodoro, L. das G.V.L., Lopes, I.C.R., Bersanetti, P.A., Carmona, A.K., Hial, V., 2008. Angiotensin-converting enzyme in pericardial fluid: comparative study with serum activity. Arq. Bras. Cardiol. 91, 156–161, 172–178.

Gong, H.C., Honjo, Y., Nangia-Makker, P., Hogan, V., Mazurak, N., Bresalier, R.S., Raz, A., 1999. The NH2 Terminus of Galectin-3 Governs Cellular Compartmentalization and Functions in Cancer Cells. Cancer Res 59, 6239–6245.

González, G.E., Rhaleb, N.-E., Nakagawa, P., Liao, T.-D., Liu, Y., Leung, P., Dai, X., Yang, X.-P., Carretero, O.A., 2014. N-acetyl-seryl-aspartyl-lysyl-proline reduces cardiac collagen cross-linking and inflammation in angiotensin II-induced hypertensive rats. Clinical science 126, 85–94.

Goossens, F., De Meester, I., Vanhoof, G., Scharpé, S., 1996. Distribution of prolyl oligopeptidase in human peripheral tissues and body fluids. Clinical Chemistry and Laboratory Medicine 34, 17–22.

Gordon, K., Balyasnikova, I.V., Nesterovitch, A.B., Schwartz, D.E., Sturrock, E.D., Danilov, S.M., 2010. Fine epitope mapping of monoclonal antibodies 9B9 and 3G8 to the N domain of angiotensin-converting enzyme (CD143) defines a region involved in regulating angiotensin-converting enzyme dimerization and shedding. Tissue Antigens 75, 136–150. https://doi.org/10.1111/j.1399-0039.2009.01416.x

Grainger, D.J., 2004. Transforming Growth Factor β and Atherosclerosis: So Far, So Good for the Protective Cytokine Hypothesis. Arterioscler Thromb Vasc Biol 24, 399–404. https://doi.org/10.1161/01.ATV.0000114567.76772.33

Graves, J.D., Krebs, E.G., 1999. Protein Phosphorylation and Signal Transduction. Pharmacology & Therapeutics 82, 111–121. https://doi.org/10.1016/S0163-7258(98)00056-4

Gray, M.O., Long, C.S., Kalinyak, J.E., Li, H.-T., Karliner, J.S., 1998. Angiotensin II stimulates cardiac myocyte hypertrophy via paracrine release of TGF-β1 and endothelin-1 from fibroblasts. Cardiovasc Res 40, 352–363. https://doi.org/10.1016/S0008-6363(98)00121-7

Grillon, C., Rieger, K., Bakala, J., Schott, D., Morgat, J.-L., Hannappel, E., Voelter, W., Lenfant, M., 1990. Involvement of thymosin β4 and endoproteinase Asp-N in the biosynthesis of the tetrapeptide AcSerAspLysPro a regulator of the hematopoietic system. FEBS Letters 274, 30–34. https://doi.org/10.1016/0014-5793(90)81322-F

Gross, O., Schulze-Lohoff, E., Koepke, M.-L., Beirowski, B., Addicks, K., Bloch, W., Smyth, N., Weber, M., 2004. Antifibrotic, nephroprotective potential of ACE inhibitor vs AT1 antagonist in a murine model of renal fibrosis. Nephrology Dialysis Transplantation 19, 1716–1723.

Guarda, E., Katwa, L.C., Myers, P.R., Tyagi, S.C., Weber, K.T., 1993. Effects of endothelins on collagen turnover in cardiac fibroblasts. Cardiovasc Res 27, 2130–2134. https://doi.org/10.1093/cvr/27.12.2130

Gundry, R.L., White, M.Y., Murray, C.I., Kane, L.A., Fu, Q., Stanley, B.A., Van Eyk, J.E., 2009. Preparation of Proteins and Peptides for Mass Spectrometry Analysis in a Bottom-Up

Proteomics Workflow. Curr Protoc Mol Biol CHAPTER, Unit10.25. https://doi.org/10.1002/0471142727.mb1025s88

Guo, L., Wu, C., 2002. Regulation of fibronectin matrix deposition and cell proliferation by the PINCH-ILK-CH-ILKBP complex. The FASEB Journal 16, 1298–1300.

Hajem, N., Chapelle, A., Bignon, J., Pinault, A., Liu, J.-M., Salah-Mohellibi, N., Lati, E., Wdzieczak-Bakala, J., 2013. The regulatory role of the tetrapeptide AcSDKP in skin and hair physiology and the prevention of ageing effects in these tissues – a potential cosmetic role. International Journal of Cosmetic Science 35, 286–298. https://doi.org/10.1111/ics.12046

Hathout, Y., 2007. Approaches to the study of the cell secretome. Expert review of proteomics 4, 239–248.

Hayashi, H., Sakai, T., 2012. Biological Significance of Local TGF-β Activation in Liver Diseases. Front. Physiol. 3. https://doi.org/10.3389/fphys.2012.00012

Hemming, M.L., Selkoe, D.J., 2005. Amyloid β-Protein Is Degraded by Cellular Angiotensin-converting Enzyme (ACE) and Elevated by an ACE Inhibitor. J. Biol. Chem. 280, 37644–37650. https://doi.org/10.1074/jbc.M508460200

Henderson, N.C., Mackinnon, A.C., Farnworth, S.L., Poirier, F., Russo, F.P., Iredale, J.P., Haslett, C., Simpson, K.J., Sethi, T., 2006. Galectin-3 regulates myofibroblast activation and hepatic fibrosis. PNAS 103, 5060–5065. https://doi.org/10.1073/pnas.0511167103

Herrera, J., Henke, C.A., Bitterman, P.B., 2018a. Extracellular matrix as a driver of progressive fibrosis. J Clin Invest 128, 45–53. https://doi.org/10.1172/JCI93557

Herrera, J., Henke, C.A., Bitterman, P.B., 2018b. Extracellular matrix as a driver of progressive fibrosis. J Clin Invest 128, 45–53. https://doi.org/10.1172/JCI93557

Ho, C.S., Lam, C.W.K., Chan, M.H.M., Cheung, R.C.K., Law, L.K., Lit, L.C.W., Ng, K.F., Suen, M.W.M., Tai, H.L., 2003. Electrospray ionisation mass spectrometry: principles and clinical applications. The Clinical Biochemist Reviews 24, 3.

Ho, J.E., Liu, C., Lyass, A., Courchesne, P., Pencina, M.J., Vasan, R.S., Larson, M.G., Levy, D., 2012. Galectin-3, a marker of cardiac fibrosis, predicts incident heart failure in the community. J Am Coll Cardiol 60, 1249–1256. https://doi.org/10.1016/j.jacc.2012.04.053

Holt, J.P., 1970. The normal pericardium. The American journal of cardiology 26, 455–465.

Hong, Y., Yao, Q., Zheng, L., 2017. Thymosin β4 attenuates liver fibrosis via suppressing Notch signaling. Biochemical and Biophysical Research Communications 493, 1396–1401. https://doi.org/10.1016/j.bbrc.2017.09.156

Hooper, N.M., 1994. Families of zinc metalloproteases. FEBS Letters 354, 1–6. https://doi.org/10.1016/0014-5793(94)01079-X

Hu, Q., Li, J., Nitta, K., Kitada, M., Nagai, T., Kanasaki, K., Koya, D., 2018. FGFR1 is essential for N-acetyl-seryl-aspartyl-lysyl-proline regulation of mitochondrial dynamics by upregulating microRNA let-7b-5p. Biochem. Biophys. Res. Commun. 495, 2214–2220. https://doi.org/10.1016/j.bbrc.2017.12.089

Hu, Q., Noll, R.J., Li, H., Makarov, A., Hardman, M., Graham Cooks, R., 2005. The Orbitrap: a new mass spectrometer. Journal of Mass Spectrometry 40, 430–443. https://doi.org/10.1002/jms.856

Hubert, C., Houot, A.M., Corvol, P., Soubrier, F., 1991. Structure of the angiotensin I-converting enzyme gene. Two alternate promoters correspond to evolutionary steps of a duplicated gene. J. Biol. Chem. 266, 15377–15383.

Hynes, R.O., Naba, A., 2012. Overview of the Matrisome—An Inventory of Extracellular Matrix Constituents and Functions. Cold Spring Harb Perspect Biol 4. https://doi.org/10.1101/cshperspect.a004903

Ignotz, R.A., Massagué, J., 1986. Transforming growth factor-beta stimulates the expression of fibronectin and collagen and their incorporation into the extracellular matrix. J. Biol. Chem. 261, 4337–4345.

Imazio, M., Gaita, F., 2015. Diagnosis and treatment of pericarditis. Heart heartjnl-2014-306362. https://doi.org/10.1136/heartjnl-2014-306362

Imazio, M., Gaita, F., LeWinter, M., 2015. Evaluation and Treatment of Pericarditis: A Systematic Review. JAMA 314, 1498–1506. https://doi.org/10.1001/jama.2015.12763

Inoki, I., Shiomi, T., Hashimoto, G., Enomoto, H., Nakamura, H., Makino, K., Ikeda, E., Takata, S., Kobayashi, K., Okada, Y., 2002. Connective tissue growth factor binds vascular endothelial growth factor (VEGF) and inhibits VEGF-induced angiogenesis. FASEB journal : official publication of the Federation of American Societies for Experimental Biology 16, 219–21. https://doi.org/10.1096/fj.01-0332fje

Inoue, K., Ikemura, A., Tsuruta, Y., Watanabe, K., Tsutsumiuchi, K., Hino, T., Oka, H., 2011. Quantification of N-acetyl-seryl-aspartyl-lysyl-proline in hemodialysis patients administered angiotensin-converting enzyme inhibitors by stable isotope dilution liquid chromatography-tandem mass spectrometry. J Pharm Biomed Anal 54, 765–771. https://doi.org/10.1016/j.jpba.2010.10.009

Ishihara, T., Ferrans, V.J., Jones, M., Boyce, S.W., Kawanami, O., Roberts, W.C., 1980. Histologic and ultrastructural features of normal human parietal pericardium. The American journal of cardiology 46, 744–753. https://doi.org/10.1016/0002-9149(80)90424-5

Isiguzo, G., Du Bruyn, E., Howlett, P., Ntsekhe, M., 2020. Diagnosis and Management of Tuberculous Pericarditis: What Is New? Curr Cardiol Rep 22, 2. https://doi.org/10.1007/s11886-020-1254-1

Iwamoto, N., Xano, H.J., Yoshioka, T., Shiraga, H., Nitta, K., Muraki, T., Ito, K., 2000. Acetyl-seryl-aspartyl-lysyl-proline is a novel natural cell cycle regulator of renal cells. Life Sciences 66, 221–226. https://doi.org/10.1016/S0024-3205(00)00460-4

Iwano, M., Plieth, D., Danoff, T.M., Xue, C., Okada, H., Neilson, E.G., 2002. Evidence that fibroblasts derive from epithelium during tissue fibrosis. Journal of Clinical Investigation 110, 341–350. https://doi.org/10.1172/JCI15518

Jaspard, E., Wei, L., Alhenc-Gelas, F., 1993. Differences in the properties and enzymatic specificities of the two active sites of angiotensin I-converting enzyme (kininase II). Studies with bradykinin and other natural peptides. Journal of Biological Chemistry 268, 9496–9503.

Jiang, C., Liu, G., Luckhardt, T., Antony, V., Zhou, Y., Carter, A.B., Thannickal, V.J., Liu, R.-M., 2017. Serpine 1 induces alveolar type II cell senescence through activating p53-p21-Rb pathway in fibrotic lung disease. Aging Cell 16, 1114–1124. https://doi.org/10.1111/acel.12643

Jonsson, J.R., Clouston, A.D., Ando, Y., Kelemen, L.I., Horn, M.J., Adamson, M.D., Purdie, D.M., Powell, E.E., 2001. Angiotensin-converting enzyme inhibition attenuates the progression of rat hepatic fibrosis. Gastroenterology 121, 148–155.

Jung, K.Y., Chen, K., Kretzler, M., Wu, C., 2007. TGF-β1 Regulates the PINCH-1–Integrin-Linked Kinase–α-Parvin Complex in Glomerular Cells. Journal of the American Society of Nephrology 18, 66–73.

Junot, C., Gonzales, M.F., Ezan, E., Cotton, J., Vazeux, G., Michaud, A., Azizi, M., Vassiliou, S., Yiotakis, A., Corvol, P., others, 2001. RXP 407, a selective inhibitor of the N-domain of angiotensin I-converting enzyme, blocks in vivo the degradation of hemoregulatory peptide acetyl-Ser-Asp-Lys-Pro with no effect on angiotensin I hydrolysis. Journal of Pharmacology and Experimental Therapeutics 297, 606–611.

Kalluri, R., Neilson, E.G., 2003. Epithelial-mesenchymal transition and its implications for fibrosis. The Journal of clinical investigation 112, 1776–1784.

Kanasaki, K., Haneda, M., Sugimoto, T., Shibuya, K., Isono, M., Isshiki, K., Araki, S., Uzu, T., Kashiwagi, A., Koya, D., 2006. N-acetyl-seryl-aspartyl-lysyl-proline inhibits DNA synthesis in human mesangial cells via up-regulation of cell cycle modulators. Biochem. Biophys. Res. Commun. 342, 758–765. https://doi.org/10.1016/j.bbrc.2006.02.019

Kanasaki, K., Koya, D., Sugimoto, T., Isono, M., Kashiwagi, A., Haneda, M., 2003. N-Acetyl-Seryl-Aspartyl-Lysyl-Proline Inhibits TGF-β–Mediated Plasminogen Activator Inhibitor-1 Expression via Inhibition of Smad Pathway in Human Mesangial Cells. JASN 14, 863–872. https://doi.org/10.1097/01.ASN.0000057544.95569.EC

Karatolios, K., Moosdorf, R., Maisch, B., Pankuweit, S., 2012. Cytokines in Pericardial Effusion of Patients with Inflammatory Pericardial Disease. Mediators of Inflammation 2012, e382082. https://doi.org/10.1155/2012/382082

Kaschina, E., Unger, T., 2003. Angiotensin AT1/AT2 receptors: regulation, signalling and function. Blood pressure 12, 70–88.

Kavian, N., Servettaz, A., Weill, B., Batteux, F., 2012. New Insights into the Mechanism of Notch Signalling in Fibrosis. Open Rheumatol J 6, 96–102. https://doi.org/10.2174/1874312901206010096

Kavvadas, P., Kypreou, K.P., Protopapadakis, E., Prodromidi, E., Sideras, P., Charonis, A.S., 2010. Integrin-linked kinase (ILK) in pulmonary fibrosis. Virchows Arch 457, 563–575. https://doi.org/10.1007/s00428-010-0976-7

Kendall, R.T., Feghali-Bostwick, C.A., 2014. Fibroblasts in fibrosis: novel roles and mediators. Frontiers in pharmacology 5, 123.

Kim, H., Lee, J., Hyun, J.W., Park, J.W., Joo, H., Shin, T., 2007. Expression and immunohistochemical localization of galectin-3 in various mouse tissues. Cell Biol. Int. 31, 655–662. https://doi.org/10.1016/j.cellbi.2006.11.036

Kim, S.M., Kim, N., Lee, S., Kim, D.K., Lee, Y.M., Ahn, S.H., Song, J.H., Choi, B.K., Wu, C., Jung, K.Y., 2007. TGF-β1-induced PINCH-1-ILK-α-parvin complex formation regulates mesangial cell proliferation and hypertrophy. Experimental & Molecular Medicine 39, 514–523. https://doi.org/10.1038/emm.2007.57

Kim, Y.S., Kim, T.H., Jeon, D.S., Lee, S.E., Yoon, S.H., Yeo, H.J., 2018. Diagnostic performance of interferon-gamma release assay for tuberculous pericarditis: A systematic review and

meta-analysis. European Respiratory Journal 52. https://doi.org/10.1183/13993003.congress-2018.PA2761

Kissin, E.Y., Lemaire, R., Korn, J.H., Lafyatis, R., 2002. Transforming growth factor β induces fibroblast fibrillin-1 matrix formation. Arthritis & Rheumatism 46, 3000–3009. https://doi.org/10.1002/art.10621

Kivirikko, K.I., Laitinen, O., Prockop, D.J., 1967. Modifications of a specific assay for hydroxyproline in urine. Analytical Biochemistry 19, 249–255. https://doi.org/10.1016/0003-2697(67)90160-1

Kohlstedt, K., Brandes, R.P., Müller-Esterl, W., Busse, R., Fleming, I., 2004. Angiotensin-converting enzyme is involved in outside-in signaling in endothelial cells. Circulation research 94, 60–67.

Kohlstedt, K., Busse, R., Fleming, I., 2005. Signaling via the Angiotensin-Converting Enzyme Enhances the Expression of Cyclooxygenase-2 in Endothelial Cells. Hypertension 45, 126–132. https://doi.org/10.1161/01.HYP.0000150159.48992.11

Kohlstedt, K., Gershome, C., Friedrich, M., Muller-Esterl, W., Alhenc-Gelas, F., Busse, R., Fleming, I., 2006. Angiotensin-Converting Enzyme (ACE) Dimerization Is the Initial Step in the ACE Inhibitor-Induced ACE Signaling Cascade in Endothelial Cells. Mol Pharmacol 69, 1725–1732. https://doi.org/10.1124/mol.105.020636

Kohlstedt, K., Shoghi, F., Müller-Esterl, W., Busse, R., Fleming, I., 2002. CK2 Phosphorylates the Angiotensin-Converting Enzyme and Regulates Its Retention in the Endothelial Cell Plasma Membrane. Circulation Research 91, 749–756. https://doi.org/10.1161/01.RES.0000038114.17939.C8

Kuiper, E.J., Nieuwenhoven, F.A.V., Smet, M.D. de, Meurs, J.C. van, Tanck, M.W., Oliver, N., Klaassen, I., Noorden, C.J.F.V., Goldschmeding, R., Schlingemann, R.O., 2008. The Angio-Fibrotic Switch of VEGF and CTGF in Proliferative Diabetic Retinopathy. PLOS ONE 3, e2675. https://doi.org/10.1371/journal.pone.0002675

Kulkarni, A.B., Huh, C.G., Becker, D., Geiser, A., Lyght, M., Flanders, K.C., Roberts, A.B., Sporn, M.B., Ward, J.M., Karlsson, S., 1993. Transforming growth factor beta 1 null mutation in mice causes excessive inflammatory response and early death. Proc. Natl. Acad. Sci. U.S.A. 90, 770–774.

Kulkarni, A.B., Ward, J.M., Yaswen, L., Mackall, C.L., Bauer, S.R., Huh, C.G., Gress, R.E., Karlsson, S., 1995. Transforming growth factor-beta 1 null mice. An animal model for inflammatory disorders. Am. J. Pathol. 146, 264–275.

Kulkarni, S.P., Alexander, K.P., Lytle, B., Heiss, G., Peterson, E.D., 2006. Long-term adherence with cardiovascular drug regimens. American Heart Journal 151, 185–191. https://doi.org/10.1016/j.ahj.2005.02.038

Kumar, N., Nakagawa, P., Janic, B., Romero, C.A., Worou, M.E., Peterson, E.L., Ongeri, E.E., Niyitegeka, J.-M.V., Rhaleb, N.-E., Carretero, O.A., 2016. The Anti-Inflammatory Peptide Ac-SDKP is Released from Thymosin β4 by Meprin α and Prolyl Oligopeptidase. The FASEB Journal 30, 969–16.

Kumar, N., Yin, C., 2018. The anti-inflammatory peptide Ac-SDKP: Synthesis, Role in ACE inhibition, and its therapeutic potential in hypertension and cardiovascular diseases. Pharmacological research.

Kumar, S., Lesch, M., 1980. Pericarditis in renal disease. Progress in Cardiovascular Diseases, Current Concepts in Cerebrovascular Disease. I 22, 357–369. https://doi.org/10.1016/0033-0620(80)90028-6

Kuno, A., Yamada, T., Masuda, K., Ogawa, K., Sogawa, M., Nakamura, S., Nakazawa, T., Ohara, H., Nomura, T., Joh, T., others, 2003. Angiotensin-converting enzyme inhibitor attenuates pancreatic inflammation and fibrosis in male Wistar Bonn/Kobori rats. Gastroenterology 124, 1010–1019.

Laemmli, U.K., 1970. Cleavage of structural proteins during the assembly of the head of bacteriophage T4. nature 227, 680–685.

Lai, P.F.H., Courtman, D.W., Stewart, D.J., 2005. NO to Small Mothers Against Decapentaplegic (Smad). Circulation Research 97, 1087–1089. https://doi.org/10.1161/01.RES.0000194559.35790.c5

Lambova, S., 2014. Cardiac manifestations in systemic sclerosis. World journal of cardiology 6, 993. https://doi.org/10.4330/wjc.v6.i9.993

Laverman, G.D., Navis, G., Henning, R.H., De Jong, P.E., De Zeeuw, D., 2002. Dual renin-angiotensin system blockade at optimal doses for proteinuria. Kidney International 62, 1020–1025. https://doi.org/10.1046/j.1523-1755.2002.00536.x

Leask, A., 2010. Potential Therapeutic Targets for Cardiac Fibrosis TGFβ, Angiotensin, Endothelin, CCN2, and PDGF, Partners in Fibroblast Activation. Circulation Research 106, 1675–1680. https://doi.org/10.1161/CIRCRESAHA.110.217737

Leffler, H., Carlsson, S., Hedlund, M., Qian, Y., Poirier, F., 2002. Introduction to galectins. Glycoconj J 19, 433–440. https://doi.org/10.1023/B:GLYC.0000014072.34840.04

Lenfant, M., Grillon, C., Rieger, K.-J., Sotty, D., Wdzieczak-Bakala, J., 1991. Formation of Acetyl-Ser-Asp-Lys-Pro, a New Regulator of the Hematopoietic System, through Enzymatic Processing of Thymosin β4a. Annals of the New York Academy of Sciences 628, 115–125. https://doi.org/10.1111/j.1749-6632.1991.tb17229.x

Lenfant, M., Wdzieczak-Bakala, J., Guittet, E., Prome, J.C., Sotty, D., Frindel, E., 1989. Inhibitor of hematopoietic pluripotent stem cell proliferation: purification and determination of its structure. PNAS 86, 779–782.

Li, J., Shi, S., Srivastava, S.P., Kitada, M., Nagai, T., Nitta, K., Kohno, M., Kanasaki, K., Koya, D., 2017. FGFR1 is critical for the anti-endothelial mesenchymal transition effect of N-acetyl-seryl-aspartyl-lysyl-proline via induction of the MAP4K4 pathway. Cell Death Dis 8, e2965. https://doi.org/10.1038/cddis.2017.353

Li, L., Li, J., Gao, J., 2014. Functions of Galectin-3 and Its Role in Fibrotic Diseases. J Pharmacol Exp Ther 351, 336–343. https://doi.org/10.1124/jpet.114.218370

Li, M., Yuan, Y., Guo, K., Lao, Y., Huang, X., Feng, L., 2020. Value of Galectin-3 in Acute Myocardial Infarction. Am J Cardiovasc Drugs 20, 333–342. https://doi.org/10.1007/s40256-019-00387-9

Lijnen, H.R., 2005. Pleiotropic functions of plasminogen activator inhibitor-1. Journal of Thrombosis and Haemostasis 3, 35–45. https://doi.org/10.1111/j.1538-7836.2004.00827.x

Lijnen, P.J., Petrov, V.V., Fagard, R.H., 2004. Collagen production in cardiac fibroblasts during inhibition of angiotensin converting enzyme and aminopeptidases. American Journal of Hypertension 17, S156–S157. https://doi.org/10.1016/j.amjhyper.2004.03.410

Lin, C.-X., Rhaleb, N.-E., Yang, X.-P., Liao, T.-D., D'Ambrosio, M.A., Carretero, O.A., 2008. Prevention of aortic fibrosis by N-acetyl-seryl-aspartyl-lysyl-proline in angiotensin II-induced hypertension. Am J Physiol Heart Circ Physiol 295, H1253–H1261. https://doi.org/10.1152/ajpheart.00481.2008

Lindsay, J., Crawley, I.S., Callaway, G.M., 1970. Chronic constrictive pericarditis following uremic hemopericardium. Am. Heart J. 79, 390–395. https://doi.org/10.1016/0002-8703(70)90426-6

Little, W.C., Freeman, G.L., 2006. Pericardial Disease. Circulation 113, 1622–1632. https://doi.org/10.1161/CIRCULATIONAHA.105.561514

Liu, F.-T., Patterson, R.J., Wang, J.L., 2002. Intracellular functions of galectins. Biochimica et Biophysica Acta (BBA) - General Subjects, Animal Lectins 1572, 263–273. https://doi.org/10.1016/S0304-4165(02)00313-6

Liu, X., Tan, M., Gong, D., Han, L., Lu, F., Huang, S., Xu, Z., 2012. Characteristics of pericardial interstitial cells and their implications in pericardial fibrocalcification. Journal of Molecular and Cellular Cardiology 53, 780–789. https://doi.org/10.1016/j.yjmcc.2012.09.008

Lok, D.J., Van Der Meer, P., de la Porte, P.W.B.-A., Lipsic, E., Van Wijngaarden, J., Hillege, H.L., van Veldhuisen, D.J., 2010. Prognostic value of galectin-3, a novel marker of fibrosis, in patients with chronic heart failure: data from the DEAL-HF study. Clinical research in cardiology 99, 323–328.

Lok, D.J.A., Van Der Meer, P., de la Porte, P.W.B.-A., Lipsic, E., Van Wijngaarden, J., Hillege, H.L., van Veldhuisen, D.J., 2010. Prognostic value of galectin-3, a novel marker of fibrosis, in patients with chronic heart failure: data from the DEAL-HF study. Clin Res Cardiol 99, 323–328. https://doi.org/10.1007/s00392-010-0125-y

Low, T.L., Goldstein, A.L., 1982. Chemical characterization of thymosin beta 4. J. Biol. Chem. 257, 1000–1006.

Low, T.L., Hu, S.K., Goldstein, A.L., 1981. Complete amino acid sequence of bovine thymosin beta 4: a thymic hormone that induces terminal deoxynucleotidyl transferase activity in thymocyte populations. PNAS 78, 1162–1166.

Ma, X., Yuan, Y., Zhang, Z., Zhang, Y., Li, M., 2014. An analog of Ac-SDKP improves heart functions after myocardial infarction by suppressing alternative activation (M2) of macrophages. International journal of cardiology 175, 376–378.

MacLean, B., Tomazela, D.M., Shulman, N., Chambers, M., Finney, G.L., Frewen, B., Kern, R., Tabb, D.L., Liebler, D.C., MacCoss, M.J., 2010. Skyline: an open source document editor for creating and analyzing targeted proteomics experiments. Bioinformatics 26, 966–968.

Maere, S., Heymans, K., Kuiper, M., 2005. BiNGO: a Cytoscape plugin to assess overrepresentation of gene ontology categories in biological networks. Bioinformatics 21, 3448–3449. https://doi.org/10.1093/bioinformatics/bti551

Maisch, B., Maisch, S., Kochsiek, K., 1982. Immune reactions in tuberculous and chronic constrictive pericarditis: Clinical data and diagnostic significance of antimyocardial

antibodies. The American Journal of Cardiology, Symposium on Verapamil Therapy for Angina Pectoris: Part III 50, 1007–1013. https://doi.org/10.1016/0002-9149(82)90409-X

Maisch, B., Seferović, P.M., Ristić, A.D., Erbel, R., Rienmüller, R., Adler, Y., Tomkowski, W.Z., Thiene, G., Yacoub, M.H., Priori, S.G., Garcia, A., Angeles, M., Blanc, J.-J., Budaj, A., Cowie, M., Dean, V., Deckers, J., Fernandez Burgos, E., Lekakis, J., Lindahl, B., Mazzotta, G., Moraies, J., Oto, A., Smiseth, O.A., Mazzotta, G., Acar, J., Arbustini, E., Becker, A.E., Chiaranda, G., Hasin, Y., Jenni, R., Klein, W., Lang, I., Lüscher, T.F., Pinto, F.J., Shabetai, R., Simoons, M.L., Soler Soler, J., Spodick, D.H., 2004. Guidelines on the Diagnosis and Management of Pericardial Diseases Executive SummaryThe Task Force on the Diagnosis and Management of Pericardial Diseases of the European Society of Cardiology. Eur Heart J 25, 587–610. https://doi.org/10.1016/j.ehj.2004.02.002

Mann, M., Ong, S.-E., Grønborg, M., Steen, H., Jensen, O.N., Pandey, A., 2002. Analysis of protein phosphorylation using mass spectrometry: deciphering the phosphoproteome. Trends in biotechnology 20, 261–268.

Mannherz, H.G., Hannappel, E., 2009. The β-thymosins: Intracellular and extracellular activities of a versatile actin binding protein family. Cell motility and the cytoskeleton 66, 839–851.

Masaki, T., 2004. Historical review: Endothelin. Trends in Pharmacological Sciences 25, 219–224. https://doi.org/10.1016/j.tips.2004.02.008

Massa, S.M., Cooper, D.N., Leffler, H., Barondes, S.H., 1993. L-29, an endogenous lectin, binds to glycoconjugate ligands with positive cooperativity. Biochemistry 32, 260–267. https://doi.org/10.1021/bi00052a033

Massague, J., Attisano, L., Wrana, J.L., 1994. The TGF-β family and its composite receptors. Trends in cell biology 4, 172–178.

Massagué, J., Blain, S.W., Lo, R.S., 2000. TGFβ signaling in growth control, cancer, and heritable disorders. Cell 103, 295–309.

Masuyer, G., Douglas, R.G., Sturrock, E.D., Acharya, K.R., 2015. Structural basis of Ac-SDKP hydrolysis by Angiotensin-I converting enzyme. Scientific reports 5, 13742.

Matozaki, T., Murata, Y., Saito, Y., Okazawa, H., Ohnishi, H., 2009. Protein tyrosine phosphatase SHP-2: a proto-oncogene product that promotes Ras activation. Cancer Sci. 100, 1786–1793. https://doi.org/10.1111/j.1349-7006.2009.01257.x

Matsuyama, K., Matsumoto, M., Sugita, T., Nishizawa, J., Yoshioka, T., Tokuda, Y., Ueda, Y., 2001. Clinical characteristics of patients with constrictive pericarditis after coronary bypass surgery. Jpn. Circ. J. 65, 480–482. https://doi.org/10.1253/jcj.65.480

Matthews, K., Deffur, A., Ntsekhe, M., Syed, F., Russell, J.B.W., Tibazarwa, K., Wolske, J., Brink, J., Mayosi, B.M., Wilkinson, R.J., Wilkinson, K.A., 2015. A Compartmentalized Profibrotic Immune Response Characterizes Pericardial Tuberculosis, Irrespective of HIV-1 Infection. Am J Respir Crit Care Med 192, 1518–1521. https://doi.org/10.1164/rccm.201504-0683LE

Mayosi, B.M., Burgess, L.J., Doubell, A.F., 2005. Tuberculous Pericarditis. Circulation 112, 3608–3616. https://doi.org/10.1161/CIRCULATIONAHA.105.543066

Mayosi, B.M., Ntsekhe, M., Bosch, J., Pandie, S., Jung, H., Gumedze, F., Pogue, J., Thabane, L., Smieja, M., Francis, V., Joldersma, L., Thomas, K.M., Thomas, B., Awotedu, A.A.,

Magula, N.P., Naidoo, D.P., Damasceno, A., Chitsa Banda, A., Brown, B., Manga, P., Kirenga, B., Mondo, C., Mntla, P., Tsitsi, J.M., Peters, F., Essop, M.R., Russell, J.B.W., Hakim, J., Matenga, J., Barasa, A.F., Sani, M.U., Olunuga, T., Ogah, O., Ansa, V., Aje, A., Danbauchi, S., Ojji, D., Yusuf, S., 2014. Prednisolone and Mycobacterium indicus pranii in Tuberculous Pericarditis. New England Journal of Medicine 371, 1121–1130. https://doi.org/10.1056/NEJMoa1407380

Mayosi, B.M., Wiysonge, C.S., Ntsekhe, M., Gumedze, F., Volmink, J.A., Maartens, G., Aje, A., Thomas, B.M., Thomas, K.M., Awotedu, A.A., Thembela, B., Mntla, P., Maritz, F., Blackett, K.N., Nkouonlack, D.C., Burch, V.C., Rebe, K., Parish, A., Sliwa, K., Vezi, B.Z., Alam, N., Brown, B.G., Gould, T., Visser, T., Magula, N., Commerford, P.J., 2008. Mortality in patients treated for tuberculous pericarditis in sub-Saharan Africa. South African Medical Journal 98, 36–40.

McLachlin, D.T., Chait, B.T., 2001. Analysis of phosphorylated proteins and peptides by mass spectrometry. Current opinion in chemical biology 5, 591–602.

McMurray, J.J.V., Ostergren, J., Swedberg, K., Granger, C.B., Held, P., Michelson, E.L., Olofsson, B., Yusuf, S., Pfeffer, M.A., CHARM Investigators and Committees, 2003. Effects of candesartan in patients with chronic heart failure and reduced left-ventricular systolic function taking angiotensin-converting-enzyme inhibitors: the CHARM-Added trial. Lancet 362, 767–771. https://doi.org/10.1016/S0140-6736(03)14283-3

Mehta, J.B., Chierico, G.C., Berk, S.H., Berk, S.L., 1990. Effect of Antituberculosis Therapy on Angiotensin-Converting Enzyme Levels in Tuberculosis Patients. Lab Med 21, 223–225. https://doi.org/10.1093/labmed/21.4.223

Mesulam, M.-M., 1978. Tetramethyl benzidine for horseradish peroxidase neurohistochemistry: a non-carcinogenic blue reaction product with superior sensitivity for visualizing neural afferents and efferents. Journal of Histochemistry & Cytochemistry 26, 106–117.

Michalski, A., Damoc, E., Hauschild, J.-P., Lange, O., Wieghaus, A., Makarov, A., Nagaraj, N., Cox, J., Mann, M., Horning, S., 2011. Mass Spectrometry-based Proteomics Using Q Exactive, a High-performance Benchtop Quadrupole Orbitrap Mass Spectrometer. Molecular & Cellular Proteomics 10, M111.011015. https://doi.org/10.1074/mcp.M111.011015

Miyazono, K., 2000. Positive and negative regulation of TGF-beta signaling. Journal of cell science 113, 1101–1109.

Morales, M.G., Cabrera, D., Céspedes, C., Vio, C.P., Vazquez, Y., Brandan, E., Cabello-Verrugio, C., 2013. Inhibition of the angiotensin-converting enzyme decreases skeletal muscle fibrosis in dystrophic mice by a diminution in the expression and activity of connective tissue growth factor (CTGF/CCN-2). Cell and tissue research 353, 173–187.

Moriya, Y., Niki, T., Yamada, T., Matsuno, Y., Kondo, H., Hirohashi, S., 2001. Increased expression of laminin-5 and its prognostic significance in lung adenocarcinomas of small size. Cancer 91, 1129–1141. https://doi.org/10.1002/1097-0142(20010315)91:6<1129::AID-CNCR1109>3.0.CO;2-C

Morris, S., Ahmad, N., André, S., Kaltner, H., Gabius, H.-J., Brenowitz, M., Brewer, F., 2004. Quaternary solution structures of galectins-1, -3, and -7. Glycobiology 14, 293–300. https://doi.org/10.1093/glycob/cwh029

Morrissey, J.J., Ishidoya, S., McCracken, R., Klahr, S., 1996. The effect of ACE inhibitors on the expression of matrix genes and the role of p53 and p21 (WAF1) in experimental renal fibrosis. Kidney international. Supplement 54, S83–7.

Morton, D.L., Glancy, D.L., Joseph, W.L., Adkins, P.C., 1973. Management of patients with radiation-induced pericarditis with effusion: A note on the development of aortic regurgitation in two of them. Chest 64, 291–297. https://doi.org/10.1378/chest.64.3.291

Moskowitz, D.W., 2002. Is "Somatic" Angiotensin I-Converting Enzyme a Mechanosensor? Diabetes Technology & Therapeutics 4, 841–858. https://doi.org/10.1089/152091502321118847

Moustakas, A., Pardali, K., Gaal, A., Heldin, C.-H., 2002. Mechanisms of TGF-β signaling in regulation of cell growth and differentiation. Immunology letters 82, 85–91.

Moustakas, A., Souchelnytskyi, S., Heldin, C.H., 2001. Smad regulation in TGF-beta signal transduction. J. Cell. Sci. 114, 4359–4369.

Mukherjee, D., Nissen, S., 2001. RIsk of cardiovascular events associated with selective cox-2 inhibitors. JAMA 286, 954–959. https://doi.org/10.1001/jama.286.8.954

Mutsaers, S.E., 2002. Mesothelial cells: Their structure, function and role in serosal repair. Respirology 7, 171–191. https://doi.org/10.1046/j.1440-1843.2002.00404.x

Mutsaers, S.E., Birnie, K., Lansley, S., Herrick, S.E., Lim, C.-B., Prêle, C.M., 2015. Mesothelial cells in tissue repair and fibrosis. Front Pharmacol 6. https://doi.org/10.3389/fphar.2015.00113

Mutyaba, A.K., Ntsekhe, M., 2017. Tuberculosis and the Heart. Cardiol Clin 35, 135–144. https://doi.org/10.1016/j.ccl.2016.08.007

Myers, R.B., Spodick, D.H., 1999. Constrictive pericarditis: clinical and pathophysiologic characteristics. Am. Heart J. 138, 219–232. https://doi.org/10.1016/S0002-8703(99)70105-5

Myöhänen, T.T., Pyykkö, E., Männistö, P.T., Carpen, O., 2012. Distribution of prolyl oligopeptidase in human peripheral tissues and in ovarian and colorectal tumors. Journal of Histochemistry & Cytochemistry 60, 706–715.

Naicker, K., Ntsekhe, M., 2020. Tuberculous pericardial disease: a focused update on diagnosis, therapy and prevention of complications. Cardiovasc Diagn Ther 10, 289–295. https://doi.org/10.21037/cdt.2019.09.20

Nakagawa, P., Romero, C.A., Jiang, X., D'Ambrosio, M., Bordcoch, G., Peterson, E.L., Harding, P., Yang, X.-P., Carretero, O.A., 2018. Ac-SDKP decreases mortality and cardiac rupture after acute myocardial infarction. PloS one 13, e0190300.

Namba, M., Nishitani, K., Kimoto, T., 1980. Characteristics of WI-38 cells (WI-38 CT-1) transformed by treatment with Co-60 gamma rays. Gann = Gan 71, 300–7.

Namsolleck, P., Recarti, C., Foulquier, S., Steckelings, U.M., Unger, T., 2014. AT(2) receptor and tissue injury: therapeutic implications. Curr. Hypertens. Rep. 16, 416. https://doi.org/10.1007/s11906-013-0416-6

Napolitano, G., Pressacco, J., Paquet, E., 2009. Imaging features of constrictive pericarditis: beyond pericardial thickening. Can Assoc Radiol J 60, 40–46. https://doi.org/10.1016/j.carj.2009.02.034

Nemir, M., Metrich, M., Plaisance, I., Lepore, M., Cruchet, S., Berthonneche, C., Sarre, A., Radtke, F., Pedrazzini, T., 2014. The Notch pathway controls fibrotic and regenerative repair in the adult heart. Eur Heart J 35, 2174–2185. https://doi.org/10.1093/eurheartj/ehs269

Newlaczyl, A.U., Yu, L.-G., 2011. Galectin-3 – A jack-of-all-trades in cancer. Cancer Letters 313, 123–128. https://doi.org/10.1016/j.canlet.2011.09.003

Noubiap, J.J., Agbor, V.N., Ndoadoumgue, A.L., Nkeck, J.R., Kamguia, A., Nyaga, U.F., Ntsekhe, M., 2019. Epidemiology of pericardial diseases in Africa: a systematic scoping review. Heart 105, 180–188. https://doi.org/10.1136/heartjnl-2018-313922

Nozaki, Y., Sato, N., Iida, T., Hara, K., Fukuyama, K., Epstein, W.L., 1992. Prolyl endopeptidase purified from granulomatous inflammation in mice. Journal of Cellular Biochemistry 49, 296–303. https://doi.org/10.1002/jcb.240490313

Ntsekhe, M., Matthews, K., Syed, F.F., Deffur, A., Badri, M., Commerford, P.J., Gersh, B.J., Wilkinson, K.A., Wilkinson, R.J., Mayosi, B.M., 2013. Prevalence, Hemodynamics, and Cytokine Profile of Effusive-Constrictive Pericarditis in Patients with Tuberculous Pericardial Effusion. PLoS ONE 8, e77532. https://doi.org/10.1371/journal.pone.0077532

Ntsekhe, M., Matthews, K., Wolske, J., Badri, M., Wilkinson, K.A., Wilkinson, R.J., Sturrock, E.D., Mayosi, B.M., 2012. Scientific letter: Ac-SDKP (N-acetyl-seryl-aspartyl-lysyl-proline) and Galectin-3 levels in tuberculous pericardial effusion: implications for pathogenesis and prevention of pericardial constriction. Heart 98, 1326–1328. https://doi.org/10.1136/heartjnl-2012-302196

Ntsekhe, M., Mayosi, B.M., 2012. Tuberculous pericarditis with and without HIV. Heart Failure Reviews 1–7. https://doi.org/10.1007/s10741-012-9310-6

Ochieng, J., Furtak, V., Lukyanov, P., 2002. Extracellular functions of galectin-3. Glycoconj J 19, 527–535. https://doi.org/10.1023/B:GLYC.0000014082.99675.2f

Oikawa, T., Freeman, M., Lo, W., Vaughan, D.E., Fogo, A., 1997. Modulation of plasminogen activator inhibitor-1 in vivo: A new mechanism for the anti-fibrotic effect of renin-angiotensin inhibition. Kidney International 51, 164–172. https://doi.org/10.1038/ki.1997.20

Olivieri, J., Smaldone, S., Ramirez, F., 2010. Fibrillin assemblies: extracellular determinants of tissue formation and fibrosis. Fibrogenesis Tissue Repair 3, 24. https://doi.org/10.1186/1755-1536-3-24

Pagès, G., Lenormand, P., L'Allemain, G., Chambard, J.C., Meloche, S., Pouysségur, J., 1993. Mitogen-activated protein kinases p42mapk and p44mapk are required for fibroblast proliferation. PNAS 90, 8319–8323.

Pandie, S., Peter, J.G., Kerbelker, Z.S., Meldau, R., Theron, G., Govender, U., Ntsekhe, M., Dheda, K., Mayosi, B.M., 2014. Diagnostic accuracy of quantitative PCR (Xpert MTB/RIF) for tuberculous pericarditis compared to adenosine deaminase and unstimulated interferon-γ in a high burden setting: a prospective study. BMC Medicine 12, 101. https://doi.org/10.1186/1741-7015-12-101

Pankuweit, S., Wädlich, A., Meyer, E., Portig, I., Hufnagel, G., Maisch, B., 2000. Cytokine activation in pericardial fluids in different forms of pericarditis. Herz 25, 748–754. https://doi.org/10.1007/PL00001993

Parameswaran, N., Patial, S., 2010. Tumor Necrosis Factor-α Signaling in Macrophages. Crit Rev Eukaryot Gene Expr 20, 87–103. https://doi.org/10.1615/CritRevEukarGeneExpr.v20.i2.10

Pasini, A.F., Garbin, U., Nava, M.C., Stranieri, C., Pellegrini, M., Boccioletti, V., Luchetta, M.L., Fabrizzi, P., Lo Cascio, V., Cominacini, L., 2007. Effect of sulfhydryl and non-sulfhydryl angiotensin-converting enzyme inhibitors on endothelial function in essential hypertensive patients. American journal of hypertension 20, 443–450.

Pawson, T., Scott, J.D., 2005. Protein phosphorylation in signaling – 50 years and counting. Trends in Biochemical Sciences 30, 286–290. https://doi.org/10.1016/j.tibs.2005.04.013

Peng, H., Carretero, O.A., Brigstock, D.R., Oja-Tebbe, N., Rhaleb, N.-E., 2003. Ac-SDKP Reverses Cardiac Fibrosis in Rats With Renovascular Hypertension. Hypertension 42, 1164–1170. https://doi.org/10.1161/01.HYP.0000100423.24330.96

Peng, H., Carretero, O.A., Liao, T.-D., Peterson, E.L., Rhaleb, N.-E., 2007. Role of N-Acetyl-Seryl-Aspartyl-Lysyl-Proline in the Antifibrotic and Anti-Inflammatory Effects of the Angiotensin-Converting Enzyme Inhibitor Captopril in Hypertension. Hypertension 49, 695–703. https://doi.org/10.1161/01.HYP.0000258406.66954.4f

Peng, H., Carretero, O.A., Peterson, E.L., Rhaleb, N.-E., 2010. Ac-SDKP inhibits transforming growth factor-β1-induced differentiation of human cardiac fibroblasts into myofibroblasts. Am J Physiol Heart Circ Physiol 298, H1357–H1364. https://doi.org/10.1152/ajpheart.00464.2009

Peng, H., Carretero, O.A., Peterson, E.L., Yang, X.-P., Santra, K., Rhaleb, N.-E., 2012. N-Acetyl-seryl-aspartyl-lysyl-proline inhibits ET-1-induced collagen production by preserving Src homology 2-containing protein tyrosine phosphatase-2 activity in cardiac fibroblasts. Pflugers Arch. 464, 415–423. https://doi.org/10.1007/s00424-012-1150-7

Peng, H., Carretero, O.A., Raij, L., Yang, F., Kapke, A., Rhaleb, N.E., 2001. Antifibrotic effects of N-acetyl-seryl-aspartyl-Lysyl-proline on the heart and kidney in aldosterone-salt hypertensive rats. Hypertension 37, 794–800.

Petersen, S.E., Aung, N., Sanghvi, M.M., Zemrak, F., Fung, K., Paiva, J.M., Francis, J.M., Khanji, M.Y., Lukaschuk, E., Lee, A.M., Carapella, V., Kim, Y.J., Leeson, P., Piechnik, S.K., Neubauer, S., 2017. Reference ranges for cardiac structure and function using cardiovascular magnetic resonance (CMR) in Caucasians from the UK Biobank population cohort. J Cardiovasc Magn Reson 19, 1–19. https://doi.org/10.1186/s12968-017-0327-9

Piersma, S.R., Knol, J.C., de Reus, I., Labots, M., Sampadi, B.K., Pham, T.V., Ishihama, Y., Verheul, H.M., Jimenez, C.R., 2015. Feasibility of label-free phosphoproteomics and application to base-line signaling of colorectal cancer cell lines. Journal of proteomics 127, 247–258.

Pilling, D., Vakil, V., Cox, N., Gomer, R.H., 2015. TNF-α–stimulated fibroblasts secrete lumican to promote fibrocyte differentiation. PNAS 112, 11929–11934. https://doi.org/10.1073/pnas.1507387112

Pokharel, S., Geel, P.P. van, Sharma, U.C., Cleutjens, J.P.M., Bohnemeier, H., Tian, X.-L., Schunkert, H., Crijns, H.J.G.M., Paul, M., Pinto, Y.M., 2004. Increased Myocardial Collagen Content in Transgenic Rats Overexpressing Cardiac Angiotensin-Converting Enzyme Is Related to Enhanced Breakdown of N-Acetyl-Ser-Asp-Lys-Pro and Increased

Phosphorylation of Smad2/3. Circulation 110, 3129–3135. https://doi.org/10.1161/01.CIR.0000147180.87553.79

Pokharel, S., Rasoul, S., Roks, A.J.M., Leeuwen, R.E.W. van, Luyn, M.J.A. van, Deelman, L.E., Smits, J.F., Carretero, O., Gilst, W.H. van, Pinto, Y.M., 2002. N-Acetyl-Ser-Asp-Lys-Pro Inhibits Phosphorylation of Smad2 in Cardiac Fibroblasts. Hypertension 40, 155–161. https://doi.org/10.1161/01.HYP.0000025880.56816.FA

Pradelles, P., Frobert, Y., Créminon, C., Ivonine, H., Frindel, E., 1991. Distribution of a negative regulator of haematopoietic stem cell proliferation (AcSDKP) and thymosin, β4 in mouse tissues. FEBS Letters 289, 171–175. https://doi.org/10.1016/0014-5793(91)81062-D

Pradelles, P., Frobert, Y., Créminon, C., Liozon, E., Massé, A., Frindel, E., 1990. Negative regulator of pluripotent hematopoietic stem cell proliferation in human white blood cells and plasma as analysed by enzyme immunoassay. Biochemical and Biophysical Research Communications 170, 986–993. https://doi.org/10.1016/0006-291X(90)90489-A

Qiu, P., Wheater, M.K., Qiu, Y., Sosne, G., 2011. Thymosin β4 inhibits TNF-α-induced NF-κB activation, IL-8 expression, and the sensitizing effects by its partners PINCH-1 and ILK. The FASEB Journal 25, 1815–1826. https://doi.org/10.1096/fj.10-167940

Reed, C.C., Iozzo, R.V., 2002. The role of decorin in collagen fibrillogenesis and skin homeostasis. Glycoconj J 19, 249–255. https://doi.org/10.1023/A:1025383913444

Reis, R.I., Nogueira, M.D., Campanha-Rodrigues, A.L., Pereira, L.M., Andrade, M.C.C., Parreiras-e-Silva, L.T., Costa-Neto, C.M., Mortara, R.A., Casarini, D.E., 2018. Regulation of Cell Signaling Pathways The binding of captopril to angiotensin I-converting enzyme triggers activation of signaling pathways.

Reuter, H., Burgess, L., Vuuren, W. van, Doubell, A., 2006. Diagnosing tuberculous pericarditis. QJM 99, 827–839. https://doi.org/10.1093/qjmed/hcl123

Reyman, T.A., 1969. Subacute constrictive uremic pericarditis. Am. J. Med. 46, 972–975. https://doi.org/10.1016/0002-9343(69)90098-9

Rhaleb, N.-E., Peng, H., Harding, P., Tayeh, M., LaPointe, M.C., Carretero, O.A., 2001a. Effect of N-acetyl-seryl-aspartyl-lysyl-proline on DNA and collagen synthesis in rat cardiac fibroblasts. Hypertension 37, 827–832.

Rhaleb, N.-E., Peng, H., Yang, X.-P., Liu, Y.-H., Mehta, D., Ezan, E., Carretero, O.A., 2001b. Long-Term Effect of N-Acetyl-Seryl-Aspartyl-Lysyl-Proline on Left Ventricular Collagen Deposition in Rats With 2-Kidney, 1-Clip Hypertension. Circulation 103, 3136–3141. https://doi.org/10.1161/01.CIR.103.25.3136

Rhaleb, N.-E., Pokharel, S., Sharma, U.C., Peng, H., Peterson, E., Harding, P., Yang, X.-P., Carretero, O.A., 2013. N-acetyl-Ser-Asp-Lys-Pro inhibits interleukin-1β-mediated matrix metalloproteinase activation in cardiac fibroblasts. Pflugers Arch - Eur J Physiol 465, 1487–1495. https://doi.org/10.1007/s00424-013-1262-8

Rieger, K.J., Saez-Servent, N., Papet, M.P., Wdzieczak-Bakala, J., Morgat, J.L., Thierry, J., Voelter, W., Lenfant, M., 1993. Involvement of human plasma angiotensin I-converting enzyme in the degradation of the haemoregulatory peptide N-acetyl-seryl-aspartyl-lysyl-proline. Biochemical Journal 296, 373.

Ristić, A.D., Pankuweit, S., Maksimović, R., Moosdorf, R., Maisch, B., 2013. Pericardial cytokines in neoplastic, autoreactive, and viral pericarditis. Heart Fail Rev 18, 345–353. https://doi.org/10.1007/s10741-012-9334-y

Roberts, W.C., 2005. Pericardial heart disease: its morphologic features and its causes. Proceedings (Baylor University. Medical Center) 18, 38. https://doi.org/10.1080/08998280.2005.11928030

Robinson, M.J., Cobb, M.H., 1997. Mitogen-activated protein kinase pathways. Current Opinion in Cell Biology 9, 180–186. https://doi.org/10.1016/S0955-0674(97)80061-0

Robinson, S., Lenfant, M., Wdzieczak-Bakala, J., Riches, A., 1993. The molecular specificity of action of the tetrapeptide acetyl-N-Ser-Asp-Lys-Pro (AcSDKP) in the control of hematopoietic stem cell proliferation. Stem Cells 11, 422–427. https://doi.org/10.1002/stem.5530110509

Rockey, D.C., Bell, P.D., Hill, J.A., 2015. Fibrosis — A Common Pathway to Organ Injury and Failure. New England Journal of Medicine 372, 1138–1149. https://doi.org/10.1056/NEJMra1300575

Rosenkranz, S., 2004. TGF-β1 and angiotensin networking in cardiac remodeling. Cardiovasc Res 63, 423–432. https://doi.org/10.1016/j.cardiores.2004.04.030

Rousseau-Plasse, A., Lenfant, M., Potier, P., 1996. Catabolism of the hemoregulatory peptide N-Acetyl-Ser-Asp-Lys-Pro: a new insight into the physiological role of the angiotensin-I-converting enzyme N-active site. Bioorganic & Medicinal Chemistry 4, 1113–1119. https://doi.org/10.1016/0968-0896(96)00104-6

Ruprecht, B., Koch, H., Domasinska, P., Frejno, M., Kuster, B., Lemeer, S., 2017. Optimized Enrichment of Phosphoproteomes by Fe-IMAC Column Chromatography, in: Comai, L., Katz, J.E., Mallick, P. (Eds.), Proteomics: Methods and Protocols, Methods in Molecular Biology. Springer New York, New York, NY, pp. 47–60. https://doi.org/10.1007/978-1-4939-6747-6_5

Ryan, U.S., Ryan, J.W., Whitaker, C., Chiu, A., 1976. Localization of angiotensin converting enzyme (kininase II). II. Immunocytochemistry and immunofluorescence. Tissue and Cell 8, 125–145. https://doi.org/10.1016/0040-8166(76)90025-2

Sagristà Sauleda, J., Permanyer Miralda, G., Soler Soler, J., 2005. Diagnosis and Management of Acute Pericardial Syndromes. Revista Española de Cardiología (English Edition) 58, 830–841. https://doi.org/10.1016/S1885-5857(06)60512-4

Sakai, L.Y., Keene, D.R., Engvall, E., 1986. Fibrillin, a new 350-kD glycoprotein, is a component of extracellular microfibrils. J. Cell Biol. 103, 2499–2509. https://doi.org/10.1083/jcb.103.6.2499

Sangaletti, S., Tripodo, C., Cappetti, B., Casalini, P., Chiodoni, C., Piconese, S., Santangelo, A., Parenza, M., Arioli, I., Miotti, S., Colombo, M.P., 2011. SPARC Oppositely Regulates Inflammation and Fibrosis in Bleomycin-Induced Lung Damage. Am J Pathol 179, 3000–3010. https://doi.org/10.1016/j.ajpath.2011.08.027

Sato, S., Hughes, R.C., 1994. Regulation of secretion and surface expression of Mac-2, a galactoside-binding protein of macrophages. J Biol Chem 269, 4424–4430.

Satoh, M., Nagasu, H., Morita, Y., Yamaguchi, T.P., Kanwar, Y.S., Kashihara, N., 2012. Klotho protects against mouse renal fibrosis by inhibiting Wnt signaling. American Journal of Physiology-Renal Physiology 303, F1641–F1651.

Sawada, T., Ishii, Y., Tojimbara, T., Nakajima, I., Fuchinoue, S., Teraoka, S., 2002. The ACE inhibitor, quinapril, ameliorates peritoneal fibrosis in an encapsulating peritoneal sclerosis model in mice. Pharmacological research 46, 505–510.

Schnee, J.M., Hsueh, W.A., 2000. Angiotensin II, adhesion, and cardiac fibrosis. Cardiovasc Res 46, 264–268. https://doi.org/10.1016/S0008-6363(00)00044-4

Schorb, W., Conrad, K.M., Singer, H.A., Dostal, D.E., Baker, K.M., 1995. Angiotensin II is a potent stimulator of MAP-kinase activity in neonatal rat cardiac fibroblasts. Journal of Molecular and Cellular Cardiology 27, 1151–1160. https://doi.org/10.1016/0022-2828(95)90051-9

Schwager, S.L., Carmona, A.K., Sturrock, E.D., 2006. A high-throughput fluorimetric assay for angiotensin I-converting enzyme. Nature Protocols 1, 1961–1964. https://doi.org/10.1038/nprot.2006.305

Schwefer, M., Aschenbach, R., Heidemann, J., Mey, C., Lapp, H., 2009. Constrictive pericarditis, still a diagnostic challenge: comprehensive review of clinical management. Eur J Cardiothorac Surg 36, 502–510. https://doi.org/10.1016/j.ejcts.2009.03.004

Seetharaman, J., Kanigsberg, A., Slaaby, R., Leffler, H., Barondes, S.H., Rini, J.M., 1998. X-ray Crystal Structure of the Human Galectin-3 Carbohydrate Recognition Domain at 2.1-Å Resolution. J. Biol. Chem. 273, 13047–13052. https://doi.org/10.1074/jbc.273.21.13047

Seo, H.T., Kim, Y.S., Ock, H.S., Kang, L.H., Byun, K.S., Jeon, D.S., Kim, S.J., 2020. Diagnostic performance of interferon-gamma release assay for diagnosis of tuberculous pericarditis: A meta-analysis. International Journal of Clinical Practice n/a, e13479. https://doi.org/10.1111/ijcp.13479

Sgalla, G., Flore, M., Siciliano, M., Richeldi, L., 2020. Antibody-based therapies for idiopathic pulmonary fibrosis. Expert Opinion on Biological Therapy 0, 1–8. https://doi.org/10.1080/14712598.2020.1735346

Shabetai, R., Fowler, N.O., Guntheroth, W.G., 1970. Symposium on Pericardial DiseasesThe hemodynamics of cardiac tamponade and constrictive pericarditis. The American Journal of Cardiology 26, 480–489. https://doi.org/10.1016/0002-9149(70)90706-X

Shabetai, R., Mangiardi, L., Bhargava, V., Ross, J., Higgins, C.B., 1979. The pericardium and cardiac function. Progress in Cardiovascular Diseases 22, 107–134. https://doi.org/10.1016/0033-0620(79)90017-3

Shalom-Feuerstein, R., Cooks, T., Raz, A., Kloog, Y., 2005. Galectin-3 Regulates a Molecular Switch from N-Ras to K-Ras Usage in Human Breast Carcinoma Cells. Cancer Res 65, 7292–7300. https://doi.org/10.1158/0008-5472.CAN-05-0775

Shannon, P., Markiel, A., Ozier, O., Baliga, N.S., Wang, J.T., Ramage, D., Amin, N., Schwikowski, B., Ideker, T., 2003. Cytoscape: A Software Environment for Integrated Models of Biomolecular Interaction Networks. Genome Res 13, 2498–2504. https://doi.org/10.1101/gr.1239303

Shenje, J., Ifeoma Adimora-Nweke, F., Ross, I.L., Ntsekhe, M., Wiesner, L., Deffur, A., McIlleron, H.M., Pasipanodya, J., Gumbo, T., Mayosi, B.M., 2015. Poor Penetration of Antibiotics Into Pericardium in Pericardial Tuberculosis. EBioMedicine 2, 1640–1649. https://doi.org/10.1016/j.ebiom.2015.09.025

Shevchenko, A., Wilm, M., Vorm, O., Mann, M., 1996. Mass spectrometric sequencing of proteins from silver-stained polyacrylamide gels. Analytical chemistry 68, 850–858.

Shibuya, K., Kanasaki, K., Isono, M., Sato, H., Omata, M., Sugimoto, T., Araki, S., Isshiki, K., Kashiwagi, A., Haneda, M., Koya, D., 2005. N-Acetyl-Seryl-Aspartyl-Lysyl-Proline Prevents Renal Insufficiency and Mesangial Matrix Expansion in Diabetic db/db Mice. Diabetes 54, 838–845. https://doi.org/10.2337/diabetes.54.3.838

Shull, M.M., Ormsby, I., Kier, A.B., Pawlowski, S., Diebold, R.J., Yin, M., Allen, R., Sidman, C., Proetzel, G., Calvin, D., 1992. Targeted disruption of the mouse transforming growth factor-beta 1 gene results in multifocal inflammatory disease. Nature 359, 693–699. https://doi.org/10.1038/359693a0

Simpson, R.J., Kalra, H., Mathivanan, S., 2012. ExoCarta as a resource for exosomal research. J Extracell Vesicles 1. https://doi.org/10.3402/jev.v1i0.18374

Singhal, P., Thavendiranathan, P., Butany, J., 2016. Chapter 16 - The Pericardium and Its Diseases, in: Buja, L.M., Butany, Jagdish (Eds.), Cardiovascular Pathology (Fourth Edition). Academic Press, San Diego, pp. 649–677. https://doi.org/10.1016/B978-0-12-420219-1.00015-X

Skeggs Jr, L.T., Kahn, J.R., Shumway, N.P., 1956. The preparation and function of the hypertensin-converting enzyme. The Journal of experimental medicine 103, 295–299.

Skeggs Jr, L.T., Marsh, W.H., Kahn, J.R., Shumway, N.P., 1954. The existence of two forms of hypertensin. The Journal of experimental medicine 99, 275–282.

Skidgel, R.A., Erdös, E.G., 1985. Novel activity of human angiotensin I converting enzyme: release of the NH2- and COOH-terminal tripeptides from the luteinizing hormone-releasing hormone. PNAS 82, 1025–1029.

Smets, P., Guettrot-Imbert, G., Hermet, M., Delevaux, I., Kemeny, J.-L., Aumaître, O., André, M., 2013. Péricardite récidivante : traquer le mésotheliome péricardique primitif. La Revue de Médecine Interne 34, 573–576. https://doi.org/10.1016/j.revmed.2013.04.021

Soderblom, E.J., Philipp, M., Thompson, J.W., Caron, M.G., Moseley, M.A., 2011. Quantitative label-free phosphoproteomics strategy for multifaceted experimental designs. Analytical chemistry 83, 3758–3764.

Song, M., Jang, H., Lee, J., Kim, J.H., Kim, S.H., Sun, K., Park, Y., 2014. Regeneration of chronic myocardial infarction by injectable hydrogels containing stem cell homing factor SDF-1 and angiogenic peptide Ac-SDKP. Biomaterials 35, 2436–2445.

Soubrier, F., Alhenc-Gelas, F., Hubert, C., Allegrini, J., John, M., Tregear, G., Corvol, P., 1988. Two putative active centers in human angiotensin I-converting enzyme revealed by molecular cloning. Proceedings of the National Academy of Sciences 85, 9386–9390.

Specks, U., Nerlich, A., Colby, T.V., Wiest, I., Timpl, R., 1995. Increased expression of type VI collagen in lung fibrosis. Am. J. Respir. Crit. Care Med. 151, 1956–1964. https://doi.org/10.1164/ajrccm.151.6.7767545

Spodick, D.H., 2003. Acute Pericarditis: Current Concepts and Practice. JAMA 289, 1150. https://doi.org/10.1001/jama.289.9.1150

Spodick, D.H., 1992. Macrophysiology, microphysiology, and anatomy of the pericardium: a synopsis. Am. Heart J. 124, 1046–1051. https://doi.org/10.1016/0002-8703(92)90990-D

Srichai, M.B., 2011. CMR Imaging in Constrictive Pericarditis: Is Seeing Believing? J Am Coll Cardiol Img 4, 1192–1194. https://doi.org/10.1016/j.jcmg.2011.09.009

Stanchi, F., Grashoff, C., Yonga, C.F.N., Grall, D., Fässler, R., Van Obberghen-Schilling, E., 2009. Molecular dissection of the ILK-PINCH-parvin triad reveals a fundamental role for the ILK kinase domain in the late stages of focal-adhesion maturation. Journal of cell science 122, 1800–1811.

Stastna, M., Van Eyk, J.E., 2012. Investigating the Secretome: Lessons About the Cells that Comprise the Heart. Circ Cardiovasc Genet 5, o8–o18. https://doi.org/10.1161/CIRCGENETICS.111.960187

Steckelings, U.M., Kloet, A. de, Sumners, C., 2017. Centrally Mediated Cardiovascular Actions of the Angiotensin II Type 2 Receptor. Trends Endocrinol. Metab. 28, 684–693. https://doi.org/10.1016/j.tem.2017.06.002

Steen, H., Jebanathirajah, J.A., Rush, J., Morrice, N., Kirschner, M.W., 2006. Phosphorylation Analysis by Mass Spectrometry: Myths, Facts, and the Consequences for Qualitative and Quantitative Measurements. Molecular & Cellular Proteomics 5, 172–181. https://doi.org/10.1074/mcp.M500135-MCP200

Sturrock, E.D., Natesh, R., Van Rooyen, J.M., Acharya, K.R., others, 2004. Structure of angiotensin I-converting enzyme. Cellular and molecular life sciences 61, 2677–2686.

Sugiura, T., Iwasaka, T., Takayama, Y., Matsutani, M., Hasegawa, T., Takahashi, N., Inada, M., 1990. Factors associated with pericardial effusion in acute Q wave myocardial infarction. Circulation 81, 477–481. https://doi.org/10.1161/01.CIR.81.2.477

Sun, X., Rentzsch, B., Gong, M., Eichhorst, J., Pankow, K., Papsdorf, G., Maul, B., Bader, M., Siems, W.E., 2010. Signal transduction in CHO cells stably transfected with domain-selective forms of murine ACE. Biological Chemistry 391, 235–244.

Sun, Y., Yang, F., Yan, J., Li, Q., Wei, Z., Feng, H., Wang, R., Zhang, L., Zhang, X., 2010. New anti-fibrotic mechanisms of n-acetyl-seryl-aspartyl-lysyl-proline in silicon dioxide-induced silicosis. Life Sci. 87, 232–239. https://doi.org/10.1016/j.lfs.2010.06.016

Supek, F., Bošnjak, M., Škunca, N., Šmuc, T., 2011. REVIGO Summarizes and Visualizes Long Lists of Gene Ontology Terms. PLOS ONE 6, e21800. https://doi.org/10.1371/journal.pone.0021800

Suwan, P.K., Potjalongsilp, S., 1995. Predictors of constrictive pericarditis after tuberculous pericarditis. Br Heart J 73, 187–189. https://doi.org/10.1136/hrt.73.2.187

Suzuki, Y., Ruiz-Ortega, M., Lorenzo, O., Ruperez, M., Esteban, V., Egido, J., 2003. Inflammation and angiotensin II. Int. J. Biochem. Cell Biol. 35, 881–900.

Syed, F.F., Mayosi, B.M., 2007. A Modern Approach to Tuberculous Pericarditis. Progress in Cardiovascular Diseases 50, 218–236. https://doi.org/10.1016/j.pcad.2007.03.002

Syed, F.F., Schaff, H.V., Oh, J.K., 2014. Constrictive pericarditis--a curable diastolic heart failure. Nat Rev Cardiol 11, 530–544. https://doi.org/10.1038/nrcardio.2014.100

Szklarczyk, D., Morris, J.H., Cook, H., Kuhn, M., Wyder, S., Simonovic, M., Santos, A., Doncheva, N.T., Roth, A., Bork, P., Jensen, L.J., von Mering, C., 2017. The STRING database in 2017:

quality-controlled protein–protein association networks, made broadly accessible. Nucleic Acids Res 45, D362–D368. https://doi.org/10.1093/nar/gkw937

Takeda, Y., Nishikimi, T., Akimoto, K., Matsuoka, H., Ishimitsu, T., 2010. Beneficial effects of a combination of Rho-kinase inhibitor and ACE inhibitor on tubulointerstitial fibrosis induced by unilateral ureteral obstruction. Hypertension Research 33, 965–973.

Taunk, N.K., Haffty, B.G., Kostis, J.B., Goyal, S., 2015. Radiation-induced heart disease: pathologic abnormalities and putative mechanisms. Front. Oncol. 5, 39. https://doi.org/10.3389/fonc.2015.00039

Thierry, J., Papet, M.P., Saez-Servent, N., Plissonneau-Haumont, J., Potier, P., Lenfant, M., 1990. Synthesis and activity of NAcSerAspLysPro analogues on cellular interactions between T-cell and erythrocytes in rosette formation. J. Med. Chem. 33, 2122–2127.

Thillai, M., Eberhardt, C., Lewin, A.M., Potiphar, L., Hingley-Wilson, S., Sridhar, S., Macintyre, J., Kon, O.M., Wickremasinghe, M., Wells, A., Weeks, M.E., Mitchell, D., Lalvani, A., 2012. Sarcoidosis and Tuberculosis Cytokine Profiles: Indistinguishable in Bronchoalveolar Lavage but Different in Blood. PLOS ONE 7, e38083. https://doi.org/10.1371/journal.pone.0038083

Thurber, D.L., Edwards, J.E., Achor, R.W.P., 1962. Secondary Malignant Tumors of the Pericardium. Circulation 26, 228–241. https://doi.org/10.1161/01.CIR.26.2.228

Timpl, R., 1989. Structure and biological activity of basement membrane proteins. Eur. J. Biochem. 180, 487–502. https://doi.org/10.1111/j.1432-1033.1989.tb14673.x

Tournier, C., Whitmarsh, A.J., Cavanagh, J., Barrett, T., Davis, R.J., 1997. Mitogen-activated protein kinase kinase 7 is an activator of the c-Jun NH2-terminal kinase. PNAS 94, 7337–7342.

Tran, D.Q., 2012. TGF-β: the sword, the wand, and the shield of FOXP3+ regulatory T cells. J Mol Cell Biol 4, 29–37. https://doi.org/10.1093/jmcb/mjr033

Trautner, B.W., Darouiche, R.O., 2001. Tuberculous Pericarditis: Optimal Diagnosis and Management. Clin Infect Dis. 33, 954–961. https://doi.org/10.1086/322621

Trautwein, C., Friedman, S.L., Schuppan, D., Pinzani, M., 2015. Hepatic fibrosis: Concept to treatment. Journal of Hepatology, Emerging Trends in Hepatology 62, S15–S24. https://doi.org/10.1016/j.jhep.2015.02.039

Trombetta-eSilva, J., Bradshaw, A.D., 2012. The Function of SPARC as a Mediator of Fibrosis. Open Rheumatol J 6, 146–155. https://doi.org/10.2174/1874312901206010146

Vincenti, M.P., Brinckerhoff, C.E., 2001. Transcriptional regulation of collagenase (MMP-1, MMP-13) genes in arthritis: integration of complex signaling pathways for the recruitment of gene-specific transcription factors. Arthritis Res Ther 4, 157. https://doi.org/10.1186/ar401

Vogiatzidis, K., Zarogiannis, S.G., Aidonidis, I., Solenov, E.I., Molyvdas, P.-A., Gourgoulianis, K.I., Hatzoglou, C., 2015. Physiology of pericardial fluid production and drainage. Front Physiol 6. https://doi.org/10.3389/fphys.2015.00062

Volkov, L., Quéré, P., Coudert, F., Comte, L., Praloran, V., 1996. The tetrapeptide AcSDKP, a physiological inhibitor of normal cell proliferation, reduces the S phase entry of continuous cell lines. Experimental cell research 223, 112–116.

Wang, B., Komers, R., Carew, R., Winbanks, C.E., Xu, B., Herman-Edelstein, M., Koh, P., Thomas, M., Jandeleit-Dahm, K., Gregorevic, P., Cooper, M.E., Kantharidis, P., 2012. Suppression of microRNA-29 Expression by TGF-β1 Promotes Collagen Expression and Renal Fibrosis. JASN 23, 252–265. https://doi.org/10.1681/ASN.2011010055

Wang, M., Liu, R., Jia, X., Mu, S., Xie, R., 2010. N-acetyl-seryl-aspartyl-lysyl-proline attenuates renal inflammation and tubulointerstitial fibrosis in rats. Int. J. Mol. Med. 26, 795–801.

Wang, R., Ibarra-Sunga, O., Verlinski, L., Pick, R., Uhal, B.D., 2000. Abrogation of bleomycin-induced epithelial apoptosis and lung fibrosis by captopril or by a caspase inhibitor. American Journal of Physiology-Lung Cellular and Molecular Physiology 279, L143–L151.

Wang, Y., Simonson, M.S., Pouyssegur, J., Dunn, M.J., 1992. Endothelin rapidly stimulates mitogen-activated protein kinase activity in rat mesangial cells. Biochem J 287, 589–594.

Wang, Y.-T., Tsai, C.-F., Hong, T.-C., Tsou, C.-C., Lin, P.-Y., Pan, S.-H., Hong, T.-M., Yang, P.-C., Sung, T.-Y., Hsu, W.-L., 2010. An informatics-assisted label-free quantitation strategy that depicts phosphoproteomic profiles in lung cancer cell invasion. Journal of proteome research 9, 5582–5597.

Wdzieczak-Bakala, J., Fache, M.P., Lenfant, M., Frindel, E., Sainteny, F., 1990. AcSDKP, an inhibitor of CFU-S proliferation, is synthesized in mice under steady-state conditions and secreted by bone marrow in long-term culture. Leukemia 4, 235–237.

Wei, L., Alhenc-Gelas, F., Corvol, P., Clauser, E., 1991. The two homologous domains of human angiotensin I-converting enzyme are both catalytically active. Journal of Biological Chemistry 266, 9002–9008.

Wei, L., Clauser, E., Alhenc-Gelas, F., Corvol, P., 1992. The two homologous domains of human angiotensin I-converting enzyme interact differently with competitive inhibitors. J. Biol. Chem. 267, 13398–13405.

Weinstock, J.V., 1986. The significance of angiotensin I converting enzyme in granulomatous inflammation. Functions of ACE in granulomas. Sarcoidosis 3, 19–26.

Whitaker, D., Papadimitriou, J.M., Walters, M.N., 1982. The mesothelium: a cytochemical study of “activated” mesothelial cells. J. Pathol. 136, 169–179. https://doi.org/10.1002/path.1711360302

Whitworth, J.A., 2003. 2003 World Health Organization (WHO)/International Society of Hypertension (ISH) statement on management of hypertension. J. Hypertens. 21, 1983–1992. https://doi.org/10.1097/01.hjh.0000084751.37215.d2

WHO | Global tuberculosis report 2019 [WWW Document], n.d. . WHO. URL http://www.who.int/tb/publications/global_report/en/ (accessed 12.19.19).

Wilkes, J.D., Fidias, P., Vaickus, L., Perez, R.P., 1995. Malignancy-related pericardial effusion. 127 cases from the roswell park cancer institute. Cancer 76, 1377–1387. https://doi.org/10.1002/1097-0142(19951015)76:8<1377::AID-CNCR2820760813>3.0.CO;2-M

Williams, P.M., Lively, T.G., Jessup, J.M., Conley, B.A., 2012. Bridging the Gap: Moving Predictive and Prognostic Assays from Research to Clinical Use. Clin Cancer Res 18, 1531–1539. https://doi.org/10.1158/1078-0432.CCR-11-2203

Wilson, M., Wynn, T., 2009. Pulmonary fibrosis: pathogenesis, etiology and regulation. Mucosal Immunol 2, 103–121. https://doi.org/10.1038/mi.2008.85

Wiśniewski, J.R., 2017. Filter-Aided Sample Preparation: The Versatile and Efficient Method for Proteomic Analysis. Meth. Enzymol. 585, 15–27. https://doi.org/10.1016/bs.mie.2016.09.013

Wiysonge, C.S., Ntsekhe, M., Thabane, L., Volmink, J., Majombozi, D., Gumedze, F., Pandie, S., Mayosi, B.M., 2017. Interventions for treating tuberculous pericarditis. Cochrane Database of Systematic Reviews. https://doi.org/10.1002/14651858.CD000526.pub2

Wong, J., Patel, R.A., Kowey, P.R., 2004. The clinical use of angiotensin-converting enzyme inhibitors. Progress in Cardiovascular Diseases, Drug Class Effects Part 2 47, 116–130. https://doi.org/10.1016/j.pcad.2004.04.003

Wu, C., 2005. PINCH, N (i) ck and the ILK: network wiring at cell–matrix adhesions. Trends in cell biology 15, 460–466.

Wu, C., 2004. The PINCH–ILK–parvin complexes: assembly, functions and regulation. Biochimica et Biophysica Acta (BBA)-Molecular Cell Research 1692, 55–62.

Wu, R., Haas, W., Dephoure, N., Huttlin, E.L., Zhai, B., Sowa, M.E., Gygi, S.P., 2011. A large-scale method to measure absolute protein phosphorylation stoichiometries. Nat Methods 8, 677–683. https://doi.org/10.1038/nmeth.1636

Wynn, T., 2008. Cellular and molecular mechanisms of fibrosis. The Journal of Pathology 214, 199–210. https://doi.org/10.1002/path.2277

Wynn, T.A., 2007. Common and unique mechanisms regulate fibrosis in various fibroproliferative diseases. J Clin Invest 117, 524–529. https://doi.org/10.1172/JCI31487

Xiao, H.D., Fuchs, S., Frenzel, K., Teng, L., Bernstein, K.E., 2004. Circulating versus Local Angiotensin II in Blood Pressure Control: Lessons from Tissue-Specific Expression of Angiotensin-Converting Enzyme (ACE). CRE 14. https://doi.org/10.1615/CritRevEukaryotGeneExpr.v14.i12.70

Xiaojun, W., Yan, L., Hong, X., Xianghong, Z., Shifeng, L., Dingjie, X., Xuemin, G., Lijuan, Z., Bonan, Z., Zhongqiu, W., 2016. Acetylated α-Tubulin Regulated by N-Acetyl-Seryl-Aspartyl-Lysyl-Proline (Ac-SDKP) Exerts the Anti-fibrotic Effect in Rat Lung Fibrosis Induced by Silica. Scientific reports 6, 32257.

Xu, H., Yang, F., Sun, Y., Yuan, Y., Cheng, H., Wei, Z., Li, S., Cheng, T., Brann, D., Wang, R., 2012. A New Antifibrotic Target of Ac-SDKP: Inhibition of Myofibroblast Differentiation in Rat Lung with Silicosis. PLoS ONE 7, e40301. https://doi.org/10.1371/journal.pone.0040301

Yamamoto, K., Mano, T., Yoshida, J., Sakata, Y., Nishikawa, N., Nishio, M., Ohtani, T., Hori, M., Miwa, T., Masuyama, T., 2005. ACE inhibitor and angiotensin II type 1 receptor blocker differently regulate ventricular fibrosis in hypertensive diastolic heart failure. J. Hypertens. 23, 393–400.

Yáñez-Mó, M., Lara-Pezzi, E., Selgas, R., Ramírez-Huesca, M., Domínguez-Jiménez, C., Jiménez-Heffernan, J.A., Aguilera, A., Sánchez-Tomero, J.A., Bajo, M.A., Alvarez, V., Castro, M.A., del Peso, G., Cirujeda, A., Gamallo, C., Sánchez-Madrid, F., López-Cabrera, M., 2003. Peritoneal dialysis and epithelial-to-mesenchymal transition of mesothelial cells. N. Engl. J. Med. 348, 403–413. https://doi.org/10.1056/NEJMoa020809

Yang, F., Yang, X.-P., Liu, Y.-H., Xu, J., Cingolani, O., Rhaleb, N.-E., Carretero, O.A., 2004. Ac-SDKP Reverses Inflammation and Fibrosis in Rats With Heart Failure After Myocardial Infarction. Hypertension 43, 229–236. https://doi.org/10.1161/01.HYP.0000107777.91185.89

Yang, H.Y.T., Erdös, E.G., Levin, Y., 1971. A dipeptidyl carboxypeptidase that converts angiotensin I and inactivates bradykinin. Biochim Biophys Acta 214, 374–376.

Yang, L., Kwon, J., Popov, Y., Gajdos, G.B., Ordog, T., Brekken, R.A., Mukhopadhyay, D., Schuppan, D., Bi, Y., Simonetto, D., Shah, V.H., 2014. Vascular Endothelial Growth Factor Promotes Fibrosis Resolution and Repair in Mice. Gastroenterology 146, 1339-1350.e1. https://doi.org/10.1053/j.gastro.2014.01.061

Yang, R.-Y., Hill, P.N., Hsu, D.K., Liu, F.-T., 1998. Role of the Carboxyl-Terminal Lectin Domain in Self-Association of Galectin-3. Biochemistry 37, 4086–4092. https://doi.org/10.1021/bi971409c

Yang, R.Y., Hsu, D.K., Liu, F.T., 1996. Expression of galectin-3 modulates T-cell growth and apoptosis. PNAS 93, 6737–6742. https://doi.org/10.1073/pnas.93.13.6737

Yang, Y., Dukhanina, O., Tang, B., Mamura, M., Letterio, J.J., MacGregor, J., Patel, S.C., Khozin, S., Liu, Z., Green, J., Anver, M.R., Merlino, G., Wakefield, L.M., 2002. Lifetime exposure to a soluble TGF-β antagonist protects mice against metastasis without adverse side effects. Journal of Clinical Investigation 109, 1607–1615. https://doi.org/10.1172/JCI15333

Yarnold, J., Vozenin Brotons, M.-C., 2010. Pathogenetic mechanisms in radiation fibrosis. Radiotherapy and Oncology, Radiotherapy related morbidity 97, 149–161. https://doi.org/10.1016/j.radonc.2010.09.002

Yoshiji, H., Kuriyama, S., Noguchi, R., Ikenaka, Y., Yoshii, J., Yanase, K., Namisaki, T., Kitade, M., Yamazaki, M., Asada, K., others, 2006. Amelioration of liver fibrogenesis by dual inhibition of PDGF and TGF-β with a combination of imatinib mesylate and ACE inhibitor in rats. International journal of molecular medicine 17, 899–904.

Yoshiji, H., Noguchi, R., Fukui, H., 2005. Combined effect of an ACE inhibitor, perindopril, and interferon on liver fibrosis markers in patients with chronic hepatitis C. Journal of gastroenterology 40, 215–216.

Yu, C.-M., Tipoe, G.L., Lai, K.W.-H., Lau, C.-P., 2001. Effects of combination of angiotensin-converting enzyme inhibitor and angiotensin receptor antagonist on inflammatory cellular infiltration and myocardial interstitial fibrosis after acute myocardial infarction. Journal of the American College of Cardiology 38, 1207–1215.

Yue, B., 2014. Biology of the Extracellular Matrix: An Overview. J Glaucoma S20–S23. https://doi.org/10.1097/IJG.0000000000000108

Zeisberg, E.M., Tarnavski, O., Zeisberg, M., Dorfman, A.L., McMullen, J.R., Gustafsson, E., Chandraker, A., Yuan, X., Pu, W.T., Roberts, A.B., Neilson, E.G., Sayegh, M.H., Izumo, S., Kalluri, R., 2007. Endothelial-to-mesenchymal transition contributes to cardiac fibrosis. Nature Medicine 13, 952. https://doi.org/10.1038/nm1613

Zeisberg, M., Bonner, G., Maeshima, Y., Colorado, P., Müller, G.A., Strutz, F., Kalluri, R., 2001. Renal Fibrosis: Collagen Composition and Assembly Regulates Epithelial-Mesenchymal Transdifferentiation. The American Journal of Pathology 159, 1313–1321. https://doi.org/10.1016/S0002-9440(10)62518-7

Zhang, L., Xu, L.-M., Chen, Y.-W., Ni, Q.-W., Zhou, M., Qu, C.-Y., Zhang, Y., 2012. Antifibrotic effect of N-acetyl-seryl-aspartyl-lysyl-proline on bile duct ligation induced liver fibrosis in rats. World J. Gastroenterol. 18, 5283–5288. https://doi.org/10.3748/wjg.v18.i37.5283

Zhang, L., Yang, F., Li, Q., Zhang, X., Wang, R., 2011. AcSDKP inhibits the proliferation and collagen expression of cardiac fibroblasts induced by PDGF through blocking the ERK1/2 and JNK pathway activation, in: Human Health and Biomedical Engineering (HHBE), 2011 International Conference On. pp. 916–919.

Zhang, X., Zhou, J., Zhu, Y., He, L., Pang, Z., Wang, Z., Xu, C., Zhang, C., Hao, Q., Li, W., Zhang, W., Zhang, Y., Li, M., 2019. d-Amino Acid Modification Protects N-Acetyl-seryl-aspartyl-lysyl-proline from Physiological Hydroxylation and Increases Its Antifibrotic Effects on Hepatic Fibrosis. IUBMB Life. https://doi.org/10.1002/iub.2037

Zhang, Y., Fonslow, B.R., Shan, B., Baek, M.-C., Yates, J.R., 2013. Protein Analysis by Shotgun/Bottom-up Proteomics. Chem. Rev. 113, 2343–2394. https://doi.org/10.1021/cr3003533

Zhang, Y.E., 2009. Non-Smad pathways in TGF-β signaling. Cell Res 19, 128–139. https://doi.org/10.1038/cr.2008.328

Zhuo, J.L., Carretero, O.A., Peng, H., Li, X.C., Regoli, D., Neugebauer, W., Rhaleb, N.-E., 2007. Characterization and localization of Ac-SDKP receptor binding sites using 125I-labeled Hpp-Aca-SDKP in rat cardiac fibroblasts. Am J Physiol Heart Circ Physiol 292, H984–H993. https://doi.org/10.1152/ajpheart.00776.2006

Zou, K., Yamaguchi, H., Akatsu, H., Sakamoto, T., Ko, M., Mizoguchi, K., Gong, J.-S., Yu, W., Yamamoto, T., Kosaka, K., Yanagisawa, K., Michikawa, M., 2007. Angiotensin-Converting Enzyme Converts Amyloid B-Protein 1–42 (Aβ1–42) to Aβ1–40, and Its Inhibition Enhances Brain Aβ Deposition. J. Neurosci. 27, 8628–8635. https://doi.org/10.1523/JNEUROSCI.1549-07.2007

Zumla, A., Maeurer, M., Moll, G., Mayosi, B.M., 2015. Host-directed therapies for tuberculous pericarditis. International Journal of Infectious Diseases 32, 30–31.